Technical University of Munich
TUM School of Life Sciences

Chemoproteomics-based target deconvolution and selectivity profiling of Histone Deacetylase inhibitors

Severin Lechner

Complete reprint of the dissertation approved by the TUM School of Life Sciences of the Technical University of Munich for the award of the Doktor der Naturwissenschaften (Dr. rer. nat.).

Chair: Prof. Dr. Martin Klingenspor

Examiners:

1. Prof. Dr. Bernhard Küster
2. Prof. Dr. Stephan A. Sieber
3. Prof. Dr. Thomas Carell

The dissertation was submitted to the Technical University of Munich on 07.06.2023 and accepted by the TUM School of Life Sciences on 12.07.2023.

Abstract

Most approved drugs are binding to proteins and modulate their function. The target proteins of drug candidates are often unknown at the outset, for instance when they are discovered as hits in phenotypic screening assays. Knowing the targets, however, is crucial to understand the mode of action of a drug candidate, to potentially allow repurposing of established drugs, and to improve the selectivity of the molecule. Chemoproteomics combines the use of chemical tools with powerful LC-MS/MS-based proteomics technology to identify drug targets among thousands of proteins in a single experiment. As such, chemoproteomic approaches are the methods of choice to identify the target space of drug candidates.

Here, I developed a new affinity-based protein profiling technology for the target deconvolution and selectivity profiling of HDAC inhibitors. The chemical toolset enabled the selectivity profiling of more than 50 metal ion-chelating drug molecules against all proteins expressed in the cellular system, including 9 of the 11 zinc-dependent HDACs and at least 8 common off-targets. This effort resulted in the most comprehensive target landscape of HDAC inhibitors, comprising affinity data for more than 850 drug-target interactions. Our results question the claimed selectivity of widely used chemical probes and drug molecules. Strikingly, more than 24 of the 32 validated hydroxamate-based HDAC inhibitors, including approved drugs, bound and inhibited the unreported off-target MBLAC2. Knockdown and inhibition of MBLAC2 led to a reconstruction of the lipidome and an accumulation of extracellular vesicles, and might therefore have a direct impact on the clinical efficacy or side effects of these drugs. Furthermore, the technology supported the chemoproteomic identification of HDACs as protein targets of lipoic acid, a drug that has been approved for diabetic neuropathy and is in use as a food supplement without a well-understood mode of action.

Overall, these findings will stimulate further investigation of potential off-target effects of HDAC inhibitors, prevent the further use of unselective probes for the study of HDAC biology, designate chemical probes for HDAC6 and HDAC10, and motivate the research community to explore the clinical relevance of lipoic acid-mediated HDAC inhibition.

Zusammenfassung

Die meisten zugelassenen Arzneimittel binden Proteine und modulieren deren Funktion. Die Zielproteine von Arzneimittelkandidaten sind zu Beginn oft nicht bekannt, zum Beispiel wenn sie als Treffer in phänotypischen Screening-Tests entdeckt werden. Die Kenntnis der Zielproteine ist jedoch von entscheidender Bedeutung, um die Wirkungsweise eines Wirkstoffkandidaten zu verstehen, um möglicherweise die Umwidmung etablierter Arzneimittel zu ermöglichen und um die Selektivität des Moleküls zu verbessern. Die Chemoproteomik kombiniert den Einsatz chemischer Werkzeuge mit der leistungsstarken LC-MS/MS-basierten Proteomik-Technologie, um in einem einzigen Experiment Wirkstoff-Zielprotein für Tausende von Proteinen zu identifizieren. Daher sind chemoproteomische Ansätze die Methoden der Wahl, um die Zielproteine von Arzneimittelkandidaten zu identifizieren.

In diesem Projekt habe ich eine neue affinitätsbasierte Proteinprofilierungstechnologie für die Zielprotein-Aufklärung und Selektivitätsprofilierung von HDAC-Inhibitoren entwickelt. Das chemische Toolset ermöglichte die Erstellung von Selektivitätsprofilen für mehr als 50 Metallionen-chelierende Wirkstoffe gegen alle im zellulären System exprimierten Proteine, darunter 9 der 11 zinkabhängigen HDACs und mindestens 8 häufig auftretende Off-Targets. Das Ergebnis dieser Bemühungen ist die umfassendste Target-Feld von HDAC-Inhibitoren, welche Affinitätsdaten für mehr als 850 Wirkstoff-Ziel-Interaktionen umfasst. Unsere Ergebnisse stellen die behauptete Selektivität von weit verbreiteten chemischen Sonden und Wirkstoffmolekülen in Frage. Auffallend ist, dass mehr als 24 der 32 validierten hydrocamat-basierten HDAC-Inhibitoren, darunter auch zugelassene Medikamente, das bisher nicht entdeckte Off-Target MBLAC2 binden und hemmen. Der Knockdown und die Hemmung von MBLAC2 führte zu einer Umstrukturierung des Lipidoms und zu einer Anhäufung von extrazellulären Vesikeln, und könnte daher direkte Auswirkungen auf die klinische Wirksamkeit oder die Nebenwirkungen dieser Medikamente haben. Darüber hinaus unterstützte die Technologie die chemoproteomische Identifizierung von HDACs als Zielproteine von Liponsäure, einem Medikament, das zur Behandlung von diabetischer Neuropathie zugelassen ist und als Nahrungsergänzungsmittel verwendet wird, ohne dass seine Wirkungsweise genau bekannt ist.

Zusammengenommen werden diese Ergebnisse die weitere Untersuchung potenzieller Off-Target-Effekte von HDAC-Inhibitoren anregen, die weitere Anwendung unselektiver Sonden für die Untersuchung der HDAC-Biologie unterbinden, chemische Sonden für HDAC6 und HDAC10 definieren und die Forschungsgemeinschaft motivieren, die klinische Relevanz der Liponsäure-vermittelten HDAC-Inhibition weiter zu untersuchen.

Table of contents

Abstract i
Zusammenfassung ii
Table of contents iii
General Introduction 1
General Methods 32
Publications 35
General discussion and outlook 44
Conclusions 76
References 77
Acknowledgements 91
Appendix 92

General Introduction

Content

Abstract i

Zusammenfassung ii

Table of contents iii

General Introduction 1

1 Chemoproteomics in drug target deconvolution and selectivity profiling 2

1.1 The value of target deconvolution in drug discovery 2

1.2 (Chemo-) Proteomics-based drug target deconvolution approaches 3

1.2.1 Whole proteome perturbation experiments 3

1.2.2 Protein stability profiling 6

1.2.3 Assessing direct drug target binding 7

1.2.4 Choosing the right target deconvolution method 12

1.2.6 Promiscuous affinity probes for the target deconvolution and selectivity profiling of large drug families 14

2 Zn^{2+}-dependent histone deacetylases as drug targets 16

2.1 The diversity of the HDAC family members 16

2. 2 The potential of HDACs as drug targets 19

2.2.1 Effects of simultaneous inhibition of class I HDAC1, HDAC2, and HDAC3 20

2.2.2 Targeting HDAC8 in cancer 21

2.2.3 Inhibiting HDAC6 in neurological and neoplastic diseases 21

2.2.4 Disturbing the polyamine homeostasis via HDAC10 inhibition 23

2.2.5 Class IIa HDACi as potential therapeutics? 24

2.2.6 Class IV HDAC11i 24

2.2.7 Target cell non-autonomous effects of HDAC inhibitors 24

2.3 Studying the selectivity of HDAC inhibitors 25

2.3.1 General design principles of HDAC inhibitor 25

2.3.2 Approaches to determine HDAC inhibitor selectivity 25

3 Objective and outline 30

1 Chemoproteomics in drug target deconvolution and selectivity profiling

1.1 The value of target deconvolution in drug discovery

Drug molecules elicit their effects via interaction with various biomolecules. Such interactions can for instance affect the functionality, localization, interaction network, or stability of the biomolecules. Depending on whether the drug interaction is a desired outcome of the drug design, the biomolecules are called targets (wanted interaction) or off-targets (unwanted interaction).
Molecules identified as hits in target-agnostic drug discovery programs, such as phenotypic screens, are initially often not assigned to any molecular target. Even in target-oriented drug discovery, the hit molecules are often only profiled against a panel of closely related target biomolecules or a safety pharmacology panel, ignoring the potential binding to various unexpected off-targets. The field of target deconvolution deals with the comprehensive identification of drug targets and off-targets and is relevant for several reasons:

(i) Identifying the molecular target can support the development of advanced molecules from the initial hit. For instance, co-crystal structures of drugs engaged with the target can inform rational drug design or enable docking of in silico drug libraries to find additional hit molecules. Moreover, assays tailored to the target can be employed for high-throughput screening, or to robustly and quickly evaluate the performance and properties of novel drug derivatives in SAR studies.
(ii) Identifying the (off-) targets might raise red flags at an early development stage. If drug molecules are found to inhibit proteins essential in a healthy physiological context, the development can be stopped. To circumvent side effects, analogs of the pharmacophore with reduced off-target affinity can be developed instead. This prevents wasting resources or risking human health and lives by progressing such drugs into clinical trial[1].
(iii) If target deconvolution after phenotypic screens finds a protein target that has been subject to drug development pipelines before, the existing drugs against this target can be repurposed for the new indication. The advantage is that repurposed drugs have already been characterized regarding their pharmacokinetics and safety profile and therefore allow to skip the time-demanding and costly clinical phase I-II studies[2].

The prominent examples of two drug modalities, BIA 10−2474 and Imatinib, shall illustrate the points made above. The designated FAAH inhibitor BIA 10−2474 entered clinical trials to treat chronic pain in cancer patients and motoric deficits in Parkinson's disease[3]. The trial abruptly came to an end after human volunteers died or had to be hospitalized due to brain tissue damage[3]. In hindsight, the neurotoxic effects of BIA 10-2474 were explained by a multitude of off-targets, while other selective FAAH inhibitors have proved safe[4, 5]. One prominent off-target effect was the covalent inhibition of the detoxifying aldehyde dehydrogenases by the des-methylated BIA 10−2474[5]. Early discovery of the vast number of off-targets should have triggered a closer analysis of potential toxic side effects to deter premature progression into clinical trials[1]. While proper target deconvolution can prevent fatal incidents in patients, Imatinib is a prime example of successful rational drug repurposing enabled by drug target deconvolution. Initially, Imatinib was designed as a selective BCR-ABL inhibitor. But soon it was shown to inhibit other receptor tyrosine kinases, such as KIT[6]. At about the same time, KIT was found to drive gastrointestinal stromal tumor (GIST)[7], and, therefore, Imatinib was repurposed and approved for treating GIST in 2002[8]. This early and successful repurposing of the drug would not have been possible without the identification of KIT as an additional target of Imatinib.

Overall, target deconvolution aids in minimizing risks, supports hit-to-lead development processes, and potentially allows to take advantage of developed drugs via drug repurposing. It is therefore desirable to submit all drugs and drug candidates to rigorous target deconvolution.

1.2 (Chemo-) Proteomics-based drug target deconvolution approaches

Proteomics is the study of the proteome, i.e. the identification and quantification of the thousands of proteins contained in a biological sample. Since most of the drugs approved today are targeting proteins, proteomic technologies are well suited for target deconvolution and elucidating the mode of action (MoA) of drugs.

In the bottom-up (or shotgun) proteomics approach, proteins from a sample are first enzymatically digested into peptides, which are then analyzed via a liquid chromatography-coupled tandem mass-spectrometer (LC-MS/MS) system to generate data for the identification and quantification of the proteins (for more details, see general methods). Depending on the sample type, sample amount, sample workup protocol, and LC-MS/MS equipment, up to 9,000 proteins can be robustly identified and quantified with modern set-ups (see for instance ref.[9]), and these numbers are rising with each year's advances in technology. Proteomics approaches therefore allow to inquire drug molecules' binding or modulation of thousands of potential protein targets in a single experiment. Assaying this large and not pre-defined space of potential targets allows to draw a comprehensive picture of the protein targets bound or otherwise modulated by a drug molecule.

Proteomics-based target deconvolution approaches cover a broad spectrum of methodologies that all come with their own set of advantages and disadvantages. On one end of the spectrum, the strategies enable the identification of direct drug-target interactions. On the other, the approaches yield only a narrowed-down set of potential targets or pathways that get perturbed by the drug. These approaches, however, additionally provide a more global view of downstream effects.

1.2.1 Whole proteome perturbation experiments

In several papers, researchers have suggested that proteome perturbation experiments directly inform the MoA or even the molecular target[10-13], arguing that the target is often regulated as a result of treating cells with the drug. For instance, one study states that the authors "[…] have previously shown that when sensitive cell lines are treated with a toxic compound, its targets, and mechanistic proteins are consistently found among the most regulated ones" [11]. Further, the authors claim to "[…] show that contrasting the proteome signature of a single compound against others highlights a given compound's target and mechanistic proteins on the top positions in most cases" [11]. Another study insinuates a similar potential of such a proteomic readout by headlining a subsection with "*Regulation of target proteins informs compound MOA"* [13].

These ideas are based on the concept that inactivation of a protein is perceived by the cell as absence of the protein, triggering feedback-loop mediated upregulation of the target protein in response. For instance, inhibiting enzyme targets would lead to accumulation of the enzyme's substrates and depletion of its products. Such a 'bottleneck' in a metabolic pathway can in theory be sensed by cells and induce the expression of the target enzyme to cope with the accumulating substrate[14]. However, such feedback mechanisms have been mostly described for bacteria. Intensive literature research did not reveal a single example of a human enzyme being overexpressed via negative feedback regulation of accumulating substrates or a declining product pool. In reality, and opposing the claims of many studies, the drug target level is often not regulated and if so, it is unlikely regulated via a specific feedback loop. In point of fact, many drugs cause a general perturbation of the cellular proteome and the targets are only a minority compared to the high number of other regulated non-target proteins. Hence, target regulation is

more likely an indirect secondary effect of a larger cellular restructuring caused by the drug. Such large proteome perturbations are particularly observed for drugs (Fig. 1) that

(i) directly affect the activation or repression of transcription and therefore the de novo protein production (e.g. (Tyrosine) Kinase inhibitors, HDAC inhibitors, BRD inhibitors)[13].

(ii) disturb the protein homeostasis and protein degradation pathways (e.g. shown for proteasome, autophagy, and HSP90 inhibitors[13]).

(iii) arrest the cells in a specific cell cycle phase with characteristic protein levels (e.g. CDK inhibitors, DNA synthesis blocking agents, topoisomerase inhibitors)[13].

(iv) cause various kinds of cellular stresses, which push the cell into a response that remodels the proteome (e.g. oxidative stress inducers)[13].

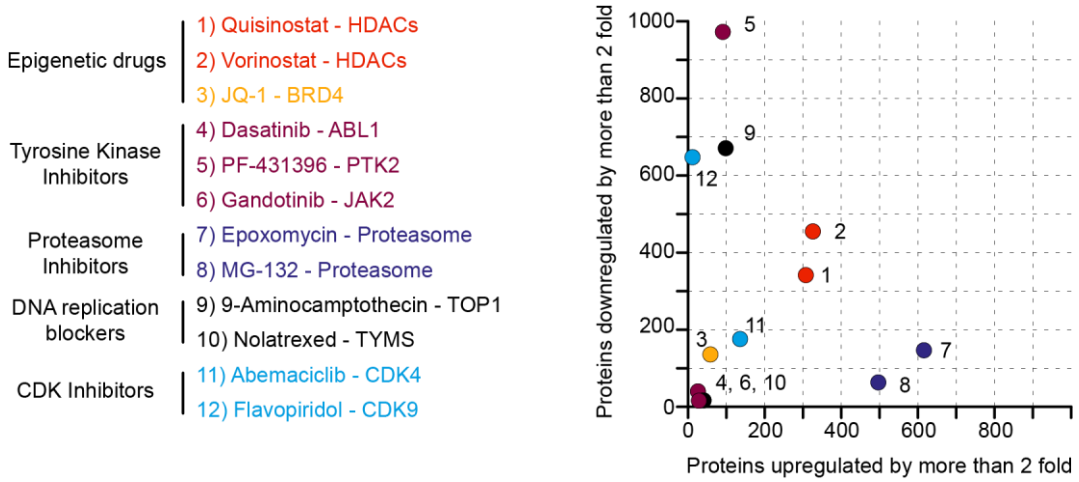

Fig. 1|Many drugs lead to the up-or downregulation of tens to hundreds of proteins. Some drug families, such as HDAC inhibitors or proteasome inhibitors lead to a substantial remodeling of the cellular proteome. The data origin of this figure is Mitchell et al.[13], supporting Table 1. HCT116 cells were treated with 10 µM drug for 24 h before proteomic analysis. Targets with an upregulation or downregulation of ≥ 2-fold. Drug names are followed by the main target, as annotated in the source data from Mitchell et al.[13].

In papers describing that drug-induced target regulation informs on the target identity (ref. [10-12]), examples have often been cherry-picked and results have been interpreted with prior knowledge of drug modes of action. In one study, HDAC4 was listed as an example of a target upregulated as a response to inhibition by the claimed HDAC4 inhibitor LMK-235[12]. However, in hindsight, LMK-235 was discovered to not even bind and inhibit HDAC4 (publication 1[15], see chapter 4.4). Overall, none of the studies (ref. [10-12]) contributed to the identification of previously unknown targets of drugs, and, therefore, do not represent suitable examples for successful drug target deconvolution approaches.

According to Mitchell et al.[13], who assessed the proteome perturbation by 875 drugs, less than 10% of drugs upregulate their target at all, and if so, only with a median fold change of 1.56. While target upregulation is therefore rather the exception from the rule, most drugs still significantly regulate tens to hundreds of other proteins not directly linked to the mode of action[13]. Further, targets can, if affected at all, either be up- or downregulated[13]. This renders de novo target deconvolution, i.e. the confident identification of the physical target of a drug, from a single proteome perturbation experiment highly unlikely (Fig. 2).

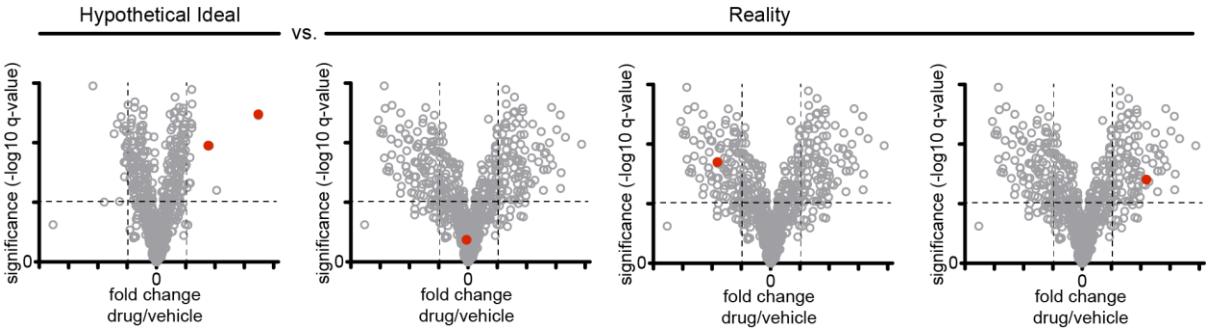

Fig. 2|Schematic representation of proteome perturbance data, comparing drug treatment (single dose) to the vehicle control. In a hypothetical scenario, drug targets are directly regulated as a response to their inhibition, and most other proteins are not regulated. This idealistic scenario is often claimed to enable drug target deconvolution by calling the most strong and most significant proteins targets (ref.[10-12]). In reality, however, most drugs induce a large perturbance of the proteome resulting in tens to hundreds of up and downregulated proteins[13]. For initial target assignment, however, it is not known whether the target protein is actually regulated at all, and if so whether it is among the crowd of down- or upregulated proteins. This renders de novo target deconvolution by proteome perturbance experiments highly unlikely.

Nevertheless, full proteome perturbation experiments are not unsuited for target deconvolution in general. The effects of drugs on the global protein expression can induce a characteristic signature of protein up- or downregulation. Such shifts can be viewed as a drug 'fingerprint' on the proteome. If this fingerprint is compared to fingerprints of drugs with known MoA, good correlations suggest interference of the drug with the same pathway or even the same target. Such methods only work well on a large scale, when a sufficient number of well-defined drugs (ideally hundreds to thousands) is investigated in the same cell line, with the same drug exposure parameters (incubation time, culturing methods), the same sample preparation protocol, and the same data processing. Similar strategies have been successfully implemented on transcriptome level (i.e., 986 features in the L1000 project[16]) or in cell painting experiments, where up to 1,500 features are extracted from microscope pictures of treated cells[17-19]. Most recently, the afore-mentioned first big proteomic study was performed by Mitchel et al.[13], investigating 875 drugs that were incubated with HCT116 cells at 10 µM concentration for 24 hours[13]. This study is the first proof of concept using the correlation of proteome perturbation fingerprints (i.e., more than 8000 features per treated cell) for the identification of potential drug MoAs. Several molecules designed for different targets clustered together. Interestingly, the molecules featured similar pharmacophores and the data suggests that the TLR7 activator imiquimod inhibits DHFR as off-target[13]. Further, ferrous ion chelation might contribute to the phenotypes induced by the CASP3 activator PAC-1[13]. However, experiments confirming these findings are still pending.

While increasing the library sizes of compounds with well-characterized MoA will allow matching to a more diverse set of MoAs and will boost the power of the fingerprinting approach, it will stay inherently incapable of unraveling unseen MoAs, which are not represented in the library of reference fingerprints. Bespoke study[13], for instance, only targeted roughly 900 proteins with their reference drug library, meaning that target deconvolution can only assign MoAs that are closely linked to the inactivation of these 900 proteins or their functional network. Besides the size of the reference library and the limited number of MoAs covered, another challenge originates from polypharmacology of drugs, i.e. drugs that inhibit several targets. This can be particularly problematic if drugs are only profiled at a fixed single dose. At 10 µM (as in mentioned study ref.[13]), even probes that are considered selective, might bind to and inhibit off-targets, blurring the fingerprint. Additionally, the reference compound might be annotated to the wrong target[20], further confounding results. Therefore, the way to the success of fingerprinting approaches lies in the improvement of yet insufficiently large and well-curated compound reference libraries. Extending the efforts to dose-dependent profiling might allow to better cope with polypharmacology. Further, complementing the drug reference libraries with, for instance,

genetic perturbances might allow to match protein inhibition fingerprints to protein knockdown fingerprints and thereby expand the space of potentially covered MoAs for targets with yet unknown inhibitors.

1.2.2 Protein stability profiling

In contrast to whole proteome perturbation experiments, protein stability profiling approaches do not necessarily lead to huge changes in the proteomic readout and are therefore more likely to directly identify the physical target of drugs. The concept of protein stability profiling is based on drug binding-mediated target stabilization (or enhanced destabilization) against destabilizers such as heat (Thermal proteome Profiling (TPP); proteome integral stability alteration (PISA))[21] (Fig. 3), solvents[22], or enzymatic digestion (limited proteolysis-coupled mass spectrometry (LiP-MS))[23, 24] (Fig. 4).

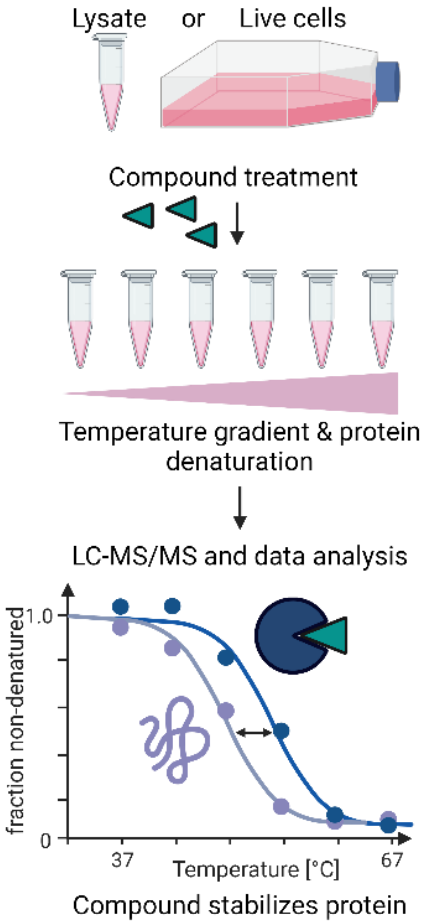

Fig. 3|Schematic representation of the TPP approach for target deconvolution. Cell lysate or intact cells are incubated with the drug of interest or vehicle control. After incubation cells or lysate are exposed to different temperatures. The temperatures lead to protein denaturation and precipitation. Proteins remaining in the soluble fraction are further processed and quantified via LC-MS/MS. Drug binding can (de-)stabilize the target protein to shift its 'melting temperature' and thereby hints at potential protein targets. The figure was created with Biorender.

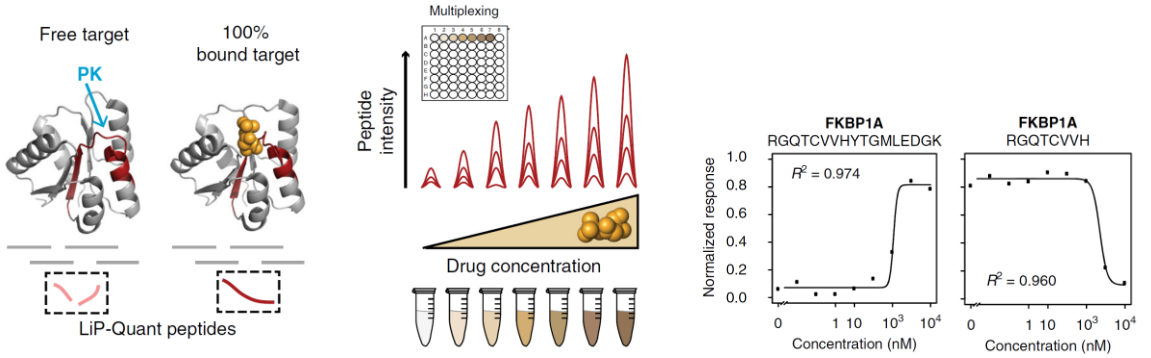

Fig. 4|Schematic representation of the LiP-MS (LiP-Quant) approach for target deconvolution (adapted with permission from ref.[24]). Binding of a compound to its target might shield the adjacent peptides from digestion with proteinase K (preference for aromatic and hydrophobic amino acids in P1). With increasing drug concentrations, higher fractions of the protein are bound by the drug and kept from cleavage. After proteomics sample preparation and LC-MS/MS analysis, the relative amount of a peptide originating from proteinase K cleavage proximal to the drug binding site, therefore, decreases with higher drug concentrations, while the amount of the full-length peptide (shielded from digestion) is increasing. This is nicely exemplified for an FKBP1A peptide. After treating HeLa lysates with Rapamycin, a known FKBP1A binder, the proteinase K cleavage of the peptide at the position RGQTCVVH-YTGMLEDGK (cleavage site indicated by a minus) is diminishing with increasing rapamycin concentrations. The curves allow to derive a binding affinity measure, the effective concentration of half-maximal target engagement (EC50), in the range of 1-10 µM.

While protein stability profiling experiments proved useful in the identification of unreported drug targets (e.g. TPP[25-27], LiP-MS[24]), chances of success in direct target identification are limited, since drugs often do not affect the target stability at all, or can lead to either stabilization or destabilization of targets[24, 28]. Especially, if these assays are carried out in living cells, downstream effects of drug treatment can change the stability of many proteins that are not direct targets[21]. For instance, kinase inhibition would lead to a quick decrease of phospho-sites downstream of the target kinase signaling pathway. The substrates' or their interaction partners' stability might be directly affected by the phosphorylation status, and hence downstream proteins, which often are kinases, might be confused with direct targets of the drug[21, 28]. Similar to whole proteome perturbation experiments, protein stability assays might therefore often produce a list of potential targets that still needs further narrowing down by alternative assays[21].

1.2.3 Assessing direct drug target binding

Direct interaction between drugs and protein targets can be determined by different methods, suited for either covalent binders or non-covalent binders. Covalent drugs form a direct physical crosslink between molecule and target protein. By introducing an enrichment handle such as a biotin tag to the drug, the drug-target complex can be pulled down from a cellular lysate with Streptavidin beads (Fig. 5). Protein(s) that are significantly enriched compared to a control can be considered direct targets. First introduced for serine hydrolases, this concept was termed activity-based protein profiling (ABPP) and has led to the identification of many targets and modes of action[29, 30].

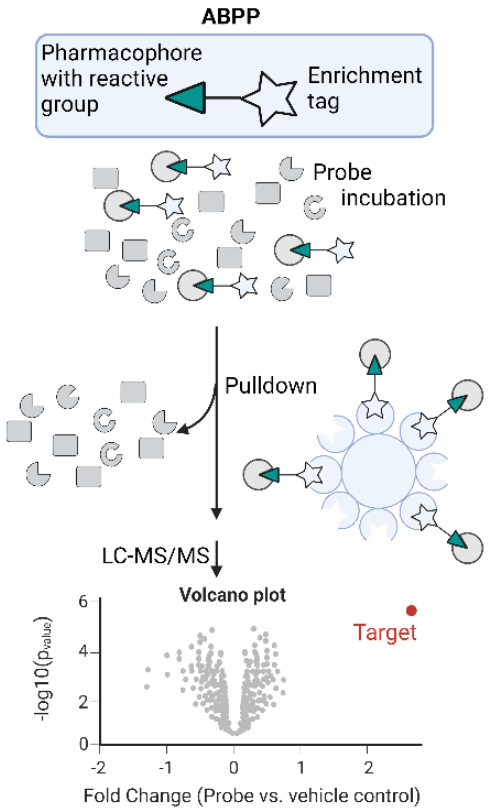

Fig. 5|Schematic representation of an ABPP workflow. The compound of interest (a pharmacophore with reactive warhead) is derivatized by attaching an enrichment handle. This handle can consist of biotin for streptavidin-biotin enrichment, alkyne or azide for copper(I)-catalyzed azide-alkyne Cycloaddition (CuAAC) click reaction, or other tags for bioorthogonal reaction. In the simplest setup, the proteins pulled down after probe treatment are compared to proteins pulled down after vehicle control treatment. The direct target of the compound should appear as most significantly and highly enriched protein amongst the background proteome of unspecific or low-affinity binders. Such data can for instance be visualized in a volcano plot. Instead of comparing vehicle to probe, an assay setup with competition between a promiscuous probe targeting a whole enzyme class (e.g. serine hydrolases[30]) and the compound of interest is conceivable. The figure was created with Biorender.

New approaches have been aiming at globally determining the reactivity of drugs with specific amino acid residues on a proteomic scale (Fig. 6). The concept was introduced as cysteine reactivity profiling[31, 32] but has been extended to other amino acids such as lysine[33, 34] or tyrosine[35]. To find targets of drugs with reactive warheads, the drugs are incubated with the lysate or cells to covalently bind to their targets. Next, a promiscuous and reactive warhead with an enrichment tag is added and binds to cysteine residues that are accessible and have not reacted with the covalent drug. The tag is then used to enrich probe-labeled cysteine residues and measure their abundance via LC-MS/MS. Reactive amino acid residues that interacted with the drug are not labeled and pulled down by the probe, resulting in their depletion. In this way, the methodology allows the indirect identification of protein sites covalently bound by drugs. Modern cysteine reactivity profiling assay setups can assess binding to thousands of cysteine residue sites on proteins[36-38].

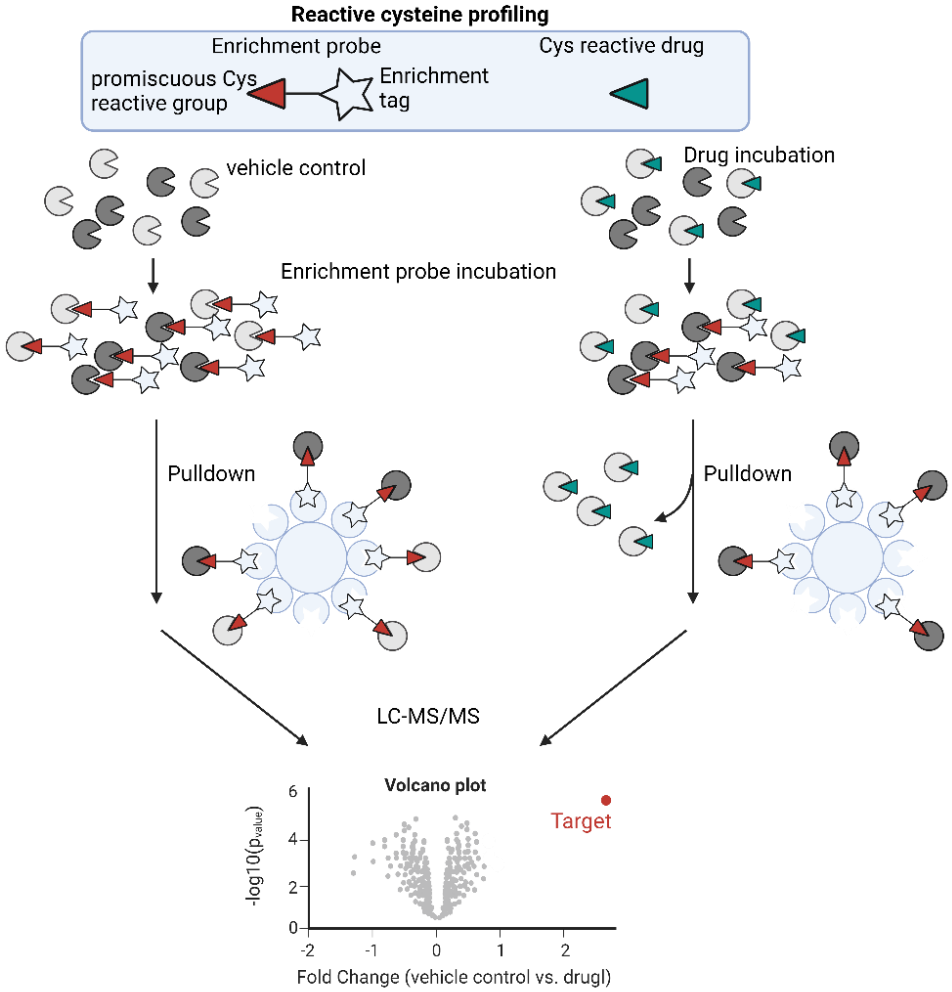

Fig. 6|Schematic representation of competitive reactivity-based protein profiling. Lysate is incubated with vehicle control or with the compound of interest, which contains a reactive warhead (such as an iodoacetamide or Michael acceptors for cysteine reactivity profiling). A promiscuous reactive probe is then incubated with the lysate. This probe contains an enrichment handle (such as moieties for click chemistry or biotin) and allows to pull down covalently bound proteins that are digested to peptides and submitted to LC-MS/MS analysis for protein identification and quantification. Reactive cysteine sites already occupied by the compound of interest can not react with the promiscuous probe anymore and are therefore depleted from the compound-treated sample. Targets should therefore be significantly and highly enriched in the vehicle control sample, as exemplified in the volcano plot. The figure was created with Biorender.

Most of the approved small molecule drugs are binding non-covalently. To be able to apply similar protocols as for ABPP, one can equip the molecule with an enrichment handle and a reactive moiety that allows it to covalently link the drug to its target for pulldown via the enrichment handle. For instance, the introduction of photo-activatable groups allows to unspecifically react the target-bound drug with amino acids in close proximity (Photo Affinity Labelling, PAL)[39]. Pulldown of the drug-linked targets and LC-MS/MS analysis allows to identify significantly enriched proteins as target candidates (Fig. 7).

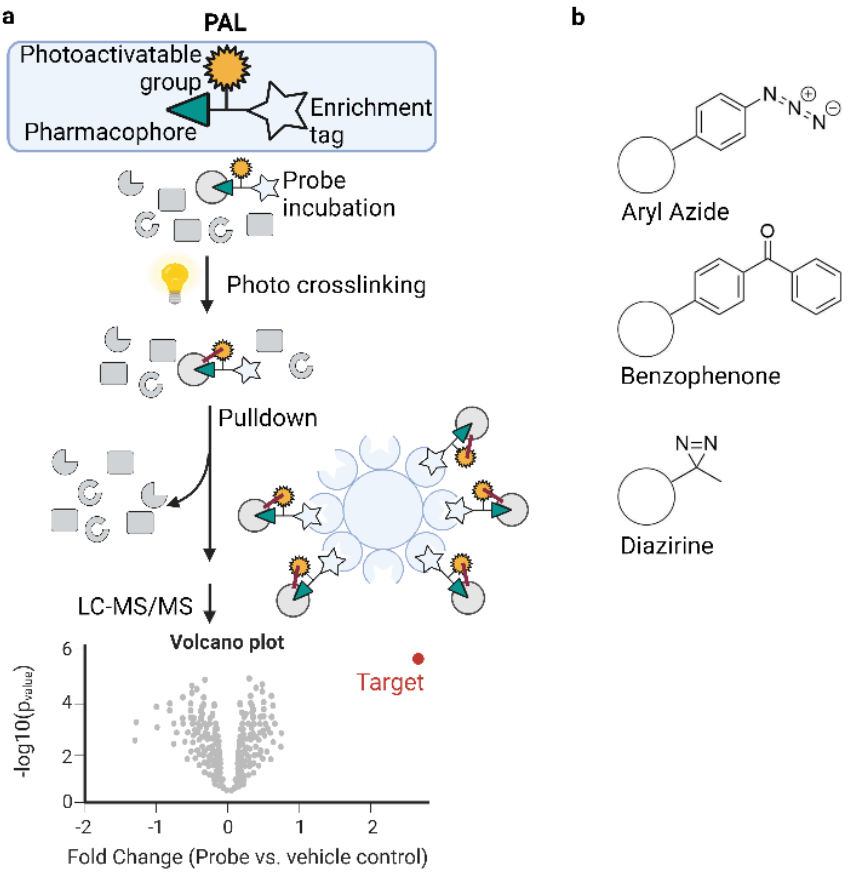

Fig. 7|Schematic representation of target deconvolution using photoaffinity labeling (PAL) probes. a, Drugs that do not contain a warhead for covalent binding to targets can be equipped with a photoactivatable group to induce unspecific covalent crosslinking of the drug-target complex after irradiating the sample with light. Additional introduction of an enrichment handle to the drug-derivative allows pulldown of targets similar to the ABPP workflow (see Fig. 5) Proteins that are significantly and highly enriched in the probe-treated sample compared to a vehicle control-treated sample are most likely direct targets of the drug. Similar to ABPP, a competition with the parent compound as additional control can help to validate the drug target. **b**, Structures of three commonly used photo-crosslinkers used for PAL. The figure was created with Biorender.

Another route of drug target deconvolution for non-covalent drugs is affinity-based protein profiling (AfBPP). Here the drug gets immobilized to create an affinity matrix that enables the pulldown of the target proteins from cell lysate (see Fig. 8).

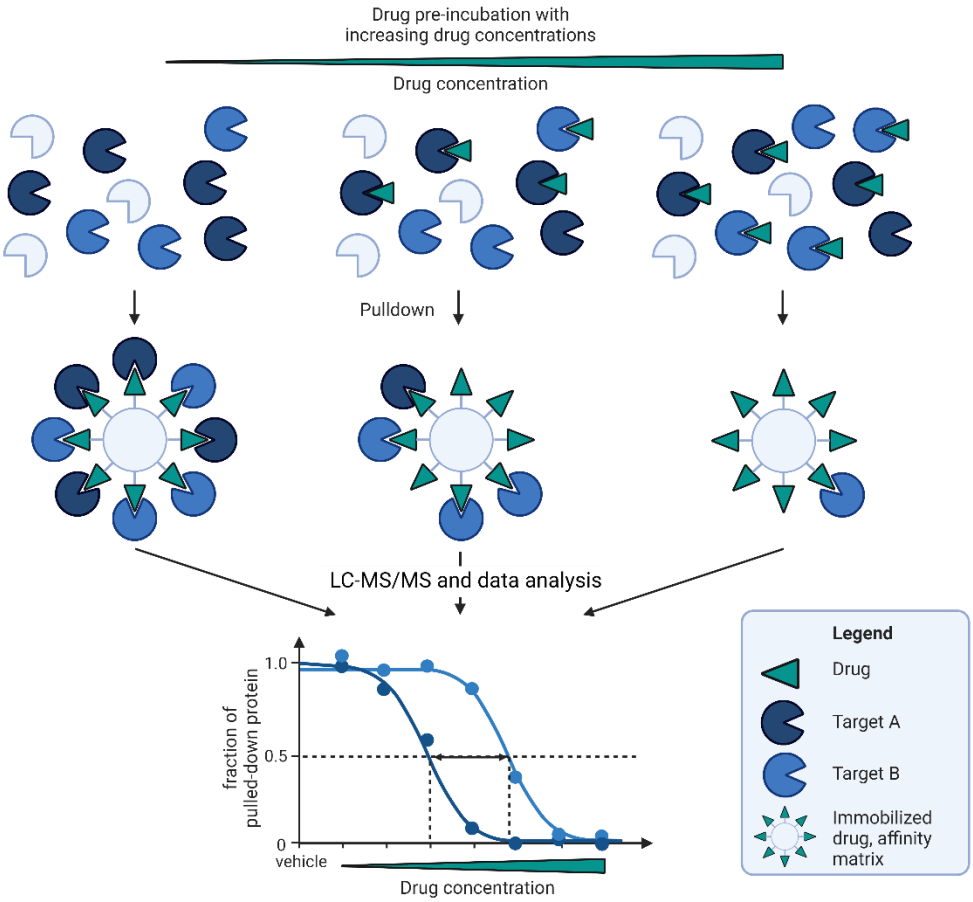

Fig. 8|Schematic representation of an affinity-based protein profiling (AfBPP) workflow in the dose-dependent competition setup. This workflow constitutes the fundament of the underlying papers (Publication 1 and 2, co-authorship 1 and 2). Drugs are covalently attached to a solid phase, such as sepharose beads, to create an affinity matrix that allows the pulldown of targets bound by the immobilized drug. Pre-incubation of the lysate with increasing concentrations of free drug leads to a dose-dependent increase in target occupancy. Target proteins already bound by the free drug cannot be pulled down by the affinity matrix. After analyzing the pulled-down proteome by LC-MS/MS, plotting the fraction of protein intensity in drug treatments relative to the vehicle control yields dose-response curves, from which EC50 values can be derived as a measure of drug target affinity. The figure was created with Biorender.

In contrast to ABPP or PAL, purely affinity-based pulldowns do not allow harsh washing conditions due to the inherent risk of losing specifically bound targets. As a result, hundreds to thousands of proteins can precipitate or bind unspecifically to the affinity matrix and specifically bound proteins might be not even among the top 1000 pulled-down proteins[15, 40]. Performing competition assays solves this issue: proteins that do not bind to the matrix in the presence of the free drug competing for the binding site, are considered targets, while proteins binding to the matrix independent of spiked in drug are not considered targets of the drug. Competition assays can be performed either at a single concentration of free drug or in a dose-dependent fashion. The dose-response provides information about target affinity (i.e. at which drug concentrations are target proteins substantially engaged by the free drug to significantly impede pulldown) in addition to simple binary information (target/no target). This information is highly relevant since it allows to conclude on drug selectivity. For instance, given the case that a drug binds target A with an affinity of 10 nM and target B with an affinity of 500 nM, this drug would be considered selective, since it completely inhibits target A at around 50 nM while target B's activity would not be affected at this low concentration. In contrast, a competition experiment performed at a single concentration of 10 µM, however, would show a significant depletion of both target A and target B, neglecting the

fact of actual selectivity. Selectivity profiling, as performed in the studies underlying this thesis, was therefore always performed in a dose-response assay setup.

1.2.4 Choosing the right target deconvolution method

All of the mentioned approaches come with a set of advantages and disadvantages. For the right choice of proteomic target deconvolution method, one needs to consider the following points in regard to the research question and also needs to take into account whether methods are feasible concerning the required equipment, resources, and time management:

(i) Some of the experiments are exclusively performed in cell lysates (AfBPP, LiP-MS), while others theoretically work in cellulo (TPP, ABPP, PAL, proteome perturbation). Cell lysis breaks up organelles and mixes the organellar environment-specific factors such as pH or redox state, and small metabolites, cofactors, or metal ions. This might inactivate proteins or create conditions where the drug binds a protein artefactually under circumstances that would never be encountered in an intact cell. Working in cellulo is therefore recommended whenever possible.

(ii) Some of the approaches usually require the generation of a tailored or promiscuous chemical probe (AfBPP, PAL, ABPP, and reactivity-based profiling), while others can investigate the drug of interest without additional efforts of chemical synthesis (proteome perturbation/fingerprinting, TPP, solvent shift assays, and LiP-MS). Synthesizing a probe that is still binding its target despite the chemical modification constitutes a major challenge. The exact attachment site of the enrichment handle can significantly impact the target binding profile. In the case of Staurosporine[41], a simple immobilization via an amidation reaction allowed the pulldown of 8 kinase targets, while unspecific photo-immobilization at different sites of the molecule allowed the binding of 9 kinase targets[41]. Strikingly, only three of the kinase targets were bound by either of the two immobilization approaches, showcasing the potential influence of drug derivatization on target affinity. Even if a proper attachment site of the enrichment handle is known, the synthesis of probes can still be quite laborious. Some molecules of interest, such as many natural products, would require enormous synthesis efforts. Luckily, photo-immobilization grants a solution to this issue for some of these molecules[41, 42]. Here, commercially available drugs or natural products are exposed to diazirine-functionalized beads, which crosslink unspecifically with the molecules upon UV irradiation. With this technology, drugs or natural products purified from plants or microorganisms can directly be immobilized without the need for laborious synthesis. Unfortunately, the approach does not work for every molecule of interest[41].

(iii) The approaches differ regarding their likelihood of directly identifying the physical targets of drugs. As discussed above, proteome perturbation experiments and protein stability profiling technologies usually lead to relative changes in many proteins and the actual target is not necessarily part of the regulated proteome. These methods, therefore, often produce a list of potential target candidates with a large fraction of false-positive hits, while potentially missing the real target. It is, therefore, unlikely to confidently pinpoint the target right away. Proteomic fingerprinting approaches can be more successful in defining the target but rely on the size of the reference data set of profiled drugs with well-defined MoA. Unseen MoAs via inhibition of novel targets or pathways are impossible to uncover with this approach. In contrast, reactive amino acid profiling allows to probe thousands of potential target residues of reactive covalent drugs and has, therefore, a good chance to detect the targets. Similarly, approaches such as ABPP, PAL,

and AfBPP, which directly assess the physical drug-target interaction, most likely lead to a small number of high-confidence target proteins. Even though interactors of targets can be co-pulled down and confused with the actual target, the pulldown of known target complex partners can increase the confidence in target ID and add a certain layer of useful information (see for instance ref.[43, 44], and publication 1[15]) instead of leading down the wrong path.

(iv) While some approaches are more likely to identify the direct protein target, others such as in-cell TPP and proteome perturbation experiments can provide additional insights into modes of action that are not necessarily linked to protein binding. Drugs that for instance target DNA, RNA, or membranes, and drugs that chelate metal ions, or induce oxidative stress can leave a corresponding fingerprint in the proteome, represented by regulation of well-established protein sets. For instance, an in-cell TPP study on the anti-metabolite drug fluorouracil uncovered that it is killing cancer cells most likely via global and unspecific RNA-related toxicity mechanisms and not via the originally proposed inhibition of DNA synthesis[45].

In general, all of the methods have some blind spots. Preparing probes that carry an enrichment tag, photo-activatable group, or a linker to a solid phase (AfBPP), might modify the drug in a way that prevents its binding to some targets. This can be partly controlled by checking whether the probe still features similar cellular phenotypes (e.g. same cancer cell killing EC50). Moreover, approaches for drugs or probes that get covalently linked to their targets (such as cysteine profiling, ABPP, or PAL) usually employ protein-extraction workflows that disrupt every non-covalent drug-target interaction. Every protein target non-covalently bound by the drug would therefore be missed. Ideally, a combination of orthogonal proteomic target deconvolution assays is carried out in a range of tissue or cell proteomes with distinct expression patterns to allow the most comprehensive exploration of the potential target space.

1.2.6 Promiscuous affinity probes for the target deconvolution and selectivity profiling of large drug families

In hindsight, many of the non-covalent small molecule drugs entering clinical phases or receiving formal approval were discovered to bind off-targets. This off-target engagement often either explains side effects or actually contributes substantially to the drug's clinical efficacy (Table 1).

Table 1|Examples of clinically advanced or approved drugs, whose off-targets contribute to clinical effects in human patients.

Drug	Originally proposed target and MoA	Novel (off-) target identified	Effect of (off-) target	Method(s) used for identification of novel (off-) targets	Reference(s)
Metformin	AMPK activation by unknown MoA	AMPK activation as a downstream effect of Metformin binding to **PEN2**	Explains the mechanism of action of the antidiabetic effects of Metformin	Chemo-proteomics, based on PAL-affinity probe	Ma *et. al*[46].
Thalidomide	unknown	Binding to CRBN-Cul4A-DDB1 E3 ubiquitin Ligase, inducing degradation of several proteins, including transcription factors (**TFs**)	Degradation of TFs that are relevant in fetal development most probably led to malformations and deaths of hundreds of unborns (Contergan scandal). Degradation of other targets might explain its beneficial effects in treating Multiple Myeloma or leprosy	AfBPP	Ito, et al.[47]
OTS167	MELK	**CDK11**	Inhibition of mitotic progression via CDK11 inhibition explains anticancer activity	RNAi, mutational scanning	Lin et al.[48]
Ralimetinib	p38α	**EGFR**	EGFR inhibition explains its anticancer activity	Multimodular approach, genetics	Bhattacharjee et al.[49]
Imatinib, other KIs	Kinases	**NQO2**	Uncertain clinical consequences	AfBPP	Bantscheff, et al.[50], Klaeger et al.[51]
Tivantinib, KIs	MET (HGFR)	**Tubulin**	Cytotoxicity via modulation of microtubules dynamics, akin to Vincristine	Phenotyping, genetic approaches	Katayama et al.[52], Basilico et al.[53]
KIs	Kinases	**FECH**	Photosensitivity as a side effect of drug treatment	AfBPP, TPP	Klaeger, et al.[54], Savitski, et al.[28]
KIs	Kinases	Other Kinases	Additional kinase targets contributing to clinical effects	AfBPP	Klaeger et al.[51]
Panobinostat	HDACs	**PAH**	Side effect: reduction of thyroid hormone levels	AfBPP, TPP	Becher et al.[26]
Ricolinostat	HDAC6	**HDAC1-3**	HDAC1-3 inhibition explains the anti-cancerous effects of Ricolinostat	AfBPP, genetic	Lin et al.[48]
Domatinostat (4SC-202)	HDAC1-3	**Tubulin**	Cytostatic effects via modulation of microtubules dynamics	Phenotyping, cell painting	Akbrazadeh et al.[19], Xue et al.[55], Wobser et al.[56]

Chemoproteomic target deconvolution strategies and in particular AfBPP aided in unraveling many of such previously unreported targets. For instance, affinity-based competition assays using the immobilized HDACi Panobinostat as probe identified Phenylalanine Hydroxylase (PAH) as a novel Panobinostat off-target[26]. Interestingly, Panobinostat treatment leads to a reduction in thyroid hormone levels in patients. Since PAH is essential for tyrosine biosynthesis, and tyrosine is a building block of thyroid hormones, this finding provides a rationale for this observed adverse effect of Panobinostat[26]. Similarly, ferrochelatase (FECH) was identified as off-target of several kinase inhibitors using kinase inhibitor (Ki)-based affinity matrices (kinobeads) in chemoproteomic competition assays[51, 54]. Interestingly, Ki-mediated FECH inhibition leads to the accumulation of protoporphyrin and is associated with undesired photosensitivity, which strongly affects patients' quality of life[51, 54, 57].

To identify off-targets and predict off-target-related adverse effects early on in drug discovery, it would be desirable to perform target deconvolution for every new drug candidate. However, this would require the synthesis and evaluation of various immobilizable chemical probe candidates. Considering the resources, capacity, or skill sets required for such extensive target deconvolution campaigns, this is often not feasible for drug-developing institutions.

How can we work around that bottleneck of synthetic effort? Ideally, a universal affinity probe is invented which allows to probe the binding of tens to hundreds of drugs to a large target space. Such a promiscuous affinity probe (or affinity matrix) must bind to and pulldown a large panel of related target proteins. This tool can then be used in chemoproteomic competition assays (see Fig. 9) to determine the binding of many drugs to the pulled-down subproteome.

Conceptually, many drug targets and related proteins (potential off-targets) bind to molecules from an overlapping chemical space. For instance, all kinases need to accommodate ATP in their active site. The ATP binding pockets of kinases are therefore well conserved and share three-dimensional physicochemical properties that predispose them to bind common ATP-mimicking pharmacophores of kinase inhibitors. While this situation complicates the development of selective drugs, it presents a chance to develop a promiscuous affinity probe that binds to a large fraction of the (off-) target family.

As design principles for such promiscuous affinity tools, analogs of the natural substrates can be employed, as seen for the ATP-based probes used in the Kinativ assay to profile kinase inhibitors[58, 59]. However, these natural substrates and their analogs often feature low target affinity hampering their suitability as affinity probes. Alternatively, highly potent but non-selective drugs can be used that cover a broad range of the target family. A systematic combination of such tool compounds extends the number of target proteins covered by the affinity matrix. For kinases, a selection of unselective but highly affine kinase inhibitor pharmacophores immobilized to sepharose spheres was iteratively refined to establish the kinobeads technology[50, 60]. Kinobeads have been used to profile hundreds of kinase inhibitors in the same experimental setup, covering a large space of the potential target spectrum (~300 of ~500 kinases)[51, 54]. Of note, kinobeads also allow to probe binding to common kinase inhibitor off-targets such as FECH and NQO2[51, 54]. Once the kinobeads technology was established, chemoproteomics target deconvolution and selectivity profiling was made accessible for all developed kinase inhibitors, without the need of designing hundreds of affinity probes for each new inhibitor type.

Establishing such a chemoproteomic toolset is most worthwhile for big drug families that target a broad range of related targets. Importantly, the target family needs to feature active site similarities that allow the design of promiscuous probes. Theoretically, this is most easily achieved for protein families that share a common substrate or co-factor space such as Kinases (ATP binding pocket), HDACs (acylated lysine binding pocket), Bromodomain proteins (acetyl-lysine binding pocket)[61, 62], or Fe^{2+}- and alpha-ketoglutarate dependent lysine demethylases (KDMs)[63].

Overall, affinity-based profiling utilizing a promiscuous affinity matrix as a generic tool offers a compromise: On the one hand, it only allows to identify targets from the pool of proteins that are bound by the promiscuous affinity matrix. The more the pharmacophores of the affinity matrix and drug of interest differ, the more likely it is to miss out on drug-specific off-targets. On the other hand, it allows to circumvent the laborious synthesis of affinity probes for every new drug, and, therefore, helps to overcome the activation barrier of performing chemoproteomic target deconvolution.

2 Zn^{2+}-dependent histone deacetylases as drug targets

Metalloenzymes are proteins that depend on one or several metal ions in the active site for full enzymatic function. The metal ions in the active site are either directly chelated by amino acid residues or by cofactor complexes such as heme. Often, the metal ion cofactors are not fully coordinated allowing interactions with substrates or reaction intermediates. About 40% of human enzymes are estimated to be metal-dependent[64].
Considering a large number of metalloenzymes and their various implications in diseases[65], unexpectedly, only a relatively small number of FDA-approved drugs (62 of 1562 = ~4%, as of Dec. 2017) inhibit metalloenzymes via direct binding to active site metal ions[64]. Of those 62 drugs, only 39 are aiming at a surprisingly small number of human single protein targets or target families[64] (Table 2).

Table 2|Human metalloenzymes that are targeted by clinically approved metal-chelating inhibitors. Data adapted from ref[64].

Target enzyme (gene)	clinical settings	Number of inhibitors (%)
Cytochrome P450 3A4 (CYP3A4)	CYP3A4i reduces the inactivation of anti-virals	1 (3%)
Tyrosinase (TYR)	Melanoma, dermatological conditions	1 (3%)
Phosphodiesterase 4 (PDE4)	Inflammation	1 (3%)
Angiotensin-converting enzyme (ACE)	Hypertension, blood circulation	10 (26%)
Histone deacetylases (HDAC1,2,3,6,8,10)	Oncological diseases	6 (15%)
Lipoxygenase (ALOX5)	Asthma	1 (3%)
Carbonic Anhydrase (CA)	Glaucoma	19 (49%)

Histone deacetylases (HDACs) are currently the largest family of metalloenzymes inhibited by approved drugs. The following sections give a short overview of the characteristics of the single HDAC family members and try to link their diverse biological functions to the mode of action (MoA) of HDAC inhibitors.

2.1 **The diversity of the HDAC family members**

The first histone deacetylase family member was discovered in 1996 by Taunton et al., who used the natural product Trapoxin A to pull down its human target protein and uncover it as histone deacetylase, HDAC1[66]. Since then, 11 Zn^{2+}-dependent deacetylases (histone deacetylases, HDAC1-11) and 7 NAD^{+}-dependent deacetylases (Sirtuins, SIRT1-7) have been discovered. According to sequence homology, HDACs are grouped into 4 classes, whose characteristics and functional diversity will be outlined below (Fig. 9)[67].

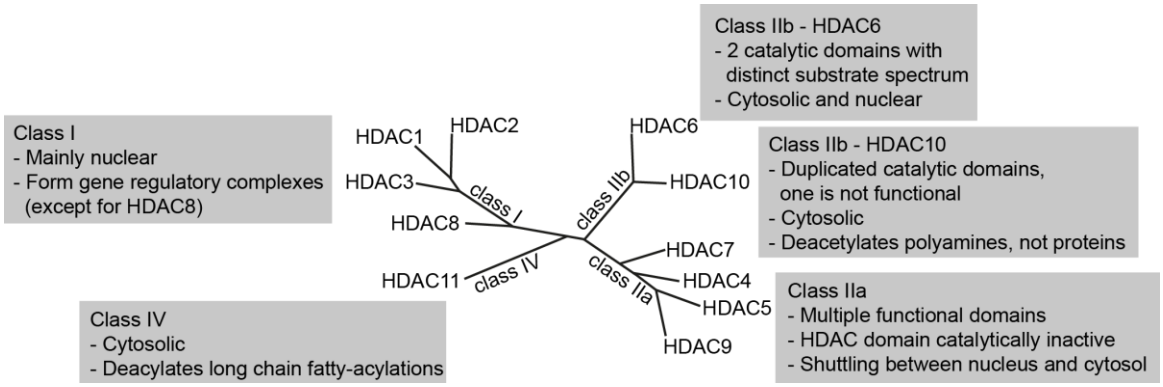

Fig. 9|The HDAC phylogenetic tree including information about the main differences between branches. The phylogenetic tree has been adapted from Arrowsmith et al.[68].

Class I histone deacetylases HDAC1, HDAC2, and HDAC3 are mainly located in the nucleus and act as eraser enzymes of the epigenetic acetylation mark on histone N-terminal tails, opposing the activity of histone acetyltransferases (HATs)[69]. In this role, HDACs are primarily known as global transcriptional suppressors (Fig. 10).

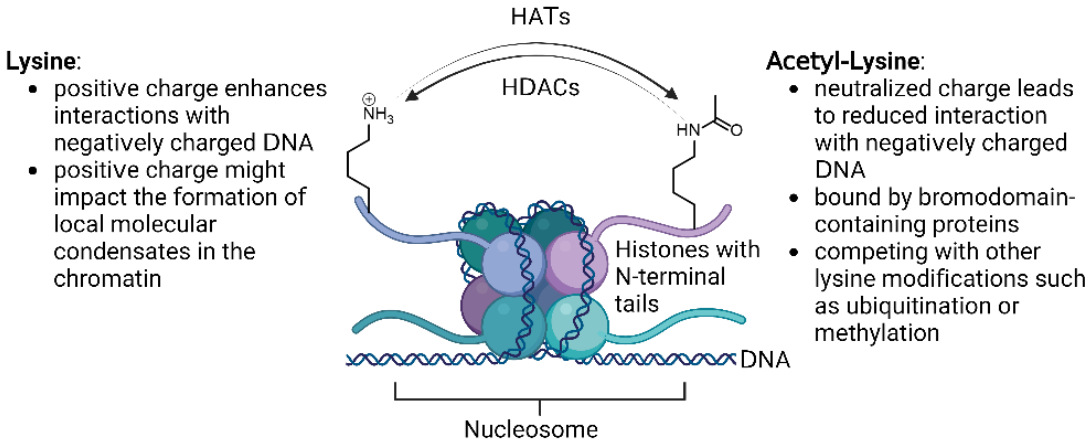

Fig. 10|HDACs and HATs regulate the acetylation status of histones and thereby modulate gene expression and chromatin properties. The figure was created with Biorender.

From a biophysical point of view, the lysines of the intrinsically disordered N-terminal histone tails provide positive charges for multivalent interactions between histones and the negatively charged DNA backbone[68]. Tight interactions between histones and DNA are dominant in highly condensed euchromatin, which is deprived of the transcription machinery[68]. By removing the neutralizing modifications from lysines and reinstalling the ionic interactions between histones and DNA, HDACs contribute to tight DNA packaging and therefore generally promote repression of gene transcription[68]. Additionally to the biophysical aspects, some histone acetylation marks directly act as transcription-promoting PTMs. For instance, H3K14ac contributes to promoter-nucleosome dissociation and H3K9ac is relevant for RNA Pol II pause release, a crucial transmission process between early elongation and transcription of the full mRNA[70]. Furthermore, acetylations on H3K9 and H3K27 are competing with transcriptional-repressive lysine methylation[71]. These pro-transcriptional roles of histone tail acetylations are counteracted by HDAC1-3, and, therefore, inhibition of HDACs has been traditionally considered as globally transcription-activating.
HDAC1-3 can be part of at least 5 chromatin modifying protein complexes. HDAC1 or HDAC2 is part of the CoREST[72], NuRD[73], Sin3[74], and the MiDAC[75] complex, while HDAC3 forms the catalytic

unit of the NCoR[76] complex. HDAC1-3 have a broad overlap in their substrate spectrum and deacetylate hundreds of acetyl-lysine sites not only located on histone N-terminal tails but also on other chromatin-associated proteins such as P53[77, 78]. HDAC1-3 have been shown to erase a broad range of acylation PTMs besides acetylation, such as crotonylation[79], iso-butyrylation[80], and lactylation[81].

HDAC8 is the exception amongst class I HDACs, as it is not known to be part of nuclear complexes and shows a distinct substrate spectrum: HDAC8 specifically deacetylates the cohesin complex subunit SMC3[82], and thereby affects chromatin 3D architecture via regulation of chromatin looping[83] (also see chapter 1.2.2). Moreover, HDAC8 has been shown to preferentially deacylate medium to long-chain fatty acid modifications of lysine residues[84].

Class IIb comprises HDAC6 and HDAC10, which contain duplicated deacetylase domains[69]. Both enzymes are mainly located in the cytosol[69], but HDAC6 also shuttles to the nucleus and has an overlapping substrate space with class I HDACs[85]. While different substrates could be specifically assigned to the two HDAC6 catalytic domains (e.g. CD2: alpha-Tubulin, HSP90, and Cortactin, CD1: preferentially C-terminal lysine acetylation)[86-88], HDAC10 substrates remained enigmatic until the recent finding that HDAC10 acts preferentially on acetylated polyamines instead of lysine side-chains[89]. It remains to be proven that HDAC10 deacetylates only these small metabolites and not additionally certain protein substrates.

Interestingly, there is no evidence for class IIa HDACs (HDAC4,5,7,9) to be catalytically active as protein deacetylases. Due to a replacement of the active site Tyr by a His (His976, His1006, His843, and His956 of HDACs 4, 5, 7, and 9, respectively) the Tyr phenol and the substrate's acetamide carbonyl oxygen interaction, which is essential for the catalytic mechanism, is lost[90, 91]. Only weak activity for the unnatural trifluoroacetylated peptides has been reported[91]. Since the mutation might still allow class IIa HDACs to bind acyl-lysine substrates, they are rather considered to act as readers of acetyl-lysines, akin to bromodomains[69, 92, 93]. Moreover, class IIa HDACs contain a 450-600 amino acid long N-terminal extension, which features several protein interaction motifs, and, therefore, implicates additional functions besides those carried out through the HDAC domain[69]. For instance, a MEF2 transcription factor binding domain contributes to gene silencing at MEF2-targeted promotors[94]. Moreover, a phospho-serine motif is responsible for their binding to 14-3-3 protein, which mediates shuttling from the nucleus to the cytosol[94]. In general, there is still a huge gap in understanding class IIa biology, which is probably caused by their multifunctionality and by the fact that no proper chemical genetic tools (i.e. isoform-specific drugs) exist to probe the single protein functions.

The most recently discovered class IV deacetylase, HDAC11, cleaves off long-chain lysine-acylations[80] and might play roles in regulating native immune reaction pathways[95].

Taken together, HDACs have a diverse set of substrates comprising hundreds of proteins, small metabolites, and a broad range of acylation modifications. Therefore, the historically grown name Histone Deacetylase, which originated from the first discovered main function, is outdated. Recent suggestions of renaming HDACs to Lysine Deacylases (KDACs) are still falling short of the diversity of HDAC functions since HDAC10 is not acting on lysine side chains and class IIa HDACs might not even be catalytically active. For these reasons, the traditional denomination of the gene name ("HDAC") will be maintained throughout this thesis.

2. 2 **The potential of HDACs as drug targets**

Even though we have only started to disentangle the versatile biological functions of HDACs and the regulatory networks they are embedded in, already four dedicated HDAC inhibitors have been approved by the U.S. FDA and 25 additional HDAC inhibiting compounds are currently in clinical trials (as of May 2023, based on *clue.io/repurposing-app*, manually curated by the author).
The first prototypic HDAC inhibitor Vorinostat (Suberoylanilide-hydroxamic acid, SAHA) (Fig. 11) has been approved in 2007 for cutaneous peripheral T-cell carcinoma (CTCL)[96]. Since then, Romidepsin has been approved for CTCL (2009) and peripheral T-cell lymphoma (PTCL) (2011), Belinostat for PTCL (2014), and Panobinostat for multiple myeloma (2015, recently withdrawn by the U.S. FDA, still approved by the EMA). Chidamide is approved by the Chinese FDA for PTCL and the Japanese FDA for adult T-cell leukemia-lymphoma[97]. Givinostat has orphan drug status in treating Duchenne Muscular atrophy in the European Union[98]. Furthermore, phenylbutyric acid and valproic acid are approved drugs that inhibit HDACs[43, 99]. Phenylbutyric acid is prescribed for urea cycle disorders, while Valproic acid is used for epilepsy, bipolar disorder, or migraine[99, 100]. However, the low affinity to HDACs and high dosing of these molecules questions whether HDAC inhibition is the only main mechanism responsible for beneficial effects. Interestingly, it is still not fully understood how HDAC inhibitors fight cancer and why they work particularly well in T-cell lymphoma but have not been proven efficacious in solid tumours so far. Indeed more than 170 additional clinical trials have been undertaken with Vorinostat and none led to formal approval in additional clinical settings (see clinicaltrials.gov).

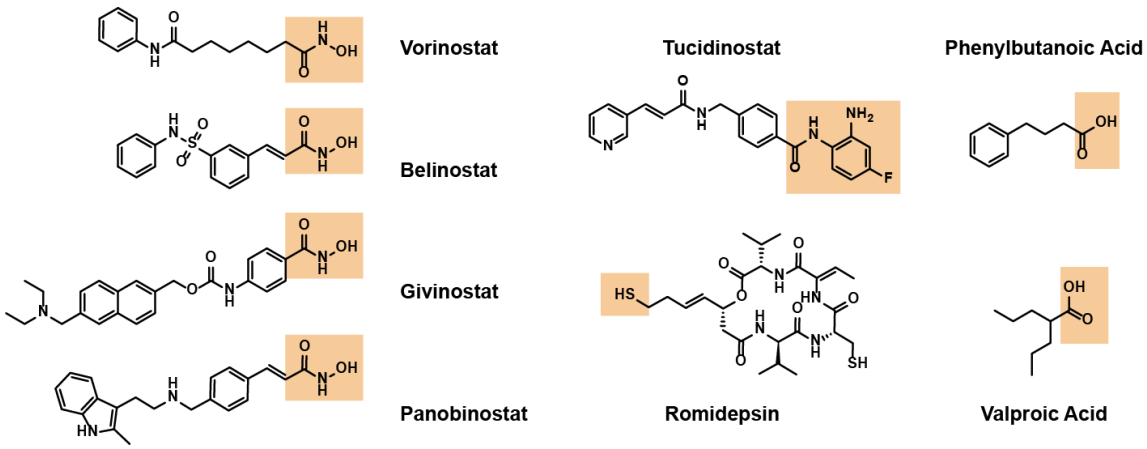

Fig. 11|Structures of clinically approved HDAC inhibitors. The Zinc-chelating warhead is highlighted with an orange box. Romidepsin is depicted in its active reduced form. The pro-drug Romidepsin is administered in its oxidized form, i.e. with a disulfide bridge between the two thiol groups.

In general, approved HDAC inhibitors inhibit at least all major epigenetic class I HDACs (HDAC1,2,3) and, therefore, interfere with global chromatin organization as well as gene transcription processes. Considering that HDACs might have up to hundreds of substrate proteins[101], whose activity, localization, and stability can be affected by deacetylation, the MoA of pan-HDACis is difficult to attribute to a main target or pathway. The pleiotropic effects of HDACis are considered to be generally cytotoxic or cytostatic[102]. While those effects might be of advantage when targeting cancer cells, they also contribute to unwanted side effects in healthy tissue and therefore limit the use of these drugs for less severe diseases outside of the oncology field.
Nevertheless, there are plenty of studies that suggest specific mechanisms of HDAC inhibitors that render cancer cells particularly sensitive. Moreover, selective inhibitors with reduced toxicity have been developed for treating neurological disorders. The following sections will review the current

state of knowledge about HDAC inhibitor-mediated effects and try to highlight the proposed main modes of action.

2.2.1 ***Effects of simultaneous inhibition of class I HDAC1, HDAC2, and HDAC3***

All HDACis approved or in clinical phases I-III target class I HDAC1, HDAC2, and HDAC3 with about the same relative affinity. Most of the clinical trials conducted on HDAC inhibitors are allocated to cancerous diseases (see clinicaltrials.gov). Although overexpression of HDACs in some cancers provides an anecdotal rationale for inhibiting these enzymes, elevated HDAC levels are not necessarily negative prognostic markers[103], and it is still unclear why HDAC inhibitors work particularly well in the treatment of CTCL[104, 105] while showing a lack of efficacy in the treatment of many solid tumours[97].
HDAC1-3 are central regulators of gene transcription and functional knockout of either HDAC3 alone, the pair of HDAC1/2, or all three class I enzymes is lethal to cells[106-109]. Due to this ubiquitous cellular dependency on HDACs, pan-HDAC inhibitors that simultaneously inhibit HDACs 1-3, have been suggested to be categorized as classic chemotherapeutics akin to DNA damaging or microtubule targeting agents, and not as targeted therapeutics[102]. However, similar to other unspecific drugs, therapeutic windows exist for HDACis[110]. This raises the question, of why (certain) cancer types are particularly sensitive to the inhibition of HDAC1-3. Several reasons have been suggested to contribute to the MoA and only the two that are currently considered most relevant will be discussed in the next paragraphs.

Preventing DNA damage repair. HDAC-mediated deacetylation of histone tails at DNA damage sites is essential for the initiation of DNA damage repair[111, 112]. Since cancer cells often feature hampered DNA repair mechanisms and cancer treatments such as DNA cross-linkers (e.g. cis-Platin) induce DNA damage, additional interference with DNA damage repair pathways by HDAC inhibition might preferentially stress cancer cells[111, 112].

Disturbing transcriptional programs. HDACs are preliminarily known for their role as global transcription suppressors (see chapter 1.2.1). With regard to cancer cell treatment, the uncontrolled HDACi-mediated transcriptional activation of otherwise repressed genes is suggested to disturb the cancer cell homeostasis, to waste important energy resources, or to reactivate the expression of tumor suppressors as well as immune system attracting factors[110, 113]. However, over recent years, the dogma that HDAC inhibition globally promotes the activation of gene transcription has been challenged. Select genes are actually transcriptionally silenced upon HDAC inhibitor treatment, including oncogenes such as c-fos, and c-jun[114, 115]. Several lines of evidence have shown that genes inactivated by HDACis are the ones that are regulated via super-enhancers. These comprise core regulatory transcription factors that define the transcription programs for cell identity and are hijacked by cancer cells[115-117]. According to this model, HDAC inhibitors interfere directly with the highly activated cancer-driving gene expression programs, which provides an attractive explanation for how HDAC inhibitors selectively disturb cancer cell programs. Interestingly, similar super-enhancer targeted mechanisms have been recently suggested to explain cis-platin activity and the unexpectedly large therapeutic window of this genotoxic drug[118].

Despite these progresses in understanding the effects of HDAC1-3 inhibition, we have yet only seen the tip of the iceberg. Considering that besides remodelling gene expression programs via histone acetylations, hundreds of additional HDAC substrates are affected downstream of HDAC inhibition, it remains difficult to tell whether a single main mechanism or whether the sum of certain downstream effects leads to the observed anti-cancer effects.

2.2.2 ***Targeting HDAC8 in cancer***

Although a few studies have identified HDAC8-specific substrates[101, 119, 120], most substrates lack independent validation by orthogonal experiments. Additionally, most potential substrate acylation sites lack functional annotation. This complicates the rational generation of a hypothesis of how HDAC8 inhibitors might be beneficial as therapeutics. Only one HDAC8-regulated process has been extensively studied. HDAC deacylates AcK105 and AcK106 on the cohesin subunit SMC3[82, 83, 121] to release cohesin from sister chromatids and reactivate chromatin looping. Opposing to HDAC8, the HAT ESCO1 acetylates cohesin and thereby pauses chromatin looping[83]. Chromatin looping defines the three-dimensional genome topology, which modulates gene expression, replication, or DNA repair[122]. Thus, unspecific HDAC inhibitors that target simultaneously HDAC1-3 and HDAC8 likely cause synergistic effects in generally disturbing chromatin organization and thus lead to cytotoxicity in cancer cells. According to the DepMap portal, knockdown or knockout of HDAC8 alone is not cytotoxic in cancer cell lines. While a study on a purportedly selective HDAC8 inhibitors reported cytotoxicity in some T-cell lymphomas or leukemias[123], it is not validated whether these effects are solely due to HDAC8 inhibition or due to off-target activity of the drug. Further work is required to fully understand the therapeutic potential of HDAC8is.

2.2.3 ***Inhibiting HDAC6 in neurological and neoplastic diseases***

HDAC6 has been highlighted as a promising target in a broad range of neurological disorders such as Charcot-Marie-Tooth disease (CMT)[124-127], Huntington disease (HD)[128], Rett Syndrome (RTT)[127, 129], or Amyotrophic Lateral Sclerosis (ALS)[130, 131].

While class I HDACs were also anecdotally reported to alleviate neurological disorder phenotypes in model systems[132], inhibition of class I HDACs in neurological disorders is problematic because of the expected toxic side effects. The advantage of selective HDAC6 inhibition is the expected lower toxicity, which might allow the use of HDAC6 inhibitors outside of the oncology field. Indeed, HDAC6$^{-/-}$ mice develop normally[133], and knockout of HDAC6 in human cell lines does not strongly reduce cell viability[48, 133, 134].

Similar to class I HDACs, HDAC6 has hundreds of substrates[101], and it is therefore very difficult to interpret which downstream events of HDAC6 inhibition alleviate disease phenotypes in model systems. However, two distinct HDAC6i modes of action in neurological disorders stand out and are the current focus of research.

Modulating microtubule dynamics. One of the best investigated HDAC6 substrate is α-tubulin[135, 136] and the HDAC6i-mediated hyperacetylation might explain some of the observed HDAC6i phenotypes. There is accumulating evidence that tubulin acetylation stabilizes microtubules (MTs) and stimulates dynamic interactions of the motor proteins kinesin and dynein with microtubules, which boosts cargo trafficking along MTs[137-139]. In some of the mentioned diseases, such as CMT or ALS, affected neurons feature deficits in the axonal transport of cargo along the microtubules[140, 141]. A characteristic of those disorders is the dying of peripheral neurons and motor neurons. The current model of disease development suggests disrupted axonal transport as a contributing factor: Reduced transport of proteins, RNA, energy-providing mitochondria, or vesicles loaded with brain-derived neurotrophic factor (BDNF) might lead to the die-back of neurons from the periphery of the axons[127, 140-142]. According to this model, particularly motor neurons are heavily affected since they can have a length of up to 1 m and therefore depend on fast axonal transport[140, 141] to bring cargo from the cell body to its periphery. Intriguingly, HDAC6 inhibitor-mediated hyperacetylation has been shown to improve axonal transport[143] and rescues neurons in models of ALS[130], CMT[124-126, 144, 145], RTT[129, 146], and Huntington's disease[147].

Modulating molecular condensates. Another role of HDAC6 inhibition in neurological disorders might be associated with its molecular condensate modulating activities[148, 149]. Molecular condensates are membrane-less 'organelles' that contain a defined and concentrated set of

proteins, RNAs, and other biomolecules, which preferentially interact amongst each other and phase separate from the surrounding environment[150]. Prominent examples of molecular condensates are stress granules (SGs), nucleoli, nuclear pores, and signaling clusters[151]. Clustering of molecules into condensates is driven by multivalent low-affinity interactions, for instance between the positive charge of lysine residues on intrinsically disordered protein domains and negative (partial) charges of the phosphates of RNA backbones or the π-systems of aromatic amino acid residues[152, 153]. These interactions are transient and highly dynamic, allowing molecules to quickly enter, diffuse within, and leave the molecular condensate[154]. Deregulation of these dynamics can lead to hardened condensates, which can mature to a solid-like irreversibly aggregated phase[151]. Akin to protein aggregation in other neurological disorders such as Lewis body dementia or Huntington's disease, these aggregates constitute a pathological hallmark of ALS and frontotemporal dementia (FTD)[151]. Indeed, genes causing aberrant condensate formation mutations (e.g. in the RNA-binding protein FUS) have been linked to ALS and the malfunction of condensates might therefore be causative[155-160]. Accordingly, these diseases have been termed condensatopathies[161]. To find cures for condensatopathies, researchers have started to search for molecules that modulate molecular condensates and, for instance, reverse or prevent the 'irreversible' aggregation[161-164]. In one such study, a large screen of 1,600 molecules identified the drug lipoic acid and its close amide analog, lipoamide, to inhibit stress granule formation[165]. The drugs also recovered cellular and organismal ALS-associated phenotypes in FUS-mutant models of neurons or drosophila melanogaster[165]. However, the molecular mechanism remained elusive. Interestingly, HDAC6 inhibitors have been shown to modulate molecular condensates related to the condensates involved in ALS[148, 149]. The HDAC6-mediated deacetylation of condensate proteins re-establishes positive charges relevant for phase separation in condensates[153]. Hyperacetylation as a result of HDAC inhibition might therefore exclude the proteins from the condensate and lead to the disassembly of condensates or impede condensate formation and maturation. Considering these recent discoveries, modulation of condensates might be one pillar of the HDAC6 MoA in neurological diseases.

Besides neurodegenerative diseases. HDAC6 also has been suggested as a target in cancer due to its roles in regulating cell motility[166, 167], in immunomodulatory tasks[168, 169], and in controlling protein homeostasis via autophagy[170] and aggresome formation[171, 172]. Considering these functions of HDAC6, the simultaneous inhibition with class I HDAC1-3 might have synergistic effects in cancer treatment. Indeed, two approved HDACis (Vorinostat, and Belinostat) are targeting HDAC1-3 and HDAC6 with relatively similar affinities[43]. Moreover, HDAC6 has a big substrate overlap with class I HDACs[101], like deacetylation of histones[85]. This might further boost the synergistic effects of targeting HDAC1-3 and HDAC6 at the same time.
Purportedly selective HDAC6 inhibitors such as Ricolinostat approached clinical phase II trials and showed activity against cancer[173]. However, there has been some controversy about the efficacy of HDAC6 selective inhibitors as single agents or for combinatorial treatment in cancer, since the observed effects of HDAC6 inhibitors might be related to a lack of selectivity and indeed result from inhibition of other HDACs or further off-targets. In the case of Ricolinostat, a study uncovered, that its anti-cancer activity does not originate from HDAC6 inhibition but from HDAC1-3 inhibition[48, 134]. This once more showcases the importance of rigorous and unbiased selectivity profiling of drugs. Confident identification of selective HDAC6 inhibitors would allow us to clear out many of the discrepancies in the literature regarding the biological functions of HDAC6 and its potential as a drug target.

2.2.4 Disturbing the polyamine homeostasis via HDAC10 inhibition

Upregulation of HDAC10 is a marker for poor treatment outcome in stage 4 neuroblastoma[174, 175]. Here, HDAC10 contributes to drug and metabolic stress resistance of the cancer cells by activating the autophagic flux, enhancing lysosomal exocytosis of drugs, and assisting in DNA damage repair[174-176].

How HDAC10 affects all these biological processes has remained elusive. However, the recent discovery that HDAC10 acts as polyamine deacetylase might explain its role in autophagy and others via polyamine-mediated processes[89, 177, 178]. The polyamines putrescine, spermidine, and spermine are small aliphatic polycationic alkylamines that can reach mM concentrations in eukaryotic cells[179]. Polyamines are indispensable for the survival and proliferation of eukaryotic cells[179, 180]. For instance, spermidine is the precursor molecule for the posttranslational hypusination of the eukaryotic initiation factor 5A (EIF5A), a modification that is necessary for the continual translation of certain amino acid combinations such as polyproline tracts[181]. Due to their ionic interactions with nucleic acids, polyamines are relevant for DNA structure and stability[182] and influence various RNA metabolic processes[179].

Polyamines can be synthesized de novo or taken up into cells via diverse routes. Biosynthesis relies on two rate-limiting steps that are catalyzed by Ornithine decarboxylase (ODC) and S-adenosylmethionine decarboxylase (AMD1), two genes that are curiously regulated by oncogenes such as MYC[183, 184]. Cellular uptake routes are not completely unraveled yet but have been shown to include direct uptake at the plasma membrane via a yet unidentified polyamine permease[185], uptake via the amino acid transporter SLC3A2[186], or uptake via endocytosis and import into the cytosol by ATP13A2 or ATP13A3[187-189].

Due to their involvement in various cellular processes, cells depend on polyamines to survive and proliferate. Particularly cancer cells require elevated polyamine levels for proliferation[190]. Indeed, polyamine-depleting therapies have shown promising effects[190]. In polyamine blocking therapies, the strategy goes beyond inhibition of de novo biosynthesis and extends to the additional blockage of polyamine uptake, for instance via inhibition of SLC3A2[190, 191]. However, as outlined above, several routes of polyamine uptake exist. The acetylated forms of polyamines might enter the cells by distinct mechanisms and provide a yet neglected source that allows cancer cells to circumvent current polyamine blockage strategies. Importantly, this source of polyamines relies on intracellular polyamine deacetylation by HDAC10 and hence could be interfered with HDAC10 inhibitors.

Unfortunately, only a few studies have yet attempted to develop HDAC10 selective inhibitors, but have not been independently confirmed and are not commercially available to the research community[178, 192]. Therefore, a chemical probe that selectively inhibits HDAC10 catalytic function is highly needed to further explore HDAC10 biological functions, clarify the HDAC10 substrate spectrum and check HDAC10's potential as a target for polyamine blocking therapy in cancerous diseases.

2.2.5 Class IIa HDACi as potential therapeutics?

There is evidence, that class IIa HDAC5 and HDAC7 are promising targets in neuroblastoma and other cancer types[193-197]. HDAC4 is claimed to be a viable target in the neurological disorders Parkinson's Disease and Huntington's Disease[198-201].
However, the biological functions of class IIa HDACs have not been well understood and therefore, the mechanisms of how and why pharmacological knock-down of class IIa functions are of advantage in those diseases remains elusive. The lack of selective inhibitors is certainly one of the reasons for the backlog in class IIa HDAC research. Additionally, many of the tool compounds that are reported in the literature and or are commercially available have not been independently confirmed to actually bind class IIa HDACs. Therefore, the use of inappropriate chemical probes might have contributed to a blurred and confounded picture of class IIa HDAC function and pharmacological relevance. Only selective and properly validated chemical probes will help to re-evaluate reported findings and declutter the controversial reports in the literature.

2.2.6 Class IV HDAC11i

HDAC11 is the most recently discovered HDAC and the least well-studied. Interestingly, HDAC11 preferentially cleaves long chain acylations from lysine side chains[80, 202], akin to HDAC8. As such, HDAC11 deacylates SHMT2, which prevents SHMT2-mediated recruitment of a deubiquitinase to the Interferon alpha receptor 1 (IFNαR1)[95]. The resulting increase in IFNαR1 ubiquitination down-regulates IFNα signaling. In turn, HDAC11 inhibition could potentiate IFN signaling in vivo, which might be a desired outcome in viral infections[203] or cancer treatment[204]. Unfortunately, most of the available HDAC inhibitors are inactive against HDAC11 and for the few reported specific HDAC11 inhibitors FT895 and SIS17[205, 206], no tools exist to confidently determine the selectivity over other HDACs. Moreover, SIS17 increased in cellulo SHMT2 acylation levels only with EC50s above 20 µM, while FT895 did not have any in cellulo activity. This underscores the need for more potent and selective inhibitors to better study the potential of HDAC11 inhibition.

2.2.7 Target cell non-autonomous effects of HDAC inhibitors

While most of the above-mentioned concepts tried to understand the HDACi MoA on a cell biology level of malfunctioning cells, systems' biological effects might be equally relevant. For instance, the targeting of immune cell populations might have an additional effect on the treatment outcome in cancer and neurodegenerative diseases. Entinostat for instance has been shown to prevent the homing of immune-suppressing myeloid-derived stem cells (MDSCs) in the tumor microenvironment and therefore de-represses the immune answer to cancer tissue[207]. The versatile effects of HDAC inhibitors on the immune system have been extensively discussed in several reviews (ref. [208, 209]).

2.3 Studying the selectivity of HDAC inhibitors

2.3.1 General design principles of HDAC inhibitor

HDAC inhibitors commonly consist of three parts: A Zn^{2+}-chelating warhead, a 'capping group', which binds to the outer rim of the active site, and a linker between those groups, which fills the active site channel akin to the alkyl-side chain of the acetyl-lysine substrate (Fig. 12). The most common Zn^{2+}-chelating group is a hydroxamic acid or an aminoanilide. Additionally, thiols can act as potent zinc chelators, as featured in the approved drug and natural product drug Romidepsin (see Fig. 11). Further, di- or tri-fluoromethyloxadiazole have been suggested as an alternative Zn^{2+}-chelating group for class IIa HDACs[210] and HDAC6[211]. Two approved drugs that target HDACs, valproic acid, and phenylbutyric acid, contain carboxylic acids as zinc chelating warhead. The interaction between carboxylic acid and zinc, is monodental and those drugs only bind with a very low affinity in the range of several hundred µM as determined by chemoproteomic binding assays[43]. The different forms of warheads feature distinct pharmacodynamics and pharmacokinetics. For instance, hydroxamates can be metabolized via glucuronidation, hydrolysis to carboxylic acids, or reduction to the amide[212-214]. The intramolecular di-sulfide in Romidepsin first needs to be reduced in the cell to expose the Zn^{2+}-chelating thiol. Interestingly, Romidepsin and aminoanilide drugs also feature extremely slow k_{on} rates and only reach binding equilibrium after hours of incubation time[44, 215]. Moreover, chemoproteomic studies revealed that aminoanilide drugs have reduced binding affinity to HDACs, as soon as those enzymes are embedded into certain gene regulatory protein complexes[43].

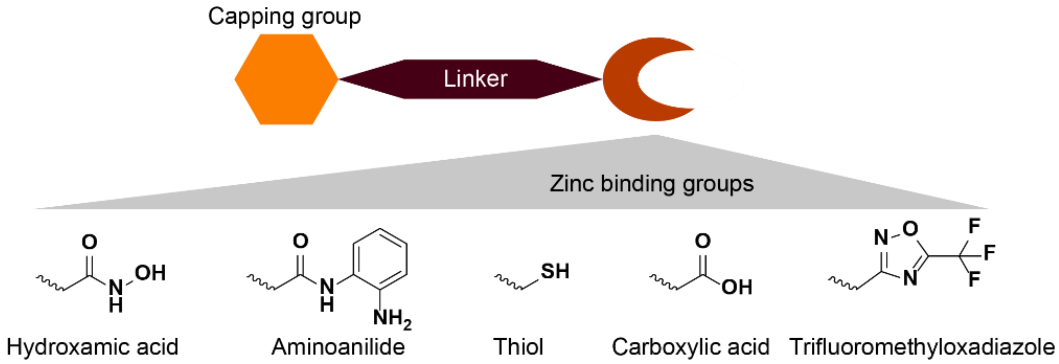

Fig. 12|General design principle of HDAC inhibitors and structures of zinc-chelating groups.

The first generations of HDAC inhibitors, including all the approved and late-stage clinical phase drugs, are not selective and inhibit class I HDACs 1-3 plus additional HDACs. Purportedly selective HDAC6 and HDAC8 inhibitors have been reported. Selectivity for class I HDACs 1-3 over all other HDACs was achieved by the discovery of the aminoanilide warhead. The aminoanilide is bulkier than the hydroxamic acid and only fits into the active sites of HDAC1-3[216]. Certain modifications of the aminoanilide head group have been suggested to gain selectivity for HDAC1-2 over HDAC3 (e.g. in BRD6929 or Cpd-60, ref. [217, 218]).

2.3.2 Approaches to determine HDAC inhibitor selectivity

The understanding of the MoA of HDACi suffers tremendously from the complicating fact that all clinical drugs inhibit several HDACs at once and therefore expand the number of pleiotropic downstream effects in HDACi-treated cells or patients. To better understand HDAC biology, selective probes are highly demanded. Moreover, selective inhibitors for class II HDACs are

proposed to have reduced toxic side effects, which are mostly mediated by class I HDAC inhibition. Thus, information on inhibitor selectivity is of high importance for current drug discovery pipelines.

A classic approach to characterize drugs regarding their potency and selectivity is to derive the inhibitory constant from enzyme activity assays. Until today, such assays are the default test setup in many medicinal chemistry studies designing novel HDAC inhibitor candidates (see for instance Ptacek et al.[211]). The first broad selectivity profiling study of HDACis was based on enzyme activity assays (Bradner et al.[93]). Unfortunately, the results obtained by enzyme activity assays are often inconsistent in the literature, probably due to different assay conditions, varying quality, and purity of recombinant HDACs. Another reason might be the inconsistent use of non-endogenous substrates such as trifluoroacetylated peptides for class IIa HDACs and peptidic substrates for HDAC10 (see Table 3 for comparison of literature IC50 values for Vorinostat)[89, 91, 93]. Further, the IC50 determined in enzyme activity assays depends on the concentration and K_m of the substrate employed. This is because of the competition between substrate and inhibitor for the same pocket of the enzyme. The substrate concentration can vary between studies, and the K_m varies between HDACs. Another drawback of enzyme activity assays is the fact that recombinant HDACs lack the natural interaction partners[43], allosteric factors such as inositol-phosphates[219], and PTMs[220, 221], which all affect their activity and potentially drug binding affinity. Indeed, recombinantly expressed HDAC3 is often used in complex with its interaction partner NCOR2 to boost its activity in assays[222].

Table 3|Overview of Vorinostat IC50 value variance, as determined by recombinant HDAC enzyme activity, assays in various publications. The IC50 values derived for HDAC inhibition by Vorinostat were normalized to the IC50 value of HDAC3 binding (ND: not determined). Color coding indicates whether the affinity for the corresponding HDAC was higher (blue) or lower (red) than compared to HDAC3. For instance, affinity values for HDAC8 range from similar affinity (~82% in Arts et al.) to 340-fold lower affinity in Schroeder et al.[218]. Further, Vorinostat class IIa affinity is sometimes estimated to be even higher than HDAC3 affinity, while several hundred-fold lower affinity values are observed for class IIa in most other studies. The data are based on published results from Bradner et al.[93], Arts et al.[223], Lauffer et al.[224], Schroeder et al.[218], Negmeldin et al.[225], and Burli et al.[226].

Class	HDAC	Bradner et al.	Arts et al.	Lauffer et al.	Schroeder et al.	Negmeldin et al.	Burli et al.
I	1	0.26	0.24	3.26	1.33	1.65	ND
I	2	0.32	0.94	13.49	3.67	4.80	ND
I	3	1.00	1.00	1.00	1.00	1.00	1.00
I	8	96.00	0.82	44.46	340.00	27.00	2.56
IIb	6	0.32	0.08	0.51	0.67	1.65	0.12
IIb	10	ND	0.59	1.56	ND	ND	ND
IIa	4	ND	0.60	>530	>10000	ND	164.00
IIa	5	720.00	0.39	>530	6000.00	ND	18.40
IIa	7	ND	9.68	>530	>10000	ND	164.00
IIa	9	ND	0.71	>530	>10000	ND	196.00

In contrast to in vitro activity assays with recombinant enzymes, HDAC nano-BRET assays have been developed, which measure drug binding affinity in cells[215]. In a nano-BRET assay, the target enzymes of interest are fused to a luciferase enzyme, which emits light of a certain wave length[227] (Fig. 13). Incubating these cells with a fluorophore-coupled reporter probe, which binds to the enzymes' active site, allows to read out the probe binding event, since the reporter probe only emits quantifiable signals via bioluminescence resonance energy transfer (BRET), when in close proximity to the luciferase[227]. In this setup, one can incubate the cells with drugs of interest that compete with the reporter binding and therefore reduce the BRET signal in case of target enzyme binding. A big advantage of this assay is that it allows measurement of intracellular binding and therefore integrates the local intracellular environment, membrane permeability, and

intracellular binding kinetics[215]. Moreover, the nanoBRET assay works independently of the use of HDAC substrates and therefore is equally well suited for probing class IIa or HDAC10 inhibitors. On the downside, the obtained binding affinities can not be generalized, since they depend on the cell line of choice and intracellular concentrations can be affected by cell-specific expression of drug importers/exporters or (pro-) drug-metabolizing enzymes. Moreover, extensive protein engineering is necessary to establish the luciferase fusion constructs. Additionally, the fusion construct does not necessarily behave like the native target enzyme since the attached luciferase might interfere with protein localization or interaction with complex partners, which have been shown to impact drug binding affinity[43].

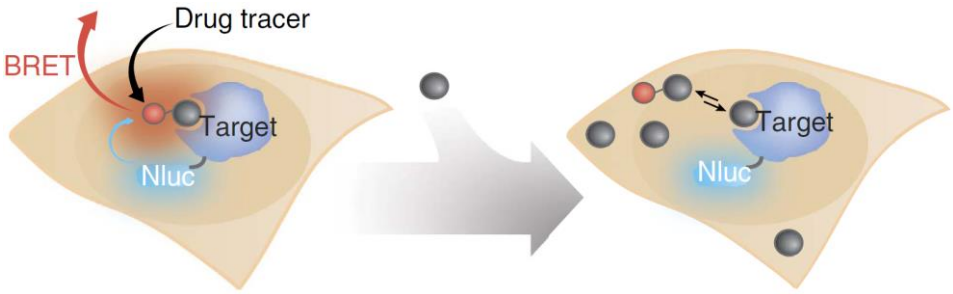

Fig. 13|Schematic representation of a nanoBRET assay for measuring in cellulo target engagement. A fluorescent tracer binds to the active site of the target of interest fused to a luciferase enzyme. Light produced by the luciferase is absorbed by the fluorescent tracer and emitted (Bioluminescence resonance energy transfer, BRET). If the cells are exposed to drugs that bind the target, the tracer is replaced and the BRET signal is lost. Figure adapted with permission from ref.[215].

Another indirect approach to determine in-cell HDAC target engagement is based on the readout of HDAC substrate acetylation sites after treatments spanning a large dose range (dose-dependent PTM readout, ddPTM). HDAC inhibition leads to a dose-dependent increase of substrate acetylation sites (Fig. 14). At full HDAC inhibition, this increase reaches a plateau. The readout for HDAC-specific substrate sites can either happen via western blotting or LC-MS/MS-based acetylomics. Plotting of the substrate intensities relative to the vehicle control treatment allows us to derive EC50 values. HDAC-specific substrate acetylation sites are acetylated TUBAA[87] or CTTN[166] for HDAC6, acetylated SMC3[82] for HDAC8, and histone acetylation sites for HDAC1-3. This method is extremely powerful, since it measures the drug effect on natural substrates and endogenously expressed proteins directly in cells.

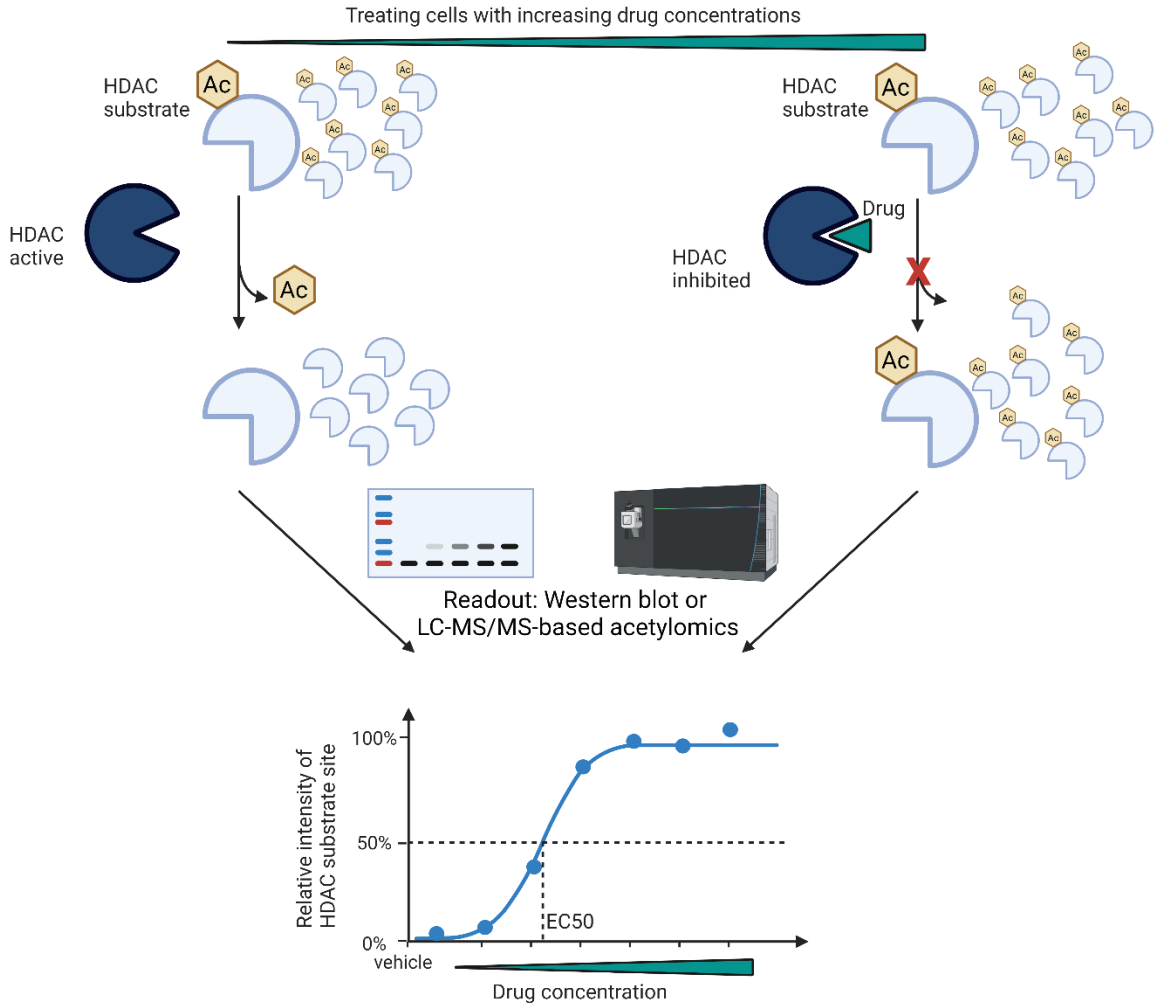

Fig. 14|Inferring in cellulo HDAC inhibition by measuring the accumulation of HDAC substrates. Cells treated with different concentrations of HDAC inhibitors show dose-dependent accumulation of HDAC substrate acetyl sites. These substrate sites can be either read out by antibodies in a western blot format or by LC-MS/MS-based acetylomics after pull down of acetyl-peptides with unspecific acetyl lysine antibodies. The dose-dependent acetylomics approach has been recently established in ref.[228] (see co-authorship 3). The figure was created with Biorender.

Unfortunately, these methods cannot be used to infer intracellular HDAC affinity for the whole phylogenetic tree, since:

(i) Class IIa HDACs are catalytically inactive, and inhibition, therefore, does not increase acetyl-site signal[91].
(ii) HDAC10 does not deacetylate protein substrates detectable via western blot or proteomics[89].
(iii) HDAC8 and HDAC11 might rather deacylate long-chain fatty acylations, which cannot be quantified via acetylomics[80, 84, 202].
(iv) HDACs 1-3 and HDAC6 have a large substrate overlap[101]. Further, there are no HDAC1, HDAC2, or HDAC3-specific substrates known. The lack of HDAC-specific substrates, which can be leveraged as HDAC-inhibition marker sites, therefore impedes differentiation between HDACs 1-3, and potentially even between HDACs 1-3 and HDAC6.
(v) Even EC50s derived from dose-dependent PTM sites of HDAC-specific substrates (e.g. histones for HDAC1-3) in one experiment can deviate from each other with a factor of 10 or even higher[228].

Despite their power in the deconvolution of drug MoAs, ddPTM approaches are therefore not the best option for HDACi selectivity profiling.

Alternatively, chemoproteomic binding assays have been employed to probe drug binding affinity to endogenous proteins in an environment close to intracellular conditions. Bantscheff *et al.* used immobilized HDAC inhibitors Vorinostat and Givinostat as an affinity matrix for the selectivity profiling of 16 HDAC inhibitors against 6 of 11 Zn^{2+}-dependent HDACs from classes I and IIb[43]. This study revealed that inhibitor binding affinity depends on the presence of target-interaction partners and also revealed a set of potential HDACi off-targets. Even though Bantscheff et al. provided a valuable resource of HDACi target interactions, their Vorinostat-based affinity matrix only covers about half of the phylogenetic tree of the HDAC family and therefore only provides incomplete selectivity data. Similarly, the two other HDAC inhibitor selectivity resources based on the nanoBRET technology or recombinant enzyme activity assays only covered an incomplete set of the HDAC target family (Fig. 15). Particularly assays for class IIa HDAC affinity probing are insufficiently developed. Overall, no selectivity profiling methods have been published that cover the whole phylogenetic tree of the HDAC family and comprehensive analysis of the selectivity landscape of HDACis is therefore still pending.

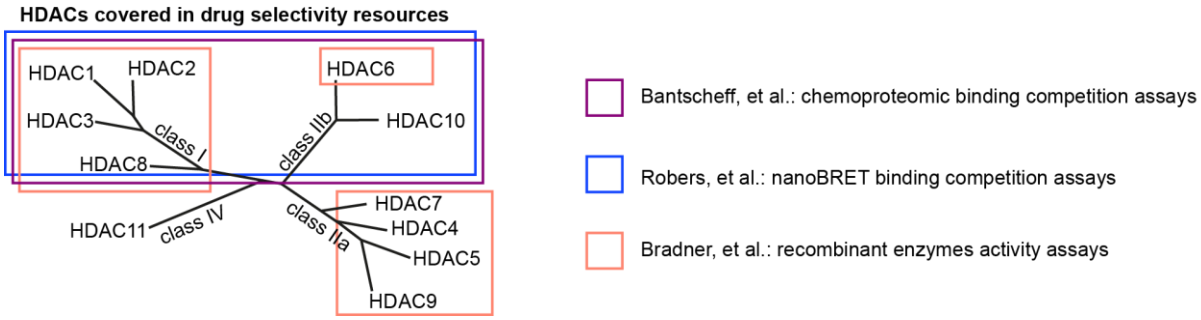

Figure 15|Coverage of the HDAC phylogenetic tree in resource papers about HDACi selectivity. None of the technologies could assess the HDAC11 affinity of drugs. Further, technologies used were either not suitable to probe either class IIa binding or to probe class IIb HDAC10 binding. Phylogenetic tree adapted according to Arrowsmith, et al.[68]. Resource papers: Bantscheff et al.[43], Robers et al.[215], Bradner et al.[93].

3 Objective and outline

Selective chemical probes are highly demanded to progress the understanding of the cell-biological functions of HDACs. Furthermore, selective class II HDAC inhibitors are proposed as promising therapeutics with reduced side-effects. Therefore, the interest in developing selective HDAC inhibitors is growing. A requirement for creating and refining the selectivity of inhibitors is to measure their target affinity. However, existing methods such as enzyme activity assays, nanoBRET assays, and chemoproteomic AfBPP (see chapter 1.1.2) have not been able to deliver comparable drug affinity and selectivity data for all HDAC family members[43, 93, 210, 215] and are often unable to identify off-targets (enzyme activity assays and nanoBRET assays)[93, 215]. Moreover, published resources of HDACi selectivity are only covering a small subset of the commercially available and clinically tested drugs.
Therefore, the primary goals of this thesis were:

(i) To develop and optimize a chemoproteomic AfBPP technology based on a promiscuous affinity matrix, which allows to pull down an extended set of HDACs (at least HDACs from classes I, IIa, and IIb; ideally all HDACs), as well as HDACi off-targets.
(ii) To employ this technology for the selectivity profiling of all commercially available HDAC inhibitors as well as chemically related compounds featuring metal-chelating warheads.

This comprehensive overview of the HDAC inhibitor target landscape informs about off-targets and unexpected selectivities that explain confounding results in literature or clinical side effects.

Accordingly, this thesis presents one study covering the development of the chemoproteomic technology and its application for selectivity profiling and drug target deconvolution of more than 50 small molecule metal chelating drugs (**Publication 1**: *Target deconvolution of HDAC pharmacopoeia reveals MBLAC2 as common off-target*[15]).
Moreover, two other papers showcase the utility of the chemoproteomic technology developed in this fundamental paper. First, the technology supported the target identification of the approved drug lipoic acid (**Publication 2**: *Chemoproteomic target deconvolution reveals Histone Deacetylases as targets of (R)-lipoic acid*). Lipoic acid was not assigned to any protein targets until now, and our results indicate that HDAC inhibition is a central part of lipoic acid's mode of action. Second, the chemoproteomic profiling technology was employed to confirm the selectivity of a first-in-class highly selective and drug-like HDAC10 inhibitor (**co-authorship 1**: *Aza-SAHA Derivatives Are Selective Histone Deacetylase 10 Chemical Probes That Inhibit Polyamine Deacetylation and Phenocopy HDAC10 Knockout*[222]).
Two additional publications complement the thesis' general focus on drug target deconvolution. One study showcases another successful example of a tailored drug-affinity probe for drug target deconvolution. The experiments uncovered NME4 and GCDH as off-targets of SIRT5-directed inhibitors (**co-authorship 2**: *Development of hetero-triaryls as a new chemotype for subtype-selective and potent Sirt5 inhibition*[229]). Another publication highlights the power of dose and time-dependent protein PTM profiling for the investigation of drug mechanism of action. This study shines light on cellular HDACi effects by analysing thousands of dose-dependent acetyl- and phosphosite regulations upon drug perturbation (**co-authorship 3**: *Decrypting drug actions and protein modifications by dose- and time-resolved proteomics*[228]).

General Methods

The papers featured in this thesis contain an extensive and detailed materials and methods section and can be found attached to the publication or in the supporting files of the publications on the journals website. This methods section therefore only covers a general summary of the main methods.

Cell culture and cell lysate preparation

Cell lines were grown in antibiotics-free growth media supplemented with 10% fetal bovine serum and tested for Mycoplasma contamination. Cells were lysed in a buffer containing a mild detergent (0.8% Igepal), a reducing agent (1 mM dithiothreitol (DTT)), and protease as well as phosphatase inhibitors. Lysates were cleared from insoluble cell debris in an ultracentrifuge and protein concentration was measured by the Bradford assay.

Gene knockdown experiments

Knockdown was performed with a pool of 20 siRNAs (siTOOLs Biotech) directed at different sites of target mRNA. The pooling of siRNAs allows the reduction of single siRNA concentration and therefore dilutes potential off-target effects. The siRNAs were transfected according to the Lipofectamine RNAiMAX protocol.

Generation of affinity matrices

The basis for the solid phase synthesis of affinity matrices were NHS-activated sepharose beads. Amino-group containing compounds were directly immobilized via amidation reaction. For carboxyl-group or alkyne-group containing probes, the sepharose matrix was first functionalized with the reactive counterpart (an amine or azide, respectively) before adding the probe and reaction catalyst. Some probes required multiple steps of on-bead synthesis followed by washing and deprotection steps. Coupling efficiency was tested by Kaiser test or LC-MS. All affinity probes were immobilized to reach a concentration of 1 µmol/mL sepharose beads.

(Competition) pulldown assay

For selectivity profiling, 0.5 mL of cell lysate (5 mg/mL protein concentration) was first incubated with increasing doses of drug and then added to 18 µL of affinity matrix for the pulldown. After washing off unspecific binders, proteins bound to beads were denatured with urea, reduced with DTT, alkylated with chloroacetamide, and then digested with trypsin. Resulting peptides were desalted on a C18 filter plate, vacuum-dried, and stored at -20 °C until LC-MS/MS analysis. In plain pulldown assays, the drug pre-incubation step was skipped.

LC-MS/MS proteome analysis

Peptides were analyzed via a Dionex UltiMate 3000 nano high-performance liquid chromatography system coupled to an Orbitrap HF or an Orbitrap Fusion Lumos mass spectrometer. Peptides were first separated on a C18 resin-loaded column using a 50 min gradient of 4-32% solvent B (0.1 % formic acid, 5 % DMSO in acetonitrile) in solvent A (0.1 % formic acid, 5 % DMSO in HPLC grade water) at a flow rate of 300 nL/min. The mass spectrometers were operated in data-dependent acquisition mode, automatically switching between MS1 and MS2 spectrum acquisition.

(Competition) pulldown assay protein identification and quantification

Protein identification and quantification were performed by the MaxQuant[230] software (with built-in Andromeda search engine), matching the LC-MS/MS spectra against a library of spectra

generated by in silico digestion of protein sequences derived from a human protein reference database. Carbamidomethylated cysteine was set as a fixed modification and oxidation as well as N-terminal acetylation were selected as variable modifications. All data were adjusted to 1% PSM and 1% protein FDR. Label-free quantification with matching between runs[230] was enabled.

(Competition) pulldown assay data analysis

Residual affinity matrix binding of drug-treated lysates was calculated relative to DMSO (vehicle) treated lysates. Plotting the relative residual binding against the drug concentrations and fitting a log-logistic regression function allowed deriving sigmoidal dose-response curves for EC50 (and pK_d^{app}) value calculation. Potential targets of inhibitors were called based on the hill-slope, curve fit (R^2), and effect size of dose-response curves. The target candidates were further filtered for only robustly quantified proteins with a sufficient number of uniquely identified peptides.

Deep proteome sample preparation after* *MBLAC2* *knockdown

Cells were lysed with 4% SDS in ddH_2O. The DNA was hydrolyzed by heating the lysate to 95 °C, adding trifluoroacetic acid (TFA), and neutralizing with N-methylmorpholine thereafter. Protein concentration was determined with a BCA assay, and proteins were cleaned up according to the SP3 protocol. Clean proteins were resuspended in HEPES buffer, reduced with DTT, alkylated with chloroacetamide, and digested by Trypsin. Before TMT10plex labeling, samples were desalted with C18 material according to the stage tips protocol. TMT-labelled peptides were fractionated via high-pH reversed-phase HPLC on a Dionex Ultra 3000 HPLC system with a Waters XBridge BEH130 column under constant 2.5 mM ammonium bicarbonate flow. During the 57 min gradient of 7-45% acetonitrile, 96 fractions were collected and then pooled to 48 fractions (fraction 1 + 49, fraction 2 + 50, and so on). Fractions were vacuum-dried and stored at -20 °C until LC-MS/MS analysis.

Deep proteome LC-MS^3 and data analysis

Peptide fractions were analyzed via an LC–MS/MS on a Dionex UltiMate 3000 RSLCnano System equipped with a Vanquish pump module coupled to an Orbitrap Fusion Lumos (Thermo Fisher Scientific) mass spectrometer. Peptides were separated on a Acclaim PepMap 100 C18 column by running a 25 min linear gradient of 4% to 32% solvent B (0.1% formic acid, 3% DMSO in acetonitrile) in solvent A (0.1% formic acid, 3% DMSO in HPLC grade water) at a flow rate of 50 µl/min. The MS was operated in data-dependent acquisition mode, automatically switching between MS1, MS2, and MS3 spectrum acquisition. MS1 and MS3 spectra were acquired by the Orbitrap, while MS2 spectra were acquired by the Ion Trap mass analyzer. Raw data were analyzed using MaxQuant[230]. Settings were allowing for automated isotope impurity corrections. Further, carbamidomethylated cysteine was set as fixed modification, and oxidation of methionine and N-terminal acetylation were set as variable modification.

Western blotting

Protein lysate concentration was determined by the Bradford assay. The same protein amounts per condition were loaded onto gels and separated by SDS-PAGE. Blots were electro-transferred to PVDF membranes, blocked by 4% bovine serum albumin and then incubated with primary antibodies. After incubation with secondary antibodies, analyte intensity was read out either by secondary antibody-based fluorescence scanning or via horseradish peroxidase-based chemiluminescence scanning.

Extracellular vesicle purification and analysis

Supernatants of cells were collected and applied to gravity-based qEV size exclusion chromatography (qEVoriginal, Izon) run with PBS elution buffer. Fractions containing particles in

the size range of 30-150 nm were submitted to nanoparticle tracking analysis on a PMX110-Z ZetaView Nanoparticle Tracking Analyzer. Particle number counting was performed with the ZetaView software.

ipidomics sample preparation

Cells were grown on glass dishes to avoid plastics-derived contamination when extracting lipids directly from the attached cells. For lipid extraction, a 2:1 (v/v) solution of methanol:chloroform was added to the cells for 10 s and then collected in a glass vials for sonication. Cell debris was removed by centrifugation and extracted lipids were stored in the extraction solution at −80 °C until LC–MS/MS analysis.

Lipidome LC-MS/MS measurement and data analysis

Lipids were were analyzed on a Nexera UHPLC system (Shimadzu) coupled to a Q-TOF mass spectrometer (TripleTOF 6600, AB Sciex) according to ref.[231]. The lipids were separated on the EH C18 2.1 × 100, 1.7 µm analytical column (Waters) with a gradient ranging from 32-97% solvent B (isopropanol–acetonitirile (90:10, v-v) with 10 mM ammonium formate and 0.1% formic acid) in solvent A (water–acetonitirile (40:60, v:v) with 10 mM ammonium formate and 0.1% formic acid). The MS was run in information-dependent acquisition mode in positive and negative mode.
Raw files from positive and negative mode were analyzed separately with the MS-DIAL4 software[232]. Potential analyte adducts were defined as ($[M + H]^+$, $[M + NH4]^+$, $[M + Na]^+$) for positive and for ($[M - H]^-$, $[M - H2O - H]^-$, $[M + FA - H]^-$) for negative mode. Only lipids identified by an MS2 spectrum matching to a reference library were considered for further analysis.

HDAC-Glo assay, HDAC10 TR-FRET assay and BRET assay.

These assays were performed according to ref.[222].

CellRox™ deep red assay for ROS quantification

The assay was performed according to the product guidelines (ThermoFisher). In brief, cells treated with compounds, stressors, or vehicle control were stained with 5 µM CellRox Deep Red for 1 hour. After washing cells with FluoroBrite DMEM (ThermoFisher) supplemented with 10 % FBS and Glutamax (ThermoFisher), CellRox signal was measured on a Leica DMI 6000B inverted microscope with a Cy5 filter set.

Assessing drug effects on stress granule counts

Cells were pre-treated with drug for 6 h, followed by a 30 min pulse of 1 mM arsenite to induce stress granule formation. Then, cells were fixed, permeabilized, and blocked by 10% goat serum in PBS. Stress granule marker G3BP1 (Aviva Systems Biology, ARP37713_T100) was detected via automatic fluorescence microscopy (ZEISS software in-built function) and quantified by ImageJ.

Publications

Publication 1 - Target deconvolution of HDAC pharmacopoeia reveals MBLAC2 as common off-target

The following article titled "Target deconvolution of HDAC pharmacopoeia reveals MBLAC2 as common off-target" has been published in Nature Chemical Biology in August, 2022. The article can be found in the appendix.

Full citation:
Lechner, S., Malgapo, M.I.P., Grätz, C. *et al.* Target deconvolution of HDAC pharmacopoeia reveals MBLAC2 as common off-target. *Nat Chem Biol* **18**, 812–820 (2022). https://doi.org/10.1038/s41589-022-01015-5

List of Authors:
Severin Lechner, Martin Ian P. Malgapo, Christian Grätz, Raphael R. Steimbach, Agnes Baron, Patrick Rüther, Simon Nadal, Carmen Stumpf, Christina Loos, Xin Ku, Polina Prokofeva, Ludwig Lautenbacher, Tino Heimburg, Vivian Würf, Chen Meng, Mathias Wilhelm, Wolfgang Sippl, Karin Kleigrewe, Josch K. Pauling, Karl Kramer, Aubry K. Miller, Michael W. Pfaffl, Maurine E. Linder, Bernhard Kuster & Guillaume Médard

Summary

Metal ions play essential functions as cofactors in enzyme active sites. Several drugs are approved that bind to the active site metal ion of target enzymes to inhibit their function. The largest metalloenzyme target family drugged are histone deacetylases with globally 7 approved drugs and many more in clinical pipelines. However, literature information on the drugs' selectivity is often contradictory and some phenotypes suggest off-target engagement. Here, we designed a chemical toolset consisting of three affinity probes that allows to profile HDAC inhibitor selectivity in a chemoproteomic competition assay. We used our optimized assay to profile 53 drugs against cellular proteomes containing 9 of the 11 human zinc-dependent HDACs and several HDAC inhibitor off-targets. This effort resulted in the most comprehensive target and selectivity landscape of HDAC inhibitors so far. Our data delineates how HDAC interaction partners influence the drug affinity to the target HDAC. For instance, HDAC1 interacting with RCOR3 was 100-fold more potently bound by certain drugs compared to HDAC1 engaged in other complexes or HDAC1 stripped off of its interaction partners. Further, many selectivity profiles obtained question the reported selectivity of widely-used molecules. Strikingly, 24 of the 32 hydroxamic acid-based HDAC inhibitors, including approved drugs, were found to potently bind and inhibit the enzyme metallo-beta-lactamase domain-containing protein 2 (MBLAC2). MBLAC2 has not yet been assigned to any biological function except for its capability to hydrolyze acyl-CoA in vitro. Our study confirmed the inhibition of its hydrolase activity and further found that knockdown and inhibition of MBLAC2 in HEK293T cells leads to a reconstruction of the lipidome and an accumulation of extracellular vesicles in the cell culture supernatant. Considering the importance of extracellular vesicles in systems biology, MBLAC2 inhibition by HDAC inhibitors may be of clinical relevance. Overall, our results question reported target profiles, designate chemical probes for the future study of HDACs, and may initiate the exploration of MBLAC2 inhibition-mediated side effects of clinically used drugs.

Author contributions

The authors' contributions were stated in the article: "G.M. conceived and directed the project. S.L., B.K. and G.M. wrote the manuscript. S.L. profiled the drugs and performed the knockdown, western blots, purification of extracellular vesicles, proteomics experiments, and lipidomics experiments. S.L. and B.K. measured the proteomics samples. M.I.P.M. and M.E.L. performed the MBLAC2 enzyme activity assays and C12-ceramidase assay. C.G. and M.W.P. performed the vesicle tracking experiments. R.R.S. and A.K.M. performed the HDAC enzyme activity assays, FRET, and NanoBRET binding assays. A.B., P.R., S.N., C.S., X.K., P.P., T.H., W.S. and G.M. performed the synthetic chemistry work. S.L, A.B., P.R., S.N., C.S., C.L., X.K. and P.P. performed the affinity matrix evaluation experiments. L.L. and M.W. made the data available in ProteomicsDB. K. Kleigrewe measured the lipidomics samples. S.L., V.W., C.M., K. Kleigrewe and J.K.P. analyzed the lipidomics data. K. Kramer performed the cell imaging experiments."

The specific contributions of the author of this thesis are detailed below:
S.L. had a leading role in the execution of the work presented. The author performed on-bead solid phase synthesis of the affinity matrices, optimized the pulldown protocol, and selected molecules for profiling. S.L. invented the affinity matrix iA. S.L. performed all chemoproteomic and proteomic experiments and performed the data analysis and interpretation. Moreover, S.L. performed knockdown experiments, western blots, sample preparation of lipidomics, and vesicle counting assays. S.L. was also main-responsible for extracellular vesicle and lipidomics data analysis and data interpretation. Planning and execution of assays performed by the collaboration partners was coordinated by S.L., B.K., and G.M.. The figures of the paper were prepared by S.L., and the original draft of the manuscript was written by S.L.

Additional supplementary material
Additional supplementary tables not suited for printing are available for download at the publisher's website (https://doi.org/10.1038/s41589-022-01015-5).

Publication 2 - Chemoproteomic target deconvolution reveals Histone Deacetylases as targets of (R)-lipoic acid

The following article titled “Chemoproteomic target deconvolution reveals Histone Deacetylases as targets of (R)-lipoic acid” was accepted to be published in Nature Communications on May 26, 2023. The unformatted but accepted article version by Nature Communications can be found in the appendix.

Full citation:
The article has not been published yet. The full citation will be added, as soon as the article is published online.

List of Authors:
Severin Lechner, Raphael R. Steimbach, Longlong Wang, Marshall L. Deline, Yun-Chien Chang, Tobias Fromme, Martin Klingenspor, Patrick Matthias, Aubry K. Miller, Guillaume Médard, Bernhard Kuster

Summary
Racemic (*R*/*S*)-lipoic acid has been has been approved drug for diabetic neuropathy for about 60 years. Furthermore, Racemic (*R*/*S*)-lipoic acid and the pure enantiomer (*R*)-lipoic have been marketed as dietary supplement with antioxidant features. Lipoic acid reaches peak plasma concentrations of up to 500 µM. In literature, lipoic acid mode of action is often related to its purportedly antioxidant properties. However, the mechanism of action of lipoic acid-induced phenotypes is still not worked out in detail. Here, we employed chemoproteomic affinity-based protein profiling to identify potential protein targets of lipoic acid. Strikingly, lipoic acid was found to bind and inhibit several HDACs with affinities in the range of 3-30 µM. HDACs were the only identified targets. Importantly, only (*R*)-lipoic acid inhibits HDACs, leads to HDAC substrate hyperacetylation, and prevents arsenate-induced stress granule formation, while (*S*)-lipoic acid was inactive. Both enantiomers, however, showed similar effects on buffering ROS in the presence of arsenite and hydroperoxides. Our data, therefore, link effects induced only by (*R*)-lipoic acid to HDAC inhibition, while effects induced by both enantiomers are attributed to lipoic acid’s physicochemical properties such as metal ion chelation, or its redox properties. The set of the two enantiomers will therefore allow to disentangle HDAC inhibition-mediated effects from additional effects, to uncover the relevance of HDAC inhibition in lipoic acid’s mode of action and clinical efficacy.

Author contributions

The authors’ contributions were stated in the article: “B.K. and G.M. conceived and directed the project. S.L. performed chemoproteomic experiments and western blots. S.L. and B.K. measured the proteomics samples. Y.C. performed proteomic experiments. R.R.S. and A.K.M. performed the HDAC enzyme activity assays, as well as BRET and FRET binding assays. L.W. and P.M. performed western blots and stress granule experiments. M.L.D., T.F., and M.K. performed the CellRox assays and data analysis. S.L. and B.K. wrote the manuscript with input from all authors.”

The contributions of the author of this thesis are detailed below:
S.L. had a leading role in conceiving and directing the project. S.L. performed and supervised the on-bead solid phase synthesis of the affinity matrices, all chemoproteomic experiments and several western blot experimets. S.L. coordinated collaboration projects together with B.K. and G.M, and was leading the experimental design as well as data analysis and interpretation of

collaboration projects. Further, S.L. prepared all figures and wrote the original draft of the paper story.

Rights and permissions

Additional supplementary material

Additional supplementary tables not suited for printing are available for download at the publisher's website.

Co-authorship publications

In addition to the two main publications, the author of this thesis contributed as co-author to three more publications that are of relevance. These publications are not printed as part of this thesis, but can be found on the corresponding journal websites.

Co-authorship 1 - Aza-SAHA Derivatives Are Selective Histone Deacetylase 10 Chemical Probes That Inhibit Polyamine Deacetylation and Phenocopy HDAC10 Knockout

The following article titled "Aza-SAHA Derivatives Are Selective Histone Deacetylase 10 Chemical Probes That Inhibit Polyamine Deacetylation and Phenocopy HDAC10 Knockout" has been published in the Journal of the American Chemical Society (JACS) on October 6th, 2022.

Full citation:
Steimbach, R.R. *et al*. Aza-SAHA Derivatives Are Selective Histone Deacetylase 10 Chemical Probes That Inhibit Polyamine Deacetylation and Phenocopy HDAC10 Knockout. J Am Chem Soc 144, 18861-18875 (2022).

List of Authors:
Raphael R. Steimbach, Corey J. Herbst-Gervasoni, **Severin Lechner**, Tracy Murray Stewart, Glynis Klinke, Johannes Ridinger, Magalie N. E. Géraldy, Gergely Tihanyi, Jackson R. Foley, Ulrike Uhrig, Bernhard Kuster, Gernot Poschet, Robert A. Casero Jr., Guillaume Médard, Ina Oehme, David W. Christianson, Nikolas Gunkel, and Aubry K. Miller

Summary
HDAC10 is a zinc-dependent enzyme from the histone deacetylase family. However, HDAC10 was recently shown to deacetylate polyamines instead of protein substrates. Potent, intracellularly active, and selective HDAC10 chemical probes are required to further study the biological functions of HDAC10 and the therapeutic potential of HDAC inhibitors. Inspired by the structure of HDAC10 polyamine structures, an amino-group was systematically inserted into different sites of the linker region of Vorinostat, which is a weak and unselective HDAC10 binder. Further optimization of the resulting pharmacophore led to the discovery of DKFZ-748, a highly potent and selective HDAC10 inhibitor. DKFZ-748 was confirmed to bind none of the common HDAC inhibitor and Vorinostat-specific off-targets. Further, the compound proved in-cell target engagement in nanoBRET assay. Treating cells with DKFZ-748 led to a dose-dependent increase in HDAC10 substrate acetyl-polyamines. In a polyamine-deprived in vitro tumor model, DKFZ-748 reduced the growth of cancer cells. We expect, that DKFZ-748 will facilitate the study of the enigmatic biological functions of HDAC10 and its role in regulating acetylated polyamine levels in physiological and pathological contexts.

Author contributions
The contributions of the author of this thesis are detailed below:
The author of this thesis performed chemoproteomic competition assays with a set of drug candidates developed in the paper. Here, S.L. was involved in experimental design, analysis and interpretation of the data, and drafted Table 2 as well as Figure S2, which summarize the results of the experiments. The data obtained led to the conclusion that the new compounds, including the lead molecule DKFZ-748, do not engage common HDAC inhibitor off-targets or HDACs besides HDAC10.

Co-authorship 2 - Development of hetero-triaryls as a new chemotype for subtype-selective and potent Sirt5 inhibition

The following article titled "Development of hetero-triaryls as a new chemotype for subtype-selective and potent Sirt5 inhibition" has been published in the Journal of the American Chemical Society (JACS) on October 6th, 2022.

Full citation:
Glas, C. *et al.* Development of hetero-triaryls as a new chemotype for subtype-selective and potent Sirt5 inhibition. *Eur J Med Chem* **240**, 114594 (2022).

List of Authors:
Carina Glas, Eli Naydenova, **Severin Lechner**, Nathalie Wössner, Liu Yang, Johannes Dietschreit, Hongyan Sun, Manfred Jung, Bernhard Küster, Christian Ochsenfeld, and Franz Bracher

Summary
Sirtuins are NAD^+-dependent enzymes catalyzing a range of lysine deacylation reactions. Seven human sirtuins have been described so far. The mitochondrial lysine deglutarylase SIRT5 is one of the least explored family members, owed in part to the lack of selective chemical probes to study its function. Recent work identified balsalazide as SIRT5 inhibitor. Balsalazide is an approved drug but has only negligible bioavailability due to rapid turnover through the intestinal microbiome. Here, we developed balsalazide-derivatives CG_209, CG_220, and CG_232 with encouraging in vitro activities ($IC50^{SIRT5}$ < 10 µM). The inhibitors showed no effect on cell viability and could enter the mitochondria to inhibit SIRT5 in cells. Affinity-based chemoproteomic target deconvolution of the lead structures identified the two potential off-targets mitochondrial nucleoside diphosphate kinase NME4 and mitochondrial glutaryl-CoA dehydrogenase GCDH. While the effect of off-target engagement remains to be elucidated, this discovery might lay the foundation for designing small molecule modulators of these yet undrugged proteins. Indeed, competition experiments with the glutaryl-CoA indicated that the compounds bind to the same pocket as the GCDH substrate. The off-target inhibition would result in accumulation of GCDH substrate glutaryl-CoA, which is the co-factor for protein glutarylation. It is, therefore, tempting to speculate about a synergistic effect between SIRT5 and GCDH inhibition in compound-mediated hyperglutarylation of SIRT5 substrates.
In summary, we discovered promising lead structures for the development of potent and selective SIRT5 inhibitors. The compounds were shown to inhibit SIRT5 in cellulo and can be used orthogonally to genetic knockdown when studying the physiological roles of SIRT5.

Author's contribution
The author of this thesis was responsible for chemoproteomic target deconvolution of the SIRT5 inhibitors developed in this publication. In detail, S.L. advised the design of the affinity probe and generated the affinity matrix for pulldown experiments. S.L. then performed chemoproteomic competition assays with Balsalazide and the lead molecules CG_220 as well as CG_232, and analyzed and interpreted the data. The data obtained confirmed that the new drugs are most likely not binding any other Sirtuins. However, novel targets of the pharmacophore, NME4 and GCDH, could be identified and might contribute to the compound's mode of action. S.L. suggested additional glutaryl-CoA competition assays to collect evidence that compound binding prevents GCDH substrate binding, likely resulting in GCDH inhibition and potentially synergistic effects. Furthermore, S.L. contributed to connecting to the collaboration partners that proved SIRT5 inhibition in mitochondria.

Co-authorship 3 - Decrypting drug actions and protein modifications by dose- and time-resolved proteomics

The following article titled "Decrypting drug actions and protein modifications by dose- and time-resolved proteomics" has been published in Science on April 7th, 2023.

Full citation:
Zecha, J. *et al*. Decrypting drug actions and protein modifications by dose- and time-resolved proteomics. Science 380, 93-101 (2023).

List of Authors:
Jana Zecha, Florian P. Bayer, Svenja Wiechmann, Julia Woortman, Nicola Berner, Julian Müller, Annika Schneider, Karl Kramer, Mar Abril-Gil, Thomas Hopf, Leonie Reichart, Lin Chen, Fynn M. Hansen, **Severin Lechner**, Patroklos Samaras, Stephan Eckert, Ludwig Lautenbacher, Maria Reinecke, Firas Hamood, Polina Prokofeva, Larsen Vornholz, Chiara Falcomatà, Madeleine Dorsch, Ayla Schröder, Anton Venhuizen, Stephanie Wilhelm, Guillaume Médard, Gabriele Stoehr, Jürgen Ruland, Barbara M. Grüner, Dieter Saur, Maike Buchner, Benjamin Ruprecht, Hannes Hahne, Matthew The, Mathias Wilhelm, and Bernhard Kuster

Summary
Posttranslational modifications (PTMs) are critical regulators of protein activity, function, stability, localization, or interaction with other biomolecules. Many cancer drugs such as kinase inhibitors or histone deacetylase inhibitors target enzymes that actively install or remove PTMs. Of note, drugs not directly targeting writers or erasers of PTMs often also induce a change in the PTM landscape as a result of the cellular response to drug perturbation. Despite this central role of PTMs in drug modes of action, little is known about the time- and dose-dependent changes of PTMs upon drug treatment. Here, we introduce the concept of proteome-wide dose- or time-dependent PTM profiling of drug-treated cells. Thousands of phosphorylation, acetylation, or ubiquitination sites were quantified after treating cells with different doses of various drugs that cover the classes of chemotherapeutics, kinase inhibitors, HDAC inhibitors, proteasome inhibitors, and antibodies. The data allowed to measure in cellulo target engagement EC50 values and shed light on drug modes of action. For instance, the dual kinase and HDAC inhibitor CUDC101 was shown to induce HDAC substrate hyperacetylation already at 100-fold lower concentrations than target kinase hypophosphorylation, questioning the pharmacological relevance of kinase inhibition by CUDC101. Furthermore, the results provide evidence that rituximab targets CD20-positive B-cells by overstimulation of B-cell receptor signaling. Overall, our results showcase the value of dose- or time-dependent PTM profiling. The 1.8 million dose-response curves of 31 drugs profiled in up to 13 cell lines are provided via ProteomicsDB as publically accessible and interactive resource for investigating drug modes of action.

Author's contribution
The authors' contributions were stated in the article: "J.Z., B.R., and B.K. conceived the decryptM approach. J.Z., F.P.B., S.Wie., J.W., N.B., A.Schn., M.A.-G., K.K., L.C., F.M.H., S.L., S.E., M.R., F.M.H., P.P., L.V., C.F., M.D., L.R., A.Schr., and A.V. performed laboratory experiments. F.P.B., J.M., T.H., P.S., L.L., G.S., M.T., J.Z., S.Wie., J.W., N.B., A.Schn., K.K., L.C., F.M.H., S.L., S.E., M.R., P.P., L.V., C.F., M.D., L.R., A.Schr., A.V., and B.K. performed data analysis. J.R., J.Z., S.Wil., B.M.G., D.S., G.M., M.B., H.H., M.T., M.W., and B.K. directed and supervised experiments and data analysis. F.P.B., A.Schn., M.T., and B.K. wrote the manuscript with input from all authors."

The contributions of the author of this thesis are detailed below:
The author of this thesis was the main-responsible author for data analysis and interpretation of the epigenetic drugs section of this paper. In detail, S.L. surveyed the dose-response plots obtained from cancer cell treatment with HDAC and HAT inhibitors. Based on the observations, S.L. generated Fig. 2 and Fig. S7 (supported by F.P.B), and wrote the original version of the manuscript for the chapter “epigenetic drugs”. S.L. was further involved in general discussion and advice regarding other sections of the paper.

General discussion and outlook

Content

General discussion and outlook 44
1 Providing a comprehensive overview of the HDAC inhibitor target landscape 45
2 Facilitating class IIa HDAC inhibitor selectivity profiling 50
3 The dependence of target-affinity on target-interaction partners 51
4 Off-targets of purportedly selective HDAC inhibitors explain unexpected phenotypes 53
5 MBLAC2 – a silent bystander or a clinically relevant target? 55
6 HDAC inhibitor off-targets with unknown drug-binding effects 58
6.1 Scriptaid binds NQO2 58
6.2 Common off-targets of Vorinostat-like drugs. 59
6.3 Further potential off-targets 63
7 Updating the list of selective chemical probes for HDAC research 65
8 Creating a drug repurposing opportunity: Lipoic acid for 'HDAC-linked diseases' and HDAC inhibitors for 'lipoic acid-linked diseases' 66
9 The value of affinity-based protein profiling for (off-) target identification 69
10 Shortcomings of chemoproteomics-based selectivity profiling and target deconvolution . 70
11 Future use cases of the promiscuous HDAC affinity matrix 72
12 Future challenges in the field of HDAC inhibitors 73

1 Providing a comprehensive overview of the HDAC inhibitor target landscape

The promiscuous affinity matrix designed in publication 1 consists of a mix of three affinity probes (iQ+iC+iA) that for the first time enable the specific pull-down of class I, IIa, and IIb HDACs in a single experiment. Furthermore, the affinity matrix allows to pull down a set of at least 11 HDACi off-targets (Fig. 16). The affinity matrix constituents complement each other: Immobilized Quisinostat iQ is pulling down all class I and IIb HDACs plus a range of off-targets and is therefore a good surrogate for previously developed affinity matrices based on the immobilization of Vorinostat (iV), Givinostat (iG), or Panobinostat (iP). Of note, iQ (as well as iP) can be readily synthesized by directly reacting the unmodified and commercially available parental drug to commercially available NHS-activated sepharose beads. The additional pulldown of class IIa HDACs and MBLAC2 is achieved by use of iC. The affinity probe iA does not add any more HDACs to the list but extends the covered off-target space (ALDHs, ISOCs, and GATD3A). The number of targets that can be profiled with the affinity matrix (iQ+iC+iA) depends on the used cell lysate and the number of profiled drugs with distinct pharmacophores. Profiling of next-generation drugs or related inhibitors with new pharmacophores or profiling in different cell lysates will presumably identify additional off-targets that can be specifically pulled down by this promiscuous affinity matrix.

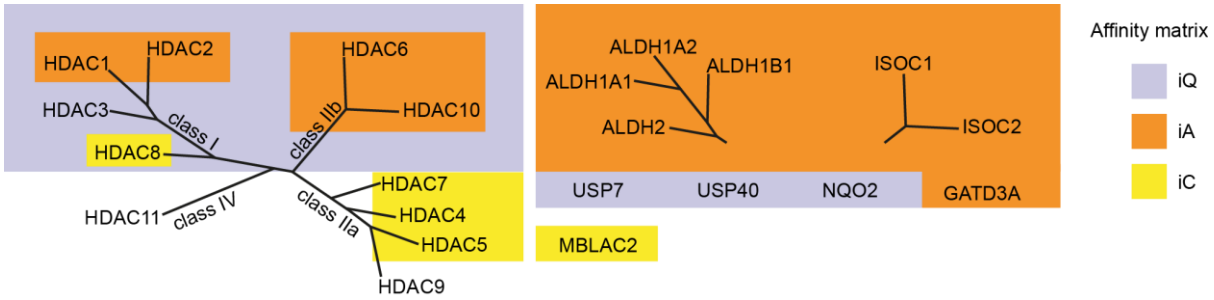

Figure 16|Coverage of the so far identified target space by the here developed affinity probes iA, iQ, and iC. HDACs and off-targets are comprehensively pulled down by a combination of iQ, iC, and iA in Lechner et al.[15]. USPs are Quisinostat-specific off-targets; NQO2 is a Scriptaid-specific off-target but pulled down by iQ; ALDH1A1, ALDH1A2, and ALDH1B1 were shown to be specifically pulled down and competed with Vorinostat in ref.[222]. HDAC9 and HDAC11 have not been identified in the pulled-down proteome. The HDAC phylogenetic tree is adapted from Arrowsmith et al.[68]. For structures of iA, iC, and iQ, see figure panel b.

HDAC9 and HDAC11 could not be identified in the pulled-down proteome. This is either related to insufficient affinity to the probes or to insufficient expression in the tested cell lines. Indeed, HDAC9 and HDAC11 are among the lowest expressed HDACs in most cell lines and tissue proteomes deposited on proteomicsDB[233-236] (Fig. 17).

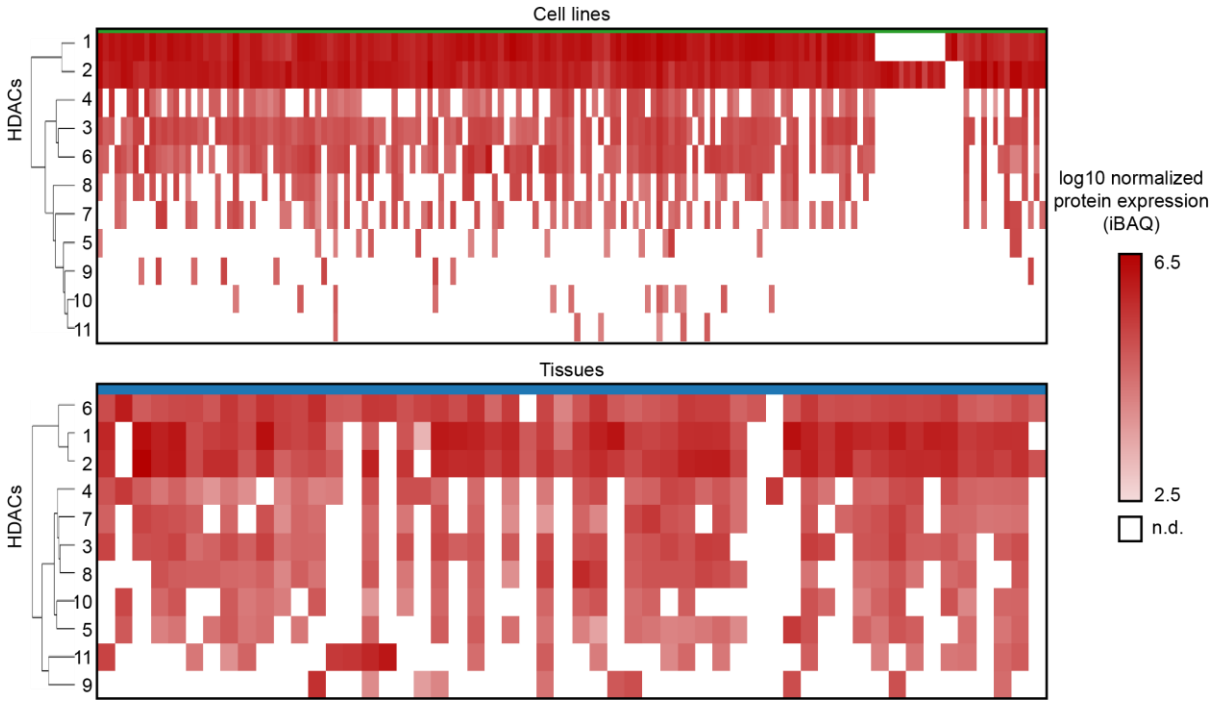

Fig. 17|Normalized HDAC expression among cell lines and tissues according to proteomics data deposited in proteomicsDB[233-236]. The HDAC order is kept according to the clustering in proteomicsDB. Both, in cell lines and tissues, HDAC9 and HDAC11 are grouped in the cluster driven by missing expression (n.d.: not detected).

Nevertheless, the here developed promiscuous affinity matrix allows to study the HDACi target and off-target space more comprehensively than all affinity matrices previously reported for chemoproteomic purposes (Fig. 18).

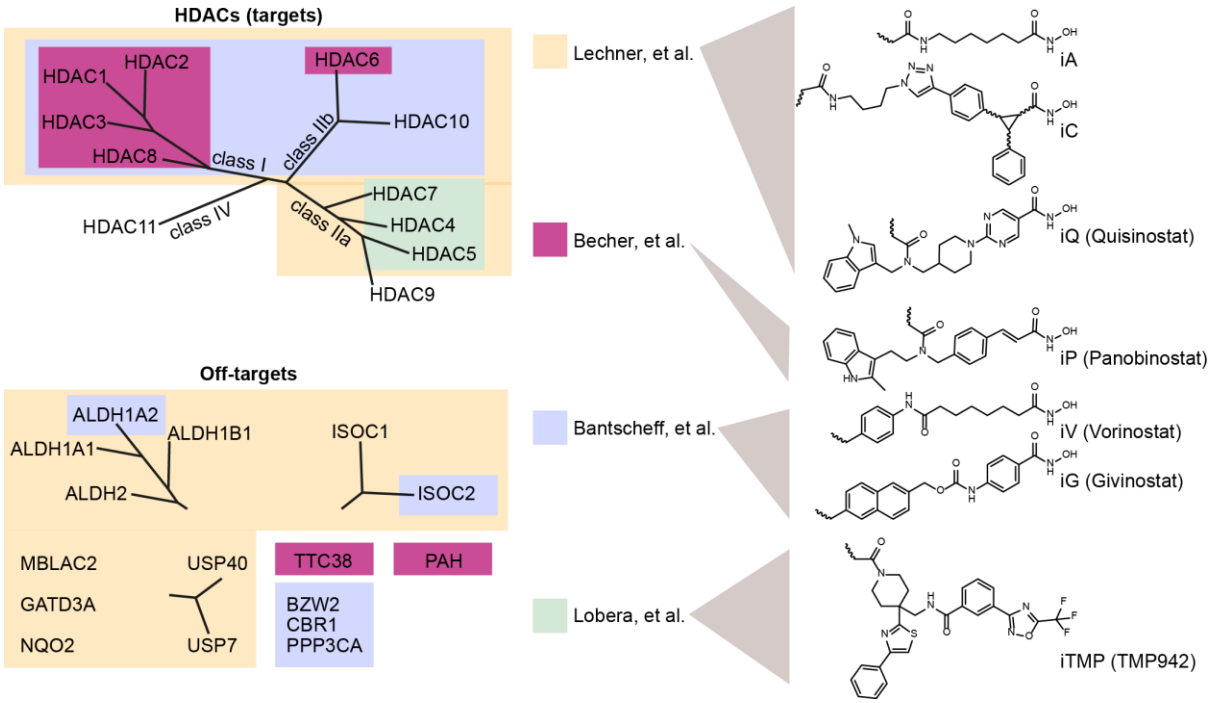

Fig. 18|Comparison of the covered target and off-target space by chemical probes employed in chemoproteomic pulldown assays targets that can be pulled down by the affinity matrices employed in different chemoproteomic studies are underlaid with the corresponding color. Data are aggregated from the following publications: Lechner et al. (iA+iC+iQ)[15, 222], Becher et al. (iP)[26], Bantscheff et al. (iV or iG)[43], and Lobera et al. (iTMP)[210].

Our chemoproteomic assay evades the disadvantages of enzyme activity and nanoBRET-based HDACi selectivity profiling assays as discussed in detail before (see 1.2.3). The assay setup developed here (publication 1[15]) determines binding to all targets in the same sample. Therefore, the relative binding affinities, i.e. selectivities, of drugs are highly reliable and comparable. While data from previous chemoproteomic profiling efforts suffered from short incubation times that led to an underestimation of slow binder affinities (i.e. aminoanilides and Romidepsin)[43, 44], we addressed this issue by determining assay-specific binding kinetics of representative HDAC inhibitors and optimizing assay conditions as well as incubation times accordingly. Our assay conditions thus guarantee that affinity values of slow binders (low k_{on}) and drugs with fast binding kinetics are comparable to each other. Additionally to having an optimized readout for HDACi target and off-target binding, our assay covers the HDAC family more comprehensively than the assays employed in the three largest previous HDACi profiling studies (enzyme activity assay, nanoBRET assay, and AfBBP) (Fig. 19).

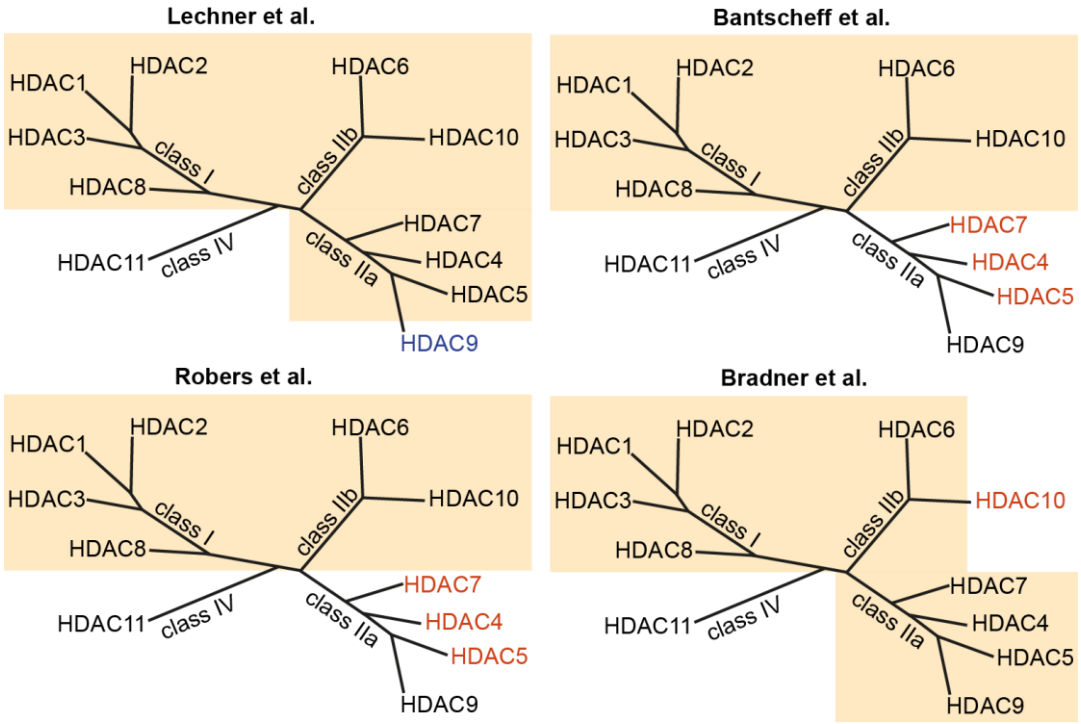

Figure 19| Comparison of HDACs covered in the largest HDAC inhibitor selectivity profiling studies. While none of the large profiling studies included class IV, the publication underlying this thesis is the only one that covers all class I and IIb enzymes as well as a substantial fraction of the class IIa proteins (Bradner et al.[93], Bantscheff et al.[43], Robers et al.[215], Lechner et al.[15]).

The established tool was used to profile the drug targets and selectivities of 53 drugs in publication 1[15] (Fig. 20). Most drugs were commercially available and four molecules were accessible only via academic collaborations at the time of profiling (TH65, TH147, CHDI00465983, and CHDI00390576). The list of drugs included 49 proposed HDAC inhibitors and 4 related compounds with metal chelating warheads (Salicylhydroxamic acid and the matrix metalloprotease inhibitors Marimastat, Ilomastat, and Batimastat) that presumably could bind HDACs or other proteins pulled down by our affinity matrix.

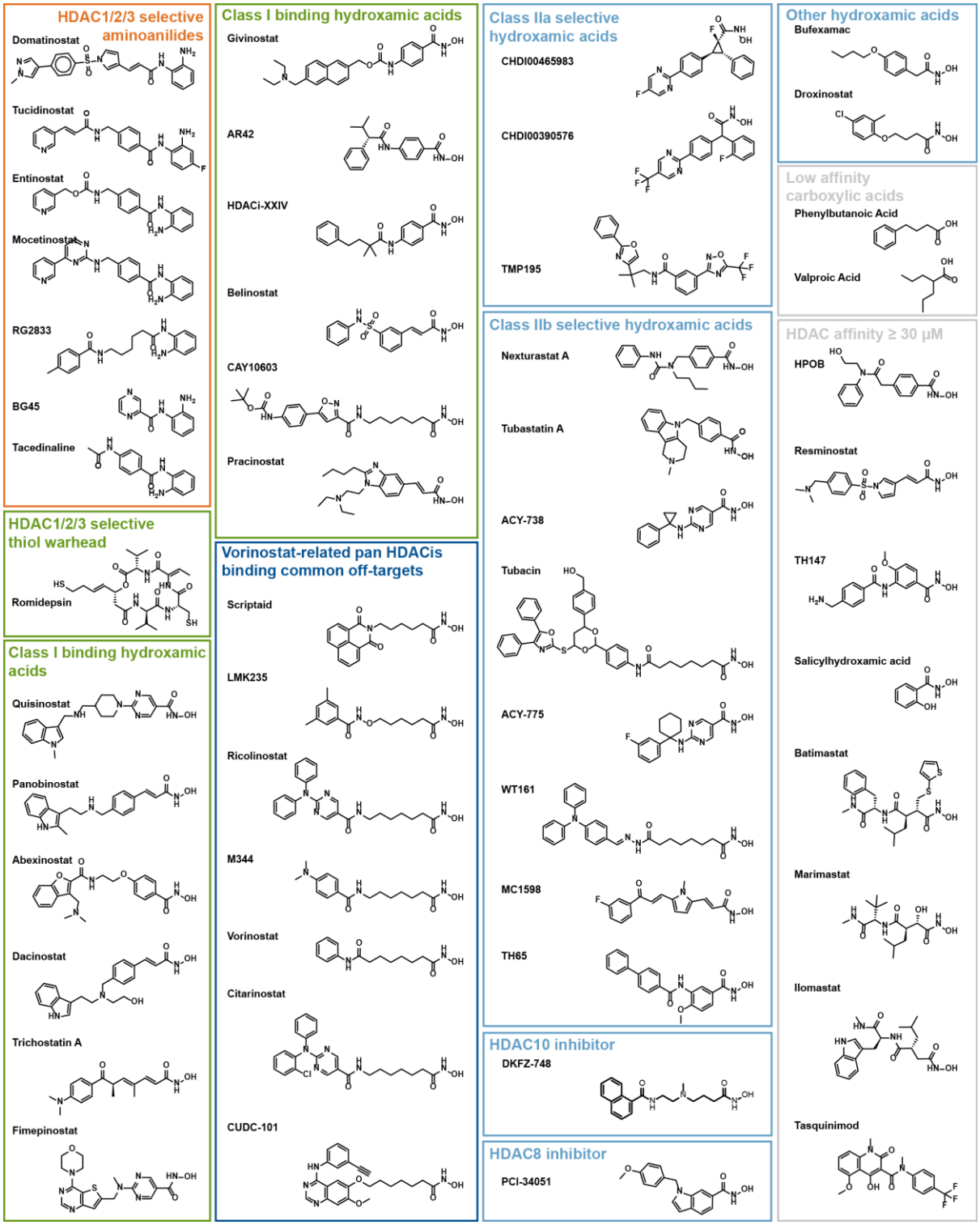

Fig. 20|Structures of compound profiled in publication 1[15] and co-authorship 1[222] (DKFZ-748). The structures are roughly sorted into groups according to their target profile and zinc-chelating warhead.

The profiled drugs partly overlapped with the drugs included in the aforementioned large HDACi selectivity profiling studies (Fig. 21a). Overall, more than 850 drug-target interactions were profiled (>50 drugs vs. 17 targets), resulting in the so far most comprehensive drug selectivity landscape of HDAC inhibitors and providing a rich resource for the research community (Fig. 21b).

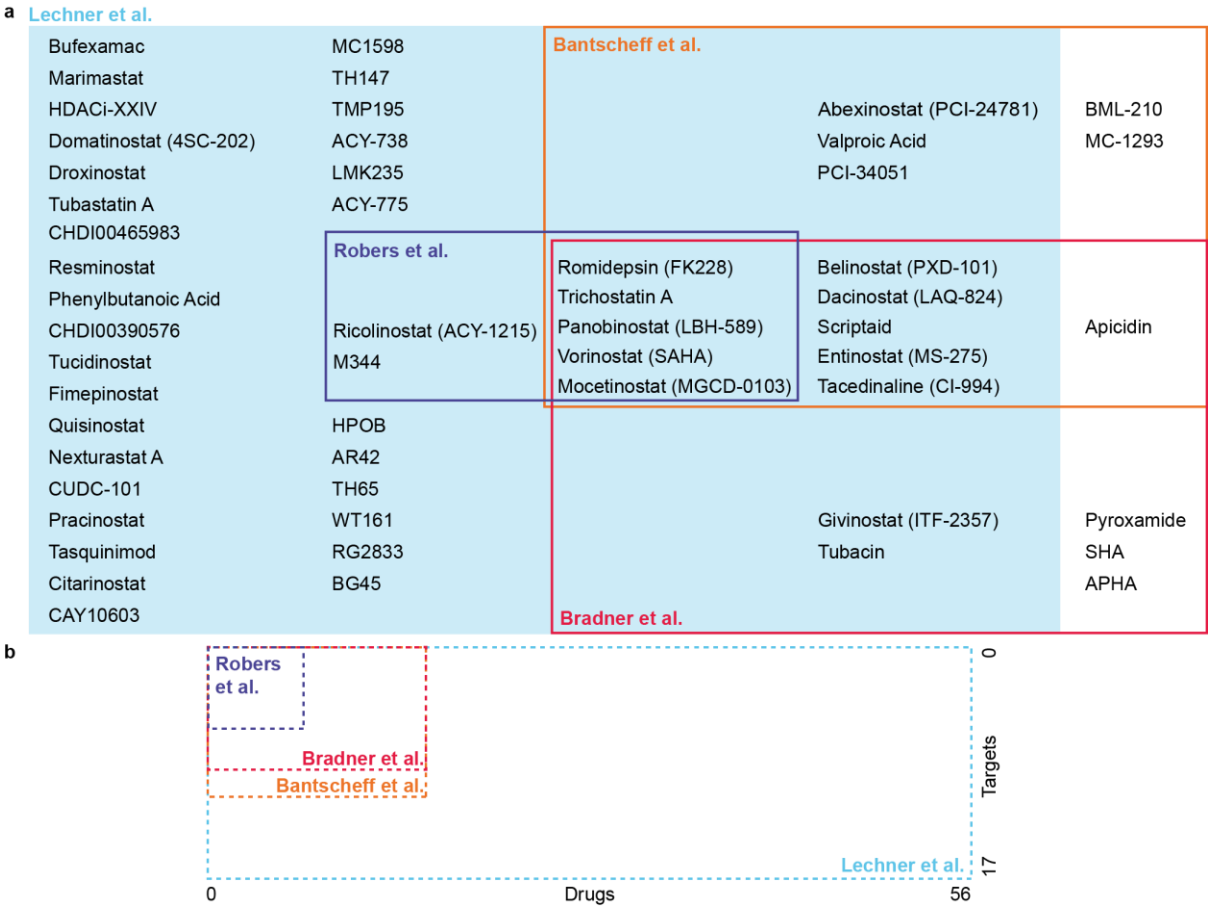

Fig. 21|Comparison of designated HDACis profiled in large selectivity profiling studies (Bradner et al.[93], Bantscheff et al.[43], Robers et al.[215], and Lechner et al.[15]). **a**, Coverage of the HDAC inhibitor space (commercially available drugs as of 2021). Five drugs have been subject to all four systematic HDACi profiling studies. 31 drugs were only covered in the study underlying this thesis. **b**, The number of drug-target pairs assayed in each study is depicted as an area, where length is the projected number of profiled drugs and height is the projected number of profiled targets (for Lechner et al.[15], only drug targets identified using the MV4-11/SW620 lysate mix are considered. Drug-specific off-targets NQO2 for Scriptaid and USP7/40 for Quisinostat are included). The panel of chemoproteomic studies will presumably grow in both dimensions with the profiling of new pharmacophores that bind to additional targets.

2 Facilitating class IIa HDAC inhibitor selectivity profiling

Our technology allowed us to derive comparable selectivity data for all class I and IIb HDACs, and, for the first time in a chemoproteomic assay setup, additionally class IIa HDACs. This led to some noteworthy findings.

First, we recognized a vast underrepresentation of class IIa targeting drugs. Indeed only 6 HDAC inhibitors bound class IIa HDACs. Three of these drugs bound other HDAC targets with 30-100 higher potency. Only 2 drugs were selectively binding class IIa over other target classes (TMP195 and CHDI00390576), albeit with low intra-class selectivity. This highlights the demand for further development of selective class IIa drugs, which are highly needed to study class IIa biology, and which might represent new therapeutic options that lack class I inhibitor-typical side effects.

Second, our data revealed that drugs commonly used to probe class IIa cell biological functions (LMK235 and MC1568) are actually not inhibiting class IIa HDACs but other targets (see also chapter 4.4). Findings about class IIa obtained by the use of these molecules are therefore misleading and need to be revised. We anticipate, that the here-developed technology will motivate and support the development of new class IIa selective agents.

3 The dependence of target-affinity on target-interaction partners

As introduced by the first large-scale chemoproteomic HDACi profiling study (ref.[43]), drug binding affinity of HDAC inhibitors can depend on the HDAC interaction partner. Dose response curves of HDAC complex partners pulled down together with the HDAC can be determined by the chemoproteomic readout and allow to infer drug affinity shifts (Fig. 22).

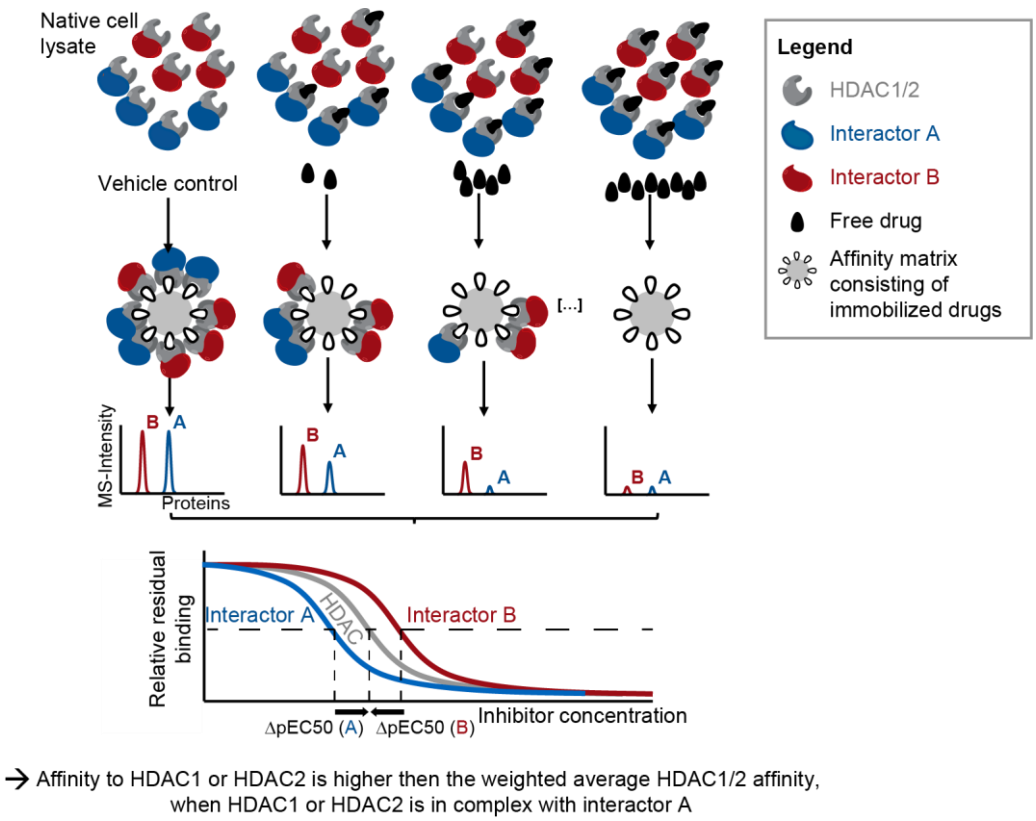

Fig. 22|Schematic representation of dose-dependent chemoproteomic competition assays for the analysis of target interaction partner-dependent drug target affinity. Depending on whether HDAC1 interacts with interactor A or interactor B, distinct drug concentrations are required to half maximally block HDAC1 pulldown by the affinity matrix. The influence of interaction partners on HDAC1 drug binding affinity is reflected by shifts in EC50 values derived from interaction partners compared against each other or against the EC50 of HDAC1. Of note, since HDAC1 participates in several complexes and is also present as single enzyme without interaction partners, the curve of HDAC1 represents a weighted average of the dose-response of all HDAC1 proteins engaged in different complexes. Similar considerations are valid for HDAC2 and HDAC3, which are also part of chromatin-regulatory protein complexes. The figure was adapted from publication 1.

Previous studies observed certain trends depending on the drug chemotypes [43, 44, 234]. Our data allowed us to confirm these observations and to draw an even more detailed picture of target-affinity dependence on target interaction partners. Aminoanilide-type inhibitors bind to HDAC1-2 that are either present as free enzymes or with reduced affinity to HDACs interacting with the CoREST complex partners. But they completely lose binding affinity to HDAC1 or HDAC2 engulfed in the NuRD, Sin3, and MiDAC complex (publication 1[15]). In contrast, most hydroxamic acid-based inhibitors have enhanced affinity to HDAC1 and HDAC2 when embedded in complexes[15]. In our study (publication 1[15]), the most drastic effect of target-interaction partners on drug-target affinity was observed for the RCOR3-based CoREST complex. Here, for some drugs, HDAC1 binding was observed to be up to 100-fold more potent if HDAC1 was interacting with RCOR3 compared

to the weighted average of HDAC1 affinities. This supports the idea that despite high active site similarity of HDAC1 and HDAC2, selectivity for targeting specific HDAC1 or HDAC2-based epigenetic complexes could be achieved. Strikingly, our data indicate that certain drugs bind to HDAC1 or HDAC2 with up to 100-fold higher affinity when these targets are engaged in the RCOR3-based CoREST complex.

Since specific and spatially defined HDAC1 and HDAC2 downstream effects are most likely guided by their interaction partners, inhibitors selectively targeting complexes would present a higher level of spatial and functional selectivity than inhibitors that are selective for HDAC1 or HDAC2 but do not differentiate between the interaction partner environments (Fig. 23). For example, CoREST selective drugs would only inhibit HDAC1/HDAC2 in chromatin regions, where the CORESTcomplex is recruited to and therefore inhibit HDACs only in a spatially confined environment. This would consequently induce spatially confined downstream effects, such as enhanced gene transcription only at CoREST sites and not globally across the whole genome.

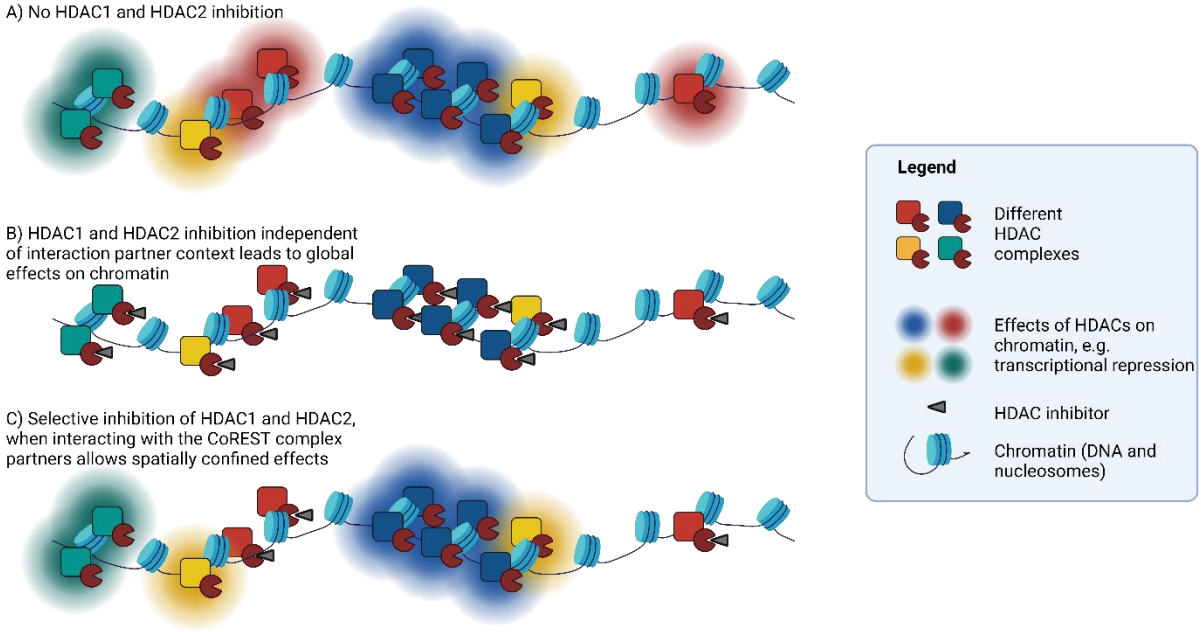

Fig. 23|Spatially confined inhibition of HDAC activity by selectively targeting HDACs in complexes. HDACs can be part of at least 5 large chromatin regulatory complexes. While the function of the complexes is not understood in detail, the current model suggests that complexes regulate HDAC activity and direct them to certain locations in the chromatin. Inhibiting HDACs independent of their complex environment leads to global hyperacetylation of HDAC substrates. Selectively inhibiting only the HDACs that are embedded in a certain complex confines the downstream effects (hyperacetylation) to the chromatin sites, where the HDAC complex is located. The figure was created with Biorender.

4 Off-targets of purportedly selective HDAC inhibitors explain unexpected phenotypes

The obtained data uncovered off-targets of chemical probes that explain confounding observations in the literature.

For instance, Tubacin is frequently used as a selective HDAC6 inhibitor to probe HDAC6 biology. Surprisingly, Tubacin was shown to induce the accumulation of extracellular vesicles independent of its HDAC6 inhibitory effects[237]. Our results indicate that this phenotype is linked to the inhibition of the previously unreported off-target MBLAC2, whose inhibition and knockdown induces accumulation of extracellular vesicles[15]. MBLAC2 is inhibited by about half of the hydroxamic acid-based HDAC inhibitors profiled in this study and might therefore be relevant for many phenotypic effects previously linked to HDAC inhibition.
A second example is the unexpected cytotoxic and cytostatic effect of LMK235, a claimed class IIa inhibitor. While class IIa inhibition, in general, does not affect cell viability[15, 210], LMK235 reduced SW620 cell viability in the same way as class I HDACis[15]. Our data unmask LMK235 as an unselective inhibitor of class I and IIb HDACs and clearly links its cytostatic and cytotoxic effects to class I HDAC inhibition. In hindsight, this finding is not very surprising, considering the structural similarity of LMK235 to Vorinostat-related molecules (class I and IIb inhibitors), and its dissimilarity to other class IIa binding molecules (Fig. 24).

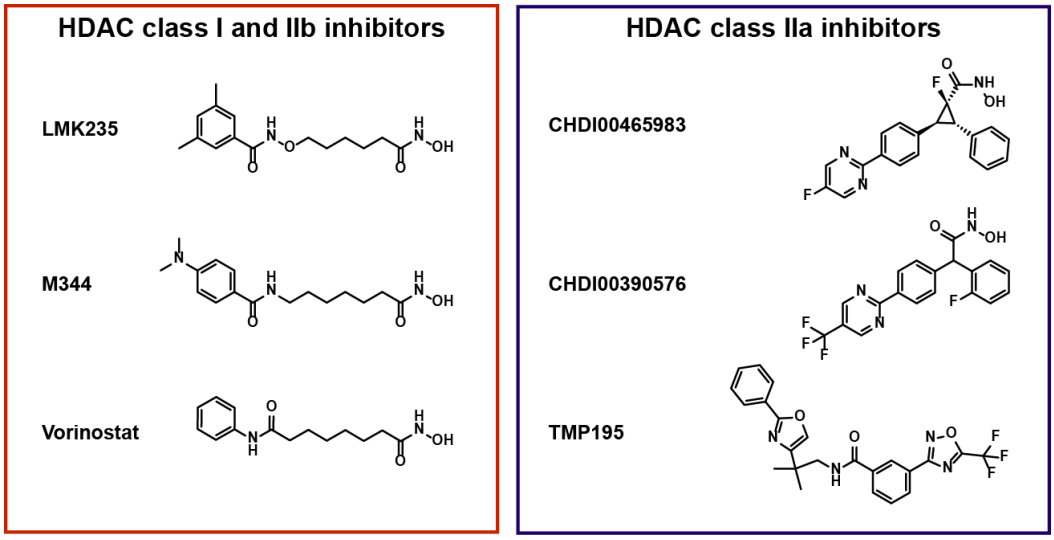

Fig 24|Structures of LMK235, the prototypical HDAC class I/IIb inhibitors M344 and Vorinostat, as well as typical HDAC class IIa binding pharmacophores. Clearly, LMK235 resembles other class I/IIb inhibitors rather than class IIa inhibitors.

Several other purportedly selective molecules used as chemical probes were uncovered to be unselective: ACY775 and WT161 are binding the aforementioned MBLAC2 with a potency similar to HDAC6. Tubastatin A has been used in more than 150 publications as chemical probe for HDAC6, but inhibits additionally HDAC10 (see also ref.[192]) and MBLAC2. CHDI00465983 is a designated class IIa selective inhibitor, which also binds HDAC8 and MBLAC2. These findings hopefully allow to reinterpret all observations made by treating cells with these molecules and should prevent their further use as chemical probes. Of note, the online vendor MedChemExpress already adapted the product description of Tubastatin A, Tubacin, ACY775, and WT161 according to our findings.

Lastly, our data from publication 1[15] support the notion that Ricolinostat is indeed not a selective HDAC6 inhibitor and that its anti-cancer effects are attributable to the inhibition of HDAC1-3[48, 134]. This is of high relevance since clinical trials with Ricolinostat are still initiated based on its perception as selective HDAC6 inhibitor[238]. According to its selectivity profile, Ricolinostat (phase II), as well as Citarinostat (phase I), resemble Vorinostat's selectivity profile (i.e. a similar relative binding affinity to HDAC1-3, about 10-fold higher affinity to HDAC6, and binding to the same off-targets). Disregarding the potentially different pharmacokinetics of Vorinostat and Ricolinostat, our data therefore suggest that for both drugs similar clinical efficacy can be expected. Considering the large number of failed Vorinostat clinical trials[102], one should probably reconsider whether testing Ricolinostat and Citarinostat for the same indications as Vorinostat is a worthwhile endeavor.

5 MBLAC2 – a silent bystander or a clinically relevant target?

Our study of 53 HDAC inhibitors found that the metallo-beta-lactamase domain-containing protein 2 (MBLAC2) was a target of about 75% of the hydroxamic acid drugs that scored in the assay. Strikingly, some of the inhibitors were more potently binding MBLAC2 than their dedicated HDAC targets. This includes Nexturastat A, a preclinical compound used as chemical probe for HDAC6, and clinical drugs such as Abexinostat (phase III), AR-42 (phase I), and Pracinostat (phase III) (Fig. 25). Strikingly, even approved drugs feature MBLAC2 off-target activity (EMA-approved Panobinostat and the orphan drug Givinostat).

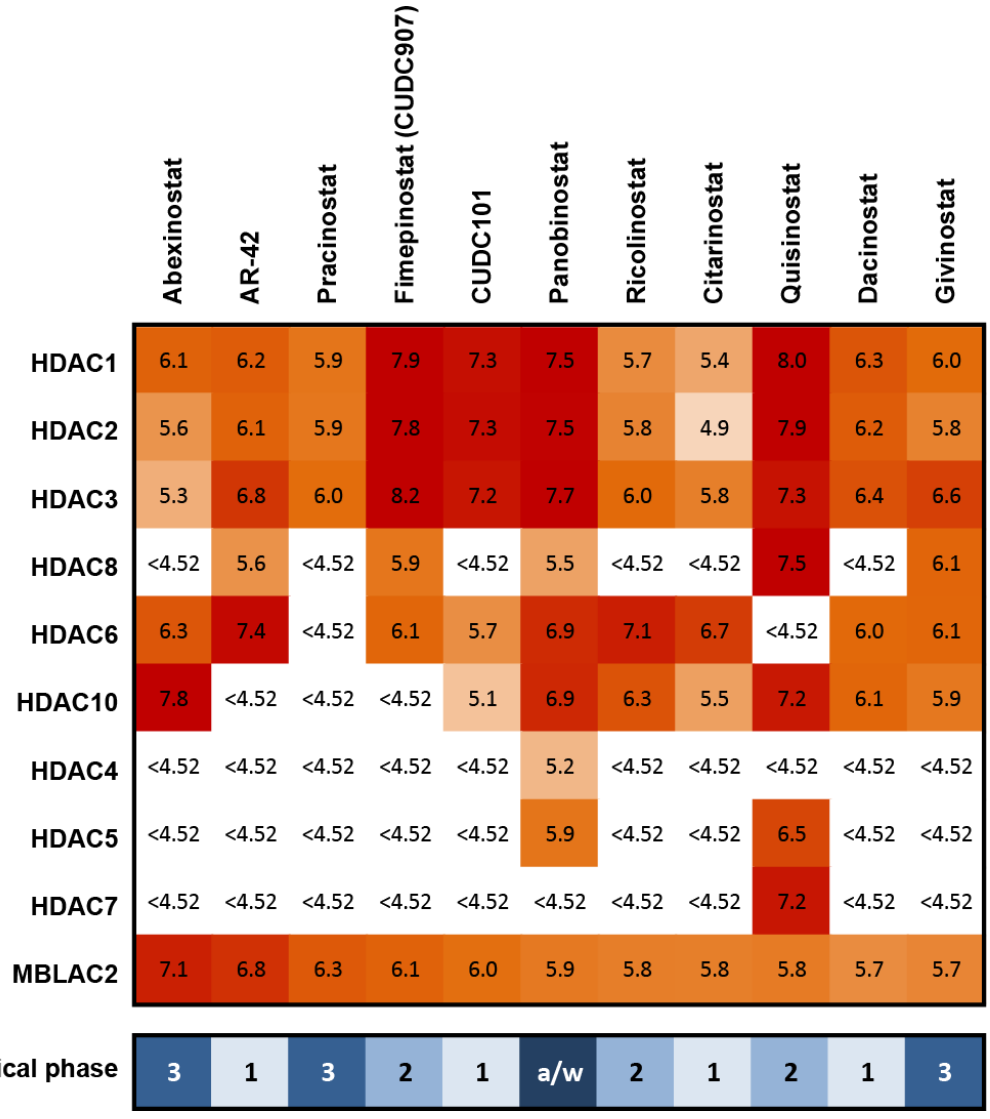

Fig. 25|Clinical phase HDAC inhibitors bound by MBLAC2. The heatmap shows the pK_d^{app} values as affinity measure for drug target interactions of HDACis. The highest clinical phase reached by the drug is indicated below (a: approved by FDA and EMA, w: withdrawn by FDA). The clinical phase information is derived from the drug repurposing hub (https://clue.io/repurposing-app). Givinostat has orphan drug status in the EU.

These findings directly raise the question of the clinical relevance of MBLAC2 inhibition. Our cell viability assay data on drug treatment in SW620 and HEK293 cells and MBLAC2 knockdown in HEK293 cells show that MBLAC2 inactivation is diminishing cell viability (publication 1[15]). Furthermore, the DepMap portal (https://depmap.org/portal/), which contains information on

the knockdown or knockout effects of a gene among hundreds of cancer cell lines, does not show any cell survival dependencies on MBLAC2. Moreover, MBLAC2 knockdown did not lead to changes in the proteome of HEK293 cells, indicating that there is no cell physiological perturbance that needs to be counteracted by up- or downregulation of other proteins[15]. Therefore, MBLAC2 inhibition as off-target effect of HDAC inhibitors most likely does not contribute directly to cancer cell killing. However, this does not preclude physiological effects of system-wide MBLAC2 inhibition in a whole organism. MBLAC2 has been shown to cleave acyl-CoA into the cofactor and the free fatty acid[239]. Further, MBLAC2 has been shown to interact with several proteins involved in vesicle generation or membrane-located biological processes, such as ZDHHC20, VAMP4, SLC9A6, and ATP11C[240]. MBLAC2 interaction with the zinc-finger DHHC-type palmitoyltransferase 20 (ZDHHC20) has been confirmed independently[239]. Interestingly, the palmitoyl-CoA substrate of ZDHHC20 is degraded by MBLAC2, which might hint at MBLAC2 being involved in regulating ZDHHC20 via locally depleting its substrate pool. Furthermore, the acyl-CoAs cleaved by MBLAC2 are the initial building blocks of ceramides, which serve as basis for the formation of the lipids sphingomyelin and hexosylceramides[241]. We showed that MBLAC2 knockdown or inhibition leads to an upregulation of sphingomyelins and a downregulation of hexosylceramides (publication 1[15]), which might cause significant tissue or cell type-specific effects. Importantly, we observed an accumulation of extracellular vesicles upon MBLAC2 knockdown or inhibition. This effect might either be caused by stimulated vesicle secretion or inhibition of vesicle uptake and might be linked to the observed lipidome remodeling. Either way, extracellular vesicles play a ubiquitous role in cell-cell communication between neurons, immune cells, or in the immune-cancer cross-talk. EVs support the immune response, for instance, by antigen presentation or in $CD8^+$ T-cell-mediated target cell killing via CD95L carrying vesicles[242, 243]. However, EVs also have been shown to serve as agents enabling tumor growth and metastasis as well as helping tumors to evade their destruction through the immune system. For instance, PDAC-secreted EVs carry tumor antigens and act as antibody decoys to scavenge tumor-targeted complement-mediated toxicity[244]. Other reports show how cancer cell EVs promote tumor growth[245] or support the formation of metastatic niches[246-248]. Further, evidence is piling up that exosomal PD-L1 suppresses anti-tumor immunity[249, 250]. Stimulation of extracellular vesicle secretion or inhibition of vesicle uptake could therefore have a direct clinical impact on cancer-immune cross-talk, and, hence, might be a beneficial or a detrimental MBLAC2 off-target activity. Most likely, MBLAC2-related off-target effects would not have been recognized as such in clinical settings, since commonly tracked adverse events would be overshadowed by the HDACi-related toxicity and potential MBLAC2-related parameters such as blood plasma EV counts are not routinely assessed.

Apart from HDAC inhibitors used in the oncology field, many of the purportedly selective HDAC6 inhibitors, which were now uncovered to be dual HDAC6/MBLAC2 inhibitors, have been investigated for their beneficial effects in neurodegenerative disease models. Since HDAC6 inhibition affects and stimulates axonal transport of vesicles[126, 129] and MBLAC2 might promote vesicle secretion, the dual inhibition could have synergistic effects on the trafficking and secretion of BDNF-containing vesicles. Due to the established roles of BDNF in neuronal survival, neurite outgrowth, and synaptic plasticity[251], this hypothetical synergy might contribute to the neuroprotective MoA observed for dual HDAC6/MBLAC2 inhibitors.

To better understand the potential effects of MBLAC2 inhibition, its molecular biological function needs to be studied. The most pressing questions are:

(i) What are the cellular substrates of MBLAC2?

(ii) Is the observed EV accumulation only a downstream effect of lipidome remodeling or does MBLAC2 play a specific role in one of the vesicle pathways?

(iii) If MBLAC2 regulates EV processes, does MBLAC2 inhibition affect endocytosis or exocytosis pathways?

The MBLAC2 inhibitors discovered here should support further research since they can be used to chemically knock down MBLAC2 function and investigate effects on endo- or exocytosis. Further, highly selective MBLAC2 inhibitors might be discovered in future chemoproteomic profiling studies of compounds related to the here discovered MBLAC2 inhibitors. Our study also provides a set of siRNAs for specific knockdown of MBLAC2. The availability of these tools should enable fundamental research about MBLAC2 cell biological functions[252]. Further, we have initiated the generation of an MBLAC2 knockout mouse within the international mouse phenotyping consortium. Here, knockout mice undergo standardized physiological tests to characterize the physiological impact of the knockout in a whole organism. Considering the versatile roles of extracellular vesicles in systems biology, MBLAC2 knockdown might indeed show effects in systems biology that cannot be observed in simple cell culture models. Once its biological role is characterized in more detail, MBLAC2 may constitute a drug target all by itself or it may turn out to be an off-target that better needs to be avoided in future drug development endeavors.

6 HDAC inhibitor off-targets with unknown drug-binding effects

MBLAC2 was not the only identified HDACi off-target. USP7 and USP40 were bound by Quisinostat with sub-micromolar affinity and Scriptaid potently bound to NQO2. Furthermore, ISOC1, ISOC2, ALDH1A1, ALDH1B1, ALDH2, and GATD3A were bound by Vorinostat and 8 chemically related drugs. The sites of drug binding and the influence of the off-targets' function are not known yet. Following chapters will outline why these findings are still of relevance.

6.1 Scriptaid binds NQO2

Scriptaid potently binds to NQO2 with submicromolar affinities as determined by chemoproteomic competition assays. The affinity probe iQ is specifically pulling down NQO2[15] (Fig. 26a,b). Scriptaid contains a naphthalimide capping group. This planar aromatic system possibly binds to NQO2's cofactor binding site by stacking onto the FAD cofactor, akin to the kinase inhibitors (e.g. Imatinib or Nilotinib) that bind and inhibit NQO2 as off-target[253, 254] (Fig. 26c). From a medicinal chemistry point of view, this would place naphthalimide as a potential pharmacophore for the development of NQO2 inhibitors, which are of interest for cancer treatment[255]. Further, confirming NQO2 inhibition by a naphthalimide would suggest that other naphthalimide-featuring drugs potentially inhibit NQO2 as well. Such drugs progressed into clinical trials but have not yet been subjected to in-depth drug target deconvolution (Fig. 26d).

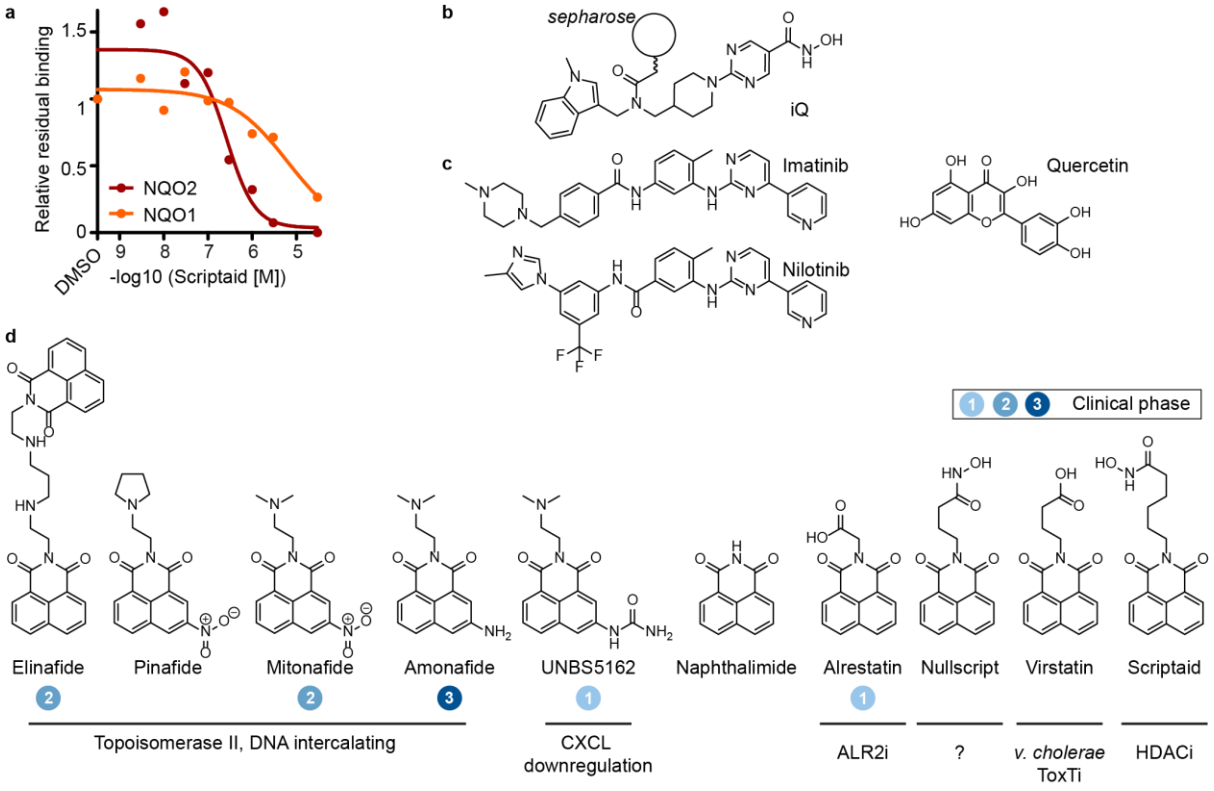

Figure 26| NQO2 is an off-target of Scriptaid. a, Scriptaid binding to NQO2 and NQO1 as determined by chemoproteomic competition assays (ref. [15]). **b,** Immobilized Quisinotat (iQ) pulls down NQO1 and NQO2 from cell lysates. **c,** Well known NQO2 binders and inhibitors Imatinib[253, 254, 256], Nilotinib[256] and Quercetin[254]. **d,** Naphthalimide-containing drug candidates that might feature NQO1 or NQO2 off-target binding similar to Scriptaid. For each drug candidate structures are depicted. Furthermore, information regarding the highest clinical phase stage reached and the purported drug mode of action is provided according to following references: Elinafide[257, 258], Pinafide[259, 260], Mitonafide[259, 261, 262], Amonafide[263], UNBS5162[264, 265], Alrestatin[266], and Virstatin[267-269]. ALR2i: Aldose reductase 2 inhibitor; ToxTi: inhibitor of transcriptional regulator ToxT.

Interestingly, it seems like NQO1 is also competed by Scriptaid at concentrations above 10 µM (Fig. 26a). This means that akin to kinobeads[270], iQ allows for chemoproteomics profiling of NQO1 and NQO2 binders. To collect further clues for the NQO2 binding mode of Scriptaid and iQ, a competition assay between iQ and reported inhibitors of NQO2, such as Imatinib or Quercetin[254, 256] (Fig. 26c), would indirectly show binding to the same site. From this finding, one could infer that Scirptaid also inhibits NQO2. In an alternative assay setup, Scriptaid would be expected to compete with kinobeads for NQO2 binding. In addition, NQO2 activity assays and co-crystal structures could demonstrate whether Scriptaid is inhibiting NQO2.

6.2 Common off-targets of Vorinostat-like drugs.

Nine of the 53 profiled HDAC inhibitors bound to the off-targets ISOC1, ISOC2, GATD3A, or ALDH2. Further experiments in different cell lysates suggest that these drugs also bind to other ALDHs, such as ALDH1A2[43] and ALDH1B1 (co-authorship 1[222]).
Six of those compounds, including clinical drugs (Vorinostat, Citarinostat, and Ricolinostat) bound more potently to ISOC2 than to any HDAC (Fig. 27a). Two drugs, Droxinostat and Bufexamac, bound to the off-targets ISOC1 (or ISOC1/2), GATD3A, and ALDH2, while showing no substantial HDAC target engagement at concentrations of up to 30 µM. Interestingly, most of the drugs binding to these off-targets have chemical characteristics common to the Vorinostat pharmacophore (Fig. 27b). This is a hydroxamic acid warhead, linked via a flexible alkyl-chain to an aromatic capping group. This pharmacophore is mimicked by the affinity probe iA (Fig. 27b), albeit the iA is missing the aromatic capping group. The direction of the amide bond in iA is reversed compared to Vorinostat but in line with the most potent ISOC2 binder Ricolinostat.

a

	ISOC2	ISOC1	ALDH2	GATD3A	HDAC1	HDAC2	HDAC3	HDAC6	HDAC10	MBLAC2
Ricolinostat	8.1	6.0	6.3	5.1	5.7	5.8	6.0	7.1	6.3	5.8
Vorinostat	7.8	6.8	6.3	5.8	6.0	6.0	6.8	6.7	5.9	<4.52
Scriptaid	7.4	5.5	6.5	4.6	5.5	6.3	7.4	7.7	<4.52	5.0
M344	7.4	6.1	6.4	5.8	4.9	5.6	5.7	6.7	5.7	<4.52
LMK235	7.2	6.1	6.1	<4.52	6.6	6.6	7.0	6.4	5.8	<4.52
Citarinostat	6.4	<4.52	5.8	5.7	5.4	4.9	5.8	6.7	5.5	5.8
CUDC101	6.0	<4.52	4.7	<4.52	7.3	7.3	7.2	5.7	5.1	6.0
Droxinostat	5.5	5.8	6.0	5.6	<4.52	<4.52	<4.52	<4.52	<4.52	5.3
Bufexamac	<4.52	5.4	6.2	5.8	<4.52	<4.52	<4.52	<4.52	<4.52	<4.52
CAY10603	<4.52	<4.52	<4.52	<4.52	5.7	5.8	5.6	6.4	<4.52	5.6
Tubacin	<4.52	<4.52	<4.52	<4.52	<4.52	<4.52	<4.52	5.8	<4.52	5.8
WT161	<4.52	<4.52	<4.52	<4.52	<4.52	<4.52	<4.52	6.1	<4.52	6.0

b

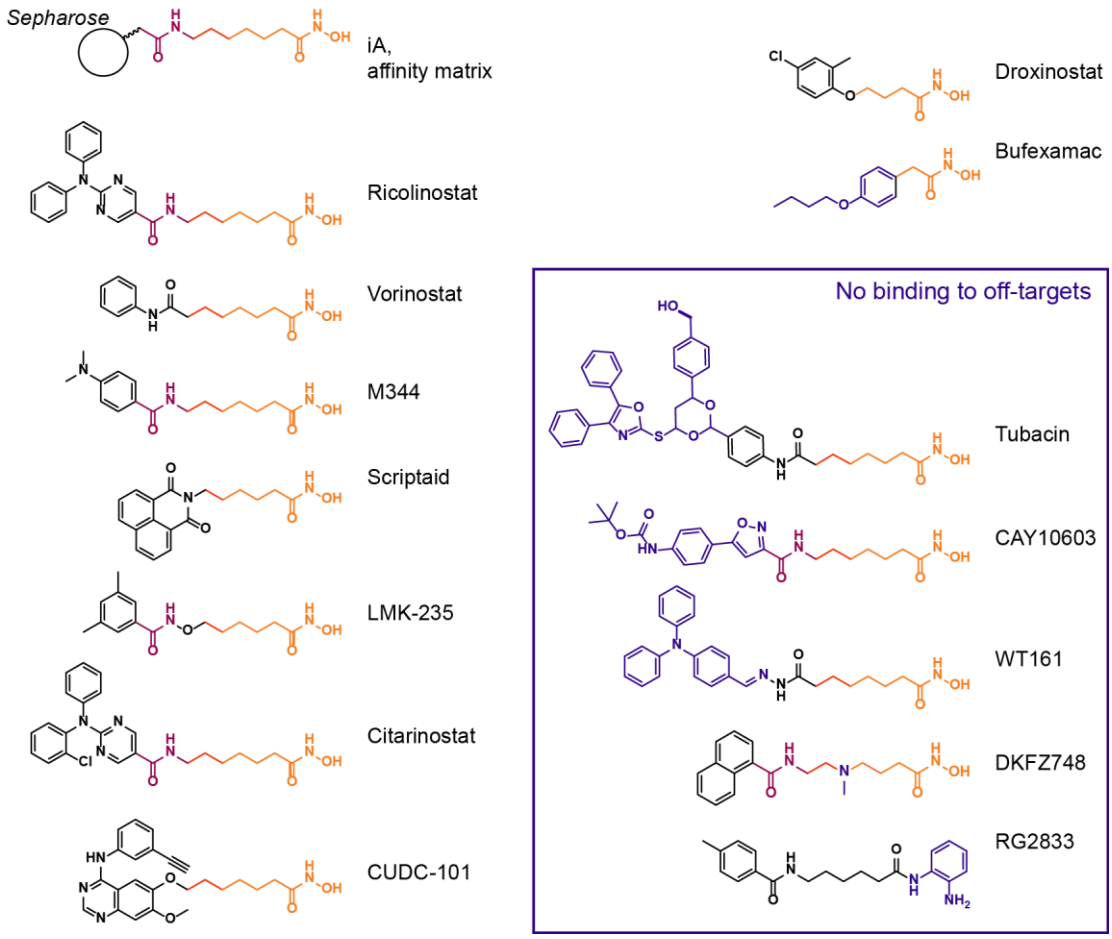

Fig. 27|Vorinostat-like drugs share the same off-target space. a, pK_d^{app} values as a measure for drug affinity as determined in the chemoproteomic HDACi profiling study (publication 1[15]). **b**, Structure of the iA affinity matrix responsible for the pulldown of the ALDH, ISOC, and GATD3A off-targets. Further shown are structures of drugs that are considered "Vorinostat-like" (on the left), structures of drugs that only share minimal similarity with Vorinostat but still bind the off-targets (Bufexamac and Droxinostat), and structures of Vorinostat-related molecules Tubacin, CAY10603, WT161, DKFZ-748, and RG2833 that lost binding affinity to the off-targets but still bind to HDACs. The molecules are sorted for decreasing ISOC2 affinity. The most common pharmacophore of off-target binders is a hydroxamic acid warhead attached to a C4 (orange) or extended C6 (orange and red) alkyl linker. The amide bond in the same distance and direction as in the affinity matrix iA is present in many off-target binding drugs and highlighted (magenta). Moieties that are unique for drugs not binding to ISOC2 and might cause the affinity loss are highlighted in blue.

Some drugs related to Vorinostat lost their affinity to off-targets (Fig. 27). Moreover, the introduction of a tertiary amine into the alkyl linker of Vorinostat-like drugs abrogates affinity to all off-targets as well as HDACs except for HDAC10 (co-authorship 1[222]). Further, HDACis that have an aminoanilide warhead instead of the hydroxamate, or a bulkier and less flexible linker (Fig. 28) can not bind the off-targets. These data, therefore, add informative details to off-target structure affinity relationships.

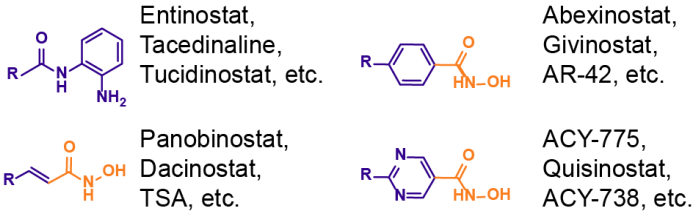

Fig. 28|HDACi warheads that, in contrast to the Vorinostat-like warhead, lead to a complete loss of affinity to ISOCs, ALDHs, and GATD3A. Listed are a few drug examples featuring the warhead motif precluding off-target binding.

Bufexamac and Droxinostat do not perfectly match the pattern since they feature a short alkyl-linker between the hydroxamic acid and an aromatic capping group. Therefore, they might alternatively bind in a different orientation, independent of the hydroxamic acid, via their common butoxybenzene pharmacophore (Fig. 29).

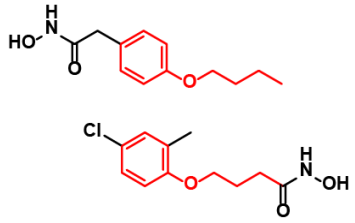

Fig. 29|A shared pharmacophore of Bufexamac and Droxinostat. The shared pharmacophore (red) that might be relevant for their off-target affinity independent of the hydroxamic acid motif.

It is surprising, that off-targets bound by Vorinostat-like drugs stem from unrelated protein families (ISOCs = isochorismatase-domain containing proteins, ALDHs = aldehyde dehydrogenases, GATD3A = Glutamine amidotransferase-like domain). This observation suggests that ALDHs, ISOCs, and GATD3A have a binding pocket with similar three-dimensional physicochemical properties, which are suitable to harbor the Vorinostat pharmacophore. Interestingly, all of the off-target proteins are known or predicted to harbor a reactive cysteine residue in their active site. Strikingly, ALDHs, ISOCs, GATD3A, and the GATD3A-related deglyoxalase PARK7 (DJ-1) belong to a target space that is also shared by drugs of a pharmacophore entirely unrelated to the Vorinostat-like drugs (Fig. 30a). The drugs feature an N-cyano pyrrolidine reactive warhead, which probably binds to the reactive amino acid cysteine located in the active site (Fig. 30b,c). While the hydroxamic acid is unlikely to covalently react with a cysteine, the big overlap in off-target space supports the idea of a similar binding pocket shared between those enzymes. Assessing binding competition between iA and N-cyano pyrrolidines might provide evidence for both pharmacophore classes binding to the same binding site, which in the case of N-cyano pyrrolidines is probably located around the active site cysteine.

a

	Panyain, *et al.*, 2021	Kooij, *et al.*, 2022	Grethe, *et al.* 2011	Grethe, *et al.* 2011
ISOC1				
ISOC2				
UCHL1				
ALDH1A2				
ALDH1B1				
ALDH2				
GATD3A				
PARK7				
lysate	HEK293	HEK293	HEK293	HEK293
Probe	MT16205	11RK72	GK16S	GK13S

b

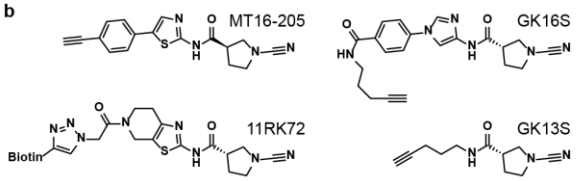

c

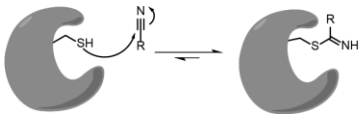

Fig. 30|Summary of a literature survey about chemically related covalent inhibitors that bind the same common off-target space as Vorinostat-like drugs. **a**, accumulating evidence that N-cyano pyrrolidine probes bind to binding ALDHs, GATD3A, PARK7, and ISOCs[271-273], similar to Vorinostat-related drugs. Blue field: the protein was amongst the significantly targeted proteins. N-cyano pyrrolidine compounds were designed as UCHL1 binders. **b**, structures of the N-cyano pyrrolidine probes used in the papers. **c**, proposed binding mode of N-cyano pyrrolidine to active site cysteines[273].

What is the effect of HDACi binding to these off-targets? Even though ALDHs and ISOCs have been found to be bound by Vorinostat in other studies (Fig. 31a)[43, 274, 275], cellular effects resulting from the binding event have never been addressed. Importantly, an in cellulo binding assay using a Vorinostat-based photo-affinity labeling probe showed in cellulo target engagement with ISOC1 and ISOC2[275]. The ISOC2 binding was confirmed by nanoBRET[275]. Drug binding as determined by the chemoproteomic competition assay is therefore unlikely to be an assay artifact and happens in cells. Considering that Vorinostat is an approved drug, it is relevant to understand whether drug binding affects the cellular functions of the off-targets. Biological roles of ISOCs are still unexplored, which complicates the investigation of drug-binding effects. Substrates have been identified for ALDHs[276] and most recently also for GATD3A[277] (Fig. 31b), which should allow to probe inhibition of their enzymatic function by Vorinostat in enzyme activity assays.

a

	in lysate				in cellulo
	Lechner, *et al.*, 2022	Steimbach, *et al.*, 2022	Bantscheff, *et al.* 2011	Fischer, *et al.*, 2011	Ohana, *et al.*, 2021
ISOC1					
ISOC2					
ALDH1A1					
ALDH1A2					
ALDH1B1					
ALDH2					
GATD3A					
PARK7					
lysate	SW620&MV4-11	BE(2)-C	K562	HEPG2	K562

b

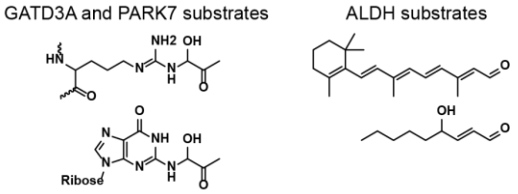

Fig. 31|Summary of a literature survey about off-targets bound by Vorinostat (and Vorinostat-derived probes). a, Accumulating evidence for ISOCs and ALDHs as potential HDACi off-targets emerges from several publications (blue fields). [15, 43, 222, 274, 275]. The binding effects have never been addressed in these studies. PARK7 (DJ-1) is a close relative to GATD3A with similar catalytic activity[277]. **b**, Structures of known substrates of ALDHs, GATD3A, and PARK7.

Even if Vorinostat-like drugs do not inhibit ISOCs, ALDHs, or GATD3A, the knowledge about this binding event can still be useful. For instance, it could be used to develop degraders of these proteins (PROTACs) or other proximity-inducing chimeras that direct the enzymatic activity of ISOCs or GATD3A to target proteins or locations in a cell. Drug target co-crystal structures would help to better understand these binding events and to find a way of developing Vorinostat-derived molecules for new purposes.

6.3 Further potential off-targets

Even though our AfBPP approach produced the most comprehensive target landscape of HDACis to date, we might still miss off-targets of certain HDACis. As mentioned before (see 1.1.2), this can be due to low expression of these off-targets in the used lysate or due to low affinity to the probes of the affinity matrix (iQ, iA, and iC). Potential off-targets of HDAC inhibitors discovered in previous studies should not stay unmentioned and are reviewed in the next paragraphs.

While PCI-34051 selectively bound HDAC8 in our study[15], TPP experiments performed in lysate of HL-60 leukemia cells identified leucine aminopeptidase 3 (LAP3) as additional off-target of PCI-34051 ($pEC50^{HDAC8}$=6.4 and $pEC50^{LAP3}$=5.9)[278]. LAP3 is a cytosolic metallohydrolase and is directly inhibited by PCI-34051[278]. These observations pose the question, of whether the observed anti-cancer effects of PCI-34051[123] are mediated by HDAC8 inhibition, LAP3 inhibition, or a combination thereof.

Another study applied TPP to discover the potential Panobinostat off-targets TTC38, FADS1, FADS2, ZNF148, and PAH in HepG2 cells[26]. TTC38 and FADS1 thermal stabilization by Panobinostat was confirmed in rat tissue[279]. TTC38 binding was further shown in PBMCs from human blood, and ZNF512, as well as ZNF148, were stabilized by Panobinostat (and Vorinostat) in human blood cells[279]. DHRS1 was stabilized only in tissue lysate and might actually be bound by products generated during Panobinostat metabolism[278, 279]. Whether Panobinostat directly binds these off-targets and whether it affects the function of these proteins remains to be confirmed. Only for PAH, AfBPP in combination with enzyme activity assays confirmed that Panobinostat and the related HDACi Belinostat bind and inhibit this off-target[26].

Belinostat was also found to either directly bind the metallo-phosphatase PP2BA (PPP3CA or calcineurin A) or to bind an interactor of PP2BA with only about 10-fold lower affinity than its designated targets HDAC1-3 and HDAC6[43]. PP2BA is a calcium-dependent phosphatase with central roles in intracellular Ca^{2+}-signaling[280] and targeted by several approved drugs[281]. When Ca^{2+} reaches high concentrations, Calmodulin binds and activates PP2BA. The presence of a metal ion cofactor in the active site of PP2BA points to direct co-factor chelation by Belinostat, akin to its HDAC binding mode. Interestingly, however, Belinostat was found to induce PTM signatures in A549 cells similar to the signature of the Calmodulin binder KN-93[282]. KN-93 is claimed to bind Ca^{2+}/Calmodulin and to prevent its interaction with and activation of CAMK2A (CaMKII)[283]. Of note, Belinostat shares a common N-phenylbenzenesulfonamide pharmacophore with KN-93 (Fig. 32). These data hint at the possibility, that Calmodulin, a PP2BA interactor, is the common direct off-target of Belinostat and KN-93.

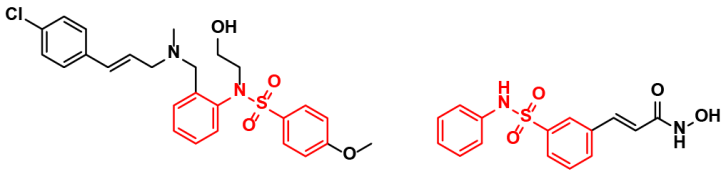

Fig. 32|Belinostat and KN-93 share a common N-phenylbenzenesulfonamide pharmacophore. Structures of the approved HDACi Belinostat and the frequently used tool-compound KN-93, which impedes CAMK2A activation via Ca^{2+}/Calmodulin. The shared N-phenylbenzenesulfonamide pharmacophore, which might explain the closely matching phenotypic signature of these compounds in A549 cells[282], is highlighted in red.

Moreover, there is evidence that some aminoanilide HDACis affect microtubule stability or dynamics. The aminoanilide-type HDAC inhibitor Domatinostat (4SC-202) inhibits microtubule formation similar to Nocodazole[19, 56]. Interestingly, another aminoanilide-type inhibitor, LT-548-133-1 has been reported to inhibit microtubule polymerization as well, while other related HDAC inhibitors such as Chidamide (Tucidinostat) were not affecting microtubules[55] (Fig. 33).

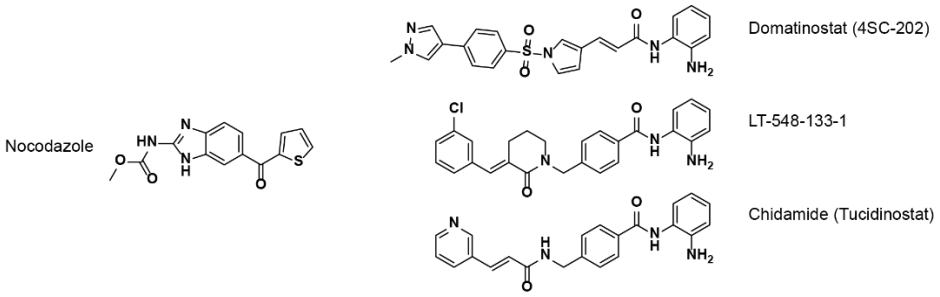

Fig. 33| Microtubule dynamics or stabilization are directly affected by certain HDAC inhibitors. Structures of the known microtubule inhibitor Nocodazole, HDAC inhibitors with reported microtubule inhibitory activity (Domatinostat and LT-548-133-1), as well as a related aminoanilide-type HDAC inhibitor without effects on microtubule (Chidamide).

Overall, evidence for additional off-targets exists, but the effect of binding events is rarely evaluated.
Finding out the clinical relevance of these binding events requires further in-depth investigations.

7 Updating the list of selective chemical probes for HDAC research

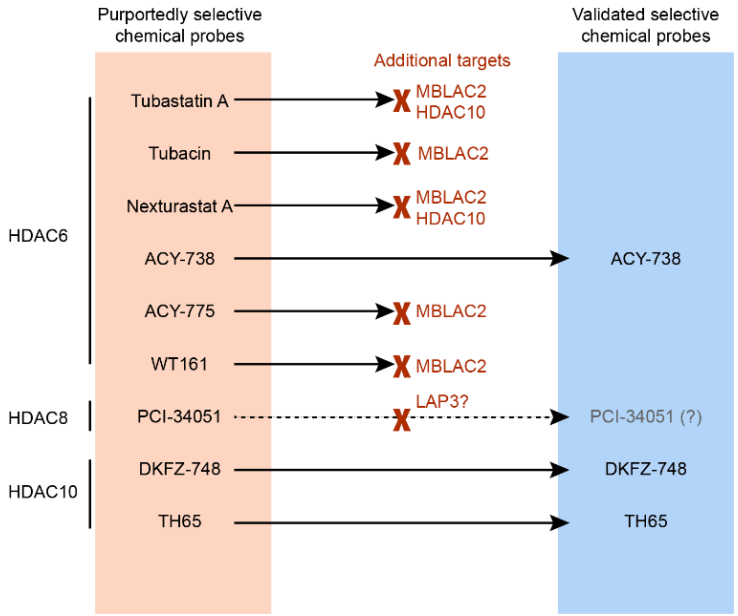

Fig. 34|Most of the previously claimed selective inhibitors lost their chemical probe status due to hitting newly discovered targets. MBLAC2 was discovered as a common off-target in publication 1[15]. HDAC10 was reported as off-target of Tubastatin A and Nexturastat A in ref.[192] and then validated in publication 1[15]. LAP3 was discovered as potential PCI-34051 off-target in ref.[278].

Although, our findings uncovered a lack of selectivity for most purportedly selective probes, the set of profiled molecules also contained three selective compounds (Fig. 34). ACY738 appears to be the only potent and selective HDAC6 inhibitor amongst all 53 profiled HDAC inhibitors. PCI-34051 was found to only bind HDAC8 in our data. However, it was reported to also bind and inhibit another off-target LAP3 (see chapter 4.6). Moreover, we serendipitously discovered TH65 as a selective HDAC10 inhibitor. TH65 was designed as *schistosoma mansonii* smHDAC8 inhibitor and has never been assessed for its binding to human HDAC10[284]. At the time of profiling, no selective and commercially available HDAC10 inhibitor was reported. Of note, our chemoproteomic profiling technology was later employed to contribute to the discovery of the highly potent and selective HDAC10i DKFZ-748[222]. This new entity proved in cellulo activity and now presents the tool of choice for studying HDAC10 functions in cells. Indeed, DKFZ-748 could already be leveraged to prove the in cellulo polyamine deacetylase activity of HDAC10[222]. In future studies, it could help to clarify, whether HDAC10 is additionally deacetylating protein substrates. LC-MS/MS-based deep analysis of the acetylated proteome after treating cells dose-dependently with DKFZ-748 could disprove or substantiate this hypothesis (see chapter 1.2.3, Fig. 14, and co-authorship 3[228]).

8 Creating a drug repurposing opportunity: Lipoic acid for 'HDAC-linked diseases' and HDAC inhibitors for 'lipoic acid-linked diseases'

Lipoic acid (LA) (Fig. 35a) has been approved for the treatment of diabetic neuropathy since the 1960s. Racemic (*R*/*S*)-LA and enantiomerically pure (*R*)-LA experience wide 'off-label' use as antioxidant in nutritional supplement pills. However, it has never been attempted to identify protein targets of lipoic acid. This might be owed to the fact that, when LA was approved as a drug, chemoproteomic target deconvolution methods did not exist, and, since then, its vaguely-defined anti-oxidant properties could be adduced as potential explanation for versatile phenotypes. Indeed, while more than 170 studies about lipoic acid were published alone in 2022 (Fig. 35b), most of the studies try to relate the putative antioxidative features to LA's cell biological effects.

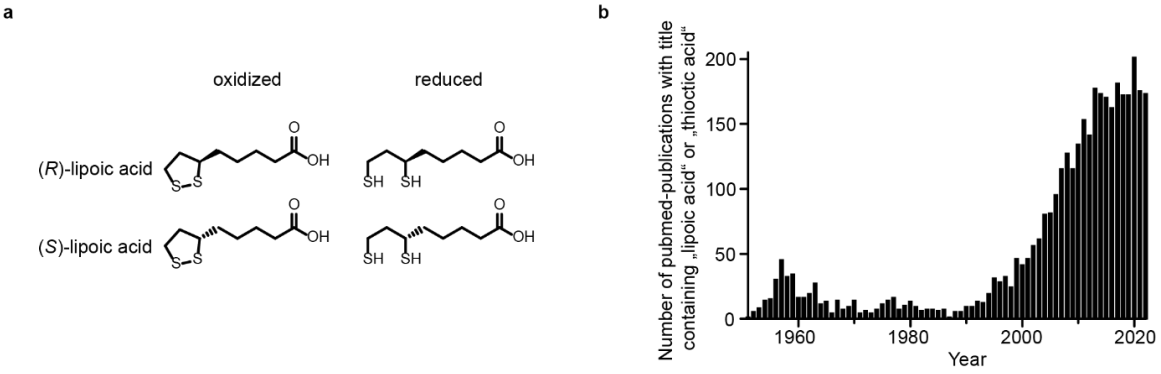

Fig. 35|Lipoic acid structure and the scientific interest in the molecule(s). a, Structures of the reduced and oxidized forms of the lipoic acid enantiomers. The racemic form, a 1:1 mixture of the enantiomers, or the pure (*R*)-enantiomer of are used as drug or food supplement. **b,** The number of papers published with "lipoic acid" or its alternative name "thioctic acid" in publication titles steadily increased over the last decades and now seems to reach a plateau of about 170 publications per year (data from pubmed).

Despite the high number of studies that try to understand lipoic acid's mode of action, the molecular mechanism of its purportedly antioxidative effects has not been explained in detail. Interestingly, lipoic acid is readily reduced in cells[285] and thereby initially consumes reductive power rather than increasing it. One hypothesis about its antioxidative effect has been related to its reactivity with reactive oxygen species (ROS)[286-288], which might allow scavenging of ROS molecules before they damage critical endogenous molecules. However, recent expert reviews have argued that small molecule scavengers are irrelevant in turning over ROS compared to the capabilities of the enzymatic machinery[289-291]. Nevertheless, lipoic acid can chelate ferrous or cuprous ions that serve as catalysts in the superoxide radical generating Fenton reaction[289-291], and might thereby prevent the generation of ROS.

The work on metal-chelating drugs 2022 (publication 1[15]) showed the strong zinc-chelating properties of the thiol group, which is featured in the most potent HDAC inhibitor Romidepsin. This observation led to the hypothesis that lipoic acid might also act via binding and inhibiting metallo-enzymes. Using chemoproteomic target deconvolution with a tailored lipoic acid-based affinity matrix, HDACs were identified as the only protein targets of (LA) and its close analog lipoamide (LM) (publication 2).

(*R*)-LA binds and inhibits HDAC in vitro with EC50s in the range of 3-30 µM, and in cellulo with EC50s in the range of 100-500 µM (publication 2). In literature, effects of lipoic acid on cells are often investigated at doses in the range of 0.5-5 mM. Hence, observed in vitro phenotypes are certainly in part driven by HDAC inhibition. The peak plasma concentration in patients is in the range of 500 µM using the highest dosing schemes, suggesting that substantial HDAC inhibition can be reached in patients. Particularly in tissues with high exposure, such as the intestine, blood,

and blood epithelium, concentrations of lipoic acid that lead to HDAC inhibition are likely to be reached. Downstream effects of HDAC inhibition thereby provide explanations for lipoic acid's phenotypic effects independent of its redox-modulating properties. For instance, HDAC inhibition directly explains LA-mediated HDAC6 substrate hyperacetylation (ref.[292] and publication 2) or LA-prevented stress granule formation (ref.[165] and publication 2). Of note, the forefront of the response to ROS is regulated via increased transcription or activation of redox enzymes, e.g. mediated via the KEAP1-NRF2 axis[289]. HDACs as part of the core transcriptional regulators might come into play during the transcriptional response to ROS. HDAC inhibitors (such as LA) might thereby impact the regulation of proteins of the ROS-response. Hence, the observed antioxidant effects of lipoic acid may be explainable by HDAC inhibition. Interestingly, lipoic acid and HDAC inhibitors have been studied for their beneficial effects on an overlapping range of diseases. Ricolinostat, a drug with an HDAC selectivity profile comparable to lipoic acid, is currently in phase II studies for diabetic neuropathy, a disease with formal approval of lipoic acid (publication 2). This suggests that LA might be an interesting alternative to HDACis and vice versa. Due to its proven safety, LA might replace HDAC inhibitors as alternative treatment option. Repurposing of lipoic acid should be feasible since it is an approved drug, is used as food supplement, has been studied extensively in clinical trials, and has a well-established pharmacokinetics profile.
However, the low bioavailability, plasma half-time, and potency of LA might actually explain, why many clinical trials did not result in convincing drug efficacy. In other words, HDAC inhibition-related effects observed at high and long-lasting exposure to lipoic acid in cell culture models might not have been recapitulated in patients because of too low dosing and low half-life of lipoic acid. If this is the case, enantiomerically pure (*R*)-LA, higher doses, or more frequent administration of lipoic acid could help to improve efficacy. Alternatively, well-established HDAC inhibitors such as Vorinostat could be considered to replace LA in disease context, where LA showed beneficial pre-clinical effects.
However, before translating these findings into clinical applications, we need to understand whether and to what extent HDAC inhibition is responsible for the phenotypes attributed to lipoic acid. Fortunately, our study uncovered that HDACs are only inhibited by (*R*)-LA and not by the enantiomer (*S*)-LA. Importantly, both enantiomers feature the same redox, metal-chelating, and ROS-scavenging properties. This finding now enables researchers to use the enantiomerically pure forms of (*S*)-LA and (*R*)-LA to differentiate between phenotypes dependent or independent of HDAC inhibition. Such experiments should help to clarify, whether either one of the effects has more clinical relevance or whether the combination of the effects is important.

Interestingly, lipoamide shows a similar but more potent HDAC inhibition profile compared to lipoic acid. In theory, lipoamide should feature the same antioxidant properties. However, lipoic acid (or thioctic acid) has been subject of 193 clinical studies (according to clinicaltrials.gov, as of March 2023), while lipoamide (or 6,8-dithiooctanoic amide) has not a single record. The amide form might allow better uptake into the cell and stabilize the molecule from beta-oxidation, which is a major degradation pathway of long-chain carboxylic acids, including lipoic acid[293]. Lipoamide has been shown to reproduce (*R*)-Lipoic and (*R*/*S*)-lipoic acid effects in terms of intracellular HDAC inhibition and prevention of SG formation (ref. [165] and publication 2). These findings might suggest to enroll clinical trials with lipoamide as alternative to lipoic acid.
If it turns out that both, the antioxidant properties of lipoic acid's five-membered disulfide 1,2-dithiolane and in addition, its HDAC inhibition have synergistic effects in certain disease states, our data might also inspire medicinal chemists to synthesize a series of (*R*)-lipoamide-derived molecules that might have increased HDAC affinity, plasma half-time, bioavailability, and at the same time keep lipoic acid's antioxidant features. Fig. 36 shows a few proposed examples. N-phenyl-(*R*)-lipoamide (derivative A) could be readily synthesized via amidation of lipoic acid.

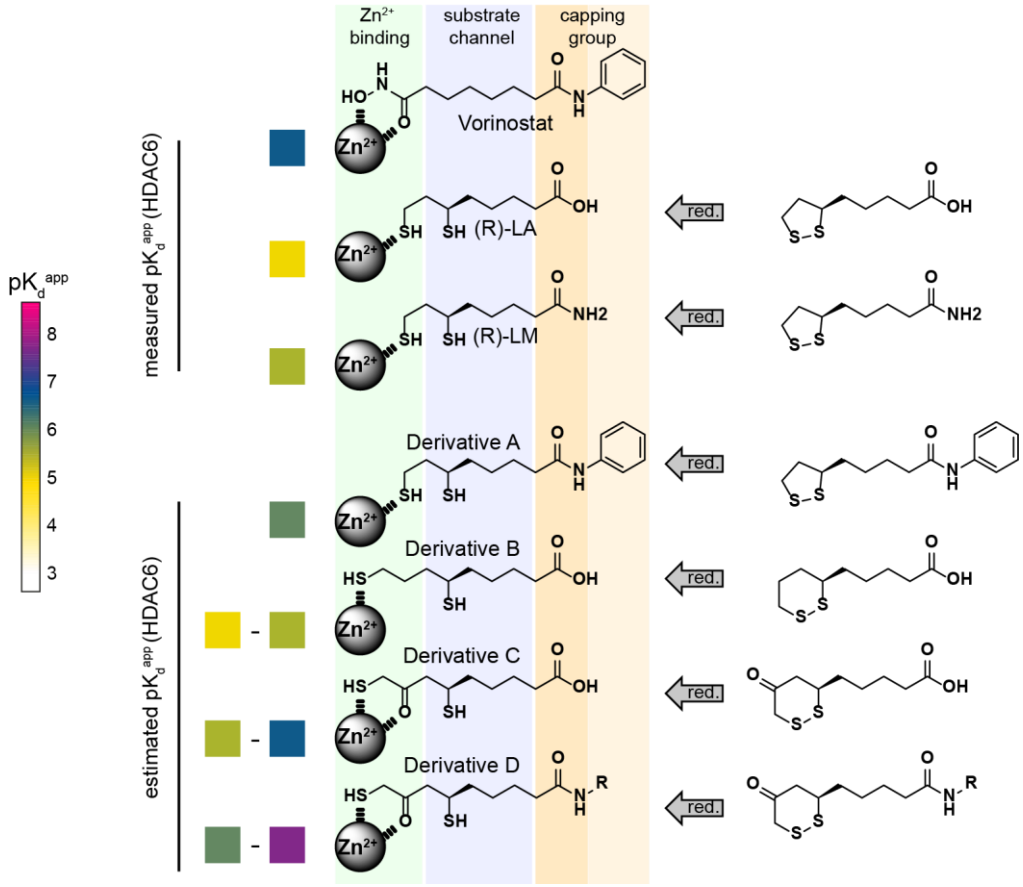

Figure 36|Proposed lipoic acid derivatives with improved affinity and pharmacokinetics. Structure of Vorinostat and the oxidized and reduced forms of lipoic acid and novel derivatives proposed in this thesis. The structures are aligned to the amide bond of the Vorinostat capping group. Measured pK_d^{app}s are indicated according to publication 1[15] and 2. Lipoic acid derivatives' affinity to HDAC6 is predicted considering the presumable affinity increase by (i) switching from acidic to amide capping group (inspired by higher potency of lipoamide compared to lipoic acid), (ii) larger capping groups for additional target interactions (inspired by Vorinostat), and (iii) changing from mono- to bidental zinc chelation. The proposed lipoic acid derivatives are not commercially available and might be challenging to synthesize.

This work on lipoic acid hopefully lays the foundations for answering clinically relevant questions regarding lipoic acid's mode of action, for potential drug repurposing endeavors, and for inspiring future drug designs.

9 The value of affinity-based protein profiling for (off-) target identification

AfBPP was used in publication 1 and 2 as well as co-authorships 1 and 2 for the target deconvolution and selectivity profiling of drugs. AfBPP allowed to map the most comprehensive target landscape of HDAC inhibitors and uncovered HDACs as the hitherto unknown targets of lipoic acid. Further, hit molecules for several so far undrugged targets were discovered. First of all, MBLAC2 was found to be inhibited by a range of drugs and notably quite selectively by Nexturastat A (publication 1)[15]. Second, target deconvolution of the dedicated SIRT5 inhibitors GC220, GC232, and Balsalazide revealed glutaryl-CoA dehydrogenase GCDH and the mitochondrial nucleoside diphosphate kinase NME4 as novel targets of these molecules (co-authorship 2[229]). Since no binder of these proteins has been published so far, these molecules provide a starting point for the development of first-in-class NME4 or GCDH targeting agents. Both projects, therefore, contributed to the extension of the proteome addressable by small molecules. Overall, the off-targets discovered in this project are yet another reminder that drugs are often less selective than claimed in original reports. Moreover, they showcase chemoproteomic AfBPP as the method of choice to unmask the lack of drug selectivity and to identify off-targets. In regard to HDACi selectivity profiling, other methodologies such as enzyme activity or nanoBRET assays are incapable of revealing such surprises since they only determine binding affinity to a pre-defined and limited set of presumed targets. Other powerful methods to globally study intracellular drug effects such as dose-dependent PTM profiling (ddPTM aka decryptM, co-publicaship 3[228]) or proteome perturbance fingerprinting[13] may not have identified most of the off-targets discovered in the underlying studies for several reasons:

(i) Off-target effects are overshadowed by cellular perturbations that are induced by on-target effects (i.e. large perturbations through pleiotropic downstream effects of HDAC inhibition).
(ii) Off-target inhibition does not lead to a perturbance of the investigated PTM or protein expression landscape (as shown for MBLAC2 knockdown[15]).
(iii) The (off-) target binding does not lead to inhibition of the (off-) target and therefore does not induce a measurable cellular perturbance.

Importantly, chemoproteomic (AfBPP) competition assays can identify any target binding event and not only active site binding (i.e. inhibition) events. Allosteric binding events that do not substantially affect the targets' activity are easily overlooked with any other methodology that probes drug effects instead of drug binding. With the advent of targeted protein degradation, simple binding events can pose a valuable starting point to tackle an undrugged protein by a PROTAC. Moreover, simple drug binding that does not affect the target's functionality can be a vantage point for other purposes, e.g. where active enzymes should be recruited to neo-substrates. For instance, one could imagine to recruit a deubiquitinase (DUB) to remove a substrate's ubiquitin chain and thereby prevent the substrate from degradation. Such a bifunctional DUB recruiter needs to retain the deubiquitinase activity and thus must not bind to the active site. AfBPP is therefore the method of choice for identifying target proteins directly bound by non-covalent drugs.

10 Shortcomings of chemoproteomics-based selectivity profiling and target deconvolution

As outlined above and in the introduction, chemoproteomics-based AfBPP has several key advantages over other drug target deconvolution approaches and has led to many impactful target identification and selectivity profiling studies (see for example ref.[15, 26, 43, 44, 50, 51, 54, 60, 222, 270]). Despite these success stories, AfBPP comes with a few shortcomings that shall not stay unmentioned.

First, it should be noted that the pK_d^{app}s and selectivity profiles of drugs derived from chemoproteomic AfBPP studies do not necessarily correlate perfectly with in cellulo or in vivo apparent pK_ds. This might have several reasons. First of all, drugs have been shown to accumulate in certain subcellular regions such as in specific molecular condensates[118] or organelles (Fig. 37). If one target is located in such a region with high drug concentration and another target is located in a drug-depleted cellular region, the in cellulo apparent pK_d will be influenced accordingly. For instance, if two targets located in different regions show the same binding affinity in vitro, their apparent in cellulo pK_d would be shifted by the ratio of local drug concentration. In other words, if a drug is 100-fold higher concentrated around target A than around target B, the apparent in cellulo K_d for target A will be 100-fold lower than for target B, even if both targets have actually the same binding affinity to the drug. Similar considerations are valid for localization of targets in different cellular organelles. Further, pK_d^{app}s determined in cell lysate can differ from in cellulo pK_d^{app}s since concentrations of co-factors, substrates, and ions that compete for drug binding or influence the protein structure, are perturbed. Finally, unselective protease inhibitor cocktails, which are routinely added in high concentrations to the lysate to keep the proteins intact, might unspecifically bind to many targets and affect their affinity to assayed drug molecules.

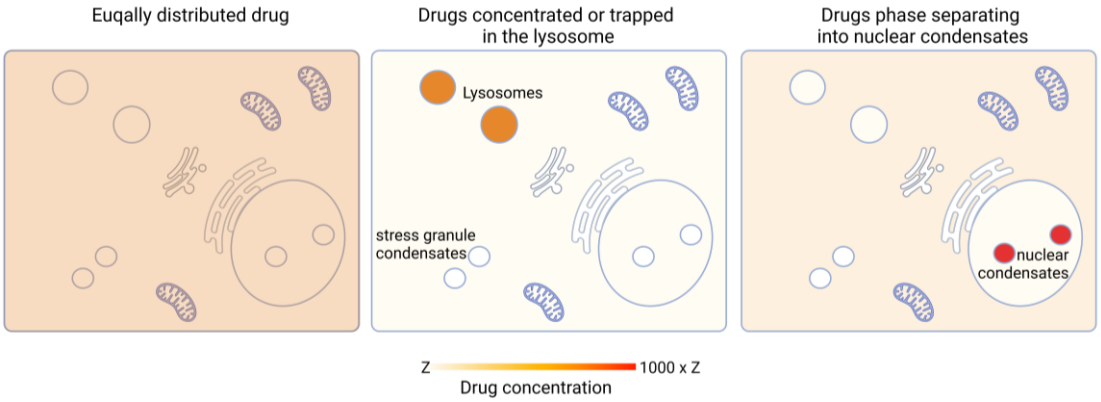

Fig. 37|Schematic of three exemplary scenarios of intracellular drug distribution. Drugs can be equally distributed but also highly concentrated in membrane-enclosed organelles such as the lysosomes or in molecular condensates. Similarly, drugs can be excluded from certain organelles such as mitochondria, or from other molecular condensates. Depending on whether the target is located in a cellular region with high or low drug concentration, the concentration required to reach the in cellulo half-maximal drug effect (EC50) may vary by several orders of magnitude. The figure was created with Biorender.

A second shortcoming, as mentioned before, is that every assay employed for drug target deconvolution, including AfBPP, has its blind spots. Therefore, the existence of additional off-targets can never be ruled out. In the following, a few reasons for incomplete target identification in an AfBPP experiment are listed.

(i) Physiologically relevant off-targets might not be present in the sample. This can be because of the low expression of the target in the cell line or tissue used for target deconvolution. For instance, Panobinostat has been profiled for its target space by chemoproteomic competition assays in three papers[15, 26, 43], but phenylalanine hydroxylase has only been identified as off-target in HepG2 liver cancer cells, which robustly express this metabolic enzyme[26]. Additionally, experiments in cell lysates do not probe binding to extracellular (secreted) proteins, since those are washed away together with the medium before the cells are harvested.

(ii) AfBPP assays are based on drug molecule derivatives equipped with a chemical handle (affinity matrix) and can only detect targets that bind to the affinity probe. The attachment of the chemical handle can cause a reduction or complete loss of target affinity and therefore loss of information about this target (see 1.1.2).

(iii) Assays working in cell or tissue lysates can be blind for identification of drug targets that are hit by a metabolized form of the drug. For instance, the enzyme SULT1A1 has been shown to attach a sulfonate group onto alcohol moieties of pro-drug molecules. Only in intact cells or tissue with active enzymes and sufficient co-factor pools, SULT1A1 transforms the pro-drug into a reactive molecule that covalently binds to a range of target proteins[294].

(iv) Chemoproteomic methods, including AfBPP, only probe for target binding or other effects visible on the proteome scale. Other biomolecular targets are missed. For instance, RNAs are frequently forming stable three-dimensional structures that can be targeted by drugs impeding the RNA's function or its processing into functional forms. Hence, RNAs pose potential off-targets of drugs. This is exemplified by the topoisomerase inhibitor Mitoxantrone, which additionally binds tau pre-mRNA, stabilizing the splicing regulatory element[295]. Such alternative drug modes of action manifesting on the transcriptome, lipidome, or metabolome level are not detectable by AfBPP and are also hard to grasp by other chemoproteomic methods.

Even though, the fundamental work of this thesis resulted in the so far most comprehensive target landscape of HDAC inhibitors, the reasons listed above suggest that there are still some off-targets awaiting their identification. Overall, every drug target deconvolution technology only assesses drug modes of action within a certain set of targets or pathways that can be enquired by the method. Ideally, a combination of orthogonal target deconvolution approaches performed on a range of biological materials are applied to increase the chances of identifying all potentially relevant modes of action.

11 Future use cases of the promiscuous HDAC affinity matrix

Profiling of more drugs. While all commonly used and clinical HDAC inhibitors available in 2019 have been profiled, there are already 20-30 new HDAC drugs listed on the vendors' websites. Some of these molecules have already entered clinical trials. Characterization of those drugs should be an ongoing endeavor to keep the HDACi target landscape up-to-date. Moreover, profiling of tool compounds from academic collaboration partners will support the characterization of the next generation of selective HDACis (such as in co-authorship 1[222]). Further, our tool might enable the discovery of selective MBLAC2 inhibitors. To find potential selective MBLAC2 inhibitors, published SAR studies should be screened for HDACi analogs of dual MBLAC2/HDAC pharmacophore (such as Nexturastat A). Analogs that lost their HDAC inhibitory activity in the SAR study may still bind MBLAC2. Screening such preselected SAR libraries with our assay might therefore reveal selective MBLAC2i candidates.

Profiling drugs in proteomes from different human cell lines and tissues. Further, profiling clinical inhibitors in lysate of a diverse set of cell lines or tissues might allow to identify novel drug targets that are not ubiquitously expressed. Of importance might be the profiling in lysates derived from liver tissue. Liver cells express a large set of specific enzymes and off-target binding in liver cells might cause toxic side effects. For instance, Panobinostat and Belinostat were found to bind and inhibit PAH in liver cells[26]. However, whether other HDACis also inhibit PAH has not been investigated yet.

Profiling drugs in proteomes from different organisms. The promiscuity of the here-developed affinity probes might allow to pull down HDACs and metalloenzymes from other organisms and to profile drugs against parasitic or bacterial enzymes. Profiling in parasites like *schistosoma mansonii* might lay the foundation for drug repurposing in infectious diseases[296] as has been shown for kinase inhibitors already[297]. Along that line, metalloenzymes are also found in bacteria of the human microbiome. Orally administered HDACis that inhibit microbial enzymes would potentially lead to a reconstruction of the gut microbiome, change the levels of microbiome-generated metabolites entering the human body, or disturb the microbiome-organism symbiosis in any other way. Disturbing the microbiome can have clinically relevant downstream effects. It would therefore be interesting to screen gut-microbiome strains for targets of orally administered HDAC inhibitors such as Vorinostat.

12 Future challenges in the field of HDAC inhibitors

The following paragraphs will give an overview of the outstanding challenges in understanding HDAC biology and their potential as drug targets.

Class I HDACs. All currently approved and late clinical-stage HDAC inhibitors target class I HDAC1, HDAC2, and HDAC3. The challenges we face in understanding their detailed MoA are:

(i) The lack of information about the roles of the HDAC1, HDAC2, and HDAC3-based gene regulatory complexes.
(ii) Missing information about the chromatin regions affected by HDACi-mediated histone hyperacetylation.
(iii) Substantial lack in functional annotation of HDAC substrate sites.
(iv) Chemical genetic tools to selectively inhibit HDAC1-3 and HDAC complex activities are not available.

No inhibitors profiled in the underlying studies showed substantial selectivity between HDAC1-3[15]. Due to the high similarity of their active sites, it has been predicted that it will be highly challenging if not impossible to design a selective probe for HDAC1, HDAC2, and HDAC3[298]. HDAC3 selective drugs might indeed be valuable therapeutics, as HDAC3 has for instance been proposed as the ideal drug target in KRAS-driven lung cancer with acquired Trametinib resistance[299]. Recently, HDAC1-2 selective inhibitors (BRD6929 or Cpd-60)[217, 218] have been proposed, but the selectivity window still needs to be validated by orthogonal assays such as the chemoproteomic assay established in the underlying study[15]. Until now, HDAC1 and HDAC2 are often used synonymous and perceived to have redundant functions. While there might be a large overlap in substrates, both HDAC1 and HDAC2 have distinct roles and might act at different spatially confined chromatin regions. Selective probes for HDAC1 and HDAC2 would allow to study these differences. Moreover, cancers that feature HDAC1 or HDAC2 deletions would be selectively targetable with inhibitors against the non-deleted class I HDAC counterpart[300]. This would kill cancer cells but spare cells that still express both HDACs since one of two enzymes can take over most of the common tasks (concept of synthetic lethality)[301].
In addition, one can also imagine inhibitors selective for one of the complexes formed around HDAC1 and HDAC2. Indeed, well-established inhibitors already showed enhanced or diminished binding affinity to HDAC1 and HDAC2, when they are embedded in a specific protein complex environment or are present as single enzymes without interaction partners (ref.[43] and publication 1). For instance, aminoanilide HDAC inhibitors did preferentially bind to HDACs that are not embedded in protein complexes, while hydroxamic acid inhibitors showed enhanced binding to HDACs that were interacting with proteins from the CoREST complex (see also chapter 4.3).
Besides these serendipitous findings of complex selectivity, a concept to selectively target complex-embedded HDACs has been proposed that is based on dual inhibitors targeting two complex members at once and thereby leverages the avidity concept to boost complex-specific affinity (Fig. 38a-b). One drug designed according to this concept is Corin[302], a dual KDM1A (LSD1) and HDAC1-3 inhibitor consisting of a tranylcypromine (KDM1A) and an aminoanilide (HDAC) warhead (Fig. 38a). Due to the fact, that KDM1A and HDAC1-2 reside both in the CoREST complex and their active sites are located in close proximity, two linked warheads that simultaneously bind to active sites of HDAC1 or HDAC2 and KDM1A would have substantially increased affinity to the CoREST complex compared to other complexes, where this drug would only bind to HDAC1-2. The linker of Corin, however, is most likely too short to allow simultaneous binding to both active sites and its claimed avidity-based selectivity still needs to be proved. Indeed, Corin's HDAC binding warhead is an aminoanilide, which already features preferred binding to CoREST compared to other HDAC complexes (publication 1). The little observed complex selectivity of Corin is therefore

most likely explainable by its intrinsic HDAC-CoREST selectivity independent of the KDM1A targeting warhead. Of note, while Corin might show some CoREST selectivity, the tranylcypromine-derived warhead is well known to bind several targets in addition to KDM1A, such as MAOA, MAOB, and others[302, 303]. This reduces Corin's overall selectivity.

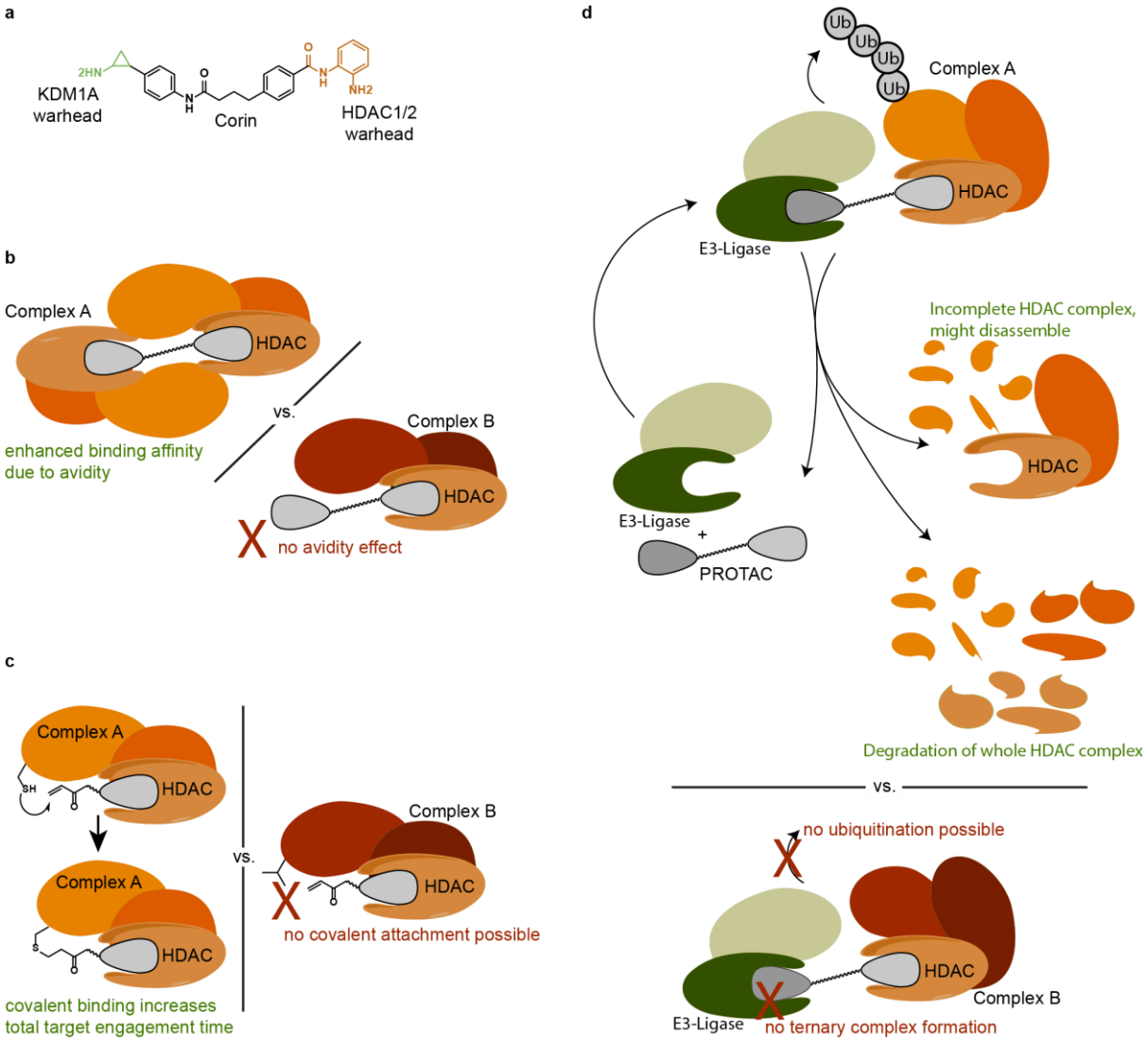

Fig. 38|Strategies to selectively target HDAC-complexes. a, Corin is a dual inhibitor of KDM1A and HDAC1-3. Moreover, it has been proposed to selectively target the HDAC1 or HDAC2 embedded in the CoREST complex because of simultaneous binding to the two complex members KDM1A and HDAC1/2 (avidity concept, see panel b). **b,** Targeting complexes selectively might be enabled by dual inhibitors that bind to two complex subunits simultaneously (avidity concept), as proposed for Corin. **c**, Targeting complexes selectively might be enabled by inhibitors that when engaged with HDACs expose a reactive warhead to an adjacent reactive amino acid. If the nucleophilic amino acid is only present on a particular complex partner and the HDACi gets covalently attached, occupancy of the drug will be selectively increased. d, complex selective degradation or destabilization by PROTACs might be achieved, if for instance the E3 ubiquitin ligase only ubiquitinates particular complex partners (depending e.g. on ternary complex formation or lysine availability).

Similarly to the idea of linking KDM1A and HDAC warheads, one could imagine to link two HDAC inhibitors at their capping groups, since some complexes are proposed to harbor two HDACs in their active core structure[298] (Fig. 38b). Potentially, more targetable pockets exist in HDAC complexes that could be leveraged for such avidity purposes. Reactive residues on complex partners located close to the active site could for instance be used to covalently anchor an HDAC

inhibitor in the complex (Fig. 38c). Finally, HDACi-based PROTACs might lead to differential degradation of complexes or complex partners and lead to the disruption or degradation of specific complexes (Fig. 38d)[304].

Class IIa HDACs. Our study revealed that class IIa targeting inhibitors are underrepresented. Indeed, only two of the 53 inhibitors profiled were specific for class IIa (publication 1). Those drugs (TMP195 and CHDI00390576), however, lack intra-class selectivity and are therefore not ideal chemical probes to study the function of HDAC4, HDAC5, or HDAC7. Indeed, the role of the HDAC domain is a major outstanding question for class II HDACs. Since the domain is not catalytically active for acetylated lysine[91], it has been suggested to act as an acetyl-lysine reader domain akin to bromodomains. However, this hypothesis has not been proved. More fundamental research is required to understand class IIa biology and judge the value of class IIa inhibitors as therapeutic option.

Class IIb – HDAC6. Hundreds of potential substrates of HDAC6 have been reported[101 88, 305]. However, only a few of these acetylation sites have been investigated for their regulatory role. To understand the mode of action of HDAC6 inhibitors, understanding the downstream effects of substrate hyperacetylation are essential. Akin to DDX3X[148], many of the substrate sites might be involved in phase separation propensity[305, 306]. Importantly, the different roles of the two catalytic domains of HDAC6 have not been investigated in detail[87, 135]. On top, differences in inhibitor affinity to the two domains have not been investigated systematically and are also not assessable by AfBPP strategies.

Class IIb – HDAC10. The recent discovery of polyamines as HDAC10 substrates and the identification of HDAC10 selective inhibitors in this work (TH65[15] and DKFZ-748[222]) presented a huge progress in understanding HDAC10 biology. Of note, inhibition of HDAC10-mediated polyamine deacetylation by DKFZ-748 has been shown to act synergistically with drugs targeting polyamine de novo biosynthesis[307]. One outstanding question will be, whether HDAC10 is indeed only a polyamine deacetylase or whether it has additional metabolite or protein substrates. The focus of understanding HDAC10's role in disease should now be shifting to the investigation of its role in polyamine metabolism, and more importantly to work out the cell biological functions of polyamines in general.

Class IV. HDAC11 is the most recent and one of the least investigated HDACs. Finding chemical probes against HDAC11 may be an important step to boost further research into identifying HDAC11-regulated substrates and pathways.

Conclusions

The publications of this thesis showcase the power of affinity-based protein profiling for target deconvolution and selectivity profiling. The design of tailored probes and promiscuous affinity matrices allowed to identify the drug targets of the approved drug lipoic acid and SIRT5-directed inhibitors, and enabled the delineation of the target landscape of HDAC inhibitors. The drug profiles of HDAC inhibitors will inform medicinal chemistry and present chemical probes to study the biology of HDACs. Identifying MBLAC2 as common HDACi off-target, uncovering its involvement in lipid and vesicle biology, and providing siRNAs as well as inhibitor tools to study this enzyme, provides the basis for investigating this hitherto poorly characterized enzyme in detail. These findings may either place MBLAC2 on the list of undesired off-targets or may highlight its contribution to the mode of action of HDAC and MBLAC2 targeting drug. Moreover, the discovery of HDAC inhibition being a potentially relevant mode of action of lipoic acid may have clinical relevance by inspiring drug repurposing or adapting lipoic acid dosing schemes. Overall, the studies underlying this thesis highlight the power of chemical proteomics in target deconvolution and drug discovery.

References

1. Pognan, F. *et al.* The evolving role of investigative toxicology in the pharmaceutical industry. *Nat Rev Drug Discov*, 1-19 (2023).
2. Pushpakom, S. *et al.* Drug repurposing: progress, challenges and recommendations. *Nat Rev Drug Discov* **18**, 41-58 (2019).
3. Butler, D. & Callaway, E. Scientists in the dark after French clinical trial proves fatal. *Nature* **529**, 263-264 (2016).
4. Huang, Z. *et al.* Global Portrait of Protein Targets of Metabolites of the Neurotoxic Compound BIA 10-2474. *ACS Chem Biol* **14**, 192-197 (2019).
5. van Esbroeck, A.C.M. *et al.* Activity-based protein profiling reveals off-target proteins of the FAAH inhibitor BIA 10-2474. *Science* **356**, 1084-1087 (2017).
6. Heinrich, M.C. *et al.* Inhibition of c-kit receptor tyrosine kinase activity by STI 571, a selective tyrosine kinase inhibitor. *Blood* **96**, 925-932 (2000).
7. Tuveson, D.A. *et al.* STI571 inactivation of the gastrointestinal stromal tumor c-KIT oncoprotein: biological and clinical implications. *Oncogene* **20**, 5054-5058 (2001).
8. Dagher, R. *et al.* Approval summary: imatinib mesylate in the treatment of metastatic and/or unresectable malignant gastrointestinal stromal tumors. *Clin Cancer Res* **8**, 3034-3038 (2002).
9. Bian, Y. *et al.* Robust, reproducible and quantitative analysis of thousands of proteomes by micro-flow LC-MS/MS. *Nat Commun* **11**, 157 (2020).
10. Chernobrovkin, A., Marin-Vicente, C., Visa, N. & Zubarev, R.A. Functional Identification of Target by Expression Proteomics (FITExP) reveals protein targets and highlights mechanisms of action of small molecule drugs. *Sci Rep* **5**, 11176 (2015).
11. Saei, A.A. *et al.* ProTargetMiner as a proteome signature library of anticancer molecules for functional discovery. *Nat Commun* **10**, 5715 (2019).
12. Ruprecht, B. *et al.* A mass spectrometry-based proteome map of drug action in lung cancer cell lines. *Nat Chem Biol* **16**, 1111-1119 (2020).
13. Mitchell, D.C. *et al.* A proteome-wide atlas of drug mechanism of action. *Nat Biotechnol* (2023).
14. Chubukov, V. *et al.* Transcriptional regulation is insufficient to explain substrate-induced flux changes in Bacillus subtilis. *Mol Syst Biol* **9**, 709 (2013).
15. Lechner, S. *et al.* Target deconvolution of HDAC pharmacopoeia reveals MBLAC2 as common off-target. *Nat Chem Biol* **18**, 812-820 (2022).
16. Subramanian, A. *et al.* A Next Generation Connectivity Map: L1000 Platform and the First 1,000,000 Profiles. *Cell* **171**, 1437-1452 e1417 (2017).
17. Bray, M.A. *et al.* Cell Painting, a high-content image-based assay for morphological profiling using multiplexed fluorescent dyes. *Nat Protoc* **11**, 1757-1774 (2016).
18. Wilke, J. *et al.* Discovery of a sigma(1) receptor antagonist by combination of unbiased cell painting and thermal proteome profiling. *Cell Chem Biol* **28**, 848-854 e845 (2021).
19. Akbarzadeh, M. *et al.* Morphological profiling by means of the Cell Painting assay enables identification of tubulin-targeting compounds. *Cell Chem Biol* **29**, 1053-1064 e1053 (2022).
20. Antolin, A.A. *et al.* The Chemical Probes Portal: an expert review-based public resource to empower chemical probe assessment, selection and use. *Nucleic Acids Res* **51**, D1492-D1502 (2023).
21. Mateus, A. *et al.* Thermal proteome profiling for interrogating protein interactions. *Mol Syst Biol* **16**, e9232 (2020).
22. Van Vranken, J.G., Li, J., Mitchell, D.C., Navarrete-Perea, J. & Gygi, S.P. Assessing target engagement using proteome-wide solvent shift assays. *Elife* **10** (2021).

23. Schopper, S. *et al.* Measuring protein structural changes on a proteome-wide scale using limited proteolysis-coupled mass spectrometry. *Nat Protoc* **12**, 2391-2410 (2017).
24. Piazza, I. *et al.* A machine learning-based chemoproteomic approach to identify drug targets and binding sites in complex proteomes. *Nat Commun* **11**, 4200 (2020).
25. Kitagawa, M. *et al.* Dual blockade of the lipid kinase PIP4Ks and mitotic pathways leads to cancer-selective lethality. *Nat Commun* **8**, 2200 (2017).
26. Becher, I. *et al.* Thermal profiling reveals phenylalanine hydroxylase as an off-target of panobinostat. *Nat Chem Biol* **12**, 908-910 (2016).
27. Dziekan, J.M. *et al.* Identifying purine nucleoside phosphorylase as the target of quinine using cellular thermal shift assay. *Sci Transl Med* **11** (2019).
28. Savitski, M.M. *et al.* Tracking cancer drugs in living cells by thermal profiling of the proteome. *Science* **346**, 1255784 (2014).
29. Cravatt, B.F., Wright, A.T. & Kozarich, J.W. Activity-based protein profiling: from enzyme chemistry to proteomic chemistry. *Annu Rev Biochem* **77**, 383-414 (2008).
30. Cravatt, B.F. Activity-based protein profiling - finding general solutions to specific problems. *Isr J Chem* **63** (2023).
31. Maurais, A.J. & Weerapana, E. Reactive-cysteine profiling for drug discovery. *Curr Opin Chem Biol* **50**, 29-36 (2019).
32. Weerapana, E. *et al.* Quantitative reactivity profiling predicts functional cysteines in proteomes. *Nature* **468**, 790-795 (2010).
33. Abbasov, M.E. *et al.* A proteome-wide atlas of lysine-reactive chemistry. *Nat Chem* **13**, 1081-1092 (2021).
34. Hacker, S.M. *et al.* Global profiling of lysine reactivity and ligandability in the human proteome. *Nat Chem* **9**, 1181-1190 (2017).
35. Hahm, H.S. *et al.* Global targeting of functional tyrosines using sulfur-triazole exchange chemistry. *Nat Chem Biol* **16**, 150-159 (2020).
36. Yan, T. *et al.* SP3-FAIMS Chemoproteomics for High-Coverage Profiling of the Human Cysteinome*. *Chembiochem* **22**, 1841-1851 (2021).
37. Boatner, L.M., Palafox, M.F., Schweppe, D.K. & Backus, K.M. CysDB: a human cysteine database based on experimental quantitative chemoproteomics. *Cell Chem Biol* (2023).
38. Vinogradova, E.V. *et al.* An Activity-Guided Map of Electrophile-Cysteine Interactions in Primary Human T Cells. *Cell* **182**, 1009-1026 e1029 (2020).
39. Burton, N.R., Kim, P. & Backus, K.M. Photoaffinity labelling strategies for mapping the small molecule-protein interactome. *Org Biomol Chem* **19**, 7792-7809 (2021).
40. Mellacheruvu, D. *et al.* The CRAPome: a contaminant repository for affinity purification-mass spectrometry data. *Nat Methods* **10**, 730-736 (2013).
41. Prokofeva, P. *et al.* Merits of Diazirine Photo-Immobilization for Target Profiling of Natural Products and Cofactors. *ACS Chem Biol* **17**, 3100-3109 (2022).
42. Kanoh, N., Honda, K., Simizu, S., Muroi, M. & Osada, H. Photo-cross-linked small-molecule affinity matrix for facilitating forward and reverse chemical genetics. *Angew Chem Int Ed Engl* **44**, 3559-3562 (2005).
43. Bantscheff, M. *et al.* Chemoproteomics profiling of HDAC inhibitors reveals selective targeting of HDAC complexes. *Nat Biotechnol* **29**, 255-265 (2011).
44. Becher, I. *et al.* Chemoproteomics reveals time-dependent binding of histone deacetylase inhibitors to endogenous repressor complexes. *ACS Chem Biol* **9**, 1736-1746 (2014).
45. Liang, Y.Y. *et al.* CETSA interaction proteomics define specific RNA-modification pathways as key components of fluorouracil-based cancer drug cytotoxicity. *Cell Chem Biol* **29**, 572-585 e578 (2022).
46. Ma, T. *et al.* Low-dose metformin targets the lysosomal AMPK pathway through PEN2. *Nature* **603**, 159-165 (2022).

47. Ito, T. *et al.* Identification of a primary target of thalidomide teratogenicity. *Science* **327**, 1345-1350 (2010).
48. Lin, A. *et al.* Off-target toxicity is a common mechanism of action of cancer drugs undergoing clinical trials. *Sci Transl Med* **11** (2019).
49. Bhattacharjee, D. & Sheltzer, J.M. A drug's most potent target is not necessarily the source of its anti-cancer activity. *bioRxiv* (2022).
50. Bantscheff, M. *et al.* Quantitative chemical proteomics reveals mechanisms of action of clinical ABL kinase inhibitors. *Nat Biotechnol* **25**, 1035-1044 (2007).
51. Klaeger, S. *et al.* The target landscape of clinical kinase drugs. *Science* **358** (2017).
52. Katayama, R. *et al.* Cytotoxic activity of tivantinib (ARQ 197) is not due solely to c-MET inhibition. *Cancer Res* **73**, 3087-3096 (2013).
53. Basilico, C. *et al.* Tivantinib (ARQ197) displays cytotoxic activity that is independent of its ability to bind MET. *Clin Cancer Res* **19**, 2381-2392 (2013).
54. Klaeger, S. *et al.* Chemical Proteomics Reveals Ferrochelatase as a Common Off-target of Kinase Inhibitors. *ACS Chem Biol* **11**, 1245-1254 (2016).
55. Xue, J. *et al.* A novel histone deacetylase inhibitor LT-548-133-1 induces apoptosis by inhibiting HDAC and interfering with microtubule assembly in MCF-7 cells. *Invest New Drugs* **39**, 1222-1231 (2021).
56. Wobser, M. *et al.* Elucidating the mechanism of action of domatinostat (4SC-202) in cutaneous T cell lymphoma cells. *J Hematol Oncol* **12**, 30 (2019).
57. Lecha, M., Puy, H. & Deybach, J.C. Erythropoietic protoporphyria. *Orphanet J Rare Dis* **4**, 19 (2009).
58. Patricelli, M.P. *et al.* Functional interrogation of the kinome using nucleotide acyl phosphates. *Biochemistry* **46**, 350-358 (2007).
59. Patricelli, M.P. *et al.* In situ kinase profiling reveals functionally relevant properties of native kinases. *Chem Biol* **18**, 699-710 (2011).
60. Medard, G. *et al.* Optimized chemical proteomics assay for kinase inhibitor profiling. *J Proteome Res* **14**, 1574-1586 (2015).
61. Bamborough, P. *et al.* Structure-Based Optimization of Naphthyridones into Potent ATAD2 Bromodomain Inhibitors. *J Med Chem* **58**, 6151-6178 (2015).
62. Dawson, M.A. *et al.* Inhibition of BET recruitment to chromatin as an effective treatment for MLL-fusion leukaemia. *Nature* **478**, 529-533 (2011).
63. Joberty, G. *et al.* Interrogating the Druggability of the 2-Oxoglutarate-Dependent Dioxygenase Target Class by Chemical Proteomics. *ACS Chem Biol* **11**, 2002-2010 (2016).
64. Chen, A.Y. *et al.* Targeting Metalloenzymes for Therapeutic Intervention. *Chem Rev* **119**, 1323-1455 (2019).
65. Jiang, Z., You, Q. & Zhang, X. Medicinal chemistry of metal chelating fragments in metalloenzyme active sites: A perspective. *Eur J Med Chem* **165**, 172-197 (2019).
66. Taunton, J., Hassig, C.A. & Schreiber, S.L. A mammalian histone deacetylase related to the yeast transcriptional regulator Rpd3p. *Science* **272**, 408-411 (1996).
67. Gregoretti, I.V., Lee, Y.M. & Goodson, H.V. Molecular evolution of the histone deacetylase family: functional implications of phylogenetic analysis. *J Mol Biol* **338**, 17-31 (2004).
68. Arrowsmith, C.H., Bountra, C., Fish, P.V., Lee, K. & Schapira, M. Epigenetic protein families: a new frontier for drug discovery. *Nat Rev Drug Discov* **11**, 384-400 (2012).
69. Seto, E. & Yoshida, M. Erasers of histone acetylation: the histone deacetylase enzymes. *Cold Spring Harb Perspect Biol* **6**, a018713 (2014).
70. Barnes, C.E., English, D.M. & Cowley, S.M. Acetylation & Co: an expanding repertoire of histone acylations regulates chromatin and transcription. *Essays Biochem* **63**, 97-107 (2019).
71. Tie, F. *et al.* CBP-mediated acetylation of histone H3 lysine 27 antagonizes Drosophila Polycomb silencing. *Development* **136**, 3131-3141 (2009).

72. Humphrey, G.W. *et al.* Stable histone deacetylase complexes distinguished by the presence of SANT domain proteins CoREST/kiaa0071 and Mta-L1. *J Biol Chem* **276**, 6817-6824 (2001).
73. Zhang, Y., LeRoy, G., Seelig, H.P., Lane, W.S. & Reinberg, D. The dermatomyositis-specific autoantigen Mi2 is a component of a complex containing histone deacetylase and nucleosome remodeling activities. *Cell* **95**, 279-289 (1998).
74. Laherty, C.D. *et al.* Histone deacetylases associated with the mSin3 corepressor mediate mad transcriptional repression. *Cell* **89**, 349-356 (1997).
75. Turnbull, R.E. *et al.* The MiDAC histone deacetylase complex is essential for embryonic development and has a unique multivalent structure. *Nat Commun* **11**, 3252 (2020).
76. Guenther, M.G., Barak, O. & Lazar, M.A. The SMRT and N-CoR corepressors are activating cofactors for histone deacetylase 3. *Mol Cell Biol* **21**, 6091-6101 (2001).
77. Liu, J. *et al.* Beclin1 controls the levels of p53 by regulating the deubiquitination activity of USP10 and USP13. *Cell* **147**, 223-234 (2011).
78. Luo, J., Su, F., Chen, D., Shiloh, A. & Gu, W. Deacetylation of p53 modulates its effect on cell growth and apoptosis. *Nature* **408**, 377-381 (2000).
79. Tan, M. *et al.* Identification of 67 histone marks and histone lysine crotonylation as a new type of histone modification. *Cell* **146**, 1016-1028 (2011).
80. Moreno-Yruela, C., Galleano, I., Madsen, A.S. & Olsen, C.A. Histone Deacetylase 11 Is an epsilon-N-Myristoyllysine Hydrolase. *Cell Chem Biol* **25**, 849-856 e848 (2018).
81. Moreno-Yruela, C. *et al.* Class I histone deacetylases (HDAC1-3) are histone lysine delactylases. *Sci Adv* **8**, eabi6696 (2022).
82. Deardorff, M.A. *et al.* HDAC8 mutations in Cornelia de Lange syndrome affect the cohesin acetylation cycle. *Nature* **489**, 313-317 (2012).
83. van Ruiten, M.S. *et al.* The cohesin acetylation cycle controls chromatin loop length through a PDS5A brake mechanism. *Nat Struct Mol Biol* **29**, 586-591 (2022).
84. Aramsangtienchai, P. *et al.* HDAC8 Catalyzes the Hydrolysis of Long Chain Fatty Acyl Lysine. *ACS Chem Biol* **11**, 2685-2692 (2016).
85. Wang, Z. *et al.* Genome-wide mapping of HATs and HDACs reveals distinct functions in active and inactive genes. *Cell* **138**, 1019-1031 (2009).
86. Valenzuela-Fernandez, A., Cabrero, J.R., Serrador, J.M. & Sanchez-Madrid, F. HDAC6: a key regulator of cytoskeleton, cell migration and cell-cell interactions. *Trends Cell Biol* **18**, 291-297 (2008).
87. Hai, Y. & Christianson, D.W. Histone deacetylase 6 structure and molecular basis of catalysis and inhibition. *Nat Chem Biol* **12**, 741-747 (2016).
88. Kutil, Z. *et al.* The unraveling of substrate specificity of histone deacetylase 6 domains using acetylome peptide microarrays and peptide libraries. *FASEB J* **33**, 4035-4045 (2019).
89. Hai, Y., Shinsky, S.A., Porter, N.J. & Christianson, D.W. Histone deacetylase 10 structure and molecular function as a polyamine deacetylase. *Nat Commun* **8**, 15368 (2017).
90. Maolanon, A.R., Madsen, A.S. & Olsen, C.A. Innovative Strategies for Selective Inhibition of Histone Deacetylases. *Cell Chem Biol* **23**, 759-768 (2016).
91. Lahm, A. *et al.* Unraveling the hidden catalytic activity of vertebrate class IIa histone deacetylases. *Proc Natl Acad Sci U S A* **104**, 17335-17340 (2007).
92. Zhang, Y., Andrade, R., Hanna, A.A. & Pflum, M.K.H. Evidence that HDAC7 acts as an epigenetic "reader" of AR acetylation through NCoR-HDAC3 dissociation. *Cell Chem Biol* **29**, 1162-1173 e1165 (2022).
93. Bradner, J.E. *et al.* Chemical phylogenetics of histone deacetylases. *Nat Chem Biol* **6**, 238-243 (2010).
94. Martin, M., Kettmann, R. & Dequiedt, F. Class IIa histone deacetylases: regulating the regulators. *Oncogene* **26**, 5450-5467 (2007).

95. Cao, J. *et al.* HDAC11 regulates type I interferon signaling through defatty-acylation of SHMT2. *Proc Natl Acad Sci U S A* **116**, 5487-5492 (2019).
96. Mann, B.S. *et al.* Vorinostat for treatment of cutaneous manifestations of advanced primary cutaneous T-cell lymphoma. *Clin Cancer Res* **13**, 2318-2322 (2007).
97. Morel, D., Almouzni, G., Soria, J.C. & Postel-Vinay, S. Targeting chromatin defects in selected solid tumors based on oncogene addiction, synthetic lethality and epigenetic antagonism. *Ann Oncol* **28**, 254-269 (2017).
98. Bettica, P. *et al.* Histological effects of givinostat in boys with Duchenne muscular dystrophy. *Neuromuscul Disord* **26**, 643-649 (2016).
99. Phiel, C.J. *et al.* Histone deacetylase is a direct target of valproic acid, a potent anticonvulsant, mood stabilizer, and teratogen. *J Biol Chem* **276**, 36734-36741 (2001).
100. Batshaw, M.L., MacArthur, R.B. & Tuchman, M. Alternative pathway therapy for urea cycle disorders: twenty years later. *J Pediatr* **138**, S46-54; discussion S54-45 (2001).
101. Scholz, C. *et al.* Acetylation site specificities of lysine deacetylase inhibitors in human cells. *Nat Biotechnol* **33**, 415-423 (2015).
102. Chang, L., Ruiz, P., Ito, T. & Sellers, W.R. Targeting pan-essential genes in cancer: Challenges and opportunities. *Cancer Cell* **39**, 466-479 (2021).
103. West, A.C. & Johnstone, R.W. New and emerging HDAC inhibitors for cancer treatment. *J Clin Invest* **124**, 30-39 (2014).
104. Zhang, Q., Wang, S., Chen, J. & Yu, Z. Histone Deacetylases (HDACs) Guided Novel Therapies for T-cell lymphomas. *Int J Med Sci* **16**, 424-442 (2019).
105. Lopez, A.T., Bates, S. & Geskin, L. Current Status of HDAC Inhibitors in Cutaneous T-cell Lymphoma. *Am J Clin Dermatol* **19**, 805-819 (2018).
106. Zhang, Y., Remillard, D., Cravatt, B.F. & Erb, M.A. Collateral lethality between HDAC1 and HDAC2 exploits cancer-specific NuRD complex vulnerabilities. *BioRxive* (2022).
107. Jamaladdin, S. *et al.* Histone deacetylase (HDAC) 1 and 2 are essential for accurate cell division and the pluripotency of embryonic stem cells. *Proc Natl Acad Sci U S A* **111**, 9840-9845 (2014).
108. Dovey, O.M. *et al.* Histone deacetylase 1 and 2 are essential for normal T-cell development and genomic stability in mice. *Blood* **121**, 1335-1344 (2013).
109. Hess, L. *et al.* A toolbox for class I HDACs reveals isoform specific roles in gene regulation and protein acetylation. *PLoS Genet* **18**, e1010376 (2022).
110. Falkenberg, K.J. & Johnstone, R.W. Histone deacetylases and their inhibitors in cancer, neurological diseases and immune disorders. *Nat Rev Drug Discov* **13**, 673-691 (2014).
111. Miller, K.M. *et al.* Human HDAC1 and HDAC2 function in the DNA-damage response to promote DNA nonhomologous end-joining. *Nat Struct Mol Biol* **17**, 1144-1151 (2010).
112. Liszczak, G., Diehl, K.L., Dann, G.P. & Muir, T.W. Acetylation blocks DNA damage-induced chromatin ADP-ribosylation. *Nat Chem Biol* **14**, 837-840 (2018).
113. Morel, D., Jeffery, D., Aspeslagh, S., Almouzni, G. & Postel-Vinay, S. Combining epigenetic drugs with other therapies for solid tumours - past lessons and future promise. *Nat Rev Clin Oncol* **17**, 91-107 (2020).
114. Hazzalin, C.A. & Mahadevan, L.C. Dynamic acetylation of all lysine 4-methylated histone H3 in the mouse nucleus: analysis at c-fos and c-jun. *PLoS Biol* **3**, e393 (2005).
115. Garzon-Porras, A.M., Chory, E. & Gryder, B.E. Dynamic Opposition of Histone Modifications. *ACS Chem Biol* (2022).
116. Gryder, B.E. *et al.* Chemical genomics reveals histone deacetylases are required for core regulatory transcription. *Nat Commun* **10**, 3004 (2019).
117. Gryder, B.E. *et al.* Histone hyperacetylation disrupts core gene regulatory architecture in rhabdomyosarcoma. *Nat Genet* **51**, 1714-1722 (2019).
118. Klein, I.A. *et al.* Partitioning of cancer therapeutics in nuclear condensates. *Science* **368**, 1386-1392 (2020).

119. Lopez, J.E., Haynes, S.E., Majmudar, J.D., Martin, B.R. & Fierke, C.A. HDAC8 Substrates Identified by Genetically Encoded Active Site Photocrosslinking. *J Am Chem Soc* **139**, 16222-16227 (2017).
120. Toro, T.B., Swanier, J.S., Bezue, J.A., Broussard, C.G. & Watt, T.J. Lysine Deacetylase Substrate Selectivity: A Dynamic Ionic Interaction Specific to KDAC8. *Biochemistry* **60**, 2524-2536 (2021).
121. Zhang, J. *et al.* Acetylation of Smc3 by Eco1 is required for S phase sister chromatid cohesion in both human and yeast. *Mol Cell* **31**, 143-151 (2008).
122. Ibrahim, D.M. & Mundlos, S. The role of 3D chromatin domains in gene regulation: a multi-facetted view on genome organization. *Curr Opin Genet Dev* **61**, 1-8 (2020).
123. Balasubramanian, S. *et al.* A novel histone deacetylase 8 (HDAC8)-specific inhibitor PCI-34051 induces apoptosis in T-cell lymphomas. *Leukemia* **22**, 1026-1034 (2008).
124. Mo, Z. *et al.* Aberrant GlyRS-HDAC6 interaction linked to axonal transport deficits in Charcot-Marie-Tooth neuropathy. *Nat Commun* **9**, 1007 (2018).
125. Benoy, V. *et al.* Development of Improved HDAC6 Inhibitors as Pharmacological Therapy for Axonal Charcot-Marie-Tooth Disease. *Neurotherapeutics* **14**, 417-428 (2017).
126. Benoy, V. *et al.* HDAC6 is a therapeutic target in mutant GARS-induced Charcot-Marie-Tooth disease. *Brain* **141**, 673-687 (2018).
127. Brindisi, M. *et al.* Old but Gold: Tracking the New Guise of Histone Deacetylase 6 (HDAC6) Enzyme as a Biomarker and Therapeutic Target in Rare Diseases. *J Med Chem* **63**, 23-39 (2020).
128. Oughtred, R. *et al.* The BioGRID database: A comprehensive biomedical resource of curated protein, genetic, and chemical interactions. *Protein Sci* **30**, 187-200 (2021).
129. Gold, W.A., Lacina, T.A., Cantrill, L.C. & Christodoulou, J. MeCP2 deficiency is associated with reduced levels of tubulin acetylation and can be restored using HDAC6 inhibitors. *J Mol Med (Berl)* **93**, 63-72 (2015).
130. Guo, W. *et al.* HDAC6 inhibition reverses axonal transport defects in motor neurons derived from FUS-ALS patients. *Nat Commun* **8**, 861 (2017).
131. Tejido, C., Pakravan, D. & Bosch, L.V.D. Potential Therapeutic Role of HDAC Inhibitors in FUS-ALS. *Front Mol Neurosci* **14**, 686995 (2021).
132. Graff, J. *et al.* An epigenetic blockade of cognitive functions in the neurodegenerating brain. *Nature* **483**, 222-226 (2012).
133. Zhang, Y. *et al.* Mice lacking histone deacetylase 6 have hyperacetylated tubulin but are viable and develop normally. *Mol Cell Biol* **28**, 1688-1701 (2008).
134. Depetter, Y. *et al.* Selective pharmacological inhibitors of HDAC6 reveal biochemical activity but functional tolerance in cancer models. *Int J Cancer* **145**, 735-747 (2019).
135. Miyake, Y. *et al.* Structural insights into HDAC6 tubulin deacetylation and its selective inhibition. *Nat Chem Biol* **12**, 748-754 (2016).
136. Hubbert, C. *et al.* HDAC6 is a microtubule-associated deacetylase. *Nature* **417**, 455-458 (2002).
137. Reed, N.A. *et al.* Microtubule acetylation promotes kinesin-1 binding and transport. *Curr Biol* **16**, 2166-2172 (2006).
138. Balabanian, L., Berger, C.L. & Hendricks, A.G. Acetylated Microtubules Are Preferentially Bundled Leading to Enhanced Kinesin-1 Motility. *Biophys J* **113**, 1551-1560 (2017).
139. Tas, R.P. *et al.* Differentiation between Oppositely Oriented Microtubules Controls Polarized Neuronal Transport. *Neuron* **96**, 1264-1271 e1265 (2017).
140. Hinckelmann, M.V., Zala, D. & Saudou, F. Releasing the brake: restoring fast axonal transport in neurodegenerative disorders. *Trends Cell Biol* **23**, 634-643 (2013).
141. Sleigh, J.N., Rossor, A.M., Fellows, A.D., Tosolini, A.P. & Schiavo, G. Axonal transport and neurological disease. *Nat Rev Neurol* **15**, 691-703 (2019).

142. Baldwin, K.R., Godena, V.K., Hewitt, V.L. & Whitworth, A.J. Axonal transport defects are a common phenotype in Drosophila models of ALS. *Hum Mol Genet* **25**, 2378-2392 (2016).
143. Chen, S., Owens, G.C., Makarenkova, H. & Edelman, D.B. HDAC6 regulates mitochondrial transport in hippocampal neurons. *PLoS One* **5**, e10848 (2010).
144. d'Ydewalle, C. *et al.* HDAC6 inhibitors reverse axonal loss in a mouse model of mutant HSPB1-induced Charcot-Marie-Tooth disease. *Nat Med* **17**, 968-974 (2011).
145. Smith, A.S.T. *et al.* HDAC6 Inhibition Corrects Electrophysiological and Axonal Transport Deficits in a Human Stem Cell-Based Model of Charcot-Marie-Tooth Disease (Type 2D). *Adv Biol (Weinh)* **6**, e2101308 (2022).
146. Xu, X., Kozikowski, A.P. & Pozzo-Miller, L. A selective histone deacetylase-6 inhibitor improves BDNF trafficking in hippocampal neurons from Mecp2 knockout mice: implications for Rett syndrome. *Front Cell Neurosci* **8**, 68 (2014).
147. Dompierre, J.P. *et al.* Histone deacetylase 6 inhibition compensates for the transport deficit in Huntington's disease by increasing tubulin acetylation. *J Neurosci* **27**, 3571-3583 (2007).
148. Saito, M. *et al.* Acetylation of intrinsically disordered regions regulates phase separation. *Nat Chem Biol* **15**, 51-61 (2019).
149. Kwon, S., Zhang, Y. & Matthias, P. The deacetylase HDAC6 is a novel critical component of stress granules involved in the stress response. *Genes Dev* **21**, 3381-3394 (2007).
150. Banani, S.F., Lee, H.O., Hyman, A.A. & Rosen, M.K. Biomolecular condensates: organizers of cellular biochemistry. *Nat Rev Mol Cell Biol* **18**, 285-298 (2017).
151. Alberti, S. & Hyman, A.A. Biomolecular condensates at the nexus of cellular stress, protein aggregation disease and ageing. *Nat Rev Mol Cell Biol* **22**, 196-213 (2021).
152. Kilgore, H.R. & Young, R.A. Learning the chemical grammar of biomolecular condensates. *Nat Chem Biol* (2022).
153. Ukmar-Godec, T. *et al.* Lysine/RNA-interactions drive and regulate biomolecular condensation. *Nat Commun* **10**, 2909 (2019).
154. Villegas, J.A., Heidenreich, M. & Levy, E.D. Molecular and environmental determinants of biomolecular condensate formation. *Nat Chem Biol* **18**, 1319-1329 (2022).
155. Niaki, A.G. *et al.* Loss of Dynamic RNA Interaction and Aberrant Phase Separation Induced by Two Distinct Types of ALS/FTD-Linked FUS Mutations. *Mol Cell* **77**, 82-94 e84 (2020).
156. Conicella, A.E., Zerze, G.H., Mittal, J. & Fawzi, N.L. ALS Mutations Disrupt Phase Separation Mediated by alpha-Helical Structure in the TDP-43 Low-Complexity C-Terminal Domain. *Structure* **24**, 1537-1549 (2016).
157. Mackenzie, I.R. *et al.* TIA1 Mutations in Amyotrophic Lateral Sclerosis and Frontotemporal Dementia Promote Phase Separation and Alter Stress Granule Dynamics. *Neuron* **95**, 808-816 e809 (2017).
158. Molliex, A. *et al.* Phase separation by low complexity domains promotes stress granule assembly and drives pathological fibrillization. *Cell* **163**, 123-133 (2015).
159. Murakami, T. *et al.* ALS/FTD Mutation-Induced Phase Transition of FUS Liquid Droplets and Reversible Hydrogels into Irreversible Hydrogels Impairs RNP Granule Function. *Neuron* **88**, 678-690 (2015).
160. Patel, A. *et al.* A Liquid-to-Solid Phase Transition of the ALS Protein FUS Accelerated by Disease Mutation. *Cell* **162**, 1066-1077 (2015).
161. Mitrea, D.M., Mittasch, M., Gomes, B.F., Klein, I.A. & Murcko, M.A. Modulating biomolecular condensates: a novel approach to drug discovery. *Nat Rev Drug Discov* (2022).
162. Vendruscolo, M. & Fuxreiter, M. Protein condensation diseases: therapeutic opportunities. *Nat Commun* **13**, 5550 (2022).
163. Kassouf, T. *et al.* Targeting the NEDP1 enzyme to ameliorate ALS phenotypes through stress granule disassembly. *Sci Adv* **9**, eabq7585 (2023).

164. Babinchak, W.M. *et al.* Small molecules as potent biphasic modulators of protein liquid-liquid phase separation. *Nat Commun* **11**, 5574 (2020).
165. Wheeler, R.J., Lee, H.O., Poser, I., Pal, A. & Hyman, A.A. Small molecules for modulating protein driven liquid-liquid phase separation in treating neurodegenerative disease. *Preprint at BioRxive* (2019).
166. Zhang, X. *et al.* HDAC6 modulates cell motility by altering the acetylation level of cortactin. *Mol Cell* **27**, 197-213 (2007).
167. Kanno, K. *et al.* Overexpression of histone deacetylase 6 contributes to accelerated migration and invasion activity of hepatocellular carcinoma cells. *Oncol Rep* **28**, 867-873 (2012).
168. Keremu, A., Aimaiti, A., Liang, Z. & Zou, X. Role of the HDAC6/STAT3 pathway in regulating PD-L1 expression in osteosarcoma cell lines. *Cancer Chemother Pharmacol* **83**, 255-264 (2019).
169. M, L. *et al.* Essential role of HDAC6 in the regulation of PD-L1 in melanoma. *Mol Oncol* **10**, 735-750 (2016).
170. Lee, J.Y. *et al.* HDAC6 controls autophagosome maturation essential for ubiquitin-selective quality-control autophagy. *EMBO J* **29**, 969-980 (2010).
171. Kawaguchi, Y. *et al.* The deacetylase HDAC6 regulates aggresome formation and cell viability in response to misfolded protein stress. *Cell* **115**, 727-738 (2003).
172. Hideshima, T. *et al.* Small-molecule inhibition of proteasome and aggresome function induces synergistic antitumor activity in multiple myeloma. *Proc Natl Acad Sci U S A* **102**, 8567-8572 (2005).
173. Vogl, D.T. *et al.* Ricolinostat, the First Selective Histone Deacetylase 6 Inhibitor, in Combination with Bortezomib and Dexamethasone for Relapsed or Refractory Multiple Myeloma. *Clin Cancer Res* **23**, 3307-3315 (2017).
174. Oehme, I., Lodrini, M., Brady, N.R. & Witt, O. Histone deacetylase 10-promoted autophagy as a druggable point of interference to improve the treatment response of advanced neuroblastomas. *Autophagy* **9**, 2163-2165 (2013).
175. Oehme, I. *et al.* Histone deacetylase 10 promotes autophagy-mediated cell survival. *Proc Natl Acad Sci U S A* **110**, E2592-2601 (2013).
176. Ridinger, J. *et al.* Dual role of HDAC10 in lysosomal exocytosis and DNA repair promotes neuroblastoma chemoresistance. *Sci Rep* **8**, 10039 (2018).
177. Eisenberg, T. *et al.* Induction of autophagy by spermidine promotes longevity. *Nat Cell Biol* **11**, 1305-1314 (2009).
178. Herbst-Gervasoni, C.J. & Christianson, D.W. Binding of N(8)-Acetylspermidine Analogues to Histone Deacetylase 10 Reveals Molecular Strategies for Blocking Polyamine Deacetylation. *Biochemistry* **58**, 4957-4969 (2019).
179. Igarashi, K. & Kashiwagi, K. Modulation of cellular function by polyamines. *Int J Biochem Cell Biol* **42**, 39-51 (2010).
180. Pegg, A.E. & Casero, R.A., Jr. Current status of the polyamine research field. *Methods Mol Biol* **720**, 3-35 (2011).
181. Shin, B.S. *et al.* Amino acid substrates impose polyamine, eIF5A, or hypusine requirement for peptide synthesis. *Nucleic Acids Res* **45**, 8392-8402 (2017).
182. Iacomino, G., Picariello, G. & D'Agostino, L. DNA and nuclear aggregates of polyamines. *Biochim Biophys Acta* **1823**, 1745-1755 (2012).
183. Bello-Fernandez, C., Packham, G. & Cleveland, J.L. The ornithine decarboxylase gene is a transcriptional target of c-Myc. *Proc Natl Acad Sci U S A* **90**, 7804-7808 (1993).
184. Bachmann, A.S. & Geerts, D. Polyamine synthesis as a target of MYC oncogenes. *J Biol Chem* **293**, 18757-18769 (2018).

185. Holbert, C.E., Cullen, M.T., Casero, R.A., Jr. & Stewart, T.M. Polyamines in cancer: integrating organismal metabolism and antitumour immunity. *Nat Rev Cancer* **22**, 467-480 (2022).
186. Gamble, L.D. *et al.* Inhibition of polyamine synthesis and uptake reduces tumor progression and prolongs survival in mouse models of neuroblastoma. *Sci Transl Med* **11** (2019).
187. Moriyama, Y., Hatano, R., Moriyama, S. & Uehara, S. Vesicular polyamine transporter as a novel player in amine-mediated chemical transmission. *Biochim Biophys Acta Biomembr* **1862**, 183208 (2020).
188. Hamouda, N.N. *et al.* ATP13A3 is a major component of the enigmatic mammalian polyamine transport system. *J Biol Chem* **296**, 100182 (2021).
189. van Veen, S. *et al.* ATP13A2 deficiency disrupts lysosomal polyamine export. *Nature* **578**, 419-424 (2020).
190. Casero, R.A., Jr., Murray Stewart, T. & Pegg, A.E. Polyamine metabolism and cancer: treatments, challenges and opportunities. *Nat Rev Cancer* **18**, 681-695 (2018).
191. Khan, A. *et al.* Dual targeting of polyamine synthesis and uptake in diffuse intrinsic pontine gliomas. *Nat Commun* **12**, 971 (2021).
192. Geraldy, M. *et al.* Selective Inhibition of Histone Deacetylase 10: Hydrogen Bonding to the Gatekeeper Residue is Implicated. *J Med Chem* **62**, 4426-4443 (2019).
193. Caslini, C., Hong, S., Ban, Y.J., Chen, X.S. & Ince, T.A. HDAC7 regulates histone 3 lysine 27 acetylation and transcriptional activity at super-enhancer-associated genes in breast cancer stem cells. *Oncogene* **38**, 6599-6614 (2019).
194. Witt, A.E. *et al.* Identification of a cancer stem cell-specific function for the histone deacetylases, HDAC1 and HDAC7, in breast and ovarian cancer. *Oncogene* **36**, 1707-1720 (2017).
195. Sun, Y. *et al.* Histone deacetylase 5 blocks neuroblastoma cell differentiation by interacting with N-Myc. *Oncogene* **33**, 2987-2994 (2014).
196. Fabian, J. *et al.* MYCN and HDAC5 transcriptionally repress CD9 to trigger invasion and metastasis in neuroblastoma. *Oncotarget* **7**, 66344-66359 (2016).
197. Cao, C. *et al.* Functional interaction of histone deacetylase 5 (HDAC5) and lysine-specific demethylase 1 (LSD1) promotes breast cancer progression. *Oncogene* **36**, 133-145 (2017).
198. Mielcarek, M. *et al.* SAHA decreases HDAC 2 and 4 levels in vivo and improves molecular phenotypes in the R6/2 mouse model of Huntington's disease. *PLoS One* **6**, e27746 (2011).
199. Lang, C. *et al.* Single-Cell Sequencing of iPSC-Dopamine Neurons Reconstructs Disease Progression and Identifies HDAC4 as a Regulator of Parkinson Cell Phenotypes. *Cell Stem Cell* **24**, 93-106 e106 (2019).
200. Mielcarek, M. *et al.* HDAC4 reduction: a novel therapeutic strategy to target cytoplasmic huntingtin and ameliorate neurodegeneration. *PLoS Biol* **11**, e1001717 (2013).
201. Federspiel, J.D., Greco, T.M., Lum, K.K. & Cristea, I.M. Hdac4 Interactions in Huntington's Disease Viewed Through the Prism of Multiomics. *Mol Cell Proteomics* **18**, S92-S113 (2019).
202. Kutil, Z. *et al.* Histone Deacetylase 11 Is a Fatty-Acid Deacylase. *ACS Chem Biol* **13**, 685-693 (2018).
203. Wranke, A. & Wedemeyer, H. Antiviral therapy of hepatitis delta virus infection - progress and challenges towards cure. *Curr Opin Virol* **20**, 112-118 (2016).
204. Medrano, R.F.V., Hunger, A., Mendonca, S.A., Barbuto, J.A.M. & Strauss, B.E. Immunomodulatory and antitumor effects of type I interferons and their application in cancer therapy. *Oncotarget* **8**, 71249-71284 (2017).
205. Son, S.I., Cao, J., Zhu, C.L., Miller, S.P. & Lin, H. Activity-Guided Design of HDAC11-Specific Inhibitors. *ACS Chem Biol* **14**, 1393-1397 (2019).

206. Martin, M.W. *et al.* Discovery of novel N-hydroxy-2-arylisoindoline-4-carboxamides as potent and selective inhibitors of HDAC11. *Bioorg Med Chem Lett* **28**, 2143-2147 (2018).
207. Lu, Z. *et al.* Epigenetic therapy inhibits metastases by disrupting premetastatic niches. *Nature* **579**, 284-290 (2020).
208. McCaw, T.R., Randall, T.D., Forero, A. & Buchsbaum, D.J. Modulation of antitumor immunity with histone deacetylase inhibitors. *Immunotherapy* **9**, 1359-1372 (2017).
209. Ellmeier, W. & Seiser, C. Histone deacetylase function in CD4(+) T cells. *Nat Rev Immunol* **18**, 617-634 (2018).
210. Lobera, M. *et al.* Selective class IIa histone deacetylase inhibition via a nonchelating zinc-binding group. *Nat Chem Biol* **9**, 319-325 (2013).
211. Ptacek, J. *et al.* Selectivity of Hydroxamate- and Difluoromethyloxadiazole-Based Inhibitors of Histone Deacetylase 6 In Vitro and in Cells. *Int J Mol Sci* **24** (2023).
212. Ginsel, C. *et al.* The Involvement of the Mitochondrial Amidoxime Reducing Component (mARC) in the Reductive Metabolism of Hydroxamic Acids. *Drug Metab Dispos* **46**, 1396-1402 (2018).
213. Dalvie, D. *et al.* Metabolism distribution and excretion of a matrix metalloproteinase-13 inhibitor, 4-[4-(4-fluorophenoxy)-benzenesulfonylamino]tetrahydropyran-4-carboxylic acid hydroxyamide (CP-544439), in rats and dogs: assessment of the metabolic profile of CP-544439 in plasma and urine of humans. *Drug Metab Dispos* **36**, 1869-1883 (2008).
214. Summers, J.B. *et al.* In vivo characterization of hydroxamic acid inhibitors of 5-lipoxygenase. *J Med Chem* **30**, 2121-2126 (1987).
215. Robers, M.B. *et al.* Target engagement and drug residence time can be observed in living cells with BRET. *Nat Commun* **6**, 10091 (2015).
216. Bressi, J.C. *et al.* Exploration of the HDAC2 foot pocket: Synthesis and SAR of substituted N-(2-aminophenyl)benzamides. *Bioorg Med Chem Lett* **20**, 3142-3145 (2010).
217. Mazitschek, R. & Payne, N. Resolving the Deceptive Isoform and Complex Selectivity of HDAC1/2 Inhibitors. *Available at SSRN: https://ssrn.com/abstract=3960267* (2022).
218. Schroeder, F.A. *et al.* A selective HDAC 1/2 inhibitor modulates chromatin and gene expression in brain and alters mouse behavior in two mood-related tests. *PLoS One* **8**, e71323 (2013).
219. Watson, P.J. *et al.* Insights into the activation mechanism of class I HDAC complexes by inositol phosphates. *Nat Commun* **7**, 11262 (2016).
220. Zhang, X. *et al.* Histone deacetylase 3 (HDAC3) activity is regulated by interaction with protein serine/threonine phosphatase 4. *Genes Dev* **19**, 827-839 (2005).
221. Bardai, F.H. & D'Mello, S.R. Selective toxicity by HDAC3 in neurons: regulation by Akt and GSK3beta. *J Neurosci* **31**, 1746-1751 (2011).
222. Steimbach, R.R. *et al.* Aza-SAHA Derivatives Are Selective Histone Deacetylase 10 Chemical Probes That Inhibit Polyamine Deacetylation and Phenocopy HDAC10 Knockout. *J Am Chem Soc* **144**, 18861-18875 (2022).
223. Arts, J. *et al.* JNJ-26481585, a novel "second-generation" oral histone deacetylase inhibitor, shows broad-spectrum preclinical antitumoral activity. *Clin Cancer Res* **15**, 6841-6851 (2009).
224. Lauffer, B.E. *et al.* Histone deacetylase (HDAC) inhibitor kinetic rate constants correlate with cellular histone acetylation but not transcription and cell viability. *J Biol Chem* **288**, 26926-26943 (2013).
225. Negmeldin, A.T., Padige, G., Bieliauskas, A.V. & Pflum, M.K. Structural Requirements of HDAC Inhibitors: SAHA Analogues Modified at the C2 Position Display HDAC6/8 Selectivity. *ACS Med Chem Lett* **8**, 281-286 (2017).
226. Burli, R.W. *et al.* Design, synthesis, and biological evaluation of potent and selective class IIa histone deacetylase (HDAC) inhibitors as a potential therapy for Huntington's disease. *J Med Chem* **56**, 9934-9954 (2013).

227. Dale, N.C., Johnstone, E.K.M., White, C.W. & Pfleger, K.D.G. NanoBRET: The Bright Future of Proximity-Based Assays. *Front Bioeng Biotechnol* **7**, 56 (2019).
228. Zecha, J. *et al.* Decrypting drug actions and protein modifications by dose- and time-resolved proteomics. *Science* **380**, 93-101 (2023).
229. Glas, C. *et al.* Development of hetero-triaryls as a new chemotype for subtype-selective and potent Sirt5 inhibition. *Eur J Med Chem* **240**, 114594 (2022).
230. Cox, J. *et al.* Accurate proteome-wide label-free quantification by delayed normalization and maximal peptide ratio extraction, termed MaxLFQ. *Mol Cell Proteomics* **13**, 2513-2526 (2014).
231. Witting, M., Maier, T.V., Garvis, S. & Schmitt-Kopplin, P. Optimizing a ultrahigh pressure liquid chromatography-time of flight-mass spectrometry approach using a novel sub-2mum core-shell particle for in depth lipidomic profiling of Caenorhabditis elegans. *J Chromatogr A* **1359**, 91-99 (2014).
232. Tsugawa, H. *et al.* A lipidome atlas in MS-DIAL 4. *Nat Biotechnol* **38**, 1159-1163 (2020).
233. Schmidt, T. *et al.* ProteomicsDB. *Nucleic Acids Res* **46**, D1271-D1281 (2018).
234. Samaras, P. *et al.* ProteomicsDB: a multi-omics and multi-organism resource for life science research. *Nucleic Acids Res* **48**, D1153-D1163 (2020).
235. Wilhelm, M. *et al.* Mass-spectrometry-based draft of the human proteome. *Nature* **509**, 582-587 (2014).
236. Lautenbacher, L. *et al.* ProteomicsDB: toward a FAIR open-source resource for life-science research. *Nucleic Acids Res* **50**, D1541-D1552 (2022).
237. Chao, O.S. *et al.* The HDAC6 Inhibitor Tubacin Induces Release of CD133(+) Extracellular Vesicles From Cancer Cells. *J Cell Biochem* **118**, 4414-4424 (2017).
238. Zeleke, T.Z. *et al.* Network-based assessment of HDAC6 activity predicts preclinical and clinical responses to the HDAC6 inhibitor ricolinostat in breast cancer. *Nat Cancer* **4**, 257-275 (2023).
239. Malgapo, M.I.P., Safadi, J.M. & Linder, M.E. Metallo-beta-lactamase domain-containing protein 2 is S-palmitoylated and exhibits acyl-CoA hydrolase activity. *J Biol Chem* **296**, 100106 (2020).
240. Huttlin, E.L. *et al.* Dual proteome-scale networks reveal cell-specific remodeling of the human interactome. *Cell* **184**, 3022-3040 e3028 (2021).
241. Turpin-Nolan, S.M. & Bruning, J.C. The role of ceramides in metabolic disorders: when size and localization matters. *Nat Rev Endocrinol* **16**, 224-233 (2020).
242. Tkach, M. *et al.* Qualitative differences in T-cell activation by dendritic cell-derived extracellular vesicle subtypes. *EMBO J* **36**, 3012-3028 (2017).
243. Robbins, P.D. & Morelli, A.E. Regulation of immune responses by extracellular vesicles. *Nat Rev Immunol* **14**, 195-208 (2014).
244. Capello, M. *et al.* Exosomes harbor B cell targets in pancreatic adenocarcinoma and exert decoy function against complement-mediated cytotoxicity. *Nat Commun* **10**, 254 (2019).
245. Wu, B. *et al.* Stiff matrix induces exosome secretion to promote tumour growth. *Nat Cell Biol* **25**, 415-424 (2023).
246. Rodrigues, G. *et al.* Tumour exosomal CEMIP protein promotes cancer cell colonization in brain metastasis. *Nat Cell Biol* **21**, 1403-1412 (2019).
247. Costa-Silva, B. *et al.* Pancreatic cancer exosomes initiate pre-metastatic niche formation in the liver. *Nat Cell Biol* **17**, 816-826 (2015).
248. Peinado, H. *et al.* Melanoma exosomes educate bone marrow progenitor cells toward a pro-metastatic phenotype through MET. *Nat Med* **18**, 883-891 (2012).
249. Poggio, M. *et al.* Suppression of Exosomal PD-L1 Induces Systemic Anti-tumor Immunity and Memory. *Cell* **177**, 414-427 e413 (2019).
250. Chen, G. *et al.* Exosomal PD-L1 contributes to immunosuppression and is associated with anti-PD-1 response. *Nature* **560**, 382-386 (2018).

251. Park, H. & Poo, M.M. Neurotrophin regulation of neural circuit development and function. *Nat Rev Neurosci* **14**, 7-23 (2013).
252. Edwards, A.M. *et al.* Too many roads not taken. *Nature* **470**, 163-165 (2011).
253. Winger, J.A., Hantschel, O., Superti-Furga, G. & Kuriyan, J. The structure of the leukemia drug imatinib bound to human quinone reductase 2 (NQO2). *BMC Struct Biol* **9**, 7 (2009).
254. Schepers, A.G. *et al.* Identification of NQO2 As a Protein Target in Small Molecule Modulation of Hepatocellular Function. *ACS Chem Biol* **16**, 1770-1778 (2021).
255. Hussein, B. *et al.* Discovery of potent 4-aminoquinoline hydrazone inhibitors of NRH:quinoneoxidoreductase-2 (NQO2). *Eur J Med Chem* **182**, 111649 (2019).
256. Rix, U. *et al.* Chemical proteomic profiles of the BCR-ABL inhibitors imatinib, nilotinib, and dasatinib reveal novel kinase and nonkinase targets. *Blood* **110**, 4055-4063 (2007).
257. https://drugs.ncats.io/drug/HL580335SI#publications.
258. Ferri, N. *et al.* Synthesis, structural, and biological evaluation of bis-heteroarylmaleimides and bis-heterofused imides. *Bioorg Med Chem* **19**, 5291-5299 (2011).
259. Rivera Cid, P., Gonzalez Fernandez, E., Martin, F.R. & Brana, M.F. The pharmacokinetics, tissue distribution, and biotransformation of a new class of antitumor agents: mitonafide and pinafide. *Eur J Drug Metab Pharmacokinet* **11**, 255-267 (1986).
260. Nekvinda, J. *et al.* Synthesis of naphthalimide-carborane and metallacarborane conjugates: Anticancer activity, DNA binding ability. *Bioorg Chem* **94**, 103432 (2020).
261. Sinha, B.K., Strong, J., Gibson, N.W. & Kalyanaraman, B. Mechanism of DNA strand breaks by mitonafide, an imide derivative of 3-nitro-1,8-naphthalic acid. *Biochem Pharmacol* **34**, 3845-3852 (1985).
262. Casado, A. *et al.* Phase II study of mitonafide in non-small cell lung cancer (NSCLC). *Invest New Drugs* **14**, 415-417 (1996).
263. Stone, R.M. *et al.* Phase III open-label randomized study of cytarabine in combination with amonafide L-malate or daunorubicin as induction therapy for patients with secondary acute myeloid leukemia. *J Clin Oncol* **33**, 1252-1257 (2015).
264. Mijatovic, T. *et al.* UNBS5162, a novel naphthalimide that decreases CXCL chemokine expression in experimental prostate cancers. *Neoplasia* **10**, 573-586 (2008).
265. Mahadevan, D. *et al.* Phase I trial of UNBS5162, a novel naphthalimide in patients with advanced solid tumors or lymphoma. *Int J Clin Oncol* **18**, 934-941 (2013).
266. Handelsman, D.J. & Turtle, J.R. Clinical trial of an aldose reductase inhibitor in diabetic neuropathy. *Diabetes* **30**, 459-464 (1981).
267. Satitsri, S., Pongkorpsakol, P., Srimanote, P., Chatsudthipong, V. & Muanprasat, C. Pathophysiological mechanisms of diarrhea caused by the Vibrio cholerae O1 El Tor variant: an in vivo study in mice. *Virulence* **7**, 789-805 (2016).
268. Hung, D.T., Shakhnovich, E.A., Pierson, E. & Mekalanos, J.J. Small-molecule inhibitor of Vibrio cholerae virulence and intestinal colonization. *Science* **310**, 670-674 (2005).
269. Thomson, J.J., Plecha, S.C. & Withey, J.H. A small unstructured region in Vibrio cholerae ToxT mediates the response to positive and negative effectors and ToxT proteolysis. *J Bacteriol* **197**, 654-668 (2015).
270. Reinecke, M. *et al.* Chemoproteomic Selectivity Profiling of PIKK and PI3K Kinase Inhibitors. *ACS Chem Biol* **14**, 655-664 (2019).
271. Panyain, N. *et al.* Activity-based protein profiling reveals deubiquitinase and aldehyde dehydrogenase targets of a cyanopyrrolidine probe. *RSC Med Chem* **12**, 1935-1943 (2021).
272. Kooij, R. *et al.* Small-Molecule Activity-Based Probe for Monitoring Ubiquitin C-Terminal Hydrolase L1 (UCHL1) Activity in Live Cells and Zebrafish Embryos. *J Am Chem Soc* **142**, 16825-16841 (2020).
273. Grethe, C. *et al.* Structural basis for specific inhibition of the deubiquitinase UCHL1. *Nat Commun* **13**, 5950 (2022).

274. Fischer, J.J. *et al.* SAHA Capture Compound--a novel tool for the profiling of histone deacetylases and the identification of additional vorinostat binders. *Proteomics* **11**, 4096-4104 (2011).
275. Friedman Ohana, R. *et al.* Streamlined Target Deconvolution Approach Utilizing a Single Photoreactive Chloroalkane Capture Tag. *ACS Chem Biol* **16**, 404-413 (2021).
276. Chen, C.H., Ferreira, J.C., Gross, E.R. & Mochly-Rosen, D. Targeting aldehyde dehydrogenase 2: new therapeutic opportunities. *Physiol Rev* **94**, 1-34 (2014).
277. Smith, A.J. *et al.* GATD3A, a mitochondrial deglycase with evolutionary origins from gammaproteobacteria, restricts the formation of advanced glycation end products. *BMC Biol* **20**, 68 (2022).
278. Kurzawa, N. *et al.* A computational method for detection of ligand-binding proteins from dose range thermal proteome profiles. *Nat Commun* **11**, 5783 (2020).
279. Perrin, J. *et al.* Identifying drug targets in tissues and whole blood with thermal-shift profiling. *Nat Biotechnol* **38**, 303-308 (2020).
280. Roy, J. & Cyert, M.S. Identifying New Substrates and Functions for an Old Enzyme: Calcineurin. *Cold Spring Harb Perspect Biol* **12** (2020).
281. Azzi, J.R., Sayegh, M.H. & Mallat, S.G. Calcineurin inhibitors: 40 years later, can't live without. *J Immunol* **191**, 5785-5791 (2013).
282. Litichevskiy, L. *et al.* A Library of Phosphoproteomic and Chromatin Signatures for Characterizing Cellular Responses to Drug Perturbations. *Cell Syst* **6**, 424-443 e427 (2018).
283. Wong, M.H. *et al.* The KN-93 Molecule Inhibits Calcium/Calmodulin-Dependent Protein Kinase II (CaMKII) Activity by Binding to Ca(2+)/CaM. *J Mol Biol* **431**, 1440-1459 (2019).
284. Heimburg, T. *et al.* Structure-Based Design and Synthesis of Novel Inhibitors Targeting HDAC8 from Schistosoma mansoni for the Treatment of Schistosomiasis. *J Med Chem* **59**, 2423-2435 (2016).
285. Felber, J.G. *et al.* Cyclic 5-membered disulfides are not selective substrates of thioredoxin reductase, but are opened nonspecifically. *Nat Commun* **13**, 1754 (2022).
286. Salehi, B. *et al.* Insights on the Use of alpha-Lipoic Acid for Therapeutic Purposes. *Biomolecules* **9** (2019).
287. Shay, K.P., Moreau, R.F., Smith, E.J., Smith, A.R. & Hagen, T.M. Alpha-lipoic acid as a dietary supplement: molecular mechanisms and therapeutic potential. *Biochim Biophys Acta* **1790**, 1149-1160 (2009).
288. Stoll, S., Hartmann, H., Cohen, S.A. & Muller, W.E. The potent free radical scavenger alpha-lipoic acid improves memory in aged mice: putative relationship to NMDA receptor deficits. *Pharmacol Biochem Behav* **46**, 799-805 (1993).
289. Forman, H.J. & Zhang, H. Targeting oxidative stress in disease: promise and limitations of antioxidant therapy. *Nat Rev Drug Discov* **20**, 689-709 (2021).
290. Sies, H. *et al.* Defining roles of specific reactive oxygen species (ROS) in cell biology and physiology. *Nat Rev Mol Cell Biol* **23**, 499-515 (2022).
291. Murphy, M.P. *et al.* Guidelines for measuring reactive oxygen species and oxidative damage in cells and in vivo. *Nat Metab* **4**, 651-662 (2022).
292. Stoner, M.W. *et al.* alpha-Lipoic acid promotes alpha-tubulin hyperacetylation and blocks the turnover of mitochondria through mitophagy. *Biochem J* **473**, 1821-1830 (2016).
293. Schupke, H. *et al.* New metabolic pathways of alpha-lipoic acid. *Drug Metab Dispos* **29**, 855-862 (2001).
294. Shi, L. *et al.* SULT1A1-dependent sulfonation of alkylators is a lineage-dependent vulnerability of liver cancers. *Nat Cancer* (2023).
295. Childs-Disney, J.L. *et al.* Targeting RNA structures with small molecules. *Nat Rev Drug Discov* **21**, 736-762 (2022).
296. Hailu, G.S. *et al.* Lysine Deacetylase Inhibitors in Parasites: Past, Present, and Future Perspectives. *J Med Chem* **60**, 4780-4804 (2017).

297. Arendse, L.B. *et al.* The anticancer human mTOR inhibitor sapanisertib potently inhibits multiple Plasmodium kinases and life cycle stages. *Sci Transl Med* **14**, eabo7219 (2022).
298. Millard, C.J., Watson, P.J., Fairall, L. & Schwabe, J.W.R. Targeting Class I Histone Deacetylases in a "Complex" Environment. *Trends Pharmacol Sci* **38**, 363-377 (2017).
299. Eichner, L.J. *et al.* HDAC3 is critical in tumor development and therapeutic resistance in Kras-mutant non-small cell lung cancer. *Sci Adv* **9**, eadd3243 (2023).
300. Zhang, Y., Remillard, D., Onubogu, U. & Erb, M.A. Collateral lethality between HDAC1 and HDAC2 exploits cancer-specific NuRD complex vulnerabilities. *bioRxiv*.
301. Kaelin, W.G., Jr. The concept of synthetic lethality in the context of anticancer therapy. *Nat Rev Cancer* **5**, 689-698 (2005).
302. Kalin, J.H. *et al.* Targeting the CoREST complex with dual histone deacetylase and demethylase inhibitors. *Nat Commun* **9**, 53 (2018).
303. Drechsel, J., Kyrousi, C., Cappello, S. & Sieber, S.A. Tranylcypromine specificity for monoamine oxidase is limited by promiscuous protein labelling and lysosomal trapping. *RSC Chem Biol* **1**, 209-213 (2020).
304. Xiong, Y. *et al.* Chemo-proteomics exploration of HDAC degradability by small molecule degraders. *Cell Chem Biol* **28**, 1514-1527 e1514 (2021).
305. Gomes, I.D., Ariyaratne, U.V. & Pflum, M.K.H. HDAC6 Substrate Discovery Using Proteomics-Based Substrate Trapping: HDAC6 Deacetylates PRMT5 to Influence Methyltransferase Activity. *ACS Chem Biol* **16**, 1435-1444 (2021).
306. Gal, J. *et al.* The Acetylation of Lysine-376 of G3BP1 Regulates RNA Binding and Stress Granule Dynamics. *Mol Cell Biol* **39** (2019).
307. Stewart, T.M. *et al.* Histone deacetylase-10 liberates spermidine to support polyamine homeostasis and tumor cell growth. *J Biol Chem* **298**, 102407 (2022).

Acknowledgements

This thesis marks the end of 4.5 years at the Kuster chair, as part of the TTTT. I am highly grateful for the inspiring environment in the lab, the help I received when things did not work out, and most of all for the fun, friendship, and good time we had at the chair during and after work.

First of all I want to thank Bernhard for being an extraordinary supervisor. I appreciate the freedom you gave me in terms of trying out new crazy ideas. This led me into many dead ends but also contributed to the most exciting discoveries made during my time in your lab. You always encouraged me to test new hypotheses or to collaborate with experts, which was crucial for the success of the paper stories published by now. I highly appreciate that you let me follow through with my HDAC story instead of the originally planned project.

Next, I want to thank Guillaume, for always playing devils advocate and being the best critic and supporter at the same time. I learned so many things from you, and you were always there for discussing new ideas and confusing results. I'll miss our discussions that inspired so many creative ideas. I was so lucky to start my Master's Thesis with you.

Of course, the time in the lab wouldn't have that much fun, without all my nice colleagues and friends. All the time we spent together at work but also after work or on weekends made us grow together, and made things easy even in difficult times. Thank you all for the good time we had.

I want to thank my family, my parents and sister, who always supported me and provided a cozy refuge at home for relaxing at weekends and during holidays. Thanks for showing me the things that are important besides work. In some way, I guess my parents laid the foundation for my scientific career: my mom always encouraged me to study and learn during school. Having good grades was a nice feeling, so I tried to stick to it when studying biochemistry. Having all that basic knowledge in mind allowed me to see connections, where others did not, as for instance in the lipoic acid story. My dad triggered my scientific curiosity already when I was a child. I learned about nature and biology during our hiking trips, but also at home when reading one of the many history, geology, physics, and biology books lying around.

Finally, I want to thank Rosi, who always supported me during tough and stressful times at work. You gave me the non-science counter balance that I needed at home to get my head clear from thinking about work all the time. It was nice to come home after work knowing that you'd be there, often waiting with freshly cooked dinner. While I finished this Thesis, you finished your 2 years project of converting a delivery van into a masterpiece of self-made camper. I am super proud about how you managed that all on your own and I am looking forward to our next big journey lying ahead.

Appendix

ARTICLES
https://doi.org/10.1038/s41589-022-01015-5
nature chemical biology

Target deconvolution of HDAC pharmacopoeia reveals MBLAC2 as common off-target

Severin Lechner[1], Martin Ian P. Malgapo[2], Christian Grätz[3], Raphael R. Steimbach[4,5], Agnes Baron[1], Patrick Rüther[1], Simon Nadal[1], Carmen Stumpf[1], Christina Loos[1], Xin Ku[1], Polina Prokofeva[1], Ludwig Lautenbacher[6], Tino Heimburg[7], Vivian Würf[8], Chen Meng[9], Mathias Wilhelm[6], Wolfgang Sippl[7], Karin Kleigrewe[9], Josch K. Pauling[8], Karl Kramer[1], Aubry K. Miller[4,10], Michael W. Pfaffl[3], Maurine E. Linder[2], Bernhard Kuster[1,9] and Guillaume Médard[1]✉

Drugs that target histone deacetylase (HDAC) entered the pharmacopoeia in the 2000s. However, some enigmatic phenotypes suggest off-target engagement. Here, we developed a quantitative chemical proteomics assay using immobilized HDAC inhibitors and mass spectrometry that we deployed to establish the target landscape of 53 drugs. The assay covers 9 of the 11 human zinc-dependent HDACs, questions the reported selectivity of some widely-used molecules (notably for HDAC6) and delineates how the composition of HDAC complexes influences drug potency. Unexpectedly, metallo-β-lactamase domain-containing protein 2 (MBLAC2) featured as a frequent off-target of hydroxamate drugs. This poorly characterized palmitoyl-CoA hydrolase is inhibited by 24 HDAC inhibitors at low nanomolar potency. MBLAC2 enzymatic inhibition and knockdown led to the accumulation of extracellular vesicles. Given the importance of extracellular vesicle biology in neurological diseases and cancer, this HDAC-independent drug effect may qualify MBLAC2 as a target for drug discovery.

HDAC inhibition has emerged as a promising therapeutic option in oncology, as well as for other conditions such as Duchenne muscular dystrophy[1]. The United States Food and Drug Administration (FDA) approval of the first-in-class HDAC inhibitor (HDACi) vorinostat in 2006 for the treatment of cutaneous T-cell lymphoma marked the start of a series of drug approvals for cancerous diseases. Notably, most clinical HDACis engage several targets across the four classes of human zinc-dependent HDACs (I, IIa, IIb and IV). Such pan-HDACis and their polypharmacological mechanisms of action might be beneficial particularly in oncology, in which several disease-relevant class I and II HDACs are inhibited simultaneously[2]. However, conditions such as amyotrophic lateral sclerosis or Huntington's disease would require class II isoform-selective inhibitors that precisely interfere with the pathological mechanism[3,4] but bypass the toxicity that arises from the inhibition of epigenetic class I HDACs[2]. Therefore, the delineation of the target spectrum of HDACis appears to be essential for the understanding of their mechanisms of action and for the development of more tailored therapies.

HDAC activity highly depends on molecular context such as post-translational modifications[5], allosteric factors[6] or participation in gene regulatory protein complexes[7]. These factors have been shown to affect drug affinity, but are not recapitulated in traditional enzyme activity assays[8,9]. To address this challenge, a landmark study[8] reported a chemoproteomic assay that probes HDACi target engagement in lysates that contains natively folded proteins with their cofactors and that maintains the biomolecular interactions. The immobilization of vorinostat allowed for the pulldown of HDAC complexes, and competitive drug binding enabled the selectivity profiling of 16 HDACis against 6 of the 11 HDACs, particularly those in classes I and IIb. These chemoproteomic experiments led to the discovery of the mitotic deacetylase complex (MiDAC), which was later shown to be relevant for correct mitotic chromosome alignment[10]. Moreover, the study revealed that aminoanilide-based HDACis exhibit reduced affinity for the Sin3–HDAC complex and slow binding kinetics[8,9]. So far, however, affinity matrices designed to profile HDAC drugs do not address class IIa HDACs[11], which are targets of increasing interest[12].

Here, we substantially extended the existing profiling technology by creating an affinity matrix that enriches 9 out of 11 zinc (Zn^{2+})-dependent HDACs, including class IIa HDACs, and mapped the target landscape of 53 HDAC and metallohydrolase drugs. The results highlight HDACis with unexpected target profiles and low selectivity. However, we also identify drugs with unparalleled selectivity for class IIb HDAC6 and HDAC10. Moreover, the quantitative data revealed that drugs interacting with HDAC1 as part of gene regulatory REST corepressor (CoREST) complexes[13] containing either RCOR1 or RCOR3 show a >10-fold difference in HDAC1 binding affinity. Surprisingly, about half of the HDACis, including clinically advanced molecules, inhibit the acyl-CoA hydrolase

[1]Chair of Proteomics and Bioanalytics, TUM School of Life Sciences, Technical University of Munich, Freising, Germany. [2]Department of Molecular Medicine, College of Veterinary Medicine, Cornell University, Ithaca, New York, USA. [3]Animal Physiology and Immunology, TUM School of Life Sciences, Technical University of Munich, Freising, Germany. [4]Cancer Drug Development, German Cancer Research Center (DKFZ), Heidelberg, Germany. [5]Faculty of Biosciences, Heidelberg University, Heidelberg, Germany. [6]Computational Mass Spectrometry, TUM School of Life Sciences, Technical University of Munich, Freising, Germany. [7]Institute of Pharmacy, Martin Luther University of Halle-Wittenberg, Halle (Saale), Germany. [8]LipiTUM, Chair of Experimental Bioinformatics, TUM School of Life Sciences, Technical University of Munich, Freising, Germany. [9]Bavarian Center for Biomolecular Mass Spectrometry (BayBioMS), Technical University of Munich, Freising, Germany. [10]German Cancer Consortium (DKTK), Heidelberg, Germany. ✉e-mail: g.medard@tum.de

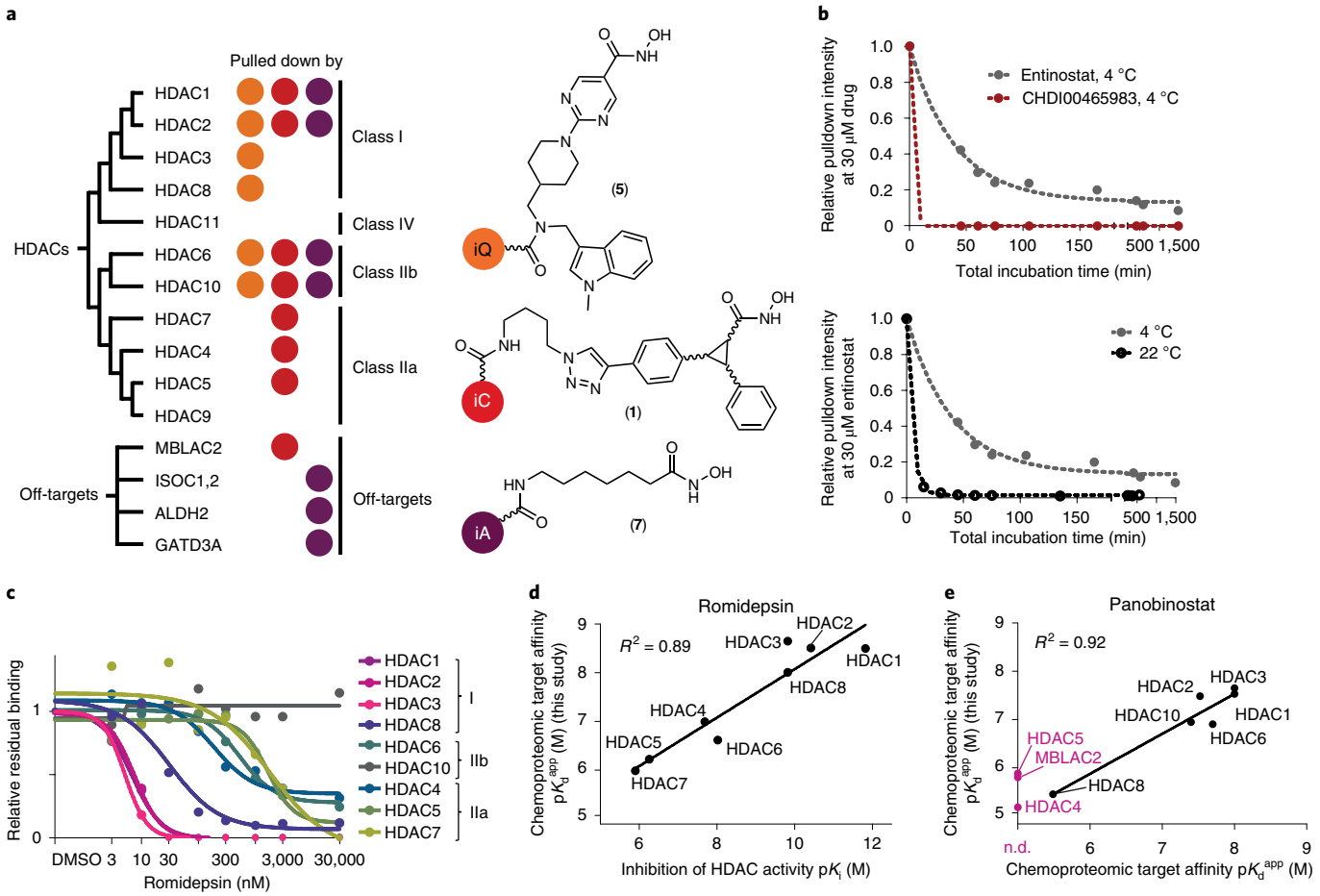

Fig. 1 | Chemical proteomics assay for HDACis. a, Contribution of each of the three selected affinity probes to the enrichment of zinc-dependent HDACs and off-targets from mixed SW620 and MV4-11 cell lysates. **b**, Temperature dependence of aminoanilide (entinostat) and hydroxamate (CHDI00465983) drugs on target engagement over time (up to 25 h). When binding equilibrium is reached, maximal occupancy of the target binding sites is obtained and minimal enrichment by the affinity matrix ensues (minimal residual binding is synonymous with maximal competition). **c**, Exemplary dose–response curves for romidepsin binding to HDACs using the optimized chemical proteomics assay. **d**, Correlation analysis of pK_d^{app} values of romidepsin. HDAC interactions are determined by the chemical proteomics assay and published pK_i values obtained by in vitro recombinant enzyme activity assays[17]. **e**, Correlation analysis of pK_d^{app} values of panobinostat. HDAC interactions are determined by the chemical proteomics assay and previously published chemical proteomics profiling[18]. Additional targets covered in this study (class IIa HDAC4 and HDAC5, and MBLAC2) are marked in pink. n.d., not determined.

MBLAC2 (ref. [14]) at nanomolar concentrations. We further demonstrate that pharmacological inhibition or knockdown of MBLAC2 triggers the accumulation of extracellular vesicles in cell culture, placing this poorly characterized protein into the context of extracellular vesicle biology.

Results

Optimized chemoproteomics assay for HDAC drugs profiling. Inspired by previous chemoproteomic studies of HDAC drugs[11], we embarked on the development of a general affinity matrix to comprehensively enrich the HDAC protein family. We synthesized 15 chemical probes (**1**–**15**) (Extended Data Fig. 1a) that represented different chemotypes, including different zinc-binding groups, and immobilized them on beads. Then, we evaluated the obtained affinity matrices for their suitability in pulling down HDACs from lysates of ten cell lines with different HDAC expression profiles, akin to the Kinobeads technology or other similar chemical proteomics approaches[15]. This led to the identification of a combination of three probes (iC, iQ and iA) (Fig. 1a) and lysates of two cell lines (MV4-11 and SW620) that together covered the widest range of targets (Fig. 1a and Extended Data Figs. 1 and 2). Specifically, iC robustly enriched seven HDACs, including class IIa HDAC4, HDAC5 and HDAC7, as well as MBLAC2. The addition of iQ improved the enrichment of HDAC3 and HDAC8, extending the coverage of the affinity matrix to 9 of the 11 zinc-dependent HDACs. We also included iA, as we observed that it enriched many metalloenzymes, including iron–sulfur cluster proteins (Extended Data Fig. 2 and Fig. 1a), as well as GATD3A, ALDH2, ISOC1 and ISOC2 that turned out to be common HDACi off-targets (see the section 'The target landscape of HDAC drugs' and Fig. 2a).

With this broad affinity matrix in hand, the target profiles of drugs can be obtained through competition experiments. Here, the drug of interest is added in increasing doses to the lysate in which it engages its targets and thereby prevents specific binding of the same targets to the matrix in a dose-dependent fashion (Supplementary Fig. 1)[8]. Plotting the relative intensities of matrix-binding proteins against increasing doses of free drug allows for the derivation of the half-maximum effective concentration (EC_{50}) and apparent dissociation constant (K_d^{app}) values that characterize the interaction (see Methods). Importantly, binding equilibrium between the molecule and the targets is essential to obtain meaningful K_d^{app} values. To account for the slow on-rates of the aminoanilide-based inhibitors[9,16], we evaluated incubation temperatures of 4 °C and 22 °C (hereafter, 22 °C is referred to as room temperature) for two

representative HDACis set to compete at 30 µM for up to 25 h. At 4 °C, the hydroxamate inhibitor CHDI00465983 engaged with class IIa HDACs within a few minutes, whereas the aminoanilide entinostat only maximally competed for target HDACs after more than 2 h. This reflects the already reported differences in binding kinetics of hydroxamates and aminoanilides, with the latter featuring extremely slow k_{on} rates[9]. However, increasing incubation temperature substantially decreased time to binding equilibrium for entinostat (Fig. 1b and Extended Data Fig. 3). We then validated a protocol with a 90-min total incubation time (60 min of drug pre-incubation and 30 min of pulldown) at 30 °C that could accommodate for very slow binders. Here, we profiled trichostatin A, mocetinostat, vorinostat, romidepsin and panobinostat and compared the results to those of previously published HDACi profiling studies[8,16,17]. In general, our data agree well with compared literature values. For instance, dose–response curves of romidepsin showed competition of HDACs from classes I, IIb and IIa (Fig. 1c), and pK_d^{app} ($-\log_{10}$[apparent dissociation constant]) values correlated well (coefficient of determination (R^2) = 0.89) with enzyme activity assays[17] (Fig. 1d) and were consistent with in-cell target engagement data based on bioluminescence resonance energy transfer (BRET)[16] (Extended Data Fig. 4). We found lower correlation with an initial chemoproteomics study[8]. In particular, the slow binder mocetinostat showed higher affinities here than those originally published[8]. However, the authors acknowledged their initial underestimation of aminoanilide affinity in a later study, in which they optimized the incubation conditions[9]. Remarkably, the K_d^{app} values for panobinostat correlated extremely well (R^2 = 0.92) to those from a more recent study using immobilized panobinostat (Fig. 1e)[18]. These experiments validate the approach and extend the assayed target spectrum over published data sets.

The target landscape of HDAC drugs. Next, we profiled 53 molecules comprising the majority of all clinical HDAC drugs, several HDAC tool compounds and five hydroxamate-based metallohydrolase drugs (see Supplementary Fig. 2 for structures). Only some of the data are highlighted in this manuscript; the complete profiling data can be dynamically explored in the freely accessible online database ProteomicsDB (https://www.proteomicsdb.org)[19]. Neither the HDAC activity modulator tasquinimod nor the five metallohydrolase inhibitors (batimastat, ilomastat, prinomastat, marimastat and salicylhydroxamic acid) bound HDACs or other metalloproteins with K_d^{app} values below 30 µM. Somewhat surprisingly, the same was observed for the four HDACis resminostat, BRD73954, HPOB and TH147. Expectedly, valproic acid and phenylbutanoic acid displayed weak (three-digit micromolar) affinities (Supplementary Data 1). By clustering the remaining 41 HDACis that have at least one micromolar target protein, we organized the compounds into four major groups (Fig. 2a). Group A comprises the aminoanilides that are selective for binding only HDAC1, HDAC2, and HDAC3. Group B comprises the thiolate romidepsin and hydroxamic acid-based pan-HDACis that often also engage MBLAC2. Interestingly, the most potent pan-HDACis (quisinostat and romidepsin) differ in the one class IIb HDAC that they engage. Romidepsin binds HDAC6 with high affinity, whereas quisinostat potently binds HDAC10 but not HDAC6, constituting an exception amongst the hydroxamic acid inhibitors. The peptidic capping group of the natural compound romidepsin does not closely mimic the nonpeptidic polyamine substrates of HDAC10, which might explain its poor affinity for HDAC10. Group C features rather unselective HDACis (including approved and clinical drugs such as vorinostat) that also bind non-HDAC off-targets, notably ALDH2 and the uncharacterized proteins ISOC1, ISOC2 and GATD3A. In contrast to groups A, B and C, group D is characterized by drugs that do not engage HDAC1, HDAC2 or HDAC3. Group D includes the most selective and potent class IIa inhibitors CHDI00390576 and CHDI00465983, which primarily target HDAC5 and HDAC7, as well as TMP195, with preferred binding for HDAC7 over HDAC4 and HDAC5. Live-cell imaging of drug-treated (at 100 nM and 1 µM) SW620 colorectal cancer cells highlighted the most potent inhibitors of HDAC1, HDAC2 and HDAC3 in groups A, B and C to affect cell vitality, whereas group D drugs did not induce an altered cell morphology (Extended Data Fig. 5). Exploring this landscape from a target perspective, we found that 29 compounds (>50% of the total) bound class I HDACs, which reflects the efforts expended in developing therapeutic modulators of these targets, and that 26 molecules bound class IIb HDACs. In contrast, only six drugs targeted class IIa HDACs. Interestingly, MC1568 and LMK235, which are frequently used as probes specific to class IIa, showed no class IIa target engagement at all in our assay, which calls into question their use as chemical probes but rationalizes the poor HDAC enrichment by probes based on these molecules (Fig. 2 and Extended Data Fig. 1e).

Selectivity of HDACis. The chemical proteomics data assembled here provided an opportunity to assess the selectivity of the HDACis for their targets. As a metric, we used the concentration- and target-dependent selectivity (CATDS) score[20], which is based on measuring the extent of target engagement by a drug. Target engagement refers to the fraction of all protein molecules that are bound by the drug at a particular drug concentration. By that definition, CATDS compares the half maximal target engagement of a particular drug to a target of interest (that is, the relative residual binding value of 0.5 for the pK_d^{app} of that drug–target interaction) to the sum of target engagements of all targets at that same drug concentration (see Methods and Supplementary Fig. 3). Systematic CATDS calculation for all drugs and targets confirmed PCI-34051 as the only selective HDAC8 inhibitor[21] (Fig. 2b and Supplementary Table 1). Interestingly, we found the HDAC6 inhibitor tubastatin A to be the second most selective HDAC10 inhibitor (CATDS = 0.67). This finding contrasts those of the original and recent reports[22] (Fig. 2c) but agrees well with published in-cell NanoBRET binding assays[23]. Furthermore, the pan-HDACi abexinostat had the highest HDAC10 affinity in the panel of drugs ($pK_d^{app,HDAC10}$ = 7.8 vs $pK_d^{app,HDAC1}$ = 6.1), in sharp contrast to the original report (pK_i^{HDAC10} = 7.6 vs pK_i^{HDAC1} = 8.2; pK_i, $-\log_{10}$[inhibition constant])[24]. Surprisingly, our analysis revealed TH65 as a selective inhibitor for HDAC10 (CATDS = 0.83, pK_d^{app} = 6.2) (Fig. 2c). TH65 was designed as an inhibitor of *Schistosoma mansoni* HDAC8 but has not been tested for human HDAC10 inhibition[25]. According to the Chemical Probes Portal (https://chemicalprobes.org), no highly selective HDAC10 probes have been reported yet, but our data designate TH65 as a novel promising chemical probe for HDAC10 with at least 30-fold selectivity (limit of our assay) over other HDACs. We profiled some selected HDACis in biochemical enzyme assays and confirmed the selectivity of TH65; TH65 inhibited HDAC10 binding with EC_{50} values comparable to those of vorinostat and ricolinostat in a fluorescence resonance energy transfer (FRET) assay, but had the lowest activity against HDAC1, HDAC2, HDAC3 and HDAC6 of the panel of drugs and, like vorinostat, had very low activity against HDAC8 (Extended Data Fig. 6a and Supplementary Table 2). We then demonstrated in-cell target engagement of TH65 by NanoBRET assays for HDAC10 and HDAC6 catalytic domain 2. In this assay, the affinity of TH65 for HDAC10 was about 5-fold higher than that for HDAC6 (Extended Data Fig. 6b and Supplementary Table 2).

For the second member of class IIb, our data examine the purported selectivity of HDAC6 probes such as tubacin, nexturastat A and tubastatin A (Fig. 2d). For instance, nexturastat A showed no substantial difference in affinity between HDAC6 and HDAC10 ($pK_d^{app,HDAC6}$ = 6.4 vs $pK_d^{app,HDAC10}$ = 6.0), contrasting reported values (pEC_{50}^{HDAC6} = 8.3 vs pEC_{50}^{HDAC10} = 5.1; pEC50, $-\log_{10}[EC_{50}]$)[26],

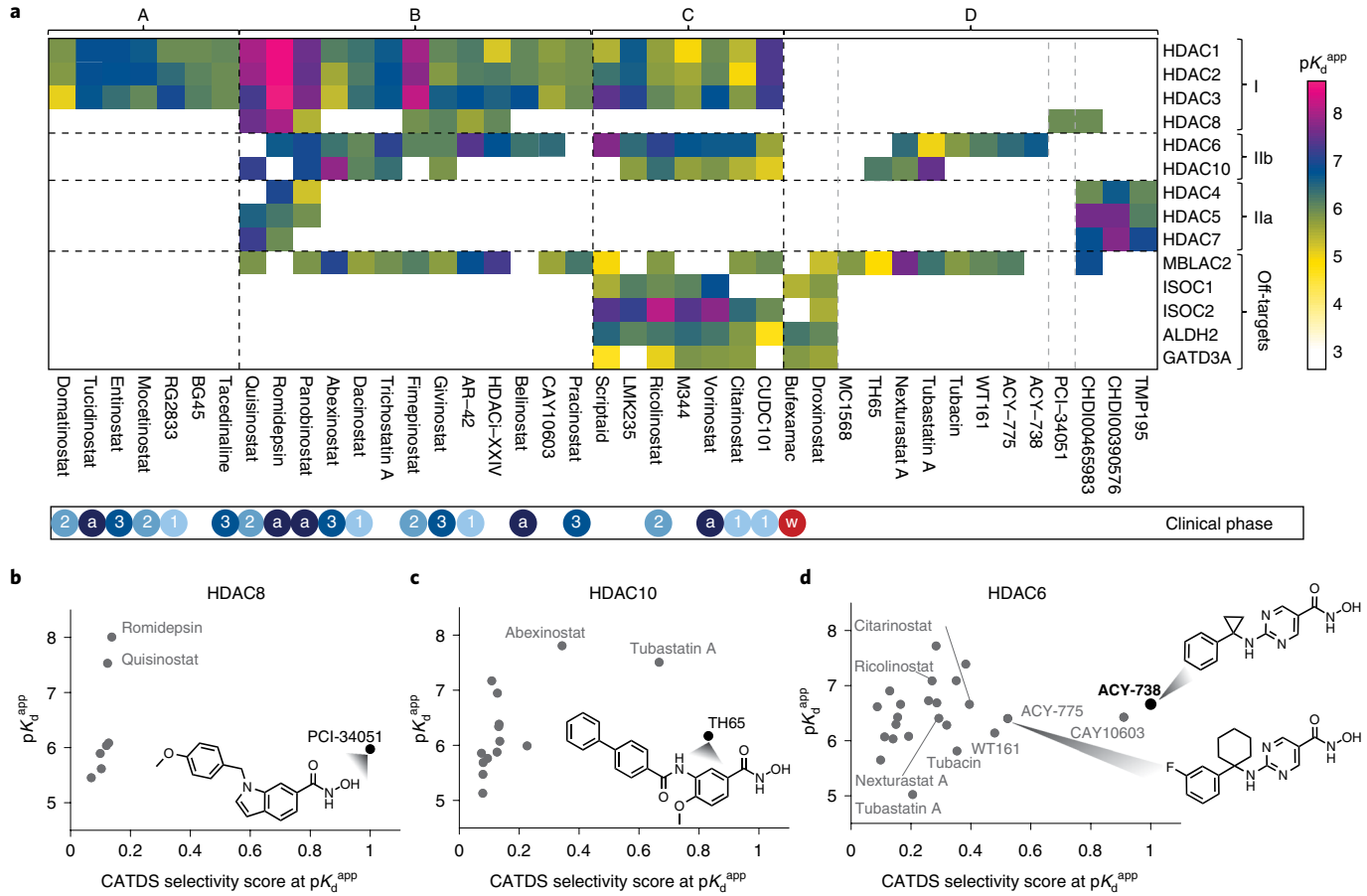

Fig. 2 | Target landscape of HDAC and metallohydrolase drugs. a, Heatmap of pK_d^{app} values obtained for 41 drugs and 14 targets using the presented chemical proteomics competition assay. A, B, C and D denote groups of drugs based on similar target profiles. Colored circles at the bottom of the panel indicate the clinical status of each drug: a, approved; w, withdrawn; 1–3, phases I–III of clinical development (https://clue.io/repurposing-app). **b**–**d**, Scatter plots displaying the affinity of drugs binding to HDAC8, HDAC10 or HDAC6 (pK_d^{app}) against their selectivity as measured by CATDS (calculated for the respective target HDAC at its pK_d^{app}; also see Supplementary Fig. 3 and text for details). The most selective compounds for a given target are marked by arrowheads and shown in bold. Structures for the most selective drugs are shown, as well as for the less-selective drug ACY-775 because of its chemical similarity to ACY-738 that we later exploit to probe MBLAC2 (see Fig. 5b).

but in line with recently reported NanoBRET data[23]. Nexturastat A also potently engages MBLAC2 (pK_d^{app} = 7.6), a novel finding that reduces the drug's apparent selectivity. Intriguingly, the two clinical designated HDAC6 inhibitors ricolinostat and citarinostat showed only slightly preferred binding for HDAC6 over class I HDACs, resulting in poor selectivity scores (Fig. 2d). Among all HDAC6-binding molecules, ACY-738 was the only compound with a perfect CATDS score of 1 (Fig. 2d). The selectivity of its close analogue ACY-775 was lower (CATDS = 0.52), owing to the nearly equipotent binding of MBLAC2. We confirmed the selectivity of ACY-738 in biochemical activity assays and its cellular target engagement in NanoBRET assays (Extended Data Fig. 6a–d and Supplementary Table 2). Considering the exquisite selectivity and its submicromolar affinity, ACY-738 currently appears to be the chemical probe of choice for HDAC6.

HDACi affinity depends on the composition of HDAC complexes. HDAC1, HDAC2 and HDAC3 exert their functions as part of protein complexes and, when tight complexes are formed, endogenous HDAC interactors are also captured by the affinity matrix. In the competition assay, complex partners are competed together with their interacting HDAC and therefore also provide dose–response curves that allow for the inference of the affinity of drugs to HDACs in complex with their respective interactors (Extended Data Fig. 7a). This allowed us to interrogate the binding of HDACis to five HDAC complexes systematically, using the acquired data. The CoREST, nucleosome remodeling and deacetylase (NuRD), Sin3 and MiDAC complexes are formed around a core of one to two isoforms of HDAC1 or HDAC2, whereas the nuclear receptor corepressor (NCoR) complex is formed around HDAC3 (ref. [13]). In accordance with published results[8,9], we did not observe a general difference between drug chemotypes with respect to preferential binding to HDAC3 that is part of the NCoR complex, nor to HDAC3 in isolation (Extended Data Fig. 7b). However, regarding HDAC1 and HDAC2-containing complexes, we observed an effect of the HDAC interactome on drug affinity. For instance, trichostatin A showed a 14-fold EC_{50} difference (ΔpEC_{50}) between HDAC1 that is part of the MiDAC complex (illustrated by its member deoxynucleotidyltransferase terminal-interacting protein 1 (DNTTIP1)) compared with HDAC1 that is not part of the complex (Fig. 3a). Even more strikingly, REST corepressor 3 (RCOR3) showed a >10-fold lower EC_{50} value compared with those of REST corepressor 1 (RCOR1) and other CoREST members, which was observed most prominently for panobinostat, romidepsin, dacinostat and M344 (Fig. 3b). These measurements support the existence of drug selectivity between variants of the same complex

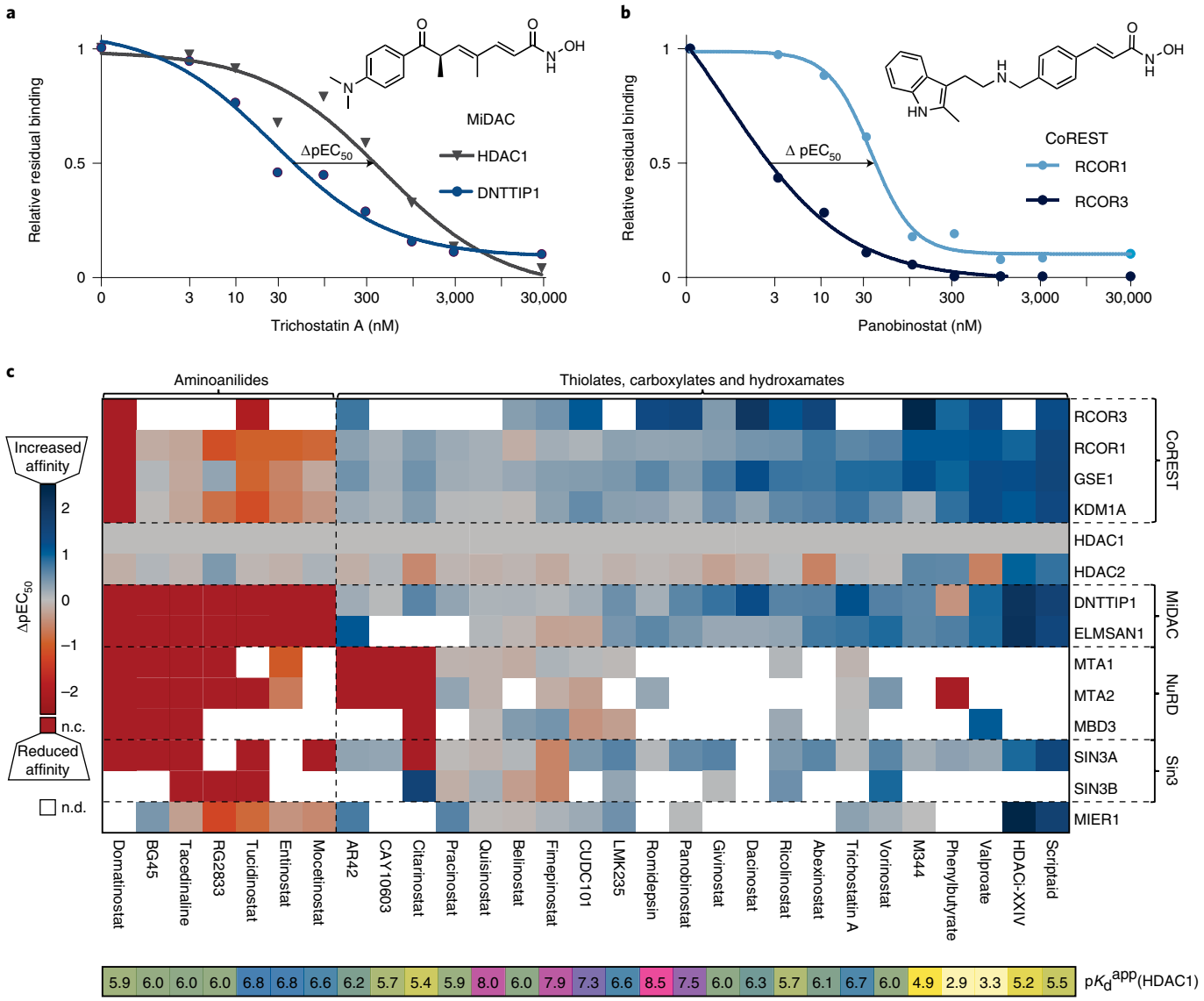

Fig. 3 | Complex selectivity of class I HDACis. a, Dose–response binding curves for trichostatin A vs HDAC1 and DNTTIP1 (representing the MiDAC complex). The difference between the two inflection points of the dose–response curve is marked by ΔpEC_{50}. **b**, Dose–response binding curves for panobinostat and the CoREST subunits RCOR1 and RCOR3. **c**, Heatmap showing ΔpEC_{50} ($pEC_{50}^{Interactor} - pEC_{50}^{HDAC1}$) values for class I HDACis and HDAC complex proteins. The bar at the bottom lists HDAC1 pK_d^{app} values of the corresponding HDACi. n.d., not determined; n.c., not competed.

depending on its (mutually exclusive) subunits. To generalize the above, we calculated ΔpEC_{50} for HDAC1 and each complex protein (Fig. 3c). This led to a clear distinction between aminoanilides and the other drugs; aminoanilides showed decreased potency for HDAC1 and HDAC2 when part of complexes (ΔpEC_{50} in red, Fig. 3c), whereas hydroxamates showed generally increased potency (ΔpEC_{50} in blue, Fig. 3c). Enhanced affinity to RCOR3-interacting HDACs was observed for the majority of hydroxamic acid inhibitors. These data confirm and extend previous observations that HDACi target engagement strongly depends on the composition of HDAC complexes and thus provides prospects for the development of further HDAC complex-specific drugs.

Acyl-CoA hydrolase MBLAC2 is a common off-target of HDACis. Perhaps the most unexpected result of this study was the observation of MBLAC2 as an off-target of 24 hydroxamate molecules (Fig. 2a). Amongst those are approved drugs such as panobinostat ($pK_d^{app} = 5.9$) and frequently used tool compounds such as nexturastat A ($pK_d^{app} = 7.6$) (Fig. 4a). To ascertain that the inhibition of binding equals the inhibition of enzymatic activity, we deployed a recombinant enzyme activity assay that measures the MBLAC2-catalyzed hydrolysis of ^{3}H-labeled palmitoyl-CoA (Fig. 4b)[14]. MBLAC2 activity was affected by nearly all binders at 300 nM drug concentration and reduced to background for 18 HDACis (Fig. 4c). HDAC drugs (for example, tucidinostat and PCI-34051) that showed no or very weak MBLAC2 binding in the chemoproteomic assay had little if any effect on enzyme activity. Full dose–response assays for 11 compounds showed that most reached the experimental EC_{50} limit of 5–10 nM (that is, pEC_{50} of ca. 8.0–8.3), which corresponds to 50% of the applied enzyme concentration. Notably, these potent inhibitors included the approved drug panobinostat ($pEC_{50} > 8.0$) and the orphan drug pracinostat ($pEC_{50} > 8.2$) (Fig. 4d and Extended Data Fig. 8). In contrast, the approved aminoanilide tucidinostat did not affect MBLAC2 activity

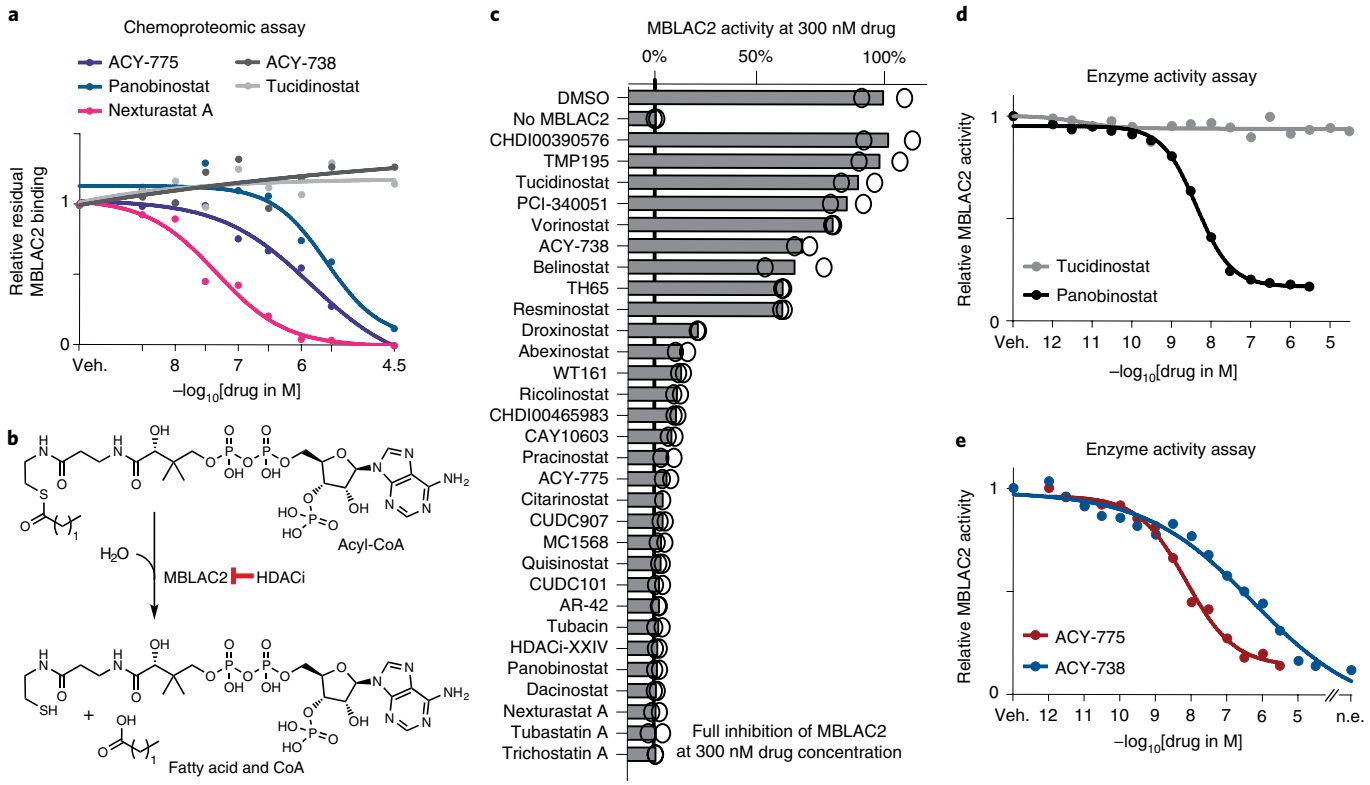

Fig. 4 | HDACis abrogate MBLAC2 acyl-CoA hydrolase activity at nanomolar concentrations. a, Chemoproteomic dose–response binding curves of MBLAC2 and five HDACis. **b**, Reaction scheme of the MBLAC2-catalyzed hydrolysis of acyl-CoA. **c**, Bar plot summarizing results of a single-dose MBLAC2 enzyme inhibition screen using HDACis. Bars represent the relative rate of [^{3}H]-palmitoyl-CoA hydrolysis in the presence of recombinant MBLAC2 (30 nM) and 24 HDACis at 300 nM drug concentration (mean of two measurements, whiskers of error bar denote s.d.). **d**, Dose-dependent inhibition of MBLAC2 activity by approved HDACis. **e**, Dose-dependent inhibition of MBLAC2 activity by two structurally related compounds. n.e., no enzyme; veh., vehicle control.

even at a 1,000-fold higher concentration. Also in concordance with the competition binding data, ACY-775 is a very potent MBLAC2 inhibitor ($pK_d^{app} = 6.1$, $pEC_{50} > 8.2$), whereas the chemically closely related compound ACY-738 is >75-fold less potent ($pK_d^{app} < 4.5$, $pEC_{50} = 6.3$; Fig. 4e).

MBLAC2 inhibition leads to accumulation of extracellular vesicles. MBLAC2 is a poorly characterized protein. Yet, it has been shown to interact with zinc-finger DHHC-type palmitoyltransferase 20 (ZDHHC20)[14], a regulator of endocytosis-mediated epidermal growth factor receptor (EGFR) internalization[27], as well as other proteins with Gene Ontology (GO) term enrichment that hints at roles in endocytosis or exocytosis (BioPlex; Supplementary Data 2)[28]. Concurring GO annotations were also found when analyzing the localization and roles of MBLAC2-coregulated proteins (ProteomeHD)[29] (Supplementary Data 2). In addition, the HDAC6 inhibitor tubacin has been shown to produce a strong vesicle phenotype that cannot be attributed to HDAC6 inhibition[30]. As we identified tubacin to inhibit MBLAC2 (Figs. 2a and 4c), we speculated that the vesicle phenotype may be related to MBLAC2 activity. Knocking down >85% of the protein in HEK293 cells using short interfering RNA (siRNA) did not have a substantial effect on the expression of 7,112 monitored proteins, including those known to be associated with MBLAC2 and vesicle biology (Extended Data Fig. 9a,b and Supplementary Data 3). However, the knockdown indeed induced accumulation of extracellular vesicles in the cell culture supernatants (Fig. 5a). This accumulation was even more pronounced upon pharmacological inhibition of MBLAC2 by ACY-775 (Fig. 5b), compared with treatment with its close analogue ACY-738 (Fig. 2a). ACY-738 and ACY-775 inhibit HDAC6 with similar potency in the chemoproteomic assay (ACY-775 $pK_d^{app} = 6.4$ vs ACY-738 $pK_d^{app} = 6.7$), and a comparable effect on acetylation of HDAC6 substrate α-tubulin is also observed (Extended Data Fig. 10). In contrast, only ACY-775 is a potent MBLAC2 binder and inhibitor ($pK_d^{app} = 6.1$, $pEC_{50} = 8.2$), whereas ACY-738 is not ($pK_d^{app} < 4.5$, $pEC_{50} = 6.3$). Together, these data suggest a role of MBLAC2 activity in extracellular vesicle levels.

Considering the involvement of lipids and particularly ceramides in vesicle budding[31], we tested whether MBLAC2 inhibition has an effect on the lipid composition of the cell. Untargeted mass spectrometry-based lipidomics following MBLAC2 knockdown revealed changes in the levels of several lipids. For instance, hexosylceramides were significantly downregulated, but sphingomyelins were generally upregulated (Fig. 5c, Extended Data Fig. 9c and Supplementary Data 4). Although we could not demonstrate ceramidase activity of MBLAC2 using a fluorescently labeled C12-ceramide model substrate (Extended Data Fig. 9d–g), the observed changes in lipid composition may still be the direct or indirect result of inhibiting one or several MBLAC2 activities and may provide a link to the well-studied effects of ceramides in vesicle biogenesis pathways[31].

Discussion

The current study makes several noteworthy contributions to the field of chemical biology. The profiling data for the 53 drugs targeting HDACs and metallohydrolases is the most comprehensive to date and constitutes a rich resource for chemical biologists and medicinal chemists. The collective data enabled several analyses that are not possible in small data sets and revealed a number of surprises.

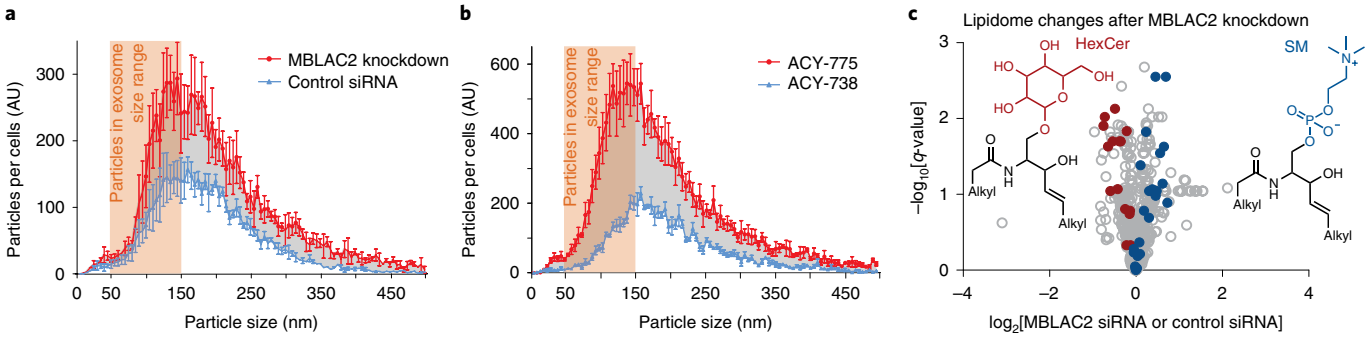

Fig. 5 | MBLAC2 knockdown or inhibition lead to vesicle accumulation in supernatants of HEK293 cells. a, Number and size distribution of extracellular vesicles isolated from HEK293 cell supernatants following MBLAC2 knockdown by siRNA pools ($n = 3$ biological replicates; data are shown as mean ± s.e.m.). The orange area marks the typical size range of exosomes. **b**, Number and size distribution of extracellular vesicles isolated from HEK293 cell supernatants following exposure to the dual HDAC6 and MBLAC2 inhibitor ACY-775 (3 μM) and the selective HDAC6 inhibitor ACY-738 (3 μM) ($n = 3$ biological replicates; data are shown as mean ± s.e.m.). **c**, Volcano plot summarizing the response of the lipidome of HEK293 cells in response to MBLAC2 knockdown ($n = 3$ experiments). Members of the hexosylceramide (HexCer) and sphingomyelin (SM) families are highlighted, and their generic structures are shown.

First, the novel affinity matrix goes beyond the state of the art[8,11,18,32], as it enriches 9 out of the 11 human zinc-dependent HDACs, including class IIa HDACs. This improvement mostly stems from the development of iC, featuring a diarylcyclopropane hydroxamic acid chemotype developed for HDAC5 inhibition[33,34]. In this series of inhibitors, enantiomerically pure CHDI00465983 is class IIa selective (Fig. 2), whereas iC (composed of three enantiomer pairs) exhibits pan-HDAC and off-target MBLAC2 binding characteristics. Immobilized quisinostat, iQ, enriches HDAC8 better than immobilized vorinostat (**6**) or any other affinity matrix tested. Off-targets GATD3A, ALDH2, ISOC1 and ISOC2 could be identified only because of their robust enrichment by iA. We note that the sterically permissive alkyl chain of iA, also found in all HDACis constituting group B (Fig. 2a and Supplementary Fig. 2), might favorably position the metal-binding hydroxamate in the active sites of many other metalloproteins leading to their enrichment (Extended Data Fig. 2). Further work aims to identify HDAC9-rich and HDAC11-rich cell lines and a dedicated HDAC11 probe. As it stands, the affinity matrix may also be leveraged to investigate HDACi repurposing against, for example, parasites such as *Schistosoma mansoni* or *Plasmodium falciparum*[35], owing to the particularly high HDAC preservation across the species phylogeny.

Second, it is obviously important to know which proteins are engaged by a given drug, how potent the drug is for that target and what its selectivity is over other targets to be able to attribute an observed biological effect to the target(s) of the compound. For example, for the designated HDAC6 inhibitors ricolinostat ($pK_d^{app,HDAC6} = 7.1$) and citarinostat ($pK_d^{app,HDAC6} = 6.7$), the narrow selectivity window is consistent with an earlier study that attributed their main anticancer effects to the inhibition of HDAC1, HDAC2 and HDAC3 (pK_d^{app} range of 4.9–6.0; Fig. 2) rather than HDAC6 (ref. [36]). More surprisingly, tubastatin A has been used in >100 publications to probe HDAC6 biology under the assumption of high HDAC6 selectivity[22]. According to our results, however, tubastatin A has a much higher potency for HDAC10 than HDAC6 ($pK_d^{app,HDAC10} = 7.5$ vs $pK_d^{app,HDAC6} = 5.0$). We hypothesize that the discrepancy between the published HDAC activity inhibition data and the chemoproteomic binding data, as well as in-cell target engagement data (NanoBRET (ref. [23])), originates from the inadequacy of the peptidic substrate used in earlier studies; HDAC10 was only recently annotated as a polyamine rather than a protein deacylase[37]. In this regard, the most potent HDAC10 binders in our assay (tubastatin A, abexinostat, pracinostat, quisinostat, panobinostat and dacinostat) all feature a positively charged amino group reminiscent of the charged polyamine substrate that interacts with the gatekeeper glutamate (Glu272 or potentially Glu22) of HDAC10 (ref. [23]). However, high selectivity is achievable. Three drugs even fulfill prime criteria for a chemical probe (submicromolar potency, 30-fold window over other targets)[38]: ACY-738 for HDAC6, PCI-34051 for HDAC8 and TH65 for HDAC10. Their identification will serve chemical biology, as, for instance, TH65 could probe the roles of HDAC10 in polyamine biology and autophagy, as well as in neuroblastoma[23,37,39,40].

Third, it is evident from the target landscape that the design of inhibitors that discriminate between the very similar active sites of HDAC1, HDAC2 and HDAC3 is challenging. Here, selectivity may be obtained with drugs that target particular HDAC complexes[13], such as CoREST-selective HDACi to treat synaptopathies[41]. Chemoproteomic profiling preserves HDAC complexes, leading to the observation that hydroxamic acid drugs tend to prefer binding to CoREST, Sin3 and MiDAC complexes (Fig. 3c). Surprisingly, some of those drugs bind with >10-fold higher affinity to HDAC1 or HDAC2 when interacting with RCOR3 instead of the alternative CoREST subunit RCOR1. In contrast to hydroxamates, aminoanilide drugs appear to bind better to HDACs that are not part of a complex. This agrees with a recent report about aminoanilide drugs engaging free HDACs and staying entrapped in the active site after the formation of a complex with rigidified HDAC dynamics[42]. The data suggest that different classes of HDAC drugs (hydroxamates vs aminoanilides) might differentially modulate the acetylation of HDAC substrates according to their preference for one of the complexes or the HDACs in isolation.

Fourth, chemoproteomic profiling is set to identify unexpected targets for otherwise well-characterized drugs. For instance, we and others have identified novel targets of kinase inhibitors within (for example, activin receptor ALK2 for the ATM inhibitor CP466722)[43] or outside the target class (for example, ferrochelatase for the BRAF inhibitor vemurafenib)[44]. The current study uncovered five such cases for HDACis, notably ALDH2 ($n = 9$ drugs, most potent $pK_d^{app} = 6.5$), GATD3A ($n = 7$ drugs, most potent $pK_d^{app} = 5.8$), ISOC1 ($n = 7$ drugs, most potent $pK_d^{app} = 6.8$), ISOC2 ($n = 8$ drugs, most potent $pK_d^{app} = 8.2$) and MBLAC2 ($n = 24$ drugs, most potent $pK_d^{app} = 7.6$). Interestingly, MBLAC2 was bound by several HDACi groups. The other off-targets seem to be preferentially bound by HDACis that have a hydroxamic acid presented via an alkyl chain. Hence, the alkyl may favor off-target binding, whereas HDACis with conjugated or aromatic linkers will be more selective for HDACs. All off-targets except ALDH2 are poorly characterized proteins,

and it remains to be investigated whether HDACi binding affects their biological function and thus affects drug efficacy. Intriguingly, ISOC1 knockdown has been reported to inhibit cancer cell proliferation and metastasis[45], which may be a desirable off-target effect of, for example, vorinostat. Droxinostat and bufexamac did not bind HDACs in our assay, but their affinity for some of the off-targets may be used to probe the function of these proteins.

Fifth, among the non-HDAC off-targets, MBLAC2 stands out for its potent and frequent binding to hydroxamic acid HDACis. This protein has recently been shown to hydrolyze acyl-CoA and, just like HDACs, it utilizes Zn^{2+} for catalysis[14]. Our data show, for the first time, that HDACis can inhibit the palmitoyl-CoA hydrolase activity of the enzyme in vitro, and several do so with single-digit nanomolar EC_{50} values. Interestingly, a study describing an HDAC6-independent stimulatory effect of tubacin on exosome biogenesis[30] led us to hypothesize that this phenotype may stem from the inhibition of MBLAC2, the only off-target of tubacin in our chemoproteomic assay. Given that MBLAC2 can hydrolyze palmitoyl-CoA, the initial building block of ceramides, we speculated that MBLAC2 might be involved in regulating ceramide levels and exosome release. In line with such a putative role, treatment with the dual MBLAC2 and HDAC6 inhibitor ACY-775 led to the accumulation of extracellular vesicles compared with treatment with the HDAC6-selective ACY-738. This finding suggests a direct or indirect role of MBLAC2 in extracellular vesicle biology, which we substantiated by conducting MBLAC2 knockdown experiments. Importantly, differential effects of ACY-775 and ACY-738 have been observed before, such as more pronounced activity on mitochondria number and axonal transport for ACY-775 than for ACY-738 in a genetic mouse model of Charcot–Marie–Tooth disease[46]. Interestingly, other inhibitors that we found to be dual MBLAC2 and HDAC6 inhibitors are investigated in neurological diseases, for instance to improve axonal transport of brain-derived neurotrophic factor (BDNF) vesicles and BDNF release[47,48]. It is therefore tempting to hypothesize a synergy between effects on the extracellular vesicle level via MBLAC2 inhibition and HDAC6-linked effects on microtubular vesicle transport and fusion[49]. We then started to explore which molecular events in the lipidome connect MBLAC2 inhibition and extracellular vesicle accumulation. Although we could not evidence MBLAC2 C12-ceramidase activity as a potential regulatory mode of vesicle budding[31], MBLAC2 might hydrolyze other lipids in cells. Such lipidase activity has indeed been elucidated for at least one of the 18 human metallo-β-lactamase domain-containing proteins, *N*-acyl-phosphatidylethanolamine-hydrolyzing phospholipase D (NAPEPLD)[50]. In fact, MBLAC2 knockdown had an effect on intracellular concentrations of some lipid families, including a general decrease of hexosylceramides and a concomitant increase of sphingomyelin levels. We anticipate that the identified MBLAC2 inhibitors will inspire biologists to further probe MBLAC2 cellular functions and help understand its connection to extracellular vesicle accumulation.

To conclude, this study has shown how the design and synthesis of promiscuous affinity probes enabled the delineation of the target landscape of HDACis. The drug profiles, assembled in ProteomicsDB, inform medicinal chemistry and highlight chemical probes to study biology. The surprising identification of MBLAC2 as an HDACi target helped to place this poorly characterized protein into a functional context and may provide the basis for future drug discovery programs focused on vesicle pathobiology.

Online content

Any methods, additional references, Nature Research reporting summaries, source data, extended data, supplementary information, acknowledgements, peer review information; details of author contributions and competing interests; and statements of data and code availability are available at https://doi.org/10.1038/s41589-022-01015-5.

Received: 22 June 2021; Accepted: 15 March 2022;
Published online: 28 April 2022

References

1. Bettica, P. et al. Histological effects of givinostat in boys with Duchenne muscular dystrophy. *Neuromuscul. Disord.* **26**, 643–649 (2016).
2. Li, Y. & Seto, E. HDACs and HDAC inhibitors in cancer development and therapy. *Cold Spring Harb. Perspect. Med.* **6**, a026831 (2016).
3. Saito, M. et al. Acetylation of intrinsically disordered regions regulates phase separation. *Nat. Chem. Biol.* **15**, 51–61 (2019).
4. Federspiel, J. D., Greco, T. M., Lum, K. K. & Cristea, I. M. Hdac4 interactions in Huntington's disease viewed through the prism of multiomics. *Mol. Cell. Proteomics* **18**, S92–S113 (2019).
5. Bardai, F. H. & D'Mello, S. R. Selective toxicity by HDAC3 in neurons: regulation by Akt and GSK3β. *J. Neurosci.* **31**, 1746–1751 (2011).
6. Watson, P. J. et al. Insights into the activation mechanism of class I HDAC complexes by inositol phosphates. *Nat. Commun.* **7**, 11262 (2016).
7. Guenther, M. G., Barak, O. & Lazar, M. A. The SMRT and N-CoR corepressors are activating cofactors for histone deacetylase 3. *Mol. Cell. Biol.* **21**, 6091–6101 (2001).
8. Bantscheff, M. et al. Chemoproteomics profiling of HDAC inhibitors reveals selective targeting of HDAC complexes. *Nat. Biotechnol.* **29**, 255–265 (2011).
9. Becher, I. et al. Chemoproteomics reveals time-dependent binding of histone deacetylase inhibitors to endogenous repressor complexes. *ACS Chem. Biol.* **9**, 1736–1746 (2014).
10. Turnbull, R. E. et al. The MiDAC histone deacetylase complex is essential for embryonic development and has a unique multivalent structure. *Nat. Commun.* **11**, 3252 (2020).
11. Weigt, D., Hopf, C. & Médard, G. Studying epigenetic complexes and their inhibitors with the proteomics toolbox. *Clin. Epigenetics* **8**, 76 (2016).
12. Asfaha, Y. et al. Recent advances in class IIa histone deacetylases research. *Bioorg. Med. Chem.* **27**, 115087 (2019).
13. Millard, C. J., Watson, P. J., Fairall, L. & Schwabe, J. W. R. Targeting class I histone deacetylases in a 'complex' environment. *Trends Pharmacol. Sci.* **38**, 363–377 (2017).
14. Malgapo, M. I. P., Safadi, J. M. & Linder, M. E. Metallo-β-lactamase domain-containing protein 2 is S-palmitoylated and exhibits acyl-CoA hydrolase activity. *J. Biol. Chem.* **296**, 100106 (2021).
15. Médard, G. et al. Optimized chemical proteomics assay for kinase inhibitor profiling. *J. Proteome Res* **14**, 1574–1586 (2015).
16. Robers, M. B. et al. Target engagement and drug residence time can be observed in living cells with BRET. *Nat. Commun.* **6**, 10091 (2015).
17. Bradner, J. E. et al. Chemical phylogenetics of histone deacetylases. *Nat. Chem. Biol.* **6**, 238–243 (2010).
18. Becher, I. et al. Thermal profiling reveals phenylalanine hydroxylase as an off-target of panobinostat. *Nat. Chem. Biol.* **12**, 908–910 (2016).
19. Samaras, P. et al. ProteomicsDB: a multi-omics and multi-organism resource for life science research. *Nucleic Acids Res.* **48**, D1153–D1163 (2020).
20. Heinzlmeir, S. et al. Chemoproteomics-aided medicinal chemistry for the discovery of EPHA2 Inhibitors. *ChemMedChem* **12**, 999–1011 (2017).
21. Balasubramanian, S. et al. A novel histone deacetylase 8 (HDAC8)-specific inhibitor PCI-34051 induces apoptosis in T-cell lymphomas. *Leukemia* **22**, 1026–1034 (2008).
22. Shen, S. et al. Structural and in vivo characterization of tubastatin A, a widely used histone deacetylase 6 inhibitor. *ACS Med. Chem. Lett.* **11**, 706–712 (2020).
23. Géraldy, M. et al. Selective inhibition of histone deacetylase 10: hydrogen bonding to the gatekeeper residue is implicated. *J. Med. Chem.* **62**, 4426–4443 (2019).
24. Buggy, J. J. et al. CRA-024781: a novel synthetic inhibitor of histone deacetylase enzymes with antitumor activity in vitro and in vivo. *Mol. Cancer Ther.* **5**, 1309–1317 (2006).
25. Heimburg, T. et al. Structure-based design and synthesis of novel inhibitors targeting HDAC8 from *Schistosoma mansoni* for the treatment of schistosomiasis. *J. Med. Chem.* **59**, 2423–2435 (2016).
26. Bergman, J. A. et al. Selective histone deacetylase 6 inhibitors bearing substituted urea linkers inhibit melanoma cell growth. *J. Med. Chem.* **55**, 9891–9899 (2012).
27. Runkle, K. B. et al. Inhibition of DHHC20-mediated EGFR palmitoylation creates a dependence on EGFR signaling. *Mol. Cell* **62**, 385–396 (2016).
28. Huttlin, E. L. et al. Dual proteome-scale networks reveal cell-specific remodeling of the human interactome. *Cell* **184**, 3022–3040.e28 (2021).
29. Kustatscher, G. et al. Co-regulation map of the human proteome enables identification of protein functions. *Nat. Biotechnol.* **37**, 1361–1371 (2019).
30. Chao, O. S. et al. The HDAC6 inhibitor tubacin induces release of CD133$^+$ extracellular vesicles from cancer cells. *J. Cell. Biochem.* **118**, 4414–4424 (2017).

31. Trajkovic, K. et al. Ceramide triggers budding of exosome vesicles into multivesicular endosomes. *Science* **319**, 1244–1247 (2008).
32. Lobera, M. et al. Selective class IIa histone deacetylase inhibition via a nonchelating zinc-binding group. *Nat. Chem. Biol.* **9**, 319–325 (2013).
33. Bürli, R. W. et al. Design, synthesis, and biological evaluation of potent and selective class IIa histone deacetylase (HDAC) inhibitors as a potential therapy for Huntington's disease. *J. Med. Chem.* **56**, 9934–9954 (2013).
34. Luckhurst, C. A. et al. Potent, selective, and CNS-penetrant tetrasubstituted cyclopropane class IIa histone deacetylase (HDAC) inhibitors. *ACS Med. Chem. Lett.* **7**, 34–39 (2016).
35. Hailu, G. S. et al. Lysine deacetylase inhibitors in parasites: past, present, and future perspectives. *J. Med. Chem.* **60**, 4780–4804 (2017).
36. Lin, A. et al. Off-target toxicity is a common mechanism of action of cancer drugs undergoing clinical trials. *Sci. Transl. Med.* **11**, eaaw8412 (2019).
37. Hai, Y., Shinsky, S. A., Porter, N. J. & Christianson, D. W. Histone deacetylase 10 structure and molecular function as a polyamine deacetylase. *Nat. Commun.* **8**, 15368 (2017).
38. Arrowsmith, C. H. et al. The promise and peril of chemical probes. *Nat. Chem. Biol.* **11**, 536–541 (2015).
39. Oehme, I. et al. Histone deacetylase 10 promotes autophagy-mediated cell survival. *Proc. Natl Acad. Sci. USA* **110**, E2592–E2601 (2013).
40. Ridinger, J. et al. Dual role of HDAC10 in lysosomal exocytosis and DNA repair promotes neuroblastoma chemoresistance. *Sci. Rep.* **8**, 10039 (2018).
41. Fuller, N. O. et al. CoREST complex-selective histone deacetylase inhibitors show prosynaptic effects and an improved safety profile to enable treatment of synaptopathies. *ACS Chem. Neurosci.* **10**, 1729–1743 (2019).
42. Mazitschek, R. & Payne, N. Resolving the deceptive isoform and complex selectivity of HDAC1/2 inhibitors. *Cell Chem. Biol.* **29**, 1–13 (2022).
43. Reinecke, M. et al. Chemoproteomic selectivity profiling of PIKK and PI3K kinase inhibitors. *ACS Chem. Biol.* **14**, 655–664 (2019).
44. Klaeger, S. et al. Chemical proteomics reveals ferrochelatase as a common off-target of kinase inhibitors. *ACS Chem. Biol.* **11**, 1245–1254 (2016).
45. Gao, B. et al. Knockdown of ISOC1 inhibits the proliferation and migration and induces the apoptosis of colon cancer cells through the AKT/GSK-3β pathway. *Carcinogenesis* **41**, 1123–1133 (2020).
46. Benoy, V. et al. Development of improved HDAC6 inhibitors as pharmacological therapy for axonal Charcot–Marie–Tooth disease. *Neurotherapeutics* **14**, 417–428 (2017).
47. Gold, W. A., Lacina, T. A., Cantrill, L. C. & Christodoulou, J. MeCP2 deficiency is associated with reduced levels of tubulin acetylation and can be restored using HDAC6 inhibitors. *J. Mol. Med.* **93**, 63–72 (2015).
48. Benoy, V. et al. HDAC6 is a therapeutic target in mutant GARS-induced Charcot–Marie–Tooth disease. *Brain* **141**, 673–687 (2018).
49. Guo, W. et al. HDAC6 inhibition reverses axonal transport defects in motor neurons derived from FUS-ALS patients. *Nat. Commun.* **8**, 861 (2017).
50. Wang, J. et al. Functional analysis of the purified anandamide-generating phospholipase D as a member of the metallo-β-lactamase family. *J. Biol. Chem.* **281**, 12325–12335 (2006).

Methods

Preparation of iC (1). 4-Azidobutanamine (1 µmol) was reacted with dimethylsulfoxide (DMSO)-washed *N*-hydroxysuccinimide (NHS)-activated (~20 µmol per ml beads) sepharose beads (1 ml) and triethylamine (20 µl) in DMSO (2 ml) on an end-over-end shaker overnight at room temperature in the dark. Aminoethanol (50 µl) was then added to inactivate the remaining NHS-activated carboxylic acid groups. After 1 h, the beads were washed with 40 ml DMSO.

Alkyne-NHOTHP (**19**) (1 µmol) (Supplementary Note) was then clicked to the azide-functionalized beads via incubation in 1:1:2 (v/v/v) DMSO:tBuOH:H_2O (2 ml total volume including beads), 0.1 mM tris(benzyltriazolylmethyl)amine (TBTA), 2 mM $CuSO_4$ and 2 mM sodium ascorbate for 16 h at room temperature in the dark on the end-over-end shaker. The beads were then washed with 20 ml of 1:1:2 (v/v/v) DMSO:tBuOH:H_2O, 30 ml of 50 mM EDTA in water and 30 ml ethanol, then reacted with 10 mM HCl in EtOH (10 ml) for 16 h at room temperature in the dark. Beads were washed with 50 ml ethanol to yield **iC**, stored at 4 °C in EtOH.

Preparation of iQ (5). Quisinostat (1 µmol) was reacted with DMSO-washed NHS-activated (~20 µmol per ml beads) sepharose beads (1 ml) and triethylamine (20 µl) in DMSO (2 ml) on an end-over-end shaker overnight at room temperature in the dark. Aminoethanol (50 µl) was then added to inactivate the remaining NHS-activated carboxylic acid groups. After 16 h, the beads were washed with 10 ml DMSO and 30 ml EtOH to yield **iQ**, stored at 4 °C in EtOH.

Preparation of iA (7). 6-Aminocaproic acid (1 µmol, 100 µl of 10 mM stock solution in 50 mM HCl tBuOH) was reacted with DMSO-washed NHS-activated (~20 µmol per ml beads) sepharose beads (1 ml) and triethylamine (15 µl) in DMSO (2 ml) on an end-over-end shaker for 16 h at room temperature in the dark (thin-layer chromatography (TLC) with Kaiser test staining was used to monitor successful conversion). Aminoethanol (50 µl) was then added to inactivate the remaining NHS-activated carboxylic acid groups. After 2 h on an end-over-end shaker at room temperature, the beads were washed with DMSO (4 × 10 ml) and resuspended in anhydrous dimethylformamide (DMF) (2 ml total volume). Hexafluorophosphate azabenzotriazole tetramethyl uronium (HATU) (10 µmol, 100 µl of 100 mM stock in DMF), *O*-(tetrahydro-2*H*-pyran-2yl)-hydroxylamine (12 µmol, 120 µl of 100 mM stock in DMF), Hünig's base (20 µmol, 100 µl of 200 mM stock in DMF) and triethylamine (20 µl) were then added, and the beads were incubated at room temperature for 16 h on an end-over-end shaker. Next, the beads were washed with 10 ml DMF and 30 ml ethanol, then reacted with 10 mM HCl in EtOH (10 ml) for 16 h at room temperature in the dark to deprotect the hydroxamate. Beads were washed with EtOH (3 × 10 ml) to yield **iA**, stored at 4 °C in EtOH.

Preparation of other affinity matrices (2–4, 6, 8–15). Amino-linkable compounds respectively **26**, **31**, **37**, commercial linkable SAHA (*p*-aminomethyl vorinostat, Toronto Research Chemicals, A617070), **44**, **45**, **52**, **57**, **60**, **64**, **66**, and **69** (Supplementary Note) were immobilized on DMSO-washed NHS-activated sepharose beads with a coupling density of 1 µmol per ml beads via incubation with 20 µl triethylamine per ml beads on an end-over-end shaker for 20 h at room temperature in the dark. Remaining free NHS groups were inactivated by blocking with 50 µl of aminoethanol per ml beads.

Preparation of cell lysates for affinity pulldown assays. Cell lines COLO-205, MV4-11, K-562, BT-549 and PC3 were grown in RPMI 1640 medium (PAN-Biotech); SW620, OVCAR-8 and MCF7 were grown in IMDM medium (PAN-Biotech), PATU-8998-S and SK-N-BE(2) were cultured in DMEM/HAM's F-12 medium (PAN-Biotech); and HEK293 was cultured in DMEM (PAN-Biotech). All media were supplemented in with 10% FBS (PAN-Biotech), and cell lines were internally tested for *Mycoplasma* contamination. Cells were lysed in lysis buffer (0.8% Igepal, 50 mM Tris-HCl pH 7.5, 5% glycerol, 1.5 mM $MgCl_2$, 150 mM NaCl, 1 mM Na_3VO_4, 25 mM NaF, 1 mM dithiothreitol (DTT) and supplemented with protease inhibitors (SigmaFast, Sigma) and phosphatase inhibitors (prepared in-house according to Phosphatase Inhibitor Cocktail 1, 2 and 3 from Sigma-Aldrich)). The protein amount of cell lysates was determined by Bradford assay and adjusted to a concentration of 5 mg ml^{-1}.

(Competition) Pulldown assays. For the selectivity profiling of HDACis, lysates from SW620 and MV4-11 cell lines were combined in a 1:1 ratio of protein amount to give a lysate mix with 5 mg ml^{-1} protein concentration. The 0.5 ml lysate mix (adjusted to 5 mg ml^{-1} protein concentration and 0.4% Igepal) was pre-incubated with nine doses of HDACi (for DMSO vehicle, 3 nM, 10 nM, 30 nM, 100 nM, 300 nM, 1,000 nM, 3,000 nM and 30,000 nM; for valproic acid and phenylbutanoic acid DMSO, 1 µM, 3 µM, 10 µM, 30 µM, 100 µM, 300 µM, 1,000 µM and 3,000 µM) for 1 h at 30 °C in an end-over-end shaker, followed by incubation with 18 µl affinity matrix (1:1:1 mixture of iC:iQ:iA) for 30 min at 30 °C in an end-over-end shaker.

To assess the degree of protein depletion from lysates by the affinity matrix, a second pulldown with fresh beads was performed using the unbound protein fraction from the vehicle control flow through.

The beads were washed (1 × 1 ml of lysis buffer without inhibitors and only 0.4% Igepal, 2 × 2 ml of lysis buffer without inhibitors and only 0.2% Igepal), and captured proteins were denatured with 8 M urea buffer, alkylated with 55 mM chloroacetamide and digested with trypsin according to standard procedures. Resulting peptides were desalted on a C18 filter plate (Sep-Pak tC18 µElution Plate, Waters), vacuum-dried and stored at −20 °C until liquid chromatography with tandem mass spectrometry (LC–MS/MS) measurement.

Other pulldown-based assays were performed according to the same protocol with minor changes. For triplicate pulldowns assessing cell line typical HDAC expression or affinity matrix enrichment properties, the pre-incubation step with HDACi and the second pulldown were omitted, and pulldown was performed at 4 °C for 45 min. For pulldown assays for probe comparison (Extended Data Fig. 1), 1 mg protein from a 1:1 mix of MV4-11 and SW620 lysate was used as input. For kinetics experiments, the pre-incubation with 30 µM compound was performed over increasing time periods (0 min, 15 min, 30 min, 1 h, 2 h, 6 h, 8 h and 24 h at 4 °C; 0 min, 15 min, 30 min, 45 min, 1 h, 2 h, 4 h, 6 h and 8 h at 22 °C) followed by pulldown at 4 °C for 45 min or at 22 °C for 15 min.

LC–MS/MS measurement of (competition) pulldown assays. Peptides were analyzed via LC–MS/MS on a Dionex UltiMate 3000 nano high-performance liquid chromatography (HPLC) coupled to an Orbitrap HF mass spectrometer (Thermo Fisher Scientific), run via Xcalibur software (Thermo Fisher Scientific). Peptides were loaded on a trap column (100 µm × 2 cm, packed in-house with Reprosil-Gold C18 ODS-3 5 µm resin, Dr. Maisch) and washed with 5 µl min^{-1} solvent A (0.1% formic acid in HPLC grade water) for 10 min. Peptides were then separated on an analytical column (75 µm × 40 cm, packed in-house with Reprosil-Gold C18 3 µm resin) using a 50 min gradient ranging from 4% to 32% solvent B (0.1% formic acid, 5% DMSO in acetonitirile) in solvent A (0.1% formic acid, 5% DMSO in HPLC grade water) at a flow rate of 300 nl min^{-1}.

The mass spectrometer was operated in data-dependent mode, automatically switching between MS1 and MS2 spectra. MS1 spectra were acquired over a mass-to-charge (m/z) range of 360–1,300 m/z at a resolution of 60,000 (at m/z 200) in the Orbitrap using a maximum injection time of 10 ms and an automatic gain control (AGC) target value of 3×10^6. Up to 15 peptide precursors were isolated (isolation width of 1.7 Th, maximum injection time of 75 ms, AGC value of 1×10^5), fragmented by higher-energy C-trap dissociation (HCD) using 25% normalized collision energy and analyzed in the Orbitrap at a resolution of 15,000. The dynamic exclusion duration of fragmented precursor ions was set to 30 s.

(Competition) Pulldown assay protein identification and quantification. Protein identification and quantification was performed using MaxQuant (v1.6.1.0)[51] by searching the LC–MS/MS data against all canonical protein sequences as annotated in the Swiss-Prot reference database (v03.12.15, 20,193 entries, downloaded 22 March 2016) using the embedded search engine Andromeda. Carbamidomethylated cysteine was set as fixed modification and oxidation of methionine and amino-terminal protein acetylation as variable modifications. Trypsin/P was specified as the proteolytic enzyme, and up to two missed cleavage sites were allowed. Precursor tolerance was set to 10 ppm, and fragment ion tolerance was set to 20 ppm. The minimum length of amino acids was set to seven, and all data were adjusted to 1% peptide spectrum matches and 1% protein false discovery rate. Label-free quantification[51] and match between runs was enabled (except for search of experiment corresponding to Supplementary Fig. 1d).

(Competition) Pulldown assay data analysis. For the competition assays, relative binding was calculated based on the protein intensity ratio to the DMSO control for every single inhibitor concentration. EC_{50} values were derived from a four-parameter log-logistic regression using an internal R script that utilizes the drc package in R. The obtained EC_{50} values were multiplied with a protein-dependent correction factor (cf), resulting in the K_d^{app} value. The correction factor is determined by calculating the ratio of the protein intensity of two consecutive pulldowns of the vehicle control sample[15]. Correction factors were set to the median of correction factors derived from all competition assays ($cf^{HDAC1} = 0.46$, $cf^{HDAC2} = 0.41$, $cf^{HDAC3} = 0.44$, $cf^{HDAC8} = 0.33$, $cf^{HDAC6} = 0.46$, $cf^{HDAC10} = 0.42$, $cf^{HDAC4} = 0.54$, $cf^{HDAC5} = 0.36$, $cf^{HDAC7} = 0.60$, $cf^{ALDH2} = 0.38$, $cf^{ISOC1} = 0.39$, $cf^{ISOC2} = 0.32$, $cf^{GATD3A} = 0.46$, $cf^{MBLAC2} = 0.54$). Targets of the inhibitors were annotated manually. A protein was considered a target or interactor of a target if the resulting binding curve showed a sigmoidal curve shape with a dose-dependent decrease of binding to the beads. Additionally, the number of unique peptides and MS/MS counts per condition were taken into account.

Heatmaps were generated using the pheatmap package in R. Initial clustering of drugs for the target landscape was based on the relative affinities using the Euclidian distance measure.

For comparison of the novel affinity matrix iA to control beads and iQ, we used iBAQ intensities (approximation to the absolute amount of proteins) obtained from MaxQuant analysis. We only calculated fold changes for proteins that were detected in all replicates of the iA pulldown. For the iQ and control beads pulldown duplicates with one missing value, we imputed the missing value by multiplying the iBAQ intensity of the valid value with the imputation factor of one plus the

mean standard deviation over all replicates without missing values (1 + mean(s.d.)), resulting in rather overestimated intensity of the protein in the control sample. To calculate the significance of the fold change, a *t*-test with Benjamini–Hochberg correction was applied. Proteins that have been identified in every replicate of the iA pulldown but in none of the iQ or control bead pulldown replicates are highly significant enriched targets, but cannot be assigned to actual values. Hence, they are listed along an arbitrary high fold change value and set to an arbitrary low *P* value for plotting with the other enriched proteins.

For kinetics experiments, we calculated the label-free quantification intensity of different drug incubation time points divided by the intensity of the vehicle control pulldown of the same experiment. This relative binding to the beads was then plotted against the total incubation time (that is, drug pre-incubation plus pulldown-incubation time) to give the binding kinetics curves.

CATDS score calculation. The general formula for the calculation of CATDS (ref. [20]) is

$$\mathrm{CATDS}_{\mathrm{target}} = \frac{(\text{target engagement})_{\text{targets of interest}}}{\sum(\text{target engagement})_{\text{all targets}}}$$

We use the term 'target engagement' as is often used in drug discovery. It refers to the fraction of all protein molecules that are bound by the drug at a particular drug concentration. By that definition, 50% target engagement corresponds to the K_d^{app} of the drug–protein interaction.

In this work, we only ever refer to selectivity at the K_d^{app} of a particular target. This simplifies the calculation as follows:

$$\mathrm{CATDS}_{\mathrm{target}} = \frac{0.5}{\sum(\text{target engagement})_{\text{all targets}}}$$

In our assay, the level of target engagement at any drug concentration of interest can be calculated as '1 − relative residual binding' at that drug concentration. Hence, this is equivalent to

$$\mathrm{CATDS}_{\mathrm{target}} = \frac{0.5}{\sum(1 - \text{relative residual binding})_{\text{all targets}}}$$

To illustrate this by example, a perfect CATDS score of 1 would mean that the drug has only a single target, which is the target of interest. If there are two equipotent targets for a drug, the CATDS score would be reduced to 0.5.

Screen for inhibitor-induced cell morphology. Twenty-four hours after seeding SW620 in microtiter plates at 3×10^3 cells per well, each compound was added in quadruplicates at concentrations of 1 µM and 0.1 µM. The morphology of the cells was monitored for 60 h of compound exposure using an automated live cell imaging system (IncuCyte S3 v2009B, Sartorius). The bright light images were processed by ilastik (ref.[52]), a supervised machine-learning image analysis tool kit, to assign and quantify different morphotypes. The areas covered by the morphotypes (number of pixels) were used to calculate the fraction of each morphology in the different wells.

HDAC-Glo assay, HDAC10 TR-FRET assay and BRET assay. The experiments were performed according to the methods in ref. [53].

Palmitoyl-CoA hydrolysis assay. MBLAC2 was expressed and purified from insect cells as previously described[14]. Palmitoyl-CoA was purchased from Sigma and stored at a stock concentration of 1 mM in 50 mM MES, pH 7.4, containing 0.05% DDM. [^{3}H]-palmitoyl-CoA was synthesized using [^{3}H]-palmitate (45 Ci mmol^{-1}, PerkinElmer Life Sciences), CoA (Sigma), and acyl-CoA synthase (Sigma) as described[54].

To screen for MBLAC2 palmitoyl-CoA hydrolase inhibitors, MBLAC2 (30 nM) was incubated with each inhibitor (300 nM) at 30 °C for 10 min. A reaction hot mix was prepared by mixing nonradioactive palmitoyl-CoA with [^{3}H]-palmitoyl-CoA to a final concentration of 6.25 µM (specific activity, 4,000 dpm pmol^{-1}). The hydrolysis reaction was initiated by adding 200 µl of the reaction hot mix to 50 µl of the enzyme inhibitor solution at 30 °C. The reaction was allowed to proceed for 10 min and then terminated with 0.5 ml of Dole's reagent (2-propanol:heptane:1 M H_2SO_4, 25:5:1). The [^{3}H]-palmitic acid product was isolated by extraction with 250 µl heptane, followed by vigorous shaking for 1 h. The organic layer collected was quantified by scintillation spectrometry. To determine the half-maximum inhibitory concentration (IC_{50}) values for selected HDACis, various concentrations of each inhibitor (3 µM to 1 pM) were prepared in 50 mM Tris, pH 7.4, prior to incubation with MBLAC2.

Ceramidase assay. The ceramidase activity of MBLAC2 was evaluated by monitoring the hydrolysis of a fluorescent ceramide analogue, C12-NBD-ceramide (Avanti Polar Lipids), as previously described[55]. Purified MBLAC2 (1 nM to 1 µM) or native cell lysate was incubated with C12-NBD-ceramide (1 µM) at 37 °C for up to 6 h. The reaction was terminated by boiling, followed by solvent evaporation. The lipids were resuspended in 30 µl of a chloroform–methanol solution (2:1, v/v) and applied to a TLC plate, which was developed with a solution of chloroform, methanol and 25% ammonium hydroxide (90:20:0.5, v/v). Separation of the lipid mixture was visualized with VersaDoc Imaging System (Bio-Rad Laboratories; Alexa Fluor 488 filter).

Knockdown of MBLAC2 in HEK293 cells. Transfection was performed using the protocol from siPOOL (siTOOLs Biotech; https://www.sitoolsbiotech.com/pdf/siPool%20Transfection%20Protocol.pdf) following the reverse transfection instructions and using a final concentration of 1 nM or 3 nM siRNA POOL (30 MBLAC2-targeting siRNAs) for knockdown of MBLAC2 or 3 nM control siRNA (pool of 30 scrambled siRNAs). Lipofectamine RNAiMAX (Invitrogen, 13778-030) was used as transfection reagent. In brief, siRNAs were pre-diluted in Opti-MEM (Gibco) and combined with a pre-mixed dilution of Opti-MEM and RNAiMax, incubated for 5 min at room temperature and transferred to the bottom of six-well cell culture plates. Detached HEK293 cells were resuspended in DMEM containing 10% exosome-depleted FBS (qualified one shot, Gibco, A27208-03) as FBS replacement (to avoid extracellular particle contamination stemming from FBS) and added to the transfection mix in six-well plates to settle down for 10 min before transfer to the incubator (37 °C, 5% CO_2, cell confluence of 15%). For the knockdown test with western blot readout, cells were incubated for 1, 2, and 3 days before lysis. For every treatment duration, cells were transfected with 3 nM control siRNA POOL, 1 or 3 nM MBLAC2 siRNA POOL. For the proteomics and extracellular vesicle counting experiment (in triplicates), knockdown cells were incubated for 3.5 days after siPOOL transfection, reaching 80% confluency. For lipidomics experiments (in triplicates), transfection and cultivation were conducted on glass dishes (to avoid plastics-derived contamination during planned lipid extraction from attached cells).

Treatment of HEK293 for exosome characterization. HEK293 cells were seeded in six-well cell culture dishes with a confluence of 15% and cultured in FBS-free DMEM (10% exosome-depleted FBS (Gibco, A27208-03)). After 4 h, cells were treated with ACY-775 or ACY-738 (triplicates, 3 µM final concentration) for 3.5 days.

Extracellular vesicle sample preparation and counting. Supernatants of ACY-775, ACY-738-treated and MBLAC2 siPOOL-transfected or control siRNA-transfected HEK293 cells were collected and stored at −80 °C. Thawed supernatant samples were applied to qEV size exclusion chromatography (35 nm, qEVoriginal, Izon) to collect supernatant samples in the size range of extracellular vesicles. In brief, the column was first washed and equilibrated with sterile PBS. Then, 1 ml of cell culture supernatant was pipetted onto the column, and 0.5 ml fractions were collected in Eppendorf reaction vessels. The fractions of column flow through (6–8; that is, 3–4.5 ml of flow through after applying sample) that contain most particles in the size range of 30–150 nm were analyzed using nanoparticle tracking analysis. The measurement of particle number and size distribution of extracellular vesicles was performed using the scatter mode of a PMX110-Z ZetaView Nanoparticle Tracking Analyzer (Particle Metrix), equipped with a 520 nm laser. Two video cycles were recorded over all 11 positions in the measurement cell while the temperature was held constant at 24 °C. The following recommended parameters were used for the measurement: sensitivity (80), shutter (70), frame rate (30), minimum brightness (20), maximum brightness (255), minimum area (5), maximum area (1000), tracking radius (100), minimum tracelength (15), nm per class (5) and classes per decade (64). Results were analyzed using the ZetaView software (v8.05.12 SP1, Particle Metrix).

Extracellular vesicle count data analysis. The particle count data from nanoparticle tracking analysis (binned in 5 nm diameter) for each fraction (fractions 6, 7 and 8, with fraction 7 containing most particles) of a replicate were summed up and normalized to the protein concentration of the corresponding replicate (as approximation for the cell volume; concentration determination by BCA assay, see below). The normalized particle size distributions of the replicates were plotted using GraphPad Prism (v5.01).

Western blot. Protein lysates were generated by harvesting cells in lysis buffer (0.8% NP40, 50 mM Tris-HCl pH 7.5, 5% glycerol, 1.5 mM $MgCl_2$, 150 mM NaCl, 1 mM Na_3VO_4, 25 mM NaF, 1 mM DTT and supplemented with protease inhibitors and phosphatase inhibitors (prepared in-house according to Phosphatase Inhibitor Cocktail 1, 2 and 3). The protein amount of cell lysates was determined by Bradford assay. Proteins were separated by SDS-PAGE and electro-transferred onto PVDF membranes. Blots were stored in Tris-buffered saline, supplemented with 0.05% Tween (TBS-T) and 4% BSA for 1 h at room temperature and then incubated with primary antibody diluted in 1X TBS, 0.05% Tween and 4% BSA overnight at 4 °C. Following antibodies were used for MBLAC2 probing: MBLAC2 (Abcam, ab122411, 0.2 mg ml^{-1}, rabbit polyclonal IgG; diluted 1:250) and β-actin (Santa Cruz Biotechnology, sc-47778, 0.2 mg ml^{-1}, monoclonal mouse IgG, diluted 1:500). For acetyl-tubulin probing, the following antibodies were used: acetyl-α-tubulin (Lys40) (Cell Signaling Technology, 12152S, monoclonal mouse IgG, diluted 1:750), and β-actin (Cell Signaling Technology, 8457S, monoclonal rabbit IgG, diluted 1:750). After antibody incubation, blots were washed in TBS-T and probed

with the corresponding fluorophore-conjugated secondary antibody (ODYSSEY donkey-anti-rabbit (926-68023), goat-anti-mouse (926-32210)) for 3 h at room temperature. The immunoreactive signals were detected by excitation of the respective fluorophore. Acquisition and quantification of the band intensities was carried out with the Odyssey imaging system and corresponding software (v3.0.29) (LI-COR Biosciences). Intensities of proteins were normalized to input β-actin. For the MBLAC2 western blot, intensities were further normalized to the control siRNA POOL transfected samples of each treatment duration to calculate the relative MBLAC2 knockdown after 1, 2, and 3 days of transfection.

Deep proteome sample preparation. *Protein digestion.* After 3.5 days of transfection or drug treatment, HEK293 cells were washed with PBS and lysed by adding 100 µl lysis buffer (4% SDS in ddH_2O) before scraping cells off the surface. Lysates were transferred to 2 ml eppendorf reaction vessels. To hydrolyze DNA and reduce viscosity, lysates were first diluted with 500 µl lysis buffer, heated at 95 °C for 10 min and then mixed with trifluoroacetic acid (TFA) to a final concentration of 2%. Next, *N*-methylmorpholine (Sigma) was added to 4% (v/v) final concentration for neutralization. Protein concentration of lysates was determined using a standard BCA assay protocol (Pierce BCA Protein Assay kit, 23225).

Protein cleanup and digestion was performed according to an adapted SP3 protocol. In brief, lysate volumes corresponding to 42 µg of protein were added to 5 µl Sera-Mag beads 1:1 mix (GE45152105050250 and GE65152105050250, GE Healthcare) before adding ethanol to a final concentration of 80% (v/v) and incubating at room temperature for 15 min under constant shaking (800 rpm). Beads were then immobilized to reaction vessel wall by magnets and washed twice with 1 ml of 80% ethanol and once with 80% acetonitrile. Beads were resuspended in 70 µl of 50 mM HEPES buffer (pH 8.5) and incubated with DTT (10 mM final concentration, 45 min at 37 °C, 600 rpm shaking) for reduction. Proteins were alkylated by adding chloroacetamide to a final concentration of 55 mM (30 min at room temperature, 600 rpm shaking in the dark). To digest the proteins, trypsin was added (trypsin:protein, 1:50) and incubated with beads at 37 °C and 800 rpm shaking for 16 h. Digested protein peptides were collected by immobilizing beads on vessel walls using magnets and transferring the peptide solution to Eppendorf reaction vessels.

StageTip desalting. To construct a StageTip, six C18 disks were packed into a 200 µl pipette tip. The StageTips were activated with 200 µl acetonitrile (centrifugation at 1,000*g*), followed by washing with 200 µl buffer B (0.1% formic acid in 50% acetonitirile) at 1,000*g* and equilibration by washing with 200 µl buffer A (0.1% formic acid in ddH_2O) at 1,000*g*. Peptide samples were acidified to a final concentration of ca. 1% formic acid (pH > 2) and loaded on StageTips with 500*g* centrifugation. The loading step was repeated with the flow through. Peptides attached to the C18 material were washed twice with 200 µl buffer A and eluted by adding twice 40 µl of buffer B and collecting the flow through. The eluent was frozen at −80 °C and vacuum-dried before further processing.

TMT labeling. Samples were reconstituted in 20 µl of 50 mM HEPES (pH 8.5) and labeled with 100 µg (5 µl of 20 µg µl^{-1}) TMT10plex (Thermo Scientific; channel 126 was used for MBLAC2 knockdown and 127N was used for control replicates) for 1 h at 25 °C under 500 rpm constant shaking. The labeling reaction was stopped by adding 3 µl 5% hydroxylamine in ddH_2O. After combining TMT-labeled samples in reaction vessel, they were acidified with 20 µl of 10% formic acid in ddH_2O. Samples were frozen at −80 °C and vacuum-dried before further processing.

High-pH RP-HPLC fractionation. In brief, the pooled TMT-labeled peptides were reconstituted in 50 µl buffer A (25 mM ammonium bicarbonate, pH 8) and separated using a Dionex Ultra 3000 HPLC system (Dionex Chromeleon (v6.80) software) equipped with an Waters XBridge BEH130 C18 3.5 µm column (2.1 × 150 mm) operated at a flow rate of 200 µl min^{-1} with a constant 10% of 25 mm ammonium bicarbonate (pH 8.0) in the running solvents. A 57 min linear gradient from 7% to 45% ACN in ddH_2O followed by a 6 min linear gradient up to 80% ACN was employed. Ninety-six fractions were collected and subsequently pooled to 48 fractions (fraction 1 + 49, fraction 2 + 50, and so on). Peptide fractions were frozen at −80 °C and dried by vacuum centrifugation.

Full proteome LC–MS/MS. Peptides were analyzed via LC–MS/MS on a Dionex UltiMate 3000 RSLCnano System equipped with a Vanquish pump module coupled to an Orbitrap Fusion Lumos (Thermo Fisher Scientific) mass spectrometer. Peptide fractions were dissolved in 1% FA and injected directly onto a commercially available Acclaim PepMap 100 C18 LC column (2 µm particle size, 1 mm ID × 150 mm; Thermo Fisher Scientific). Peptides were separated using a 25 min linear gradient ranging from 4% to 32% solvent B (0.1% formic acid, 3% DMSO in acetonitrile) in solvent A (0.1% formic acid, 3% DMSO in HPLC grade water) at a flow rate of 50 µl min^{-1}.

The mass spectrometer was operated in data-dependent mode, automatically switching between MS1, MS2 and MS3 spectra, with cycle time set to 1.2 s. MS1 spectra were acquired over a *m/z* range of 360–1,560 *m/z* at a resolution of 60,000 in the Orbitrap (OT) using a maximum injection time of 50 ms, an AGC target value of 4×10^5 and dynamic exclusion set to 50 s.

For MS2 spectra, the intensity threshold was set to 1×10^4, default charges were set to state 2–6. The isolation width was set to 0.6 *m/z*, and HCD collision energy [%] was set to 32. The AGC target value was 1.2×10^4, and the first mass was fixed at 100 *m/z*. The Iontrap was used to detect the MS2 spectra with the rapid scan function. The maximum injection time was 40 ms. Regarding MS3-Filter, precursor selection range was set to 400–2,000, and exclusion mass widths were set to 20 *m/z* for low and 5 *m/z* for high. For MS3 scans, Synchronous precursor selection was enabled, the number of SPS precursors was set to 8, the MS isolation window was 1.2 *m/z* and HCD collision energy was 55%. The Orbitrap was used to detect the MS3 spectra at 50,000 resolution and over a scan range of 100–1,000. The AGC target was 1×10^5 with a maximum IT of 86 ms.

The raw data was analyzed using MaxQuant (v1.6.10.2) and default settings, except for minor changes; isotope impurities of the TMT lot (TE268169) were specified to allow MaxQuant the automated correction of TMT intensities. TMT-labeling modification was set for lysine and N-terminal aminogroups and ITMS was set to a match tolerance of 0.4. For all searches, carbamidomethylated cysteine was set as fixed modification and oxidation of methionine and N-terminal protein acetylation as variable modifications. Trypsin/P was specified as the proteolytic enzyme with up to two missed cleavage sites allowed. Searches were based on canonical Swiss-Prot reference database (v03.12.15, 20,193 entries, downloaded 22 March 2016, annotated in-house with PFAM domains).

Full proteome data analysis. For data analysis and visualization, mostly Microsoft Excel, GraphPad Prism, RStudio (v4.0.2), and the Perseus software (v1.6.2.3) were used[56]. Firstly, all reversed hits and 'only identified by site' protein entries were removed from the MaxQuant output. Then, the reporter intensities of channels 1, 2 and 5 (that is, TMT126, TMT127N, and TMT128C, corresponding to MBLAC2 knockdown, control siPOOL transfection and DMSO control) were log_2-transformed and median-centered to the overall median of the respective dataset. Further, samples were adjusted with ComBat[57] from the sva package (v3.30.1) to remove batch effects between replicates. Protein groups without missing values were analyzed in Perseus[56] (v1.6.2.2) by using the built-in two-sample *t*-test function and Benjamini–Hochberg multiple testing correction (MBLAC2/control; S0, 0.107; FDR, 1%). Resulting table containing fold changes, *P* values and *q*-values was exported and used to plot volcano plots in GraphPad Prism.

Lipidomics sample preparation. HEK293 cells were cultured on glass dishes for 45 h after transfection in DMEM (containing 10% exosome-depleted FBS, Gibco, A27208-03) until they reached a confluency of 80%. The supernatant was discarded, and cells were gently washed with PBS. For lipid extraction, 500 µl of 2:1 (v:v) methanol:chloroform was pipetted twice onto cells in the glass dish, and broken-up cell fragments were collected in glass vials and sonicated for 10 min. After centrifugation to remove cell debris, extracted lipids were stored in extraction buffer at −80 °C until injection to LC–MS/MS.

Lipidomics LC–MS/MS measurement. The lipid analysis was performed using a Nexera UHPLC system (Shimadzu) coupled to a Q-TOF mass spectrometer (TripleTOF 6600, AB Sciex) according to a published analytical method[58]. Separation of the lipid extract was performed using a UPLC BEH C18 2.1 × 100, 1.7 µm analytical column (Waters) with a flow rate of 300 µl min^{-1}. The mobile phase was water–acetonitirile (40:60, v:v) with 10 mM ammonium formate and 0.1% formic acid (eluent A), and isopropanol–acetonitirile (90:10, v-v) with 10 mM ammonium formate and 0.1% formic acid (eluent B). The gradient profile was 32% B from 0 to 1.5 min raising to 97% B at 21 min, which was held for 4 min. Afterwards, the column was equilibrated at starting conditions. A volume of 5 µl per sample was injected. The autosampler was cooled to 10 °C, and the column oven was heated to 40 °C. The samples have been measured in the Information Dependent Acquisition mode. MS settings in the positive mode were as follows: gas 1, 55; gas 2, 65; curtain gas, 35; temperature, 500 °C; ion spray voltage, 5500; and declustering potential, 80. The mass range of the TOF MS and MS/MS scans were 100–2,000 *m/z*, and the collision energy was set to 35 V with a 15 V spread. MS settings in the negative mode were as follows: gas 1, 55; gas 2, 65; cur, 35; temperature, 500 °C; ion spray voltage, −4500; and declustering potential, −80. The mass range of the TOF MS and MS/MS scans were 100–2,000 *m/z*, and the collision energy was set to −35 V with a 15 V spread.

Lipidomics data analysis. Data was analyzed using MS-DIAL4 software (v4.38)[59]. Raw files from positive and negative ion mode were analyzed separately and loaded as lipidomics profile data type. Changes or specifications regarding the default parameter settings were as follows: defining solvent type as $HCOONH_4$, allowing all adduct types for all lipid classes for identification, and selecting adduct types for positive mode ($[M+H]^+$, $[M+NH_4]^+$, $[M+Na]^+$) or negative mode ($[M-H]^-$, $[M-H_2O-H]^-$, $[M+FA-H]^-$). Data from knockdown and control were aligned as class and normalized using the mTIC normalization function of MS-DIAL4. The raw MS-DIAL4 outputs for negative and positive mode were processed separately. Lipids that were present in less than half of the samples or that showed a retention time of <1 min were discarded. Additionally, only the lipids that were identified based on their MS2 spectrum were included in the further analysis. Quotient

normalization[60] and $\log_2$-transformation were applied to the data. For the volcano plots, the $\log_2$[fold change] between control and knockdown was calculated and a *t*-test was performed. The resulting *P* values were adjusted for multiple testing using the Benjamini–Hochberg procedure supplied by the statsmodels package. For visualization, *t*-test results of positive and negative mode data were combined and presented in a volcano plot generated in GraphPad Prism. As some detected fragment ions had very low abundance in positive ion mode, we decided to remove acyl chain information and use only the sum species annotation for lipids identified in positive mode (Fig. 5c and Supplementary Data 4).

Reporting Summary. Further information on research design is available in the Nature Research Reporting Summary linked to this article.

Data availability

Chemoproteomics data are freely accessible in ProteomicsDB (https://www.proteomicsdb.org). The mass spectrometry proteomics data, including the used Swiss-Prot reference database, have been deposited to the ProteomeXchange Consortium via the PRIDE partner repository with the dataset identifier PXD026657. The untargeted metabolomics data for lipidomics are made available on MetaboLights repository with the identifier MTBLS3557 and can further be accessed on Zenodo (https://zenodo.org/record/5914128#.Yfe59_jTVhE).

References

51. Cox, J. et al. Accurate proteome-wide label-free quantification by delayed normalization and maximal peptide ratio extraction, termed MaxLFQ. *Mol. Cell. Proteomics* **13**, 2513–2526 (2014).
52. Berg, S. et al. ilastik: interactive machine learning for (bio)image analysis. *Nat. Methods* **16**, 1226–1232 (2019).
53. Steimbach, R. R. et al. Aza-SAHA derivatives are selective histone deacetylase 10 chemical probes that inhibit polyamine deacetylation. Preprint at https://chemrxiv.org/engage/chemrxiv/article-details/615c1710b564b66c716cfbd4 (2021).
54. Jennings, B. C. et al. 2-Bromopalmitate and 2-(2-hydroxy-5-nitro-benzylidene)-benzo[*b*]thiophen-3-one inhibit DHHC-mediated palmitoylation in vitro. *J. Lipid Res.* **50**, 233–242 (2009).
55. Okino, N., Tani, M., Imayama, S. & Ito, M. Purification and characterization of a novel ceramidase from *Pseudomonas aeruginosa*. *J. Biol. Chem.* **273**, 14368–14373 (1998).
56. Tyanova, S. & Cox, J. Perseus: a bioinformatics platform for integrative analysis of proteomics data in cancer research. *Methods Mol. Biol.* **1711**, 133–148 (2018).
57. Johnson, W. E., Li, C. & Rabinovic, A. Adjusting batch effects in microarray expression data using empirical Bayes methods. *Biostatistics* **8**, 118–127 (2007).
58. Witting, M., Maier, T. V., Garvis, S. & Schmitt-Kopplin, P. Optimizing a ultrahigh pressure liquid chromatography-time of flight-mass spectrometry approach using a novel sub-2 µm core–shell particle for in depth lipidomic profiling of *Caenorhabditis elegans*. *J. Chromatogr. A* **1359**, 91–99 (2014).
59. Tsugawa, H. et al. A lipidome atlas in MS-DIAL 4. *Nat. Biotechnol.* **38**, 1159–1163 (2020).
60. Dieterle, F., Ross, A., Schlotterbeck, G. & Senn, H. Probabilistic quotient normalization as robust method to account for dilution of complex biological mixtures. Application in ^{1}H NMR metabonomics. *Anal. Chem.* **78**, 4281–4290 (2006).

Acknowledgements

We thank W. Greentree (Cornell University) and L. Wanat (Technical University of Munich) for technical support. We gratefully acknowledge funding by the Deutsche Forschungsgemeinschaft (DFG) (SFB 1309, project 401883058 and project 407391208). M.I.P.M. and M.E.L. acknowledge support from the National Institutes of Health (grant GM121540). Contributions by V.W. and J.K.P. are funded by the Bavarian State Ministry of Science and the Arts within the framework of the Bavarian Research Institute for Digital Transformation (bidt). A.K.M. acknowledges the Helmholtz Drug Initiative for financial support. We also thank the CHDI foundation for generously providing CHDI00465983 and CHDI00390576.

Author contributions

G.M. conceived and directed the project. S.L., B.K. and G.M. wrote the manuscript. S.L. profiled the drugs and performed the knockdown, western blots, purification of extracellular vesicles, proteomics experiments and lipidomics experiments. S.L. and B.K. measured the proteomics samples. M.I.P.M. and M.E.L. performed the MBLAC2 enzyme activity assays and C12-ceramidase assay. C.G. and M.W.P. performed the vesicle tracking experiments. R.R.S. and A.K.M. performed the HDAC enzyme activity assays, FRET and NanoBRET binding assays. A.B., P.R., S.N., C.S., X.K., P.P., T.H., W.S. and G.M. performed the synthetic chemistry work. S.L, A.B., P.R., S.N., C.S., C.L., X.K. and P.P. performed the affinity matrix evaluation experiments. L.L. and M.W. made the data available in ProteomicsDB. K. Kleigrewe measured the lipidomics samples. S.L., V.W., C.M., K. Kleigrewe and J.K.P. analyzed the lipidomics data. K. Kramer performed the cell imaging experiments.

Competing interests

M.W. and B.K. are cofounders and shareholders of OmicScouts and msAId. They have no operational role in either company. The remaining authors declare no competing interests.

Additional information

Extended data is available for this paper at https://doi.org/10.1038/s41589-022-01015-5.

Supplementary information The online version contains supplementary material available at https://doi.org/10.1038/s41589-022-01015-5.

Correspondence and requests for materials should be addressed to Guillaume Médard.

Peer review information *Nature Chemical Biology* thanks Christian Olsen, Hongyan Sun, Zheng-Jiang Zhu and the other, anonymous, reviewer(s) for their contribution to the peer review of this work.

Reprints and permissions information is available at www.nature.com/reprints.

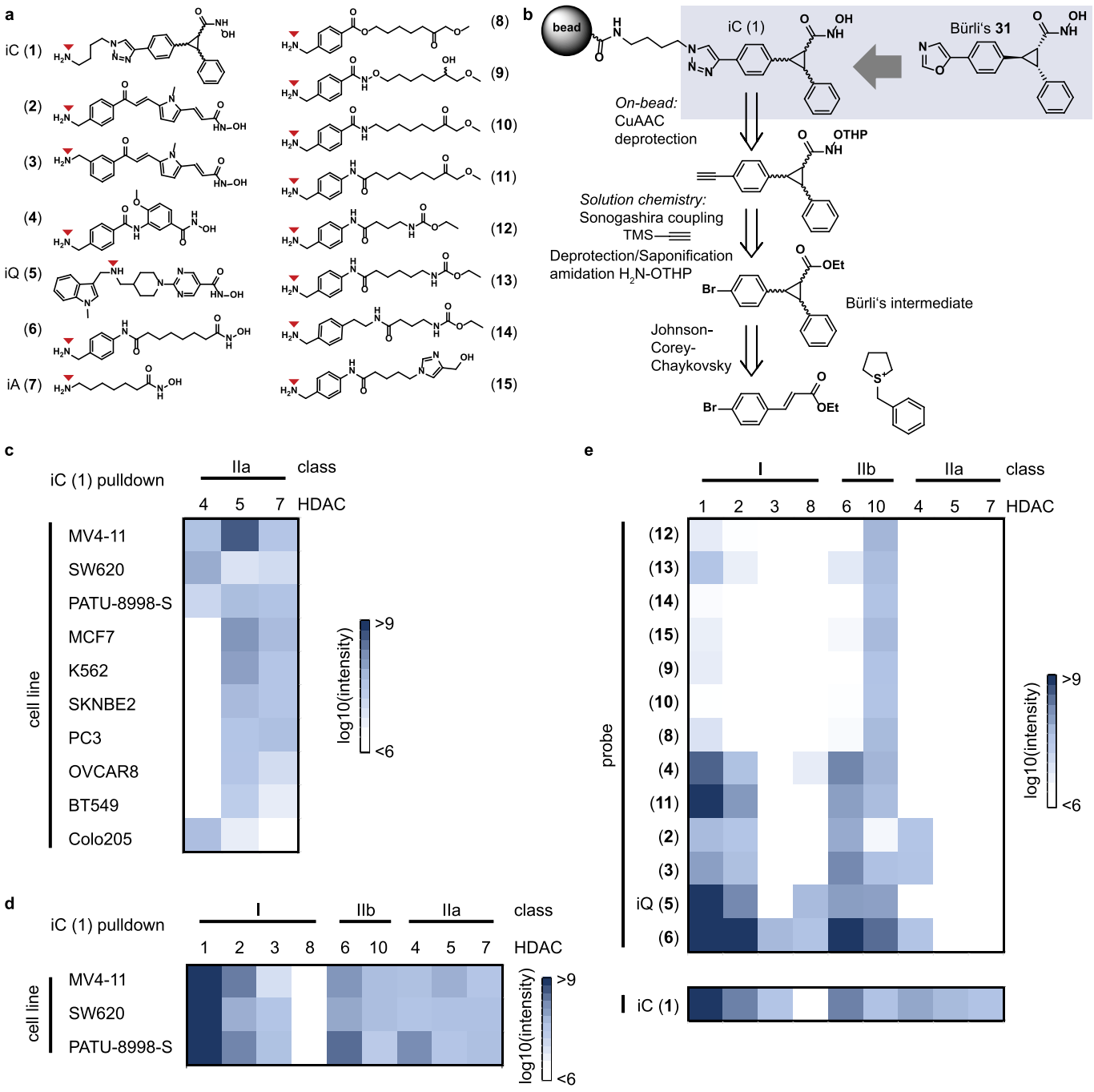

Extended Data Fig. 1 | Evaluation of affinity probes for capturing HDACs in cancer cell lysates. a, Structures of synthesized HDAC affinity probes 1-15. Positions for on-bead immobilisation are marked with red triangles. Probes **2** and **3** are respectively *para* and *meta* linkable analogues of reported class IIa inhibitor MC1568[1]. Probe **4** is an analogue of a HDAC8 inhibitor[2,3]. Probe **6** is a linkable analogue of Vorinostat[4]**. 8-15** feature alternative chelating groups to hydroxamate, grafted on hybrid structures of Vorinostat, Santacruzamate and LMK235: methoxymethyl ketone (8, 10, 11) found in a bicyclic tetrapeptide[5], ethyl carbamate (12, 13, 14) found in Santacruzamate[6] and 4-hydroxymethylimidazole (15) computationally suggested as superior to hydroxamic acid[7]. **b**, Strategy and retro-synthesis scheme for the design and preparation of class IIa affinity probe iC (**1**). The analogation of lead oxazole **31**[8] to a triazole allows for immobilisation on Sepharose beads. The matrix is conveniently obtained by on-bead Copper-catalysed Azide-Alkyne Cycloaddition (CuAAC) of a hydroxamate-protected alkyne precursor with azide-functionalised beads, followed by deprotection. The alkyne precursor was prepared by converting Bürli's bromo ester intermediate in 3 steps: Sonogashira coupling with TMS-acetylene, simultaneous deprotection/saponification and conversion to protected hydroxamic acid. An almost equimolar mixture of 3 enantiomer pairs (only all-*cis* isomers are not obtained during the Johnson-Corey-Chaykovsky synthetic step) constitute iC. (See Supporting Note) **c**, Screening cancer cell lines for class IIa HDAC expression using iC affinity probe. The heatmap depicts the average protein intensity of class IIa HDACs pulled down by iC (MS raw intensity). **d**, Intensities of HDACs pulled down by iC from three most promising cell lines from a different lysis batch. **e**, Evaluating HDAC affinity matrices for HDAC pulldown capabilities. The heatmap shows protein intensities of pulled down HDACs by 14 distinct affinity probes using cell lysate mixes of MV4-11 and SW620. For probes 2-15 a 1:1 mix of SW620 and MV4-11 cell lysate was used, while the heatmap for probe 1 represents an average of detected protein intensities from 2 single pulldowns in SW620 and MV4-11 cell lysate. All pulldowns were performed in three technical replicates.

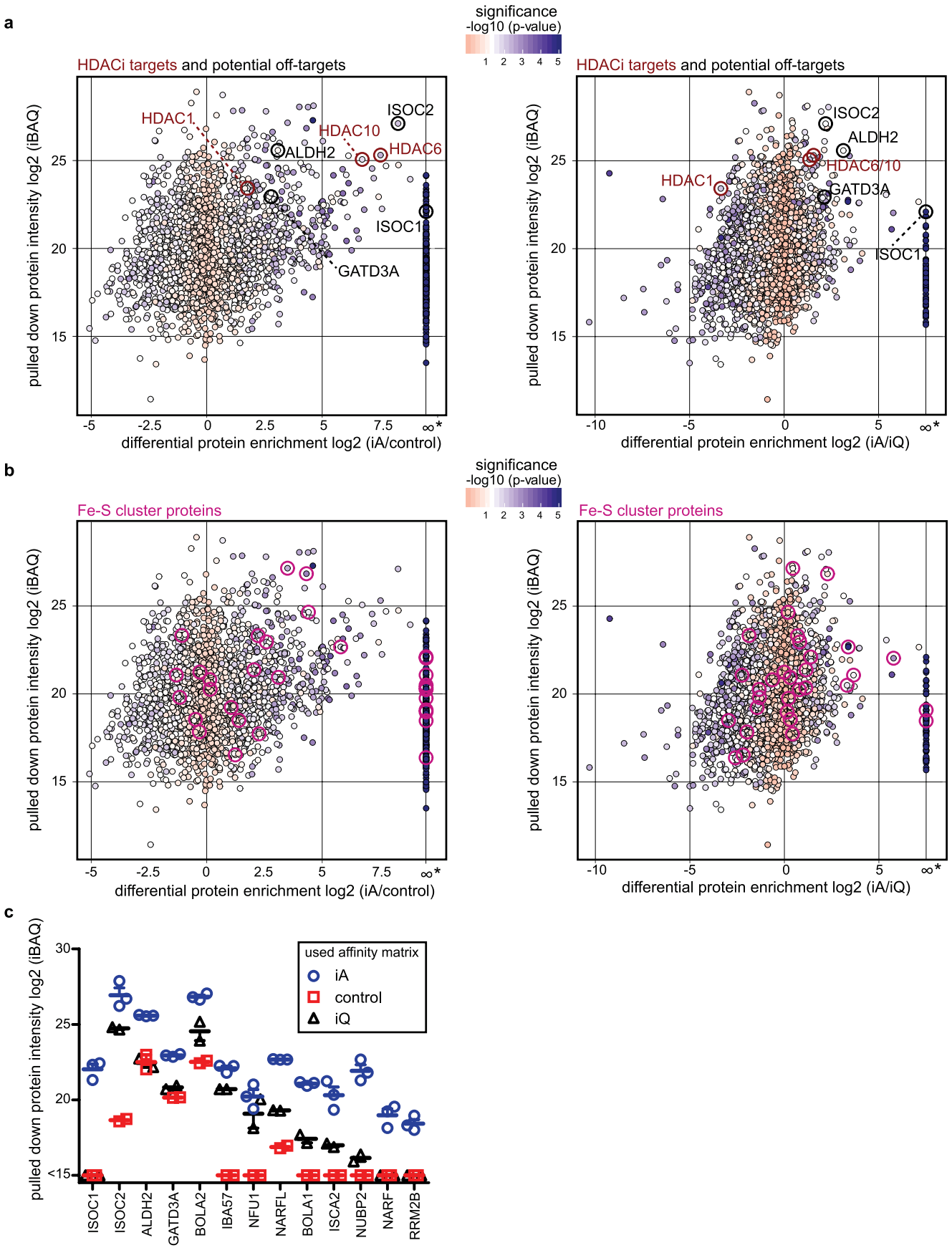

Extended Data Fig. 2 | See next page for caption.

Extended Data Fig. 2 | Evaluation of metalloprotein affinity matrix iA for pulling down metalloproteins. a and **b**, enrichment of proteins from PATU-8998-S lysate by iA relative to control beads or iQ is plotted against the intensity of the corresponding proteins in iA pulldown. iBAQ intensity values were employed as proxy for the protein amount. Asterisks on the x-axis mark proteins that have been identified in each replicate of the iA pulldown but in none of control or iQ replicates and thus represent highly significantly enriched proteins. **a**, enriched HDACs and proposed off-targets are highlighted (two sided t-test, p value without multiple testing correction). **b**, differential chemoproteomic enrichment of FeS-cluster proteins (pink circles) as an example for iA-enriched metalloprotein classes compared to control beads and iQ (two sided t-test, p-value without multiple testing correction). **c**, iBAQ intensities of selected significantly enriched proteins from the single pulldown experiments. All pulldowns were performed in technical replicates (duplicates for control and iQ, triplicates for iA) and data are shown as mean +/− SEM. As control beads we used the same sepharose beads for affinity matrix generation, but, instead of affinity probes, we coupled 2-aminoethanol to the NHS-activated Sepharose.

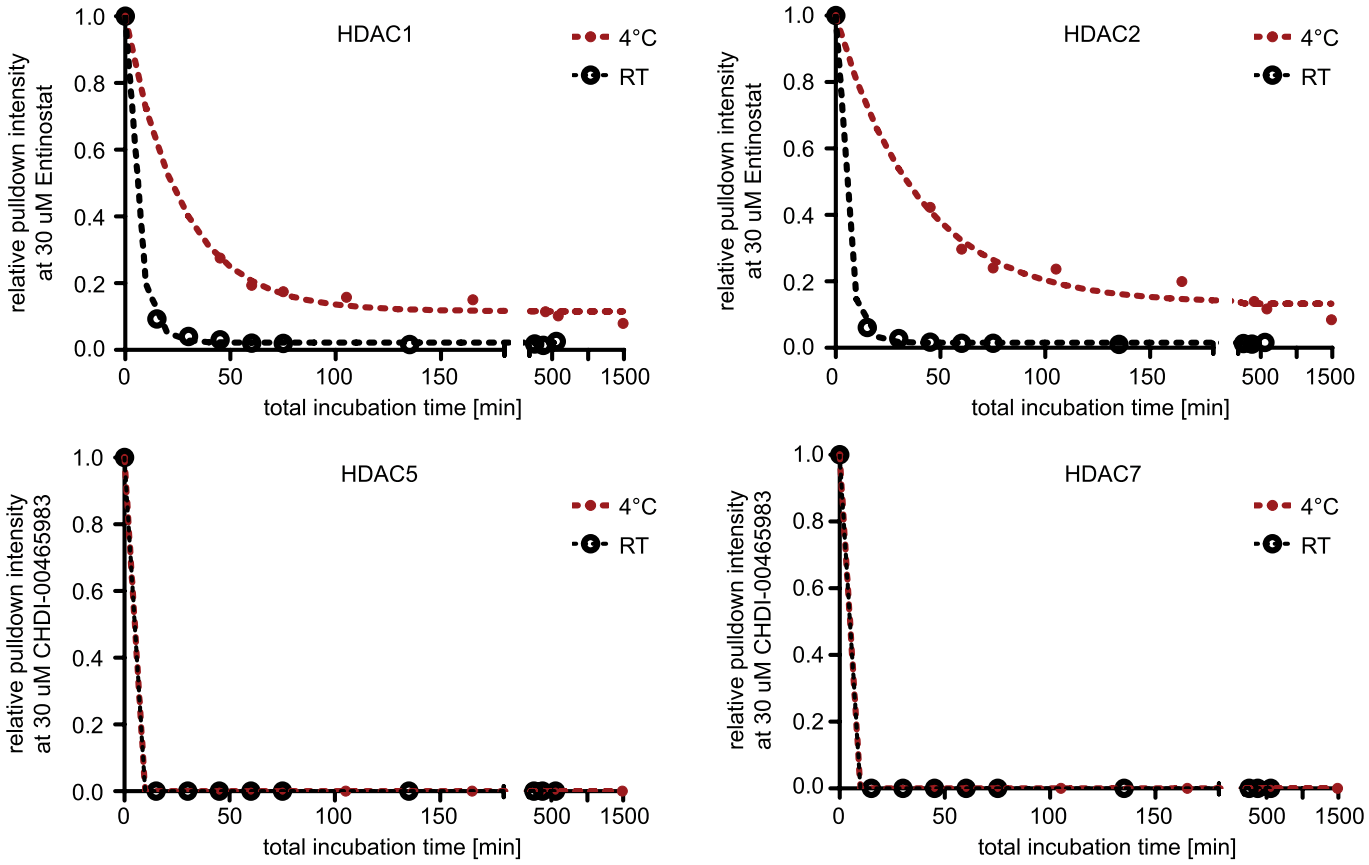

Extended Data Fig. 3 | Evaluation of binding kinetics at different incubation temperatures for Entinostat and CHDI00465983. A 1:1 mix of SW620 and MV4-11 cell lysate was incubated with excess drug (30 μM) for different periods of time at either room temperature (22 °C) or 4 °C before pulling down HDACs with iQ (for Entinostat) or iC (for CHDI00465983). HDAC1 and HDAC2 competition depends on the incubation temperature and Entinostat shows relatively slow binding kinetics compared to CHDI00465983.

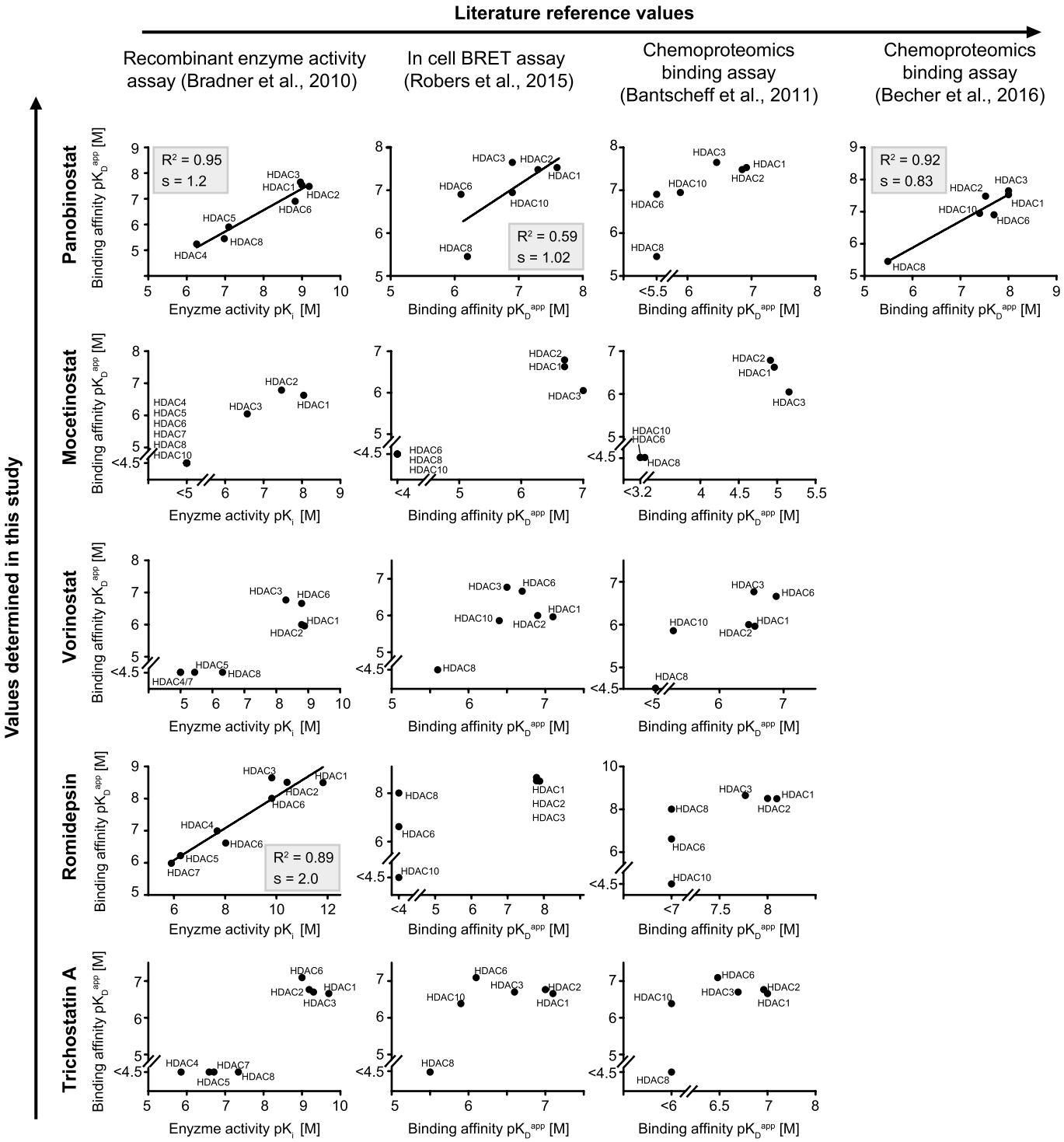

Extended Data Fig. 4 | Comparison of acquired affinity data to literature data. pK_d^{app} values determined in this study were plotted against pK_d values from three former HDACi profiling studies[4,9,10] and in case of Panobinostat to another optimized chemoproteomics study using immobilized Panobinostat as probe[9]. For data sets without missing values, regression lines were plotted (s = slope of regression line). In general good correlation is observable between recombinant enzyme activity assay data (Bradner et al.)[10] and our study as well as for the comparison to the optimized chemoproteomics assay using immobilized Panobinostat as affinity matrix (Becher et al.)[9].

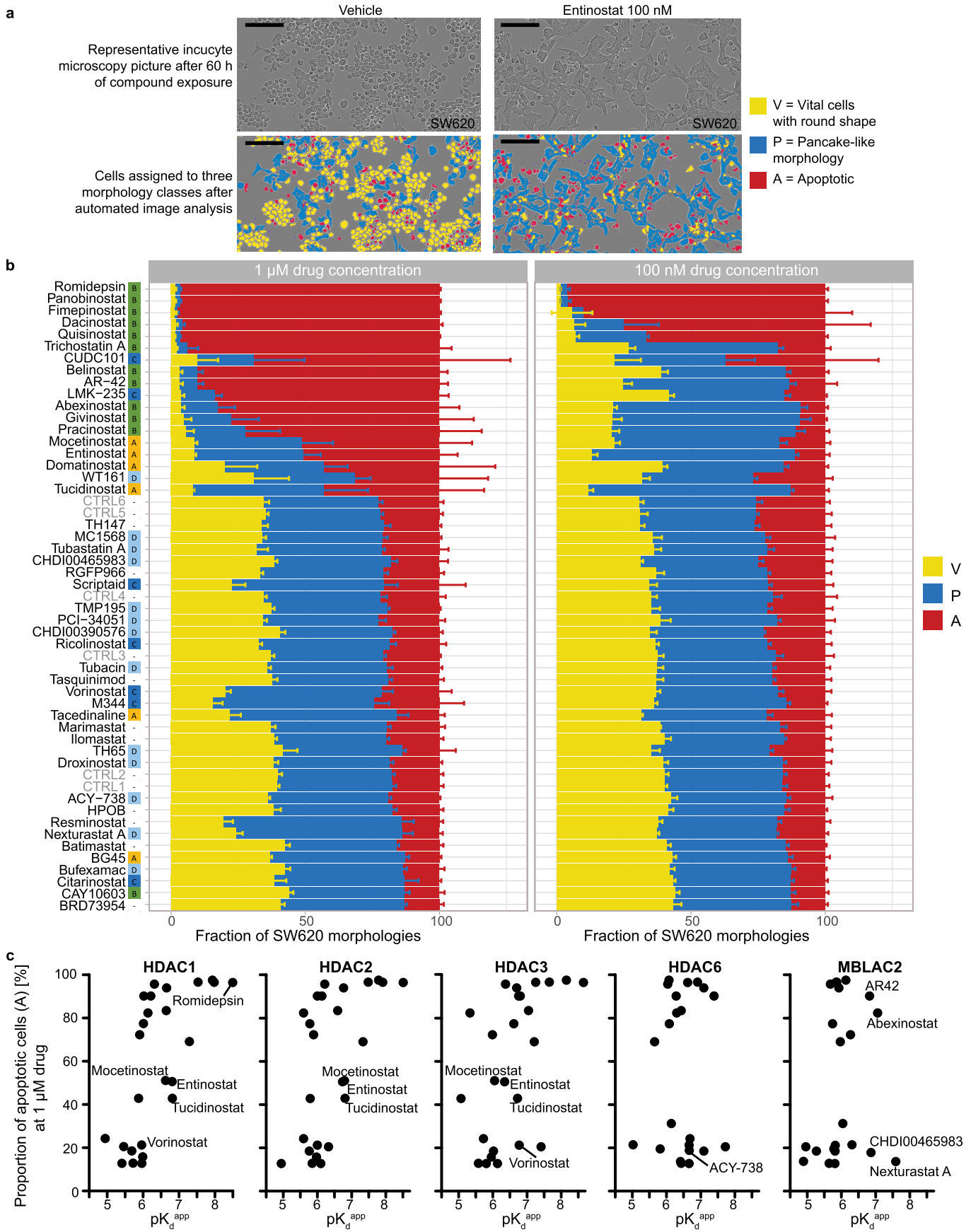

Extended Data Fig. 5 | See next page for caption.

Extended Data Fig. 5 | 2-Dose cell viability and morphology screen with HDACi library on SW620 cells. a, Representative images of vehicle (DMSO) and drug treated cells (100 nM Entinostat) after 60 h of incubation. Bright light images (upper panel) were recorded using an Incucyte S3 and processed by ilastik[11], a supervised machine learning toolkit for automated image analysis. Vital round shaped (V), flattened/pancake-like shaped (P) and apoptotic cell morphologies (A) were identified and labelled accordingly (lower panel). Scale bar corresponds to 100 µm length. **b**, Relative areas covered by the the three cell morphologies after drug treatment, performed in quadruplicates. Pixels of the ilastic software output classification were counted and divided by the sum of all cells pixels: bar chart displays the means and standard deviations of quadruplicate experiments in 96-well plates. Treatments were ranked from highest to lowest cytotoxicity (that is high proportion of apoptotic cells (A) for the 100 nM and 1 µM treatment). Control DMSO treatments are listed as CTRL1-6. Drugs are assigned to groups according to their target spectrum (see Fig. 2c). **c**, Correlation between drug affinities (pK_d^{app} of HDAC1,2,3,6 and MBLAC2) and proportion of apoptotic cells after 1 µM drug treatment. Representative clinical drugs Romidepsin (depsipeptide), aminoanilides (Mocetinostat, Entinostat, Tucidinostat) and hydroxamates (Vorinostat, AR-42, Abexinostat) as well as some particularly interesting tool compounds (ACY-738, Nexturastat A, CHDI00465983) are highlighted in the plots for orientation. In accordance to literature, class I inhibition correlated with cytotoxicity, while HDAC6 and MBLAC2 inhibition does not correlate with cytotoxicity but clusters into two clouds, defined by the drugs additional class I target affinity (cytotoxicity mainly mediated by class I inhibition). As expected, drugs of similar class I target affinity show distinct cytotoxicity, most probably reflecting distinct intracellular drug concentrations (for example via cellular uptake, metabolism, active export). Chemically similar drugs (Mocetinostat, Entinostat, and Tucidinostat) that share the same target space and most probably similar intracellular distributions according to their similar physicochemical properties cluster together.

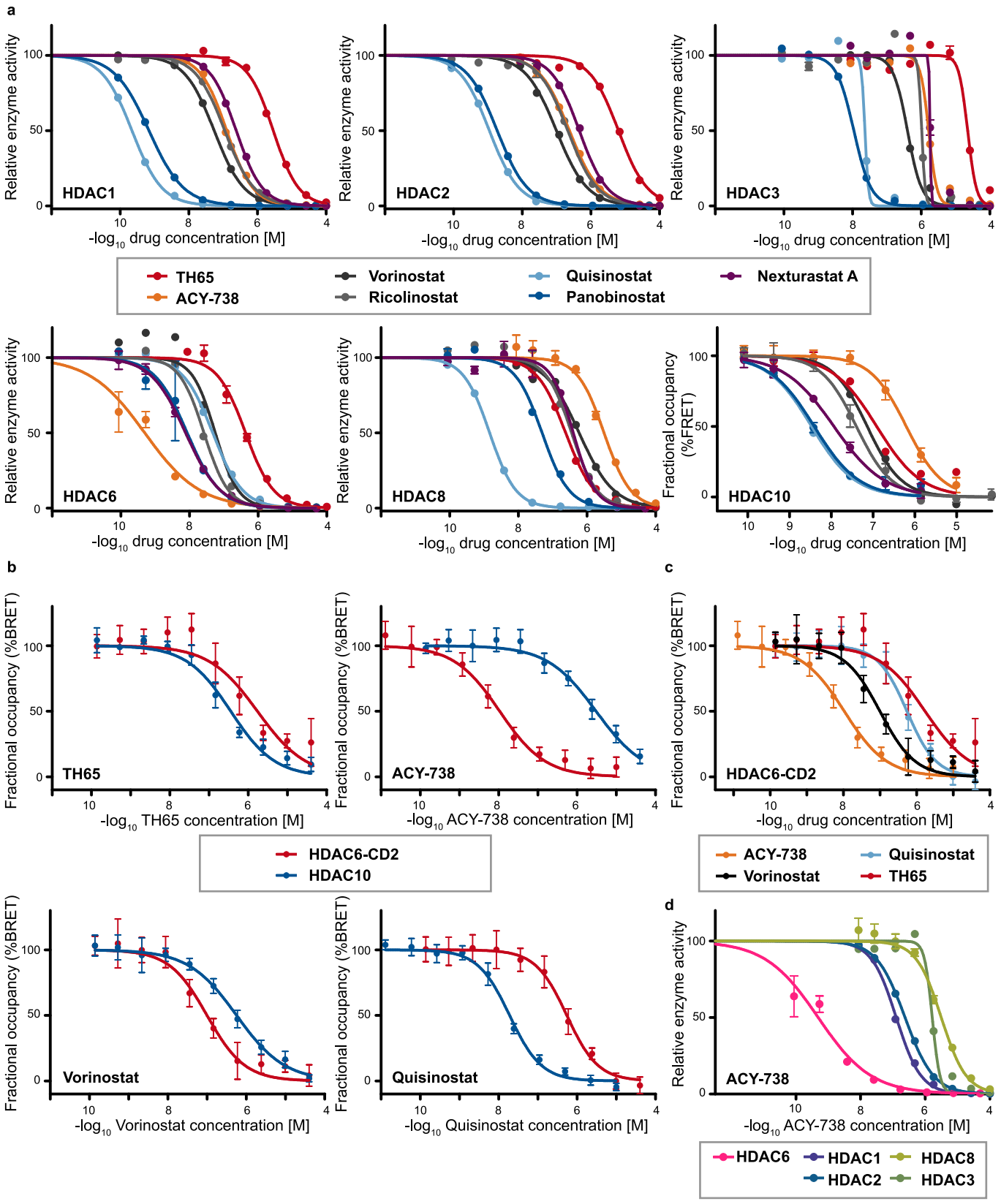

Extended Data Fig. 6 | See next page for caption.

Extended Data Fig. 6 | Confirming selectivity of ACY-738 (HDAC6i) and TH65 (HDAC10i) with orthogonal biochemical assays. a, Dose-dependent in vitro HDAC activity assays were performed using the HDAC-Glo assay for HDAC1/2/3/6/8. In vitro HDAC10 target engagement was determined by the TR-FRET assay (mean of triplicates with SD). **b** and **c**, HDAC6 and HDAC10 nano-BRET assays for in-cellulo target engagement measurement were performed with the selective compounds TH65 and ACY738 as well as with Vorinostat and Quisinostat for comparison. Of note, the HDAC6 nano-BRET only determines in-cell binding affinity to HDAC6 catalytic domain 2 (CD2) and not to CD1. **d**, Dose-dependent in vitro activity assay data for ACY-738 as determined by the HDAC-Glo assay shows the selectivity of ACY-738 over class I HDACs 1/2/3/8. a, d: HDAC-Glo assay was performed in three replicates; b, c: TR-FRET assay was performed in six replicates. Data are presented as mean values +/- SD.

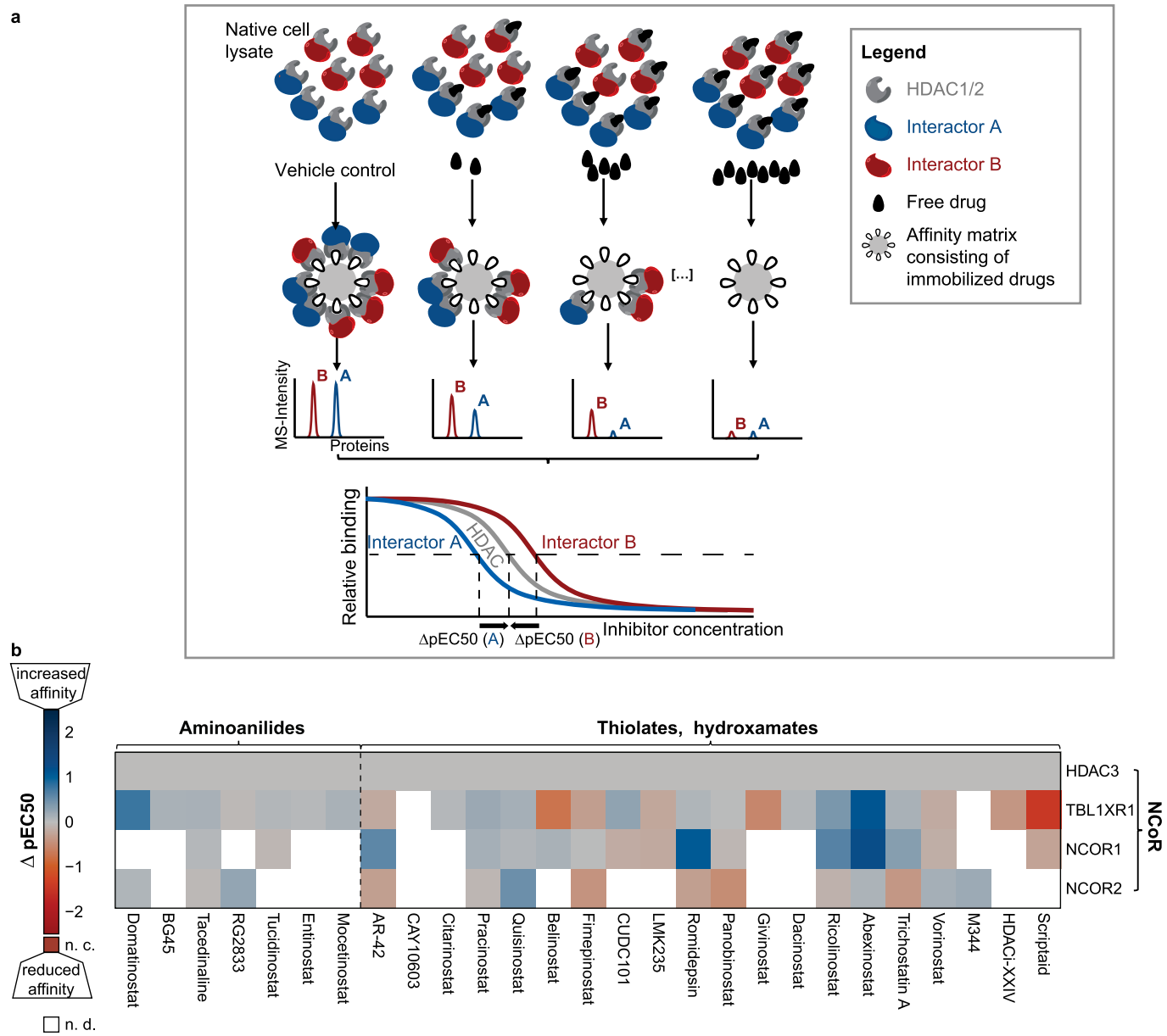

Extended Data Fig. 7 | Complex selectivity of class I HDACis. Schematic representation of acquiring HDAC complex selectivity data. Different interaction partners of the same HDAC (Interactor A and B) can impact the binding affinity of drugs to the HDAC target enzyme, for instance by inducing conformational changes. Since HDACs are bound by competing drugs or affinity probes when in complex with their interactors, all the complex partners show dose-response curves. These curves allow to infer the affinity of drugs to HDACs in complex with the respective interactor (A/B). As a result, the observed curve for the corresponding HDAC is an aggregation of all the potential complex variants and single HDACs, which are not part of complexes. **b**, Complex selectivity map for class I HDACis. The colours of the heatmap indicate differences in affinity to HDAC3 (ΔpEC_{50}) depending on its interaction partners of the NCoR complex. Colour shades of blue show that HDACi affinity is increased upon interaction between HDAC3 and the corresponding interaction partner, red shades indicate that HDACi loses binding affinity to HDACs interacting with the corresponding interaction partner (Blank space: lack of robust protein quantification prevents precise EC_{50} value determination).

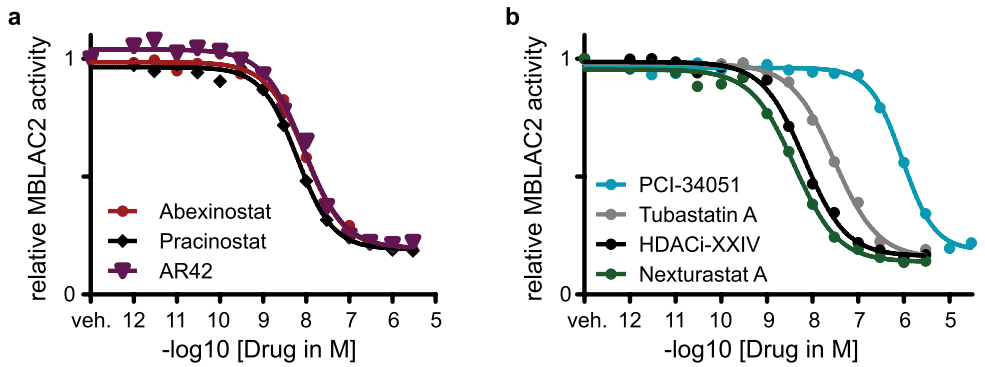

Extended Data Fig. 8 | Dose dependent inhibition of MBLAC2 hydrolase activity by HDAC inhibitors. a, Clinical drugs Abexinostat, Pracinostat and AR-42 all show EC_{50} inhibition values below 10 nM (assay threshold). **b**, Tool compounds and pre-clinical drugs also engage with MBLAC2. While potent MBLAC2 binders from the chemoproteomic profiling show inhibition with nanomolar affinities, PCI-34051 (non-binder chemoproteomic assay) shows over 100-fold lower activity against MBLAC2 ($pEC_{50} = 6.0$).

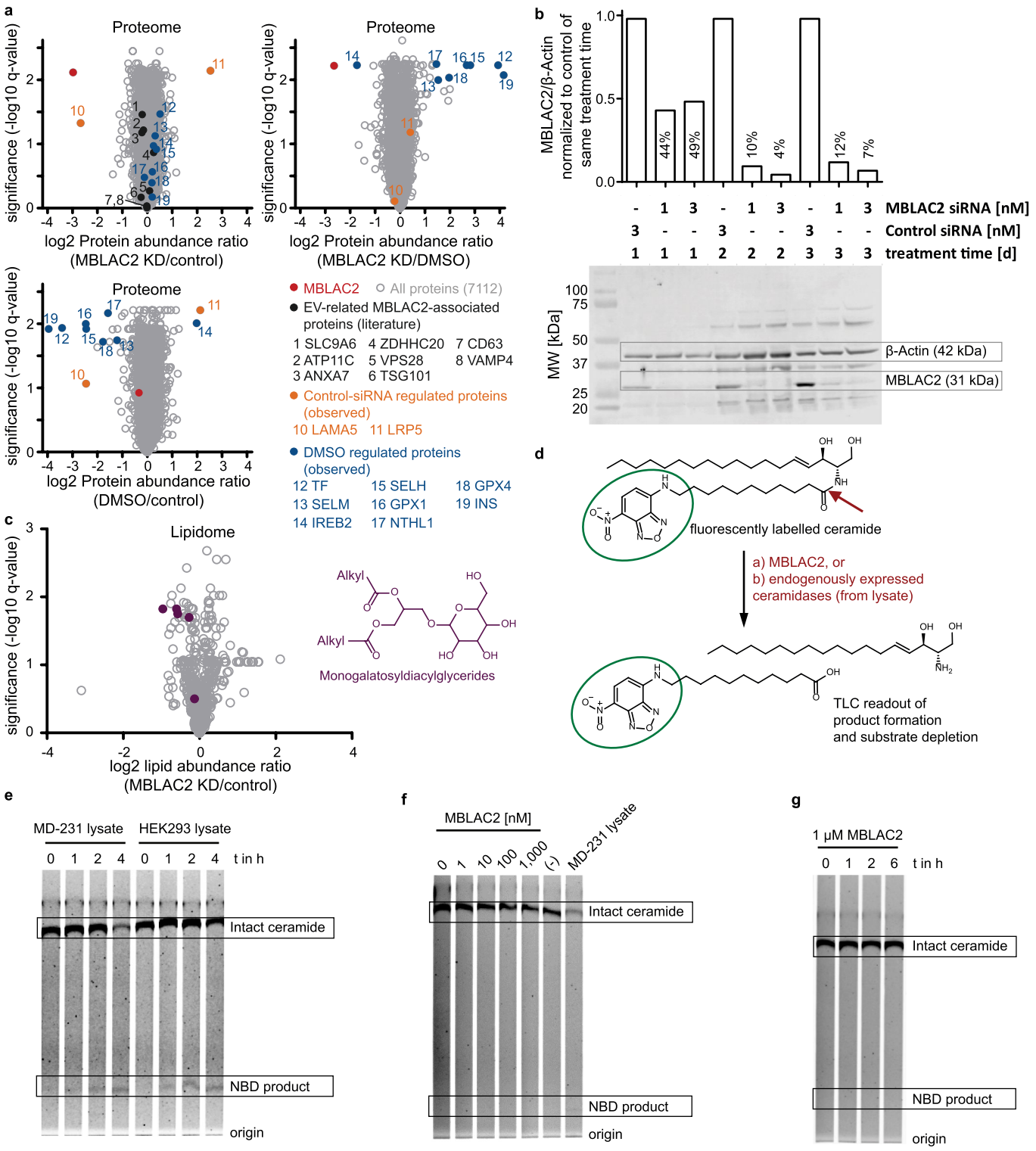

Extended Data Fig. 9 | See next page for caption.

Extended Data Fig. 9 | MBLAC2 inhibition and knockdown effects on proteome and lipidome. siRNA-mediated MBLAC2 knockdown does not lead to major changes of intracellular protein levels. Volcano plots display the difference in protein abundances of HEK293 cells after DMSO treatment of transfection with MBLAC2-directed siPOOL or control siPOOL (biological triplicates). HEK293 were lysed and submitted to a deep bottom-up proteomics workflow, including SP3-bead protein digestion protocol and TMT-labelling for robust quantification. While MBLAC2 knockdown is still efficient 3.5 d after transfection with siRNA POOL (13% compared to control siRNA), the whole proteome is generally unaffected. Intracellular levels of proteins involved in extracellular vesicle biogenesis and associated to MBLAC2 do not change significantly (labelled in grey are potential interaction partners or co-regulated proteins TSG101, ATP11C, SLC9A6, VAMP4, ZHHDC20, CD63, ANXA7, VPS28). We attribute the apparent LRP5 upregulation and LAMA5 downregulation (orange) to effects caused by transfection with control siRNA, since they are only affected in control siRNA pool treated cells. In analogy, proteins marked in blue are only regulated in DMSO treated cells and therefor attributed to DMSO-related effects (for example oxidative mechanisms). **b**, Western blot against human MBLAC2 (and beta-Actin as loading control), showing knockdown efficiencies in dependence of transfection amount and duration. Bands were quantified with the Licor software (see Methods) and normalized to the loading control. This normalized MBLAC2 expression was then again normalized to control siRNA treated cells of corresponding knockdown duration to give a relative and time-dependent knockdown efficiency of MBLAC2. In concordance with the full proteome data, knockdown is still sufficient three days after transfection. **c**, MBLAC2 knockdown leads to abundance changes of intracellular lipid families. MBLAC2 knockdown leads to global intracellular downregulation of monogalactosylceramides (general structure scaffold indicated) in HEK293 cells. Volcano plot shows the ratio and statistical significance (q-value) of lipid quantities between MBLAC2 knockdown (MBLAC2-KD - siRNA POOL in triplicate) and control (control siRNA in triplicate), as measured by mass-spectrometry based lipidomics, after MeOH/CHCl3 lipid extraction. **d**, Schematic of Ceramidase activity assay. A fluorescently labelled C12-NBD-Ceramide was incubated for different time periods with varying concentrations of WT MBLAC2 or native cell lysates containing endogenously expressed ceramidases. The reaction was terminated by boiling and solvent evaporated. The reaction products were resuspended in $CHCl_3$/MeOH run on a TLC plate and developed with $CHCl_3$/MeOH/NH_4OH. Fluorescent substrates and products were read out at 488 nm. **e**, Ceramidase assay evaluation. Incubation of the fluorescently labelled ceramide with native cell lysates from MD-231 and HEK293 cells at 37 °C shows turnover of the substrate after 4 h of incubation and confirms the functional setup. **f**, Incubation of fluorescently labelled Ceramide with increasing concentration of MBLAC2 for 2 h at 37 °C does not show notable turnover compared to negative control (-), while incubation with cell lysate reduces substantially the signal of intact ceramide substrate. **g**, Extended incubation of ceramide substrate with 1 μM WT MBLAC2 at 37 °C for increasing periods of time does not lead to notable substrate turnover even after 6 h incubation.

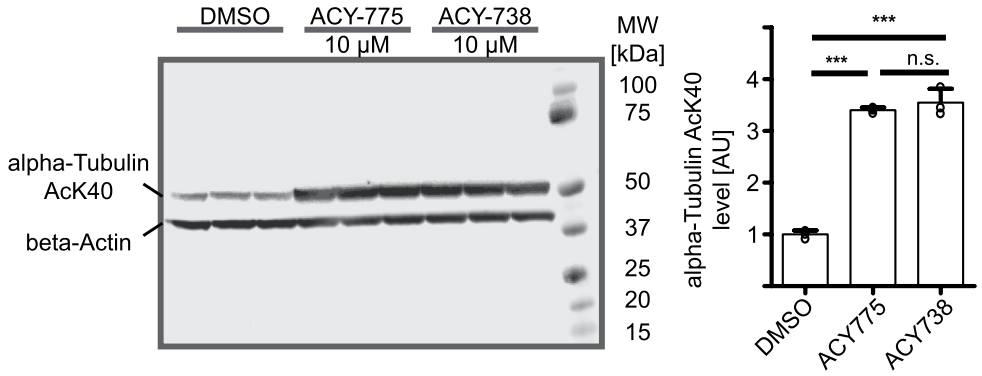

Extended Data Fig. 10 | ACY-738 and ACY-775 induce similar HDAC6 substrate overacetylation. SW620 cells were treated for 6 h with ACY-738, ACY-775 or DMSO control and the lysates were used for western blots against acetylated alpha-Tubulin (Lys40). The intensities of analyte bands were normalized to beta-actin intensities of the same lane to control for loading amount biases. ACY-775 as well as ACY-738 induced significant overacetylation of alpha-Tubulin Lys40 (***: $p < 0.0001$, n.s: $p = 0.4147$). Similar overacetylation of alpha-Tubulin indicates comparable target engagement of HDAC6 inhibitors. Data of bar chart are represented as mean +/− SD of three biological replicates (2-sided t-test).

nature research

Corresponding author(s): Guillaume Médard

Last updated by author(s): Feb 24, 2022

Reporting Summary

Nature Research wishes to improve the reproducibility of the work that we publish. This form provides structure for consistency and transparency in reporting. For further information on Nature Research policies, see our Editorial Policies and the Editorial Policy Checklist.

Statistics

For all statistical analyses, confirm that the following items are present in the figure legend, table legend, main text, or Methods section.

n/a	Confirmed
☐	☒ The exact sample size (*n*) for each experimental group/condition, given as a discrete number and unit of measurement
☐	☒ A statement on whether measurements were taken from distinct samples or whether the same sample was measured repeatedly
☐	☒ The statistical test(s) used AND whether they are one- or two-sided *Only common tests should be described solely by name; describe more complex techniques in the Methods section.*
☒	☐ A description of all covariates tested
☐	☒ A description of any assumptions or corrections, such as tests of normality and adjustment for multiple comparisons
☐	☒ A full description of the statistical parameters including central tendency (e.g. means) or other basic estimates (e.g. regression coefficient) AND variation (e.g. standard deviation) or associated estimates of uncertainty (e.g. confidence intervals)
☐	☒ For null hypothesis testing, the test statistic (e.g. *F*, *t*, *r*) with confidence intervals, effect sizes, degrees of freedom and *P* value noted *Give P values as exact values whenever suitable.*
☒	☐ For Bayesian analysis, information on the choice of priors and Markov chain Monte Carlo settings
☒	☐ For hierarchical and complex designs, identification of the appropriate level for tests and full reporting of outcomes
☐	☒ Estimates of effect sizes (e.g. Cohen's *d*, Pearson's *r*), indicating how they were calculated

Our web collection on statistics for biologists contains articles on many of the points above.

Software and code

Policy information about availability of computer code

Data collection	Thermo Scientific Xcalibur (v 4.1.31.9) was used to collect mass spectrometry data. Dionex Chromeleon (v 6.80) was used for proteome fractionation. Sartorius IncuCyte S3 software (v 2009B) was used to acquire live cell imaging data. Odyssey Li-COR application software (v 3.0.29) was used for Western Blot scanning. Versadoc Imaging System was used for the ceramidase assay. ZetaView Software (v 8.05.12 SP1) by Particle Metrix was used for nanoparticle tracking analysis.
Data analysis	MaxQuant (v 1.6.1.0) with embedded search engine Andromeda together with Swissprot reference database (v 03.12.15) were used to analyse the proteomics experiments. Microsoft Excel (2013), Internal R script based on 'drc' and 'pheatmap' packages were further used to analyse the pulldown and dose-response chemoproteomics data. ComBat from the 'sva' package (v 3.30.1), Perseus (v1.6.2.2), Microsoft Excel (2013), and GraphPad PRISM (v5.01) were further used to analyse the full proteome data. Ilastik and an ad-hoc R script were used to analyse the live-cell imaging assay. MS-DIAL4 software (v 4.38), Python 'statsmodels' package and GraphPad PRISM (v5.01) were used to analyse the lipidomics data.

For manuscripts utilizing custom algorithms or software that are central to the research but not yet described in published literature, software must be made available to editors and reviewers. We strongly encourage code deposition in a community repository (e.g. GitHub). See the Nature Research guidelines for submitting code & software for further information.

Data

Policy information about availability of data

All manuscripts must include a data availability statement. This statement should provide the following information, where applicable:

- Accession codes, unique identifiers, or web links for publicly available datasets
- A list of figures that have associated raw data
- A description of any restrictions on data availability

Chemoproteomics data are freely accessible on ProteomicsDB.org. The mass spectrometry proteomics data including the Swissprot reference database have been deposited to the ProteomeXchange Consortium via the PRIDE partner repository with the dataset identifier PXD026657. The untargeted metabolomics data for lipidomics are made available on MetaboLights repository with the identifier MTBLS3557 and can further be accessed on Zenodo (https://zenodo.org/record/5914128#.Yfe59_jTVhE).

Field-specific reporting

Please select the one below that is the best fit for your research. If you are not sure, read the appropriate sections before making your selection.

☒ Life sciences ☐ Behavioural & social sciences ☐ Ecological, evolutionary & environmental sciences

For a reference copy of the document with all sections, see nature.com/documents/nr-reporting-summary-flat.pdf

Life sciences study design

All studies must disclose on these points even when the disclosure is negative.

Sample size	No sample size calculations have been performed.
Data exclusions	In Extended Data Fig. 2, one replicate was omitted for the iQ/iA comparison and in Fig. 4 one replicate was omitted for Citarinostat due to obvious experimental errors.
Replication	Replication of the enrichment by the new affinity matrix was controlled for every drug using the vehicle control. Chemoproteomics profiling and activity assay constitute orthogonal techniques to validate the drugs as MBLAC2 inhibitors. Pharmacological inhibition and knock-down of MBLAC2 cross-validate MBLAC2 effect on extracellular vesicles. Biochemical and cell biology experiments were performed in triplicates (duplicates for the MBLAC2 single dose activity assay), morphotyping in biological quadruplicates. Chemoproteomics dose-response profiling were profiled once for each drug.
Randomization	The order of drug profiling was random.
Blinding	Blinding of drug identity was implemented for MBLAC2 activity assays. Blinding of treatment conditions was implemented for EV counting.

Reporting for specific materials, systems and methods

We require information from authors about some types of materials, experimental systems and methods used in many studies. Here, indicate whether each material, system or method listed is relevant to your study. If you are not sure if a list item applies to your research, read the appropriate section before selecting a response.

Materials & experimental systems

n/a	Involved in the study
☐	☒ Antibodies
☐	☒ Eukaryotic cell lines
☒	☐ Palaeontology and archaeology
☒	☐ Animals and other organisms
☒	☐ Human research participants
☒	☐ Clinical data
☒	☐ Dual use research of concern

Methods

n/a	Involved in the study
☒	☐ ChIP-seq
☒	☐ Flow cytometry
☒	☐ MRI-based neuroimaging

Antibodies

Antibodies used	MBLAC2 (Abcam #ab122411, rabbit polyclonal IgG, Lot GR3180549-2), beta-actin (Santa Cruz Biotechnology #sc-47778, monoclonal mouse IgG, Lot D2817), acetyl-alpha-tubulin (Lys40) (Cell Signaling Technology, #12152S, monoclonal mouse IgG, Lot 1), beta-actin (Cell Signaling Technology, #8457S, monoclonal rabbit IgG); fluorophore-conjugated secondary antibodies (ODYSSEY donkey-anti-rabbit (#926-68023, Lot C01119-01), goat-anti-mouse (#926-32210, Lot C00816-01)).
Validation	According to the manufacturer, anti-beta-actin antibody is recommended for detection of beta-actin from mouse, rat, human, avian,

Validation	bovine, canine, porcine, rabbit, Dictyostelium discoideum and Physarum polycephalum per WB, IP, IF, IHC(P) and ELISA. According to the manufacturer, anti-MBLAC2 antibody is recommended for detection of MBLAC2 from human samples and suitable for ICC/IF, IHC-P, WB. According to the manufacturer, anti acetyl-alpha-tubulin antibody is specific for detection of acetyl-alpha-tubulin and has been widely used by others and confirmed to be specific.

Eukaryotic cell lines

Policy information about cell lines

Cell line source(s)	COLO-205, MV4-11, K-562, SK-N-BE(2), HEK293, BT-549, PC3, SW620, OVCAR-8, MCF7, have been previously used in-house (10.1021/pr5012608, 10.1038/s41467-020-17336-9, 10.1016/j.celrep.2013.07.018) whereas PATU-8998-S was acquired from DSMZ (#ACC 204).
Authentication	Multiplex human Cell line Authentication Test (MCA) was performed by multiplexion using SNP profiling, for COLO-205, MV4-11, K-562, SK-N-BE(2), and PATU-8998-S. Other cell lines were not authenticated
Mycoplasma contamination	All cell lines were tested negative for mycoplasma contamination.
Commonly misidentified lines (See ICLAC register)	None.

Chemoproteomic target deconvolution reveals Histone Deacetylases as targets of (*R*)-lipoic acid

Severin Lechner[1], Raphael R. Steimbach[2,3], Longlong Wang[4,5], Marshall L. Deline[6], Yun-Chien Chang[1], Tobias Fromme[6,7], Martin Klingenspor[6,7,8], Patrick Matthias[4,5], Aubry K. Miller[2,9], Guillaume Médard[1], Bernhard Kuster[1,9,10]

[1]*Chair of Proteomics and Bioanalytics, TUM School of Life Sciences, Technical University of Munich, Freising, Germany.*
[2]*Cancer Drug Development, German Cancer Research Center (DKFZ), Heidelberg, Germany.*
[3]*Biosciences Faculty, Heidelberg University, Heidelberg, Germany.*
[4]*Friedrich Miescher Institute for Biomedical Research, 4058 Basel, Switzerland.*
[5]*Faculty of Sciences, University of Basel, 4031 Basel, Switzerland.*
[6]*Chair of Molecular Nutritional Medicine, TUM School of Life Sciences, Technical University of Munich, Freising, Germany.*
[7]*EKFZ - Else Kröner Fresenius Center for Nutritional Medicine, Technical University of Munich, Freising, Germany*
[8]*ZIEL Institute for Food & Health, Technical University of Munich, Freising, Germany.*
[9]*German Cancer Consortium (DKTK), Heidelberg, Germany.*
[10]*Bavarian Center for Biomolecular Mass Spectrometry (BayBioMS), Technical University of Munich, Freising, Germany.*

Correspondence and requests for materials should be addressed to Bernhard Kuster (kuster@tum.de).

Abstract

Lipoic acid is an essential enzyme cofactor in central metabolic pathways. Due to its claimed antioxidant properties, racemic (*R*/*S*)-lipoic acid is used as a food supplement but is also investigated as a pharmaceutical in over 180 clinical trials covering a broad range of diseases. Moreover, (*R*/*S*)-lipoic acid is an approved drug for the treatment of diabetic neuropathy. However, its mechanism of action remains elusive. Here, we performed chemoproteomics-aided target deconvolution of lipoic acid and its active close analog lipoamide. We find that histone deacetylases HDAC1, HDAC2, HDAC3, HDAC6, HDAC8, and HDAC10 are molecular targets of the reduced form of lipoic acid and lipoamide. Importantly, only the naturally occurring (*R*)-enantiomer inhibits HDACs at physiologically relevant concentrations and leads to hyperacetylation of HDAC substrates. The inhibition of HDACs by (*R*)-lipoic acid and lipoamide explain why both compounds prevent stress granule formation in cells and may also provide a molecular rationale for many other phenotypic effects elicited by lipoic acid.

Introduction

The disulfide-containing fatty acid lipoic acid (LA) is an endogenously produced molecule and is essential for aerobic metabolism both in prokaryotes and eukaryotes[1]. When attached via an amide bond to a lysine side chain (lipoylation), (*R*)-LA acts as a cofactor for several enzymes including the pyruvate dehydrogenase complex at the intersection between glycolysis and the citric acid cycle[1]. Lipoic acid can be synthesized in cells but is also taken up by cells from exogenous sources. The racemic mixture of LA enantiomers ((*R*/*S*)-LA) is used as a food supplement and as a therapeutic drug, purportedly because of its property as an antioxidant[2]. This is attributed to the fact that, following cellular uptake, the disulfide bond in LA is readily reduced[3] and the thiols may chelate metal ions or scavenge reactive oxygen or nitrogen species. At the time of writing, LA was subject to 187 clinical trials (22 phase 4 trials; clinicaltrials.gov) covering, for instance, endocrine, neurological, and autoimmune diseases such as diabetes mellitus, peripheral nervous system disorders, or multiple sclerosis, respectively[4]. Lipoic acid has been proven efficacious in diabetic neuropathy[5], which affects approximately 16% of diabetes patients[6] and, as such, is frequently prescribed for treating diabetic neuropathy and neuropathic pain[7-9]. Lipoic acid is well tolerated at clinically relevant doses ranging from 600 – 2400 mg/day (both orally and intravenously) and reaches peak plasma concentrations of 100-500 µM[10]. Despite its widespread use, the mechanism of action (MoA) of LA remains unclear. Much attention has been placed on its redox properties and ability to scavenge reactive oxygen species (ROS). Intriguingly, lipoic acid and the closely related amide lipoamide (LM) were recently discovered as hits in an *in vitro* screen for molecules that disrupt stress granules in Amyotrophic Lateral Sclerosis (ALS) model systems[11]. However, the targets underlying the observed phenotype remain elusive.

Here, we applied a chemoproteomic approach to identify direct protein targets of LA and LM. This revealed that Zn^{2+}-dependent histone deacetylases (HDACs) are protein targets of racemic (*R*/*S*)-LM as well as of (*R*)-LA, but not (*S*)-LA. (*R*)-LA and (*R*/*S*)-LM bind HDACs with low two-digit µM affinities and inhibit their enzymatic activity resulting in increased acetylation of HDAC substrates. The inhibition of HDACs also affects the hyperacetylation of the stress granule-forming protein DDX3X. Lipoamide and (*R*)-LA but not the inactive (*S*)-enantiomer prevented the formation of stress granules in A549 cells, suggesting that HDAC inhibition is the cellular MoA underlying this cellular phenotype.

Results

HDACs are targets of lipoic acid and lipoamide

To identify proteins directly bound by lipoic acid, we employed a chemoproteomic competition assay[12]. Briefly, (*R*/*S*)-LA was immobilized on sepharose beads via an amidation reaction to form an affinity matrix (abbreviated as iL; **Fig. 1a**). This affinity matrix can be incubated with cell lysate to pull down potential LA or LM target proteins and identify these targets via bottom-up proteomics. In a competition assay, free LA or LM were incubated with lysate at different concentrations before pulling down and quantifying target proteins. This pre-incubation leads to the dose-dependent reduction of pulled-down target proteins and allows to derive EC50 (effective concentration to reduce affinity matrix binding by 50%) values as well as apparent dissociation constants (K_d^{app}, expressed as $pK_d^{app} = -\log_{10} K_d^{app}$)[13] (**Fig. 1b,** see methods for details). Pulldowns using a lysate of the colorectal cancer cell line SW620 showed clear dose-dependent competition of HDAC1, HDAC2 (including co-competed members of the HDAC1/2 containing CoREST complex), and HDAC6 for both (*R*/*S*)-LA and (*R*/*S*)-LM with affinities in the range of 3-33 µM (**Fig. 1c, Supplementary Fig. 1a, Supplementary Data 1**). The lysate buffer used in this assay contains 1 mM DTT to mimic the intracellular reductive milieu and to reduce lipoic acid and lipoamide. The same experiment performed using the leukemia cell line MV4-

11 validated HDAC1 (K_d^{app} = 16 µM), HDAC2 (K_d^{app} = 14 µM), and HDAC6 (K_d^{app} = 21 µM) and identified HDAC3 (K_d^{app} = 13 µM) and HDAC10 (K_d^{app} = 5 µM) as additional targets of (*R*/*S*)-LM (**Fig. 1d**). Additional competition assays performed in lung adenocarcinoma cell A549 lysate also identified HDAC1, HDAC2, and HDAC6 as targets (**Supplementary Fig. 1b**). Amongst the three cell lines tested, HDACs were the only confidently identified targets across the 1500-3000 proteins quantified in these assays. Several HDAC complex members were co-competed, suggesting that LA and LM also engage the class I HDACs as part of gene regulatory complexes (**Fig. 1d, Supplementary Fig. 1a-d**). We validated the results by analogous pulldown competition assays using two other affinity matrices prepared via the immobilization of either the HDAC inhibitor Quisinostat (iQ) and an analog of the class IIa HDAC inhibitor Bürli's 31[14] (iC)[12]. We have previously shown that these affinity matrices specifically bind to the active sites of HDACs and have used them for HDACi selectivity profiling[12]. Indeed, binding of (*R*/*S*)-LA and (*R*/*S*)-LM to HDAC1, HDAC2, HDAC3, HDAC6, and, to a lesser extent, HDAC8 was confirmed in these assays (**Supplementary Fig. 1c-d)**. No binding to class IIa HDACs or the recently discovered common HDAC inhibitor off-target MBLAC2 was observed (**Supplementary Fig. 1e**)[12]. Interestingly, the competition assay data indicated that (*R*/*S*)-LA does not bind HDAC10, while (*R*/*S*)-LM binds HDAC10 with an even higher affinity than other HDACs. This observation might reflect electrostatic repulsion between the HDAC10 active site gate-keeper glutamic acid residues[15, 16] and the terminal carboxylic acid of LA.

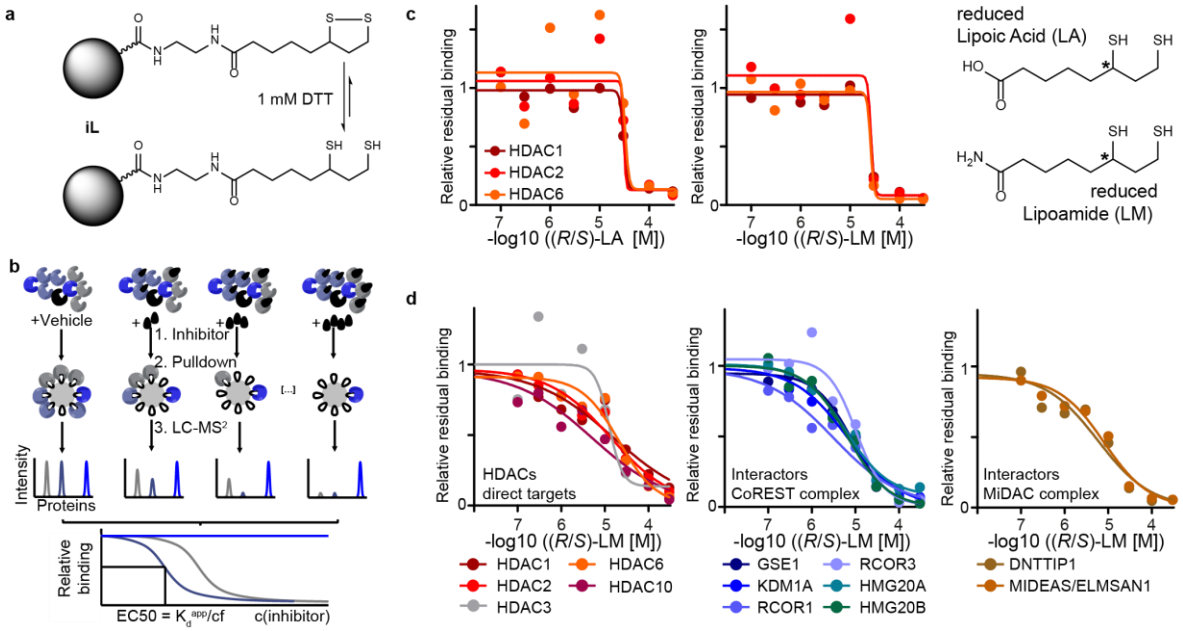

Figure 1|Chemoproteomics identifies HDACs as targets of lipoic acid and lipoamide. a, an affinity matrix iL was synthesized by immobilizing racemic (*R*/*S*)-lipoic acid to sepharose beads. The resulting affinity matrix resembles lipoamide and is reduced to dihydrolipoamide under assay conditions (1 mM DTT). **b**, Schematic representation of the competition pulldown assay used in this study. Lysate containing correctly folded proteins interacting with endogenous cofactors or macromolecular binding partners is incubated with the affinity matrix to pull down target proteins. In a competition experiment, the lysate is first incubated with different doses of the free drug of interest (black droplet symbol) before pull down. LC-MS/MS is used to quantify target proteins. The intensities are plotted against the drug concentration to yield dose-response curves, from which binding EC50s and K_d^{app} can be derived (cf=correction factor; see methods). **c**, Dose-response curves for lipoic acid and lipoamide using lysate of SW620 cancer cells. Structures of drugs are shown in the reduced form and the chiral center is indicated by an asterisk. **d**, Dose-response curves for (*R*/*S*)-LM using lysate of MV4-11 cancer cells showing HDACs and HDAC complex partners of the CoREST (blue) and MiDAC (brown) complexes. Source data are provided as a Source Data file.

The reduced forms of (*R*)-lipoic acid and racemic lipoamide inhibit HDACs

To validate the inhibition of HDACs by LA and LM and elaborate on the structure-activity relationship (SAR) of enantiomers as well as oxidized versus reduced forms of the molecules, we performed enzyme activity assays for recombinant HDAC1,2,3,6,8 as well as a FRET-based binding assay for recombinant HDAC10. We included the clinically approved HDAC inhibitor Vorinostat (SAHA) as a positive control. To measure the potential dependence of HDAC inhibition on the redox state of the molecules, experiments were performed in the presence or absence of TCEP, a reducing agent with no effect on HDAC activity and HDAC inhibitor binding under the assay conditions (**Supplementary Fig. 2a**). Reduced (*R*/*S*)-LA and (*R*/*S*)-LM inhibit HDAC1,2,3,6,8 (EC50 = 1 – 44 µM) while the oxidized form of (*R*/*S*)-LA showed diminished activity. No activity at all was detected for oxidized (*R*/*S*)-LM (**Fig. 2a, Supplementary Fig. 2b-c**). Performing the same experiment using reduced racemic dihydrolipoic acid yielded affinity values comparable to racemic lipoic acid in the presence of TCEP, suggesting complete reduction and dithiolane ring opening under the assay conditions (**Supplementary Fig. 2d**). As observed in the chemoproteomic experiments, potent HDAC10 binding of (*R*/*S*)-LM could be confirmed. While (*R*/*S*)-LM affinity for HDAC10 was only 5-fold lower than that of Vorinostat, (*R*/*S*)-LA showed almost 200-fold lower affinity to HDAC10 compared to Vorinostat (**Supplementary Fig. 2e**). The (*S*)-enantiomer of lipoic acid had no activity against any HDAC at concentrations of up to 500 µM (**Fig. 2b, c**). This makes (*S*)-LA an ideal negative control for the assessment of which of the phenotypic effects elicited by lipoic acid are related to HDAC inhibition and which are related to other physicochemical properties of the molecule such as metal ion chelation or reactive oxygen species (ROS) scavenging.

In summary, the above data indicate that reduced (*R*)-LA, as well as (*R*/*S*)-LM feature an HDAC selectivity profile similar (albeit less potent) compared to that of clinical drugs such as Vorinostat and Ricolinostat (Fig. 2d, Supplementary Fig. 2f). All these molecules inhibit HDAC1-3 with similar affinity and HDAC6 with 5 to 15-fold higher relative potency. Given that the cytosol is a disulfide-reducing environment, and lipoic acid is readily reduced once inside the cell[3], both lipoic acid and lipoamide, most probably, exist in cells in their reduced and, therefore, HDAC-inhibiting forms.

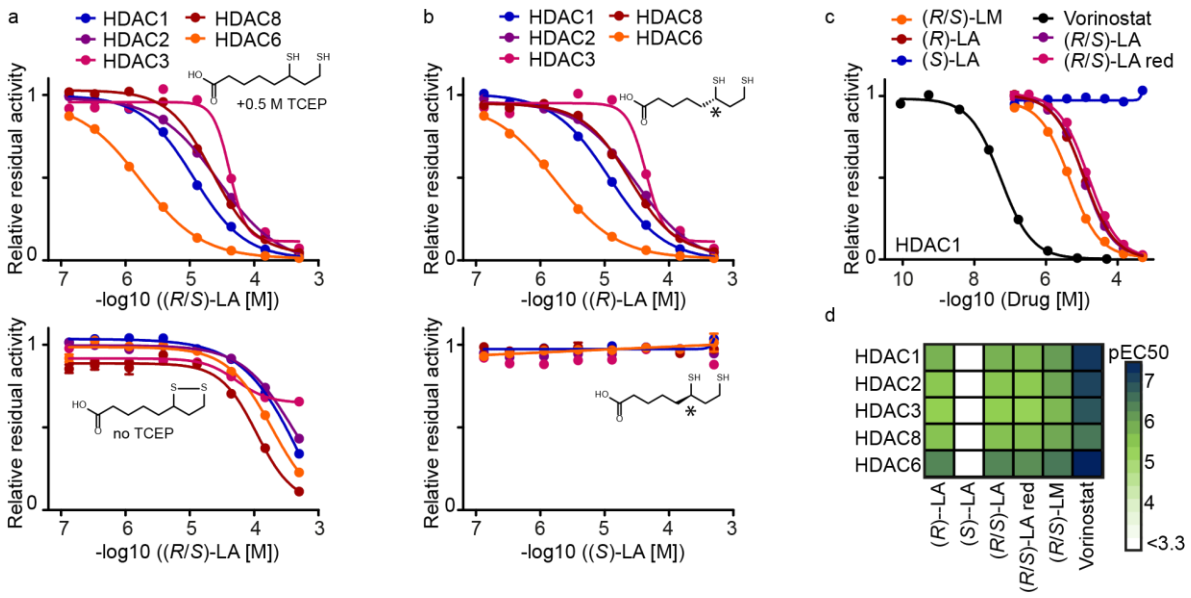

Figure 2|HDAC activity assays confirming the inhibitory effects of the reduced forms of (*R*)-lipoic acid, (*R*/*S*)-lipoic acid, and (*R*/*S*)-lipoamide. a, Influence of the reducing agent TCEP (0.5 M) on (*R*/*S*)-LA mediated HDAC enzymatic activity via reduction and ring opening of the drug (for (*R*/*S*)-LM see Supplementary Fig. 2b) (n = 3 technical replicates, data are represented as mean value +/- SEM). **b,** HDAC inhibitory effect of the (*R*)-enantiomer of lipoic acid compared to the (*S*)-

enantiomer (n = 3 technical replicates, data are represented as mean value +/- SEM). **c,** exemplary dose-response profiles of all compounds tested for HDAC1 inhibition in the presence of 0.5 M TCEP ((*R*/*S*)-LA red = (*R*/*S*)-dihydrolipoic acid). n = 3 technical replicates. **d**, Summary of EC50 values derived from dose-dependent HDAC inhibition curves. Source data are provided as a Source Data file.

(*R*)-lipoic acid engages HDACs in cells and induces HDAC substrate hyperacetylation

To verify that (*R*)-LA and (*R*/*S*)-LM inhibit HDACs in cells, we treated a set of cell lines (HEK293T, A549, HeLa S3) with racemic or enantiomerically pure lipoic acid, racemic lipoamide, the HDAC6/MBLAC2 inhibitor Tubacin, the potent HDAC6 selective inhibitor ACY-738[12], and the unselective HDAC1,2,3,6 inhibitor Vorinostat and probed for HDAC substrate hyperacetylation. Western blot analysis confirmed that (*R*/*S*)-LA and (*R*/*S*)-LM dose-dependently increased acetylation levels of the well-established HDAC6 substrate α-Tubulin AcK40 (**Supplementary Fig. 3a**) and showed substantial increase of acetylation at concentrations as low as 50 µM after 7h of drug incubation. In another experiment, HEK293T cells were probed for acetylation of the stress granule protein DDX3X K118, another well-established HDAC6 substrate site[17]. Again lipoic acid and lipoamide both dose-dependently increased acetylation levels of α-Tubulin AcK40 (3.4-fold with 1 mM (*R*/*S*)-LA; 4.0-fold with 1 mM (*R*/*S*)-LM) and DDX3X AcK118 (2.4-fold at 1 mM (*R*/*S*)-LA and (*R*/*S*)-LM). The extent of DDX3X hyperacetylation induced by 1 mM (*R*/*S*)-LA or (*R*/*S*)-LM was in the same range as for ACY-738 (3.0-fold at 5 µM) (**Fig. 3a, Supplementary Fig. 3b**) and the HDAC6/10 inhibitor Tubastatin A (ref.[17], 2.6-fold at 10 µM). Importantly, in contrast to HDAC-inhibiting (*R*)-lipoic acid and Vorinostat, (*S*)-lipoic acid did not lead to a substantial increase of α-Tubulin AcK40 or Histone H4 AcK5/8/12/16 in HEK293T cells or A549 lung adenocarcinoma cells at concentrations of up to 500 µM (**Fig. 3b, Supplementary Fig. 3c**). HDAC substrate hyperacetylation is commonly used to demonstrate in-cellulo inhibition of HDACs and our data, therefore, provides evidence for HDAC-inhibitory activity of (*R*)-lipoic acid and (*R*/*S*)-lipoamide in cells. Of note, (*R*/*S*)-lipoic acid has previously been shown to increase α-Tubulin acetylation but direct HDAC6 inhibition was not proposed as the underlying mode of action[18]. Given that LA and LM inhibit several HDACs (nuclear HDAC1, HDAC2, HDAC3, HDAC8, and cytosolic HDAC6) that collectively have hundreds of substrates[19], we reasoned that LA and LM may increase acetylation levels of many cellular proteins. Indeed, western blot analysis for global acetylation levels in (*R*/*S*)-LA treated HeLa S3 cells showed elevated levels of acetylation of proteins in the size range of histones (11-16 kDa), α-Tubulin (50 kDa) and others (**Fig. 3c, Supplementary Fig. 3c**). Similarly, time-dependent treatment of HeLa S3 cells with (*R*/*S*)-LA clearly showed upregulation of acetylation on a broad range of proteins within 1 h and peaking between 3-8 h (**Supplementary Fig. 3d-e**). To show that hyperacetylation is a direct result of HDAC inhibition, we performed nanoBRET-based intracellular target engagement assays using (*R*)-LA, (*S*)-LA, (*R*/*S*)-LM, and Vorinostat against HDAC6 and HDAC10 in HeLa cells. Indeed, (*R*)-LA as well as (*R*/*S*)-LM showed dose-dependent intracellular binding to HDAC6 and HDAC10, while (*S*)-LA was inactive. HDAC6 was half maximally inhibited at 35 µM (*R*/*S*)-LM and 170 µM (*R*)-LA. These values agree well with the observed HDAC substrate hyperacetylation using 2-3 digit µM doses of the molecules and are below the clinically observed maximal peak plasma concentration of lipoic acid. Together, these results suggest that lipoic acid and lipoamide engage and inhibit HDACs in cells.

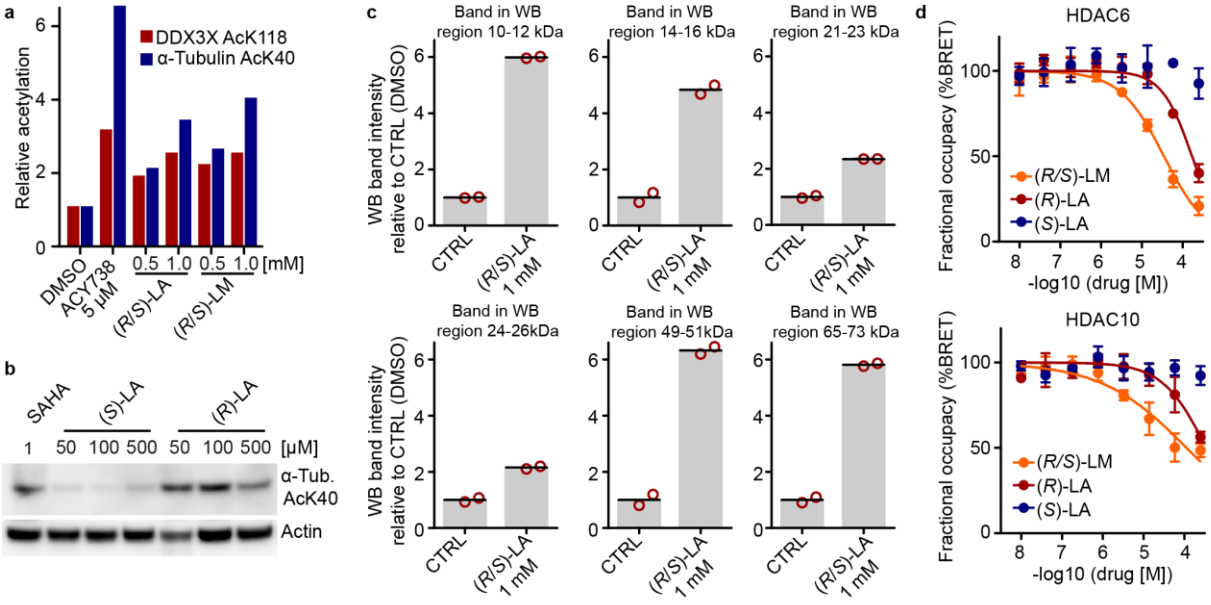

Figure 3 | (*R*/*S*)-Lipoic acid and (*R*/*S*)-lipoamide lead to hyperacetylation of HDAC substrates in cells. a, Western blot analysis of acetylation levels of HDAC6 substrates following 12 h treatment of HEK293T cells with (*R*/*S*)-LA, (*R*/*S*)-LA, and the HDAC6 inhibitor ACY738 (see also Supplementary Fig. 3a). **b,** Western blot for α-Tubulin AcK40 acetylation levels after 12 h treatment of A549 cells with SAHA (Vorinostat), (R)-LA, and (S)-LA. **c,** Western blot analysis for global lysine acetylation levels of HeLa S3 cells treated with (*R*/*S*)-LA (16 h; n = 2 independent biological experiments, error bars represent standard deviation; see also Supplementary Fig. 3c). The histograms show hyperacetylation of proteins in the size range of established HDAC substrates, such as Histones (11-16 kDa), Peroxiredoxin (22 kDa)[20], α-Tubulin (50 kDa) and others. **d,** HDAC6 and HDAC10 nano-BRET assays demonstrating in-cellulo target engagement in HEK293T cells (n = 3 independent experiments, data are represented as mean value +/- SD; curve fitted with a variable slope; bottom constrained to 0 and top constrained to 100). Source data are provided as a Source Data file.

(*R*)-lipoic acid and (*R*/*S*)-lipoamide inhibit stress granule formation in cells

The acetylation status of proteins can affect their macromolecular associations and the tendency of proteins to phase-separate into liquid condensates such as stress granules[17]. Interestingly, lipoic acid and lipoamide have recently been identified as modulators of stress granule formation[11]. To investigate whether stress granule formation can be attenuated by LA or LM-mediated HDAC inhibition, A549 cells were treated with (*S*)-LA (no HDAC inhibition) or the HDAC inhibitors (*R*)-LA, (*R*/*S*)-LM and Vorinostat. After pre-incubation of cells with compound, stress granule formation was induced using 30 min of arsenite treatment (1 mM). After treatment, cells were fixed for immunofluorescence detection of stress granules via the common stress granule marker protein G3BP1[21]. Importantly, only the HDAC inhibitors (*R*)-LA, (*R*/*S*)-LM, and Vorinostat, but not the HDAC-inactive (*S*)-LA led to a dose-dependent reduction of stress granule numbers per cell (**Fig. 4 a,b**).

To understand, whether the purportedly antioxidant effects of lipoic acid play a role in the observed phenotypes, we performed assays to read out reactive oxygen species (ROS) levels in A549 cells exposed to stressors after drug pre-treatments. Levels of ROS induced by 2 h treatment of 200 µM tert-butyl hydroperoxide (tBuOOH) were significantly reduced to 60-70% by both (*S*)-LA and (*R*)-LA or the racemic form at concentrations of 100 µM (**Fig. 4c, Supplementary Fig. 4**). Another thiol-containing molecule and antioxidant, N-acetyl-cysteine (NAC), reduced oxidative stress levels to a similar extent as lipoic acid. Thus, while having differential activity on HDAC inhibition, protein acetylation, and stress granule formation, (*S*)-LA and (*R*)-LA showed comparable ROS buffering effects (**Supplementary Fig. 5**). The reduction of oxidative stress might be explained by the molecules'

capability of chelating ferrous or cuprous ions to suppress the Fenton reaction[22, 23]. Scavenging of ROS by the molecules' thiol groups could in theory play a role but the published literature concludes that this is kinetically irrelevant compared to enzyme-catalyzed ROS turnover[22-24]. Of note, physiological intracellular hydrogen peroxide concentrations are estimated to be in the low nanomolar range[24, 25] and 200 µM tBuOOH treatment, therefore, constitutes an extreme and highly non-physiological peroxide stress. Interestingly, in contrast to tBuOOH, exposing A549 cells for 30 min to 1 mM arsenite did not significantly induce ROS according to the CellRox assay (**Fig. 4d, Supplementary Fig. 4**). Thus, in the absence of extreme oxidative stress conditions as induced by 200 µM tBuOOH, neither NAC nor (*S*)-LA and (*R*)-LA pre-treatment had a significant ROS reducing effect in A549 cells. This finding supports the conclusion that the distinct effects of (*S*)-LA and (*R*)-LA on arsenite-induced stress granule formation are independent of the molecules' potential as antioxidants, i.e. as metal ion chelators or scavengers of ROS. Considering the well-established role of HDACis in preventing arsenite-induced stress granule formation and the evidence for in cellulo HDAC inhibition by R-Lipoic acid, we propose that enantioselective HDAC inhibition is a major contributor to differential phenotypes observed between (*S*)-LA and (*R*)-LA treatments.

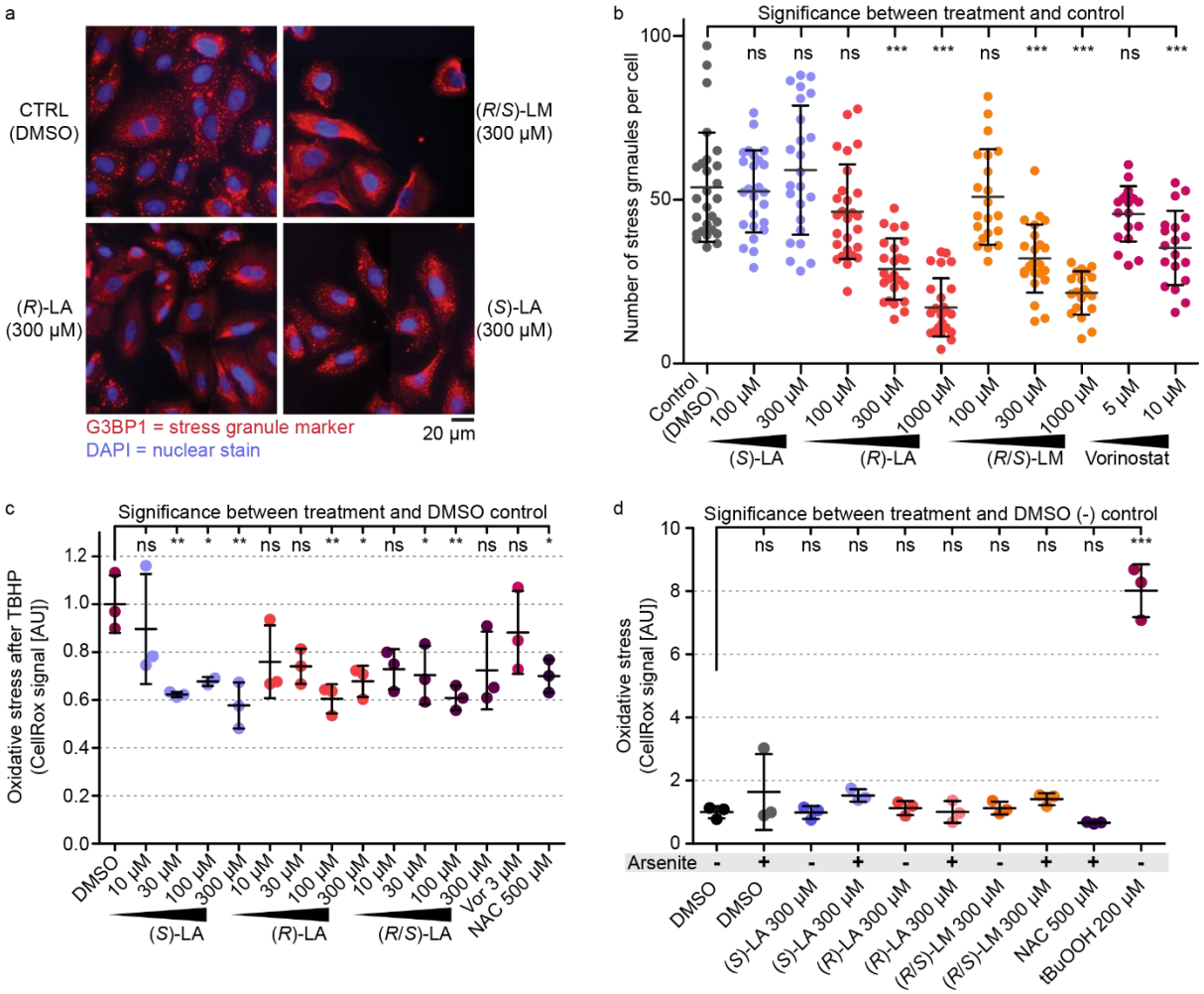

Figure 4|Lipoic acid and lipoamide reduce stress granule formation in cells. a, Immunofluorescence detection of the stress granule marker G3BP1 in A549 cancer cells. Stress granules appear as red foci in the DMSO control and cells treated with (HDAC-inactive) (*S*)-LA. The reduction of defined stress granules in response to (*R*)-LA and (*R*/*S*)-LA is apparent from the blurred red areas. **b,** Quantification of the number of stress granules per cell. Each treatment was performed in n = 3 independent biological experiments and between 140 and 150 cells were submitted to stress granule counting. **c,** Levels of oxidative stress induced by 2 h treatment with 200 µM Tertbutylhydroperoxide (BuOOH) after 1h pre-treatment with drugs (Vor: Vorinostat, NAC: N-acetylcysteine) in A549 cells. Oxidative stress levels were assessed using the CellRox assay. Every

data point corresponds to one biological replicate and is the mean CellRox intensity from 9-10 pictures capturing 60 – 180 cells in total (n = 2 biologically independent samples for 100 µM (*S*)-LA, n = 3 biologically independent samples for all other treatments, AU: arbitrary units). **d,** Levels of oxidative stress in A549 cells after 1.5 h drug pre-treatment, optionally followed by a 30 min arsenite (1 mM) pulse. Oxidative stress levels were assessed using the CellRox assay. Every data point corresponds to one biological replicate and equals the mean CellRox intensity from 10 - 15 pictures capturing 60 – 180 cells in total (n = 3 biologically independent samples for each drug dose, AU: arbitrary units). **b – d**, Statistical significance was calculated between the control and drug pre-treatments by one-way ANOVA following the Dunnett test for multiple comparison using the GraphPad Prism software. Data are presented as means ± SD. ns: not significant; *** : P-value ≤ 0.001, ** : P-value ≤ 0.01, * : P-value ≤ 0.05 in one-way ANOVA after Dunnett's multiple comparison test). Source data are provided as a Source Data file.

Discussion

Many of the metalloenzyme inhibitors widely used today, such as the angiotensin-converting enzyme inhibitor Captopril, contain thiols as metal chelating warheads. One of the most potent HDAC inhibitors, Romidepsin, features an intramolecular disulfide bond, which is intracellularly reduced to expose a thiol group that binds to the Zn^{2+}-ion in the active site of HDACs. Both lipoic acid and lipoamide also feature an intramolecular disulfide bridge that is known to be readily reduced in cells[3]. Therefore, we speculated that lipoic acid and lipoamide might target metalloproteins by one or both of the thiols functioning as a metal-chelating warhead. In line with this idea, chemoproteomic affinity profiling using immobilized lipoic acid identified Zn^{2+}-dependent HDACs as the only proteins bound specifically by lipoic acid and lipoamide. This does not exclude the possibility that other targets may exist, as pulldown experiments were only performed in MV4-11, SW620, and A549 cells, which may not express all potential target proteins. Of note, the affinity matrix was created by immobilizing (*R*/*S*)-LA via an amidation of its carboxylic acid group. Any target protein that may rely on an interaction with the negatively charged carboxy-group, would not score in the assay. Importantly, the same argument clearly opposes the published hypothesis that lipoic acid might inhibit HDACs akin to other nutritional short chain fatty acids by zinc chelation via its carboxy group[26, 27]. We confirmed HDAC binding and inhibition by recombinant enzyme activity assays, demonstrated HDAC target engagement in cells by nano-BRET assays and showed HDAC substrate hyperacetylation as the result of HDAC inhibition by lipoic acid. Cellular HDAC inhibition by lipoic acid occurred at 10 to 100-fold higher concentrations compared to the in vitro recombinant HDAC inhibition assay. This might be explained by incomplete intracellular reduction, lower intracellular compound concentration, or metabolic conversion of lipoic acid. However, the determined target affinities and inhibitory concentrations (low two-digit micromolar range) are still well below the dose range commonly applied in phenotypic studies of lipoic acid (1-5 mM). They are also below the peak plasma concentration of about 0.5 mM in humans[10]. This suggests that HDAC inhibition occurs *in vivo* at sites with high lipoic acid exposure (e.g. the blood or intestine epithelial cells) and that HDAC inhibition may at least in part explain several of the previously described phenotypes observed in response to lipoic acid.

The mode of action of lipoic acid has often been attributed to its metal ion chelation, antioxidant, and ROS scavenging properties, as well as to its potential impact on mitochondrial metabolism and biogenesis[28, 29]. However, increased mitochondrial metabolism should not result from a presumed increased availability of lipoic acid as an enzyme cofactor, because cells are capable of producing lipoic acid as needed. Considering a conservatively estimated 50 mM concentration of thiols in cells (mostly provided by glutathione), even intracellular concentrations of 0.5 mM lipoic acid would increase the availability of ROS scavenging thiols by only 1-2%[3]. Additionally, small molecule scavengers of ROS are considered kinetically irrelevant compared to the ROS turnover catalyzed by enzymes[22-24]. Antioxidant

effects of lipoic acid might therefore rather be linked to cuprous or ferrous ion chelation, which prevents the metal ion-catalyzed creation of highly reactive hydroxyl radicals from the poorly reactive hydrogen peroxide (Fenton reaction)[22-24]. In line with that, both (*S*)-LA and (*R*)-LA buffered oxidative stress levels to 60-70% under extreme peroxide exposure (200 µM). In contrast, under non-stressed or arsenite-stressed conditions, lipoic acid did not significantly affect the oxidative stress levels in A549 cells. While metal ion chelation or ROS scavenging are physicochemical properties independent of lipoic acid stereochemistry, the enantiomer selective prevention of stress granule formation by (*R*)-LA argues for a specific mode of action.

In light of the data presented above, pan-HDAC inhibition by LA provides an attractive alternative way to explain many of the described cellular phenotypes of LA. For instance, our results relate the inhibition of stress granule formation by lipoic acid or lipoamide to HDAC inhibition and the consequential hyperacetylation of stress granule proteins. Indeed, it has been shown that posttranslational modifications can regulate the phase separation behavior of proteins[30, 31]. This includes protein acetylation[17, 32, 33], possibly by neutralizing positive charges in intrinsically disordered regions, which are important for protein-RNA or protein-protein interactions[34]. For instance, the stress granule protein DDX3X showed increased acetylation upon lipoic acid or lipoamide treatment akin to HDAC6 inhibitors (Fig. 3a) and the particular acetylation site has been linked to the regulation of DDX3X phase separation and stress granule maturation[17].

Aberrant phase separation and maturation of stress granules is a hallmark of several neurodegenerative diseases such as ALS[35, 36]. Interestingly, a recent screen of 1600 compounds[11] identified lipoic acid and lipoamide as the most promising hits for the disruption of ALS-associated stress granules. However, the data could not explain the underlying mode of action. In line with reports of HDAC6 inhibitors that modulate the formation of stress granules[17, 37] and that are discussed as promising drug candidates to ameliorate certain disease phenotypes of neurological diseases[38, 39], our findings suggest that HDAC inhibition is at least a contributing mode of action of lipoic acid and lipoamide. Thus, the current study adds to the notion that HDAC inhibitors are general modulators of liquid condensates. Such modulators are now increasingly explored for their therapeutic potential in a broad range of diseases termed condensatopathies[40]. Intriguingly, there is some overlap between the use of lipoic acid in clinical trials and those disease areas, where HDAC6 inhibition is a potential therapeutic strategy. These diseases mostly comprise neurologic pathologies such as ALS[11, 41] or peripheral neuropathy and neuropathic pain [5, 9, 42, 43]. Strikingly, Ricolinostat, an HDAC inhibitor with a target selectivity profile similar to that of lipoic acid and Vorinostat[12] (**Supplementary Fig. 2f**), is in clinical phase II trials for neuropathic pain – a condition for which lipoic acid is an approved medicine[7]. As we propose that HDAC inhibition is an important underlying mode of action, the current work provides a rationale for testing more advanced HDAC inhibitors in clinical trials for diseases, where lipoic acid showed promising effects. Vice versa, lipoic acid may be an alternative to designated HDAC inhibitors in diseases where the toxicity of current HDAC drugs is a concern.

Interestingly, no clinical trial has been conducted with lipoamide yet. Lipoamide shows a slightly different target profile than lipoic acid, including HDAC10 inhibition and is a somewhat more potent pan-HDAC inhibitor. Its effects on intracellular acetylation and prevention of stress granule formation are comparable to lipoic acid. One may speculate that lipoamide could have better bioavailability than lipoic acid owing to its lower polarity and a lower propensity for degradation via beta-oxidation, which is one of the major metabolic routes of lipoic acid[44]. Therefore, it may be an advantageous alternative to lipoic acid.

Methods

Preparation of iC[12]. 4-Azidobutanamine (1 µmol) was reacted with dimethylsulfoxide (DMSO)-washed N-hydroxysuccinimide (NHS)-activated (~20 µmol per ml beads) sepharose beads (1 ml) and triethylamine (20 µl) in DMSO (2 ml) on an end-over-end shaker overnight at room temperature in the dark. Aminoethanol (50 µl) was then added to inactivate the remaining NHS-activated carboxylic acid groups. After 1 h, the beads were washed with 40 ml DMSO. Alkyne-NHOTHP (19) (1 µmol) (Supplementary Note) was then clicked to the azide-functionalized beads via incubation in 1:1:2 (v/v/v) DMSO:tBuOH:H2O (2 ml total volume including beads), 0.1 mM tris(benzyltriazolylmethyl)amine (TBTA), 2 mM CuSO4 and 2 mM sodium ascorbate for 16 h at room temperature in the dark on the end-over-end shaker. The beads were then washed with 20 ml of 1:1:2 (v/v/v) DMSO:tBuOH:H2O, 30 ml of 50 mM EDTA in water and 30 ml ethanol, then reacted with 10 mM HCl in EtOH (10 ml) for 16 h at room temperature in the dark. Beads were washed with 50 ml ethanol to yield iC, stored at 4 °C in EtOH.

Preparation of iQ[12]. Quisinostat (1 µmol) was reacted with DMSO-washed NHS-activated (~20 µmol per ml beads) sepharose beads (1 ml) and triethylamine (20 µl) in DMSO (2 ml) on an end-over-end shaker overnight at room temperature in the dark. Aminoethanol (50 µl) was then added to inactivate the remaining NHS-activated carboxylic acid groups. After 16 h, the beads were washed with 10 ml DMSO and 30 ml EtOH to yield iQ, stored at 4 °C in EtOH.

Preparation of iL. Ethylenediamine (1 µmol, in DMSO) was reacted with DMSO-washed NHS-activated (~20 µmol/mL beads) sepharose beads (1 mL) and triethylamine (15 µL) in DMSO (2 mL) on an end-over-end shaker for 16 h at RT in the dark. (TLC with Kaiser test staining was used to monitor successful conversion). Aminoethanol (50 µL) was then added to inactivate the remaining NHS-activated carboxylic acid groups. After 2 h on an end-over-end shaker at RT, the beads were washed with DMSO (4 x 10 mL) and resuspended in anhydrous DMF (2 mL total volume). HATU (10 µmol, 100 µL of 100 mM stock in DMF), racemic Lipoic acid (12 µmol, 120 µL of 100 mM stock in DMSO), Hünig's base (20 µmol, 100 µL of 200 mM stock in DMF) and triethylamine (20 µL) were then added and the beads were incubated at RT for 16 h on an end-over-end shaker. Next, the beads were washed twice with 10 mL DMF and thrice with 10 mL ethanol. Beads were stored at 4 °C in EtOH.

Preparation of cell lysates for chemoproteomic assays. Cell lines MV4-11 (ATCC: CRL-9591) was grown in RPMI 1640 medium (PAN Biotech), SW620 (from NCI60 panel), HeLa S3 (ATCC: CCL-2.2), and A549 (ATCC: CCL-185) were grown in DMEM medium (PAN Biotech). All media were supplemented with 10% FBS (PAN Biotech) and cell lines were internally tested for Mycoplasma contamination. Cells were lysed in lysis buffer (0.8% Igepal, 50 mM Tris-HCl pH 7.5, 5% glycerol, 1.5 mM $MgCl_2$, 150 mM NaCl, 1 mM Na_3VO_4, 25 mM NaF, 1 mM DTT and supplemented with protease inhibitors (SigmaFast, Sigma) and phosphatase inhibitors (prepared in-house according to Phosphatase inhibitor cocktail 1, 2 and 3 from Sigma-Aldrich)). The protein amount of cell lysates was determined by Bradford assay and adjusted to an Igepal concentration of 0.4% and protein concentration of 5 mg/mL.

Chemoproteomic competition assays[12]. Cell lysate was pre-incubated with different doses of the small molecule of interest and a DMSO vehicle control for 1 h at 30 °C in an end-over-end shaker, followed by incubation with 18 µL affinity matrix (iL, iQ, or iC) for 30 min at 30 °C in an end-over-end shaker. To assess the degree of protein depletion from lysates by the affinity matrix, a second pulldown (PDPD) with fresh beads was performed using the unbound protein fraction from the vehicle control flow through. The beads were washed (1x 1 mL of lysis buffer without inhibitors and only 0.4% Igepal, 2x 2mL of lysis buffer without inhibitors and only 0.2% Igepal), and captured proteins were denatured with 8 M urea buffer, alkylated with 55 mM chloroacetamide and digested with Trypsin

according to standard procedures. The resulting peptides were desalted on a C18 filter plate (Sep-Pak® tC18 µElution Plate, Waters), vacuum dried, and stored at -20 °C until LC-MSMS measurement.

LC-MS/MS measurement of chemoproteomic assays. Peptides were analyzed via LC-MS/MS on a Dionex Ultimate3000 nano HPLC coupled to an Orbitrap HF (Thermo Fisher Scientific) or either one of two Orbitrap Fusion Lumos mass spectrometer, operated via the Thermo Scientific Xcalibur software. Peptides were loaded on a trap column (100 µm x 2 cm, packed in-house with Reprosil-Gold C18 ODS-3 5 µm resin, Dr. Maisch, Ammerbuch) and washed with 5 µL/min solvent A (0.1 % formic acid in HPLC grade water) for 10 min. Peptides were then separated on an analytical column (75 µm x 40 cm, packed in-house with Reprosil-Gold C18 3 µm resin, Dr. Maisch, Ammerbuch) using a 50 min gradient ranging from 4-32 % solvent B (0.1 % formic acid, 5 % DMSO in acetonitrile) in solvent A (0.1 % formic acid, 5 % DMSO in HPLC grade water) at a flow rate of 300 nL/min.

The mass spectrometers were operated in data-dependent mode, automatically switching between MS1 and MS2 spectra. MS1 spectra were acquired over a mass-to-charge (m/z) range of 360-1300 m/z at a resolution of 60,000 (at m/z 200) in the Orbitrap using a maximum injection time of 10 ms (HF) or 50 ms (Lumos) and an automatic gain control (AGC) target value of 3e6 (HF) or 4e5 (Lumos). Up to 15 (HF) or 12 (Lumos) peptide precursors were isolated (isolation width of 1.2 Th for HF and Lumos2 and 1.2 for Lumos1, maximum injection time of 75 ms, AGC value of 1e5 for HF and 2e5 for Lumos), fragmented by HCD using 25 % (HF) or 30% (Lumos) normalized collision energy (NCE) and analyzed in the Orbitrap at a resolution of 15,000 (Lumos2) or 30,000 (HF and Lumos1). The dynamic exclusion duration of fragmented precursor ions was set to 20s (Lumos1) or 30 s (HF, Lumos2).

Protein identification and quantification. Protein identification and quantification were performed using MaxQuant[45] (v 1.6.1.0) by searching the LC-MS/MS data against all canonical protein sequences as annotated in the Swissprot reference database (v03.12.15, 20193 entries, downloaded 22.03.2016) using the embedded search engine Andromeda. Carbamidomethylated cysteine was set as fixed modification and oxidation of methionine and N-terminal protein acetylation as variable modifications. Trypsin/P was specified as the proteolytic enzyme and up to two missed cleavage sites were allowed. The precursor tolerance was set to 10 ppm and fragment ion tolerance to 20 ppm. The minimum length of amino acids was set to seven and all data were adjusted to 1% PSM and 1% protein FDR. Label-free quantification[45] and match between runs was enabled.

Chemoproteomic competition assay data analysis. For the competition assays, relative binding was calculated based on the protein intensity ratio to the DMSO control for every single inhibitor concentration. EC_{50} values were derived from a four-parameter log-logistic regression with variable slope (constrain: bottom > 0). The obtained EC_{50} values were multiplied with a protein-dependent correction factor (cf), resulting in the apparent K_d value (K_d^{app}). The correction factor is determined by calculating the ratio of the protein intensity of two consecutive pulldowns of the vehicle control sample[13]. Targets of the inhibitors were annotated manually according to published procedures[12, 46, 47]. In brief, a protein was considered a target or interactor of a target if the resulting binding curve showed a sigmoidal curve shape with a dose-dependent decrease of binding to the beads. Additionally, the number of unique peptides and MSMS counts per condition were taken into account. Positive target binding across several independent experiments performed with different cell lysates further substantiated our confidence for a true positive drug-target binding event.

HDAC-Glo assay. The experiments were performed according to ref.[48]. HDAC6 and class I HDAC inhibition was tested using the HDAC-Glo™ I/II Assay and Screening System (G6421, Promega) with recombinant human HDACs (BPS Bioscience; HDAC1 cat. #50051; HDAC2 cat. #50002; HDAC3/NcoR2 complex cat. #50003; HDAC6 cat. #50006; HDAC8 cat. #50008). The assay was carried out in a 384-

well plate (Corning 4512) format according to the manufacturer's description. Drug dosing was performed with a D300e Digital Dispenser (Tecan). HDACs (7 ng/mL for HDAC1, 25 ng/mL for HDAC2, 200 ng/mL for HDAC3/Ncor2 complex, 100 ng/mL for HDAC6, 200 ng/mL for HDAC8) and inhibitors were incubated together at room temperature (RT) for 30 min. After addition of the HDAC-Glo™ I/II reagent, plates were shaken (800 rpm orbital shaker, 30 s), centrifuged (300 g, 1 min) and incubated at RT for 30 min. Luminescence was detected with a CLARIOstar (BMG Labtech) plate reader. Luminescence signal was normalized with 100 µM SAHA treated inhibition controls and uninhibited positive controls. pIC50 values were calculated from log(inhibitor) vs. normalized luminescence by nonlinear regression in GraphPad Prism.

HDAC10 TR-FRET assay.[48]. TR-FRET assays were performed in white 384-well plates (Corning 4512) using 50 mM HEPES pH 8.0, 150 mM NaCl, 10 mM MgCl2, 1 mM EGTA and 0.01% Brij-35 as buffer. The concentrations of reagent in 15 µL final assay volume were 5 nM TwinStrep-GST-HDAC10, 25 nM "Tubastatin-AF647-Tracer" and 0.1 nM DTBTA-Eu^{3+}-labelled Streptactin. Inhibitors with a D300e Digital Dispenser (Tecan). After drug dosing to the premixed assay reagents in buffer, plates were shaken (800 rpm orbital shaker, 30 s), centrifuged (300 g, 1 min) and incubated at RT in the dark for 90 min. TR-FRET was measured with a CLARIOstar (BMG Labtech) plate reader, equipped with TR-FRET filters. Sample wells were excited with 100 flashes and fluorescence emission detected at 665 nm and 620 nm. FRET ratios were calculated from 665 nm/620 nm ratio and normalized for each plate using 50 µM SAHA treated inhibition controls and uninhibited positive controls. pIC50 values were calculated as described in the HDAC-Glo assay.

HDAC6 and HDAC10 BRET assay[48]. For the production of transfected HeLa mono-clones stably expressing HDAC-nanoBRET fusion proteins of HDAC10 and HDAC6-catalytic domain 2 (HDAC6CD2), plasmids expressing a fusion of HDAC10 with nanoluciferase were obtained from Promega (N2170). HeLa cells (0.75×10^6) were seeded in a 6 cm dish and after 24 h were transfected with a mix of 10 µg plasmid and 3 µL Fugene in 200 µL OptiMEM. The intracellular target engagement assay on HDAC10 and HDAC6CD2 was performed using the NanoBRET™ Target Engagement Intracellular HDAC Assay (Promega N2081 and N2090) as described by the kit manufacturer in a 96-well plate (Corning 3600) format with 2×104 cells per well and a tracer concentration of 0.3 µM. Inhibitors were dosed with a D300e Digital Dispenser (Tecan). DMSO concentrations were normalized to 0.5 % for all wells. After dosing, assay plates were shaken at 800 rpm and incubated at 37 °C for 2 h followed by measurement of 450 nm and 650 nm luminescence (80 nm bandwidth) at room temperature with a CLARIOstar (BMG Labtech) plate reader 2 min after NanoLuc substrate addition. BRET ratios were calculated from 650 nm/450 nm luminescence and normalized for each plate using 50 µM SAHA treated negative controls and uninhibited positive controls. pIC50 values were calculated as described in the HDAC-Glo assay.

DDX3X and α-tubulin acetylation detection by western blot. 0.2×10^6 HEK293T (ATCC: CRL-3216) cells were transfected with pcDNA 3.1-HA CBP plasmids (1 µg/well for 6 well plate) by FuGENE. After 2 days, cells were treated with ACY-738, Lipoic acid, and Lipoamide for 7 h, then were washed by ice-cold PBS and lysed in Triton lysis buffer (50 mM Tris, pH 8.0, 150 mM NaCl, 1 mM EDTA, 0.1% TritonX-100 and complete EDTA-free protease inhibitors (Roche)) for analysis. To detect protein acetylation, 0.2 µM Trichostatin A and 5 mM nicotinamide were added to PBS for washing, and 10 µM trichostatin A, 10 mM nicotinamide, and 50 mM sodium butyrate were added to Triton lysis buffer. Samples were boiled for 10 min in SDS–PAGE sample buffer, and separated with 4–12% NuPAGE gels (Invitrogen). Proteins were transferred onto PVDF membranes (Immobilon-P, Millipore), probed with the primary antibodies (Anti-HDAC6, rabbit mAb, CST#7558, diluted 1:1000; anti-HA-Tag (C29F4) Rabbit mAb CST#3724, diluted 1:1000; anti-DDX3X (Millipore#09-860), diluted 1:1000; anti-acetyl-DDX3X

produced in house[17], diluted 1:1000, Monoclonal anti- α -tubulin antibody produced in mouse, Sigma-Aldrich Cat#T9026, diluted 1:2000; anti-acetyl- α-tubulin (Lys40) Monoclonal Antibody (6-11B-1), Catalog # 32-2700, Invitrogen, diluted 1:1000) overnight and secondary antibody for 1 h under 5% non-fat dry milk in TBS or 5% BSA, 0.1% Tween20 in TBS blocking conditions. HRP-based chemiluminescence was detected with Amersham Imager 680 using ECL western blotting reagent (GE Healthcare).

Histone H4 and α-tubulin AcK western blot in A549 and HEK293T. $0.3x10^6$ A549 and HEK293T cells were seeded to each well of 6 well plate at Day 0. On Day 2, cells were treated with drugs for 6 hours. Then cells were harvested by Cell Lifter (CORNING:3008) and lysed by RIPA buffer (supplied with cOmplete™ Protease Inhibitor Cocktail). Protein concentration was determined by BCA assay and the same protein input amount for each condition was loaded onto gels. Proteins were transferred onto PVDF membranes (Immobilon-P, Millipore), and probed with specific primary antibody overnight (AcK-H4 antibody: Anti-acetyl-histone H4 antibody, catalog#06-866, Sigma, diluted 1:1000; Actin: Pan-actin antibody Sigma-Aldrich Cat#SAB4502632, diluted 1:2000; RRID: AB_10746710; α-tubulin: Monoclonal anti- α -tubulin antibody produced in mouse, Sigma-Aldrich Cat#T9026; RRID: AB_477593, diluted 1:2000; AcK-α-tubulin: Acetyl- α-tubulin (Lys40) Monoclonal Antibody (6-11B-1), Catalog # 32-2700, Invitrogen, diluted 1:1000). Then the secondary antibody was added for 1 h under 5% non-fat dry milk in TBS blocking conditions. HRP based chemiluminescence was detected with Amersham Imager 680 using ECL western blotting reagent (GE Healthcare).

Global Acetyl-lysine detection by western blot. HeLa S3 was grown in DMEM medium (PAN Biotech) supplemented with 10% FBS (PAN Biotech) and treated with drugs (final concentration of 0.1% DMSO) for indicated periods**.** Protein lysates were generated by harvesting cells in lysis buffer (0.8% NP40, 50 mM Tris-HCl pH 7.5, 5% glycerol, 1.5 mM $MgCl_2$, 150 mM NaCl, 1 mM Na_3VO_4, 25 mM NaF, 1 mM DTT and supplemented with protease inhibitors (SigmaFast, Sigma) and phosphatase inhibitors (prepared in-house according to Phosphatase inhibitor cocktail 1, 2 and 3 from Sigma-Aldrich)). The protein amount of cell lysates was determined by Bradford assay. Samples were boiled for 10 min in SDS–PAGE sample buffer, and separated with 4–12% NuPAGE gels (Invitrogen). Proteins were separated by SDS-PAGE and electro-transferred onto PVDF membranes. Blots were kept in Tris-buffered saline, supplemented with 0.05 % Tween (TBS-T) and 4% BSA for 1 h at room temperature and then incubated with primary antibody diluted in 1xTBS, 0.05% Tween and 4% BSA overnight at 4 ºC. Following antibodies were used: Acetylated-Lysine Antibody (Cell Signaling Technology, #9441S, polyclonal rabbit IgG, diluted 1:1000), and beta-Actin Antibody (Santa Cruz Biotechnology, #sc-47778, 0.2 mg/mL, monoclonal mouse IgG, diluted 1:500). After antibody incubation, blots were washed in TBS-T and probed with the corresponding fluorophore-conjugated secondary antibody (ODYSSEY donkey-anti-rabbit (#926-68023), goat-anti-mouse (#926-32210)) for 30 min at room temperature. Acquisition and quantification of the band fluorescence intensities were carried out with the Odyssey (Licor) imaging system and corresponding software (v 3.0.29). Intensities of proteins were normalized to input beta-Actin and further normalized to the control treatments to calculate the relative acetylation change.

Lipoic acid effect on stress granule formation. 0.03×10^6 A549 cells were seeded at 4-chamber slides (Thermo, Nunc) and cultured at 37 °C overnight. Cells were treated with HDAC inhibitor SAHA and Lipoic acid or Lipoamide for 6 h, followed by 1 mM Arsenite for 30 mins. Cells were fixed by 4% PFA and permeabilized by 0.5% Triton X-100/PBS. 10% Goat serum in PBS was used for blocking. After manually selecting an area with cell confluency of 50-80%, 16 pictures were taken randomly around the central point (ZEISS software in-built function). Stress granule marker G3BP1 (Aviva Systems Biology, ARP37713_T100) was visualized and quantified by ImageJ. Statistical analysis was performed with GraphPad Prism.

CellRox™ deep red assay for tBuOOH induced ROS. A549 cells were maintained in DMEM (Sigma) supplemented with 10 % fetal bovine serum (Pan Biotech). Cells were seeded onto a 24-well plate with flat and clear bottom (Ibidi) 24 hours before imaging. The CellRox assay was performed according to the product guidelines (ThermoFisher). Briefly, cells were treated with lipoic acid, N-acetyl-cysteine (NAC), or vector control (DMSO) for 1 hour, followed by a 2 h treatment with 200 µM tert-butyl hydroperoxide, and then stained with 5 µM CellRox Deep Red for 1 hour. Cells were washed twice with FluoroBrite DMEM (ThermoFisher) supplemented with 10 % FBS before imaging. CellRox Deep Red signal intensity was measured on a Leica DMI 6000 B epifluorescent microscope with a Cy5 filter set. Mean signal intensity per cell was determined from 60-180 (on average ~125) cells per replicate. Significance was calculated by ANOVA with a post hoc Dunnett's multiple comparisons test against the DMSO control (GraphPad).

CellRox™ deep red assay for ROS quantification. A549 cells were maintained in DMEM (Sigma) supplemented with 10 % fetal bovine serum (Pan Biotech). Cells were seeded onto a 24-well plate with flat and clear bottom (Ibidi) 24 hours before imaging. The CellRox assay was performed according to the product guidelines (ThermoFisher). Briefly, cells were treated with 300 µM lipoic acid, lipoamide, N-acetyl-cysteine, 200 µM tert-butyl hydroperoxide, or vector control (DMSO) for 1 hour, and then stained with 5 µM CellRox Deep Red for 1 hour with additional 1 mM arsenite treatment 30 min into staining where indicated. Cells were washed twice with FluoroBrite DMEM (ThermoFisher) supplemented with 10 % FBS and Glutamax (ThermoFisher) before imaging. CellRox Deep Red signal intensity was measured on a Leica DMI 6000B inverted microscope with a Cy5 filter set. Mean signal intensity per cell was determined from 60-180 (on average ~100) cells per replicate. Significance was calculated by ANOVA with a post hoc Dunnett's multiple comparisons test against the DMSO control (GraphPad).

Statistics and reproducibility. All information on statistical tests is provided within the figure legends. All experiments resulting in figures and data provided with this manuscript were performed once.

Data availability. The mass spectrometry proteomics data, including the used Swiss-Prot reference database and .pdfs from initial data analysis, have been deposited in the MassIVE proteomics database with the dataset identifier MSV000091758 (https://massive.ucsd.edu/ProteoSAFe/static/massive.jsp). Source data are provided with this paper.

References

1. Rowland, E.A., Snowden, C.K. & Cristea, I.M. Protein lipoylation: an evolutionarily conserved metabolic regulator of health and disease. *Curr Opin Chem Biol* **42**, 76-85 (2018).
2. Khan, H., Singh, T.G., Dahiya, R.S. & Abdel-Daim, M.M. alpha-Lipoic Acid, an Organosulfur Biomolecule a Novel Therapeutic Agent for Neurodegenerative Disorders: An Mechanistic Perspective. *Neurochem Res* **47**, 1853-1864 (2022).
3. Felber, J.G. *et al.* Cyclic 5-membered disulfides are not selective substrates of thioredoxin reductase, but are opened nonspecifically. *Nat Commun* **13**, 1754 (2022).
4. Xie, H. *et al.* Role of lipoic acid in multiple sclerosis. *CNS Neurosci Ther* **28**, 319-331 (2022).
5. Ziegler, D., Low, P.A., Freeman, R., Tritschler, H. & Vinik, A.I. Predictors of improvement and progression of diabetic polyneuropathy following treatment with alpha-lipoic acid for 4 years in the NATHAN 1 trial. *J Diabetes Complications* **30**, 350-356 (2016).
6. Daousi, C. *et al.* Chronic painful peripheral neuropathy in an urban community: a controlled comparison of people with and without diabetes. *Diabet Med* **21**, 976-982 (2004).

7. Ziegler, D. *et al.* Screening, diagnosis and management of diabetic sensorimotor polyneuropathy in clinical practice: International expert consensus recommendations. *Diabetes Res Clin Pract* **186**, 109063 (2022).
8. Papanas, N. & Ziegler, D. Efficacy of alpha-lipoic acid in diabetic neuropathy. *Expert Opin Pharmacother* **15**, 2721-2731 (2014).
9. Ziegler, D., Reljanovic, M., Mehnert, H. & Gries, F.A. Alpha-lipoic acid in the treatment of diabetic polyneuropathy in Germany: current evidence from clinical trials. *Exp Clin Endocrinol Diabetes* **107**, 421-430 (1999).
10. Dorsam, B. & Fahrer, J. The disulfide compound alpha-lipoic acid and its derivatives: A novel class of anticancer agents targeting mitochondria. *Cancer Lett* **371**, 12-19 (2016).
11. Wheeler, R.J., Lee, H.O., Poser, I., Pal, A. & Hyman, A.A. Small molecules for modulating protein driven liquid-liquid phase separation in treating neurodegenerative disease. *Preprint at BioRxive* (2019).
12. Lechner, S. *et al.* Target deconvolution of HDAC pharmacopoeia reveals MBLAC2 as common off-target. *Nat Chem Biol* **18**, 812-820 (2022).
13. Medard, G. *et al.* Optimized chemical proteomics assay for kinase inhibitor profiling. *J Proteome Res* **14**, 1574-1586 (2015).
14. Burli, R.W. *et al.* Design, synthesis, and biological evaluation of potent and selective class IIa histone deacetylase (HDAC) inhibitors as a potential therapy for Huntington's disease. *J Med Chem* **56**, 9934-9954 (2013).
15. Geraldy, M. *et al.* Selective Inhibition of Histone Deacetylase 10: Hydrogen Bonding to the Gatekeeper Residue is Implicated. *J Med Chem* **62**, 4426-4443 (2019).
16. Hai, Y., Shinsky, S.A., Porter, N.J. & Christianson, D.W. Histone deacetylase 10 structure and molecular function as a polyamine deacetylase. *Nat Commun* **8**, 15368 (2017).
17. Saito, M. *et al.* Acetylation of intrinsically disordered regions regulates phase separation. *Nat Chem Biol* **15**, 51-61 (2019).
18. Stoner, M.W. *et al.* alpha-Lipoic acid promotes alpha-tubulin hyperacetylation and blocks the turnover of mitochondria through mitophagy. *Biochem J* **473**, 1821-1830 (2016).
19. Scholz, C. *et al.* Acetylation site specificities of lysine deacetylase inhibitors in human cells. *Nat Biotechnol* **33**, 415-423 (2015).
20. Parmigiani, R.B. *et al.* HDAC6 is a specific deacetylase of peroxiredoxins and is involved in redox regulation. *Proc Natl Acad Sci U S A* **105**, 9633-9638 (2008).
21. Panas, M.D. *et al.* Phosphorylation of G3BP1-S149 does not influence stress granule assembly. *J Cell Biol* **218**, 2425-2432 (2019).
22. Forman, H.J. & Zhang, H. Targeting oxidative stress in disease: promise and limitations of antioxidant therapy. *Nat Rev Drug Discov* **20**, 689-709 (2021).
23. Murphy, M.P. *et al.* Guidelines for measuring reactive oxygen species and oxidative damage in cells and in vivo. *Nat Metab* **4**, 651-662 (2022).
24. Sies, H. *et al.* Defining roles of specific reactive oxygen species (ROS) in cell biology and physiology. *Nat Rev Mol Cell Biol* **23**, 499-515 (2022).
25. Chance, B., Sies, H. & Boveris, A. Hydroperoxide metabolism in mammalian organs. *Physiol Rev* **59**, 527-605 (1979).
26. Myzak, M.C., Ho, E. & Dashwood, R.H. Dietary agents as histone deacetylase inhibitors. *Mol Carcinog* **45**, 443-446 (2006).
27. Dashwood, R.H. & Ho, E. Dietary histone deacetylase inhibitors: from cells to mice to man. *Semin Cancer Biol* **17**, 363-369 (2007).
28. Zhao, L. *et al.* Lipoamide Acts as an Indirect Antioxidant by Simultaneously Stimulating Mitochondrial Biogenesis and Phase II Antioxidant Enzyme Systems in ARPE-19 Cells. *Plos One* (2015).

29. Shen, W., Hao, J. & Liu, J. Lipoamide or lipoic acid stimulates mitochondrial biogenesis in 3T3-L1 adipocytes via the endothelial NO synthase-cGMP-protein kinase G signalling pathway. *BJP* (2010).
30. Hofweber, M. *et al.* Phase Separation of FUS Is Suppressed by Its Nuclear Import Receptor and Arginine Methylation. *Cell* **173**, 706-719 e713 (2018).
31. Monahan, Z. *et al.* Phosphorylation of the FUS low-complexity domain disrupts phase separation, aggregation, and toxicity. *EMBO J* **36**, 2951-2967 (2017).
32. Cohen, T.J. *et al.* An acetylation switch controls TDP-43 function and aggregation propensity. *Nat Commun* **6**, 5845 (2015).
33. Li, X. *et al.* Deacetylation induced nuclear condensation of HP1gamma promotes multiple myeloma drug resistance. *Nat Commun* **14**, 1290 (2023).
34. Kilgore, H.R. & Young, R.A. Learning the chemical grammar of biomolecular condensates. *Nat Chem Biol* (2022).
35. Molliex, A. *et al.* Phase separation by low complexity domains promotes stress granule assembly and drives pathological fibrillization. *Cell* **163**, 123-133 (2015).
36. Patel, A. *et al.* A Liquid-to-Solid Phase Transition of the ALS Protein FUS Accelerated by Disease Mutation. *Cell* **162**, 1066-1077 (2015).
37. Kwon, S., Zhang, Y. & Matthias, P. The deacetylase HDAC6 is a novel critical component of stress granules involved in the stress response. *Genes Dev* **21**, 3381-3394 (2007).
38. Guo, W. *et al.* HDAC6 inhibition reverses axonal transport defects in motor neurons derived from FUS-ALS patients. *Nat Commun* **8**, 861 (2017).
39. Brindisi, M. *et al.* Old but Gold: Tracking the New Guise of Histone Deacetylase 6 (HDAC6) Enzyme as a Biomarker and Therapeutic Target in Rare Diseases. *J Med Chem* **63**, 23-39 (2020).
40. Mitrea, D.M., Mittasch, M., Gomes, B.F., Klein, I.A. & Murcko, M.A. Modulating biomolecular condensates: a novel approach to drug discovery. *Nat Rev Drug Discov* (2022).
41. Tejido, C., Pakravan, D. & Bosch, L.V.D. Potential Therapeutic Role of HDAC Inhibitors in FUS-ALS. *Front Mol Neurosci* **14**, 686995 (2021).
42. Vallianou, N., Evangelopoulos, A. & Koutalas, P. Alpha-lipoic Acid and diabetic neuropathy. *Rev Diabet Stud* **6**, 230-236 (2009).
43. English, K. & Barton, M.C. HDAC6: A Key Link Between Mitochondria and Development of Peripheral Neuropathy. *Front Mol Neurosci* **14**, 684714 (2021).
44. Schupke, H. *et al.* New metabolic pathways of alpha-lipoic acid. *Drug Metab Dispos* **29**, 855-862 (2001).
45. Cox, J. *et al.* Accurate proteome-wide label-free quantification by delayed normalization and maximal peptide ratio extraction, termed MaxLFQ. *Mol Cell Proteomics* **13**, 2513-2526 (2014).
46. Klaeger, S. *et al.* The target landscape of clinical kinase drugs. *Science* **358** (2017).
47. Reinecke, M. *et al.* Chemoproteomic Selectivity Profiling of PIKK and PI3K Kinase Inhibitors. *ACS Chem Biol* **14**, 655-664 (2019).
48. Steimbach, R.R. *et al.* Aza-SAHA Derivatives Are Selective Histone Deacetylase 10 Chemical Probes That Inhibit Polyamine Deacetylation and Phenocopy HDAC10 Knockout. *J Am Chem Soc* **144**, 18861-18875 (2022).

Acknowledgements. Supported by the Deutsche Forschungsgemeinschaft (DFG) SFB1309, project 401883058 (S.L.). P.M. and L.W. thank the European Research Council—ERC Synergy grant number 856581 and the Novartis Research Foundation. M.K. and T.F. thank the Else Kröner Fresenius Stiftung (2017_A108 – EKFZ) for funding. M.L.D. and T.F. thank the Science Program grants by the Heising-Simons Foundation (#2017-0496 and #2020-2427) for supporting this study.

Author Contributions. B.K. and G.M. conceived and directed the project. S.L. performed chemoproteomic experiments and western blots. S.L. and B.K. measured the proteomics samples. Y.C. performed proteomic experiments. R.R.S. and A.K.M. performed the HDAC enzyme activity assays, as well as BRET and FRET binding assays. L.W. and P.M. performed western blots and stress granule experiments. M.L.D., T.F., and M.K. performed the CellRox assays and data analysis. S.L. and B.K. wrote the manuscript with input from all authors.

Competing Interests. B.K. is a cofounder and shareholder of OmicScouts and msAId. He has no operational role in either company. The remaining authors declare no competing interests.

Supplementary Information

Chemoproteomic target deconvolution reveals Histone Deacetylases as targets of (*R*)-lipoic acid

Severin Lechner[1], Raphael R. Steimbach[2,3], Longlong Wang[4,5], Marshall L. Deline[6], Yun-Chien Chang[1], Tobias Fromme[6,7], Martin Klingenspor[6,7,8], Patrick Matthias[4,5], Aubry K. Miller[2,9], Guillaume Médard[1], Bernhard Kuster[1,9,10]

[1]Chair of Proteomics and Bioanalytics, TUM School of Life Sciences, Technical University of Munich, Freising, Germany.
[2]Cancer Drug Development, German Cancer Research Center (DKFZ), Heidelberg, Germany.
[3]Biosciences Faculty, Heidelberg University, Heidelberg, Germany.
[4]Friedrich Miescher Institute for Biomedical Research, 4058 Basel, Switzerland.
[5]Faculty of Sciences, University of Basel, 4031 Basel, Switzerland.
[6]Chair of Molecular Nutritional Medicine, TUM School of Life Sciences, Technical University of Munich, Freising, Germany.
[7]EKFZ - Else Kröner Fresenius Center for Nutritional Medicine, Technical University of Munich, Freising, Germany
[8]ZIEL Institute for Food & Health, Technical University of Munich, Freising, Germany.
[9]German Cancer Consortium (DKTK), Heidelberg, Germany.
[10]Bavarian Center for Biomolecular Mass Spectrometry (BayBioMS), Technical University of Munich, Freising, Germany.

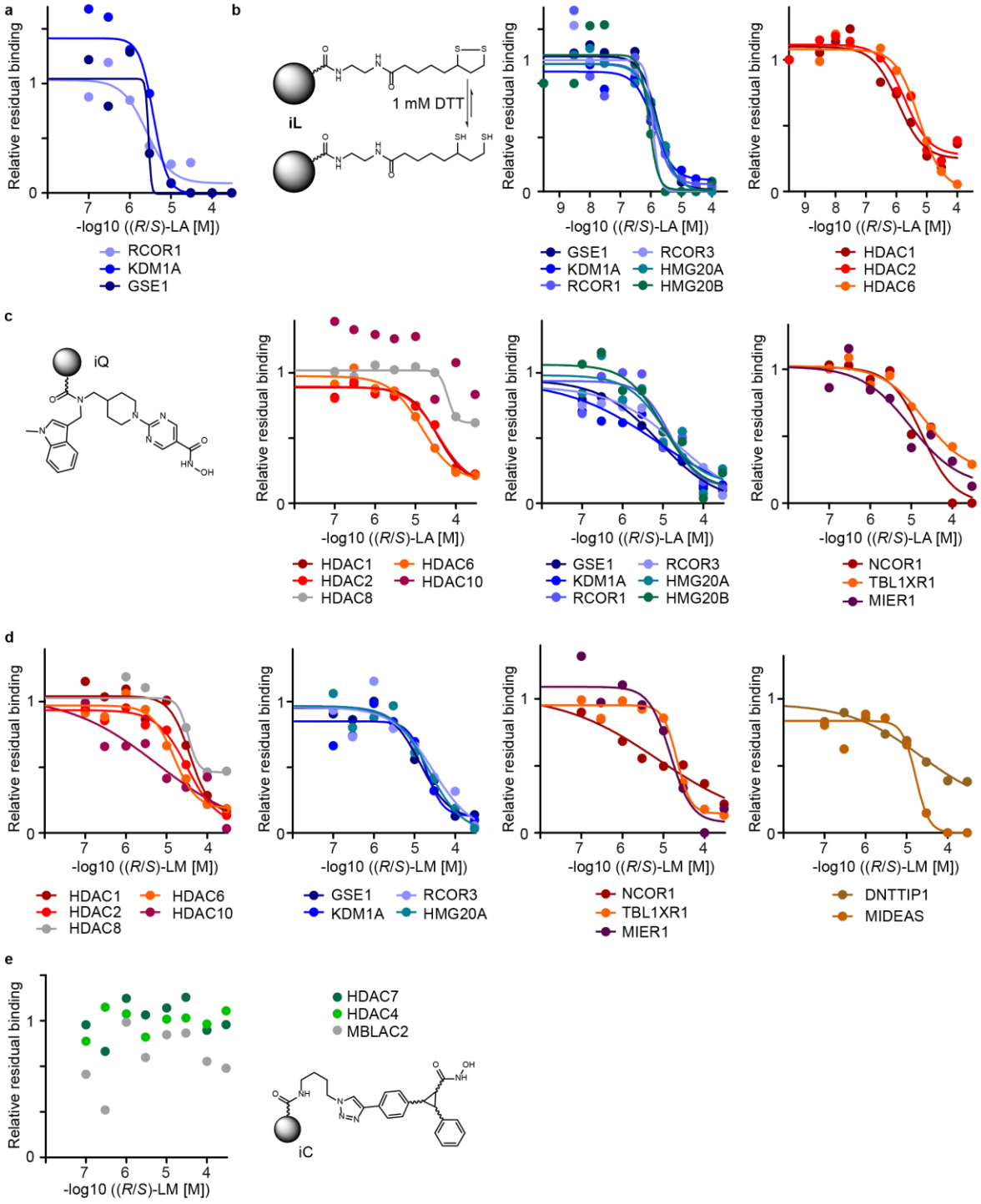

Supplementary Fig. 1|Chemoproteomics identifies HDACs as targets of lipoic acid and lipoamide. a, Dose-response curves of HDAC CoREST complex partners from the LA-iL competition experiment in SW620 cell lysate. **b**, Dose-response curves of HDACs and CoREST complex partners from the LA-iL competition experiment in A549 cell lysate. **c**, Dose-response curves from the LA-iQ competition assay in SW620 cell lysate. HDAC interactor MIER1 and complex partners of the HDAC3 NCoR complex (NCoR1, TBL1XR1) as well as the HDAC1/2 CoREST complex (RCOR1/3, KDM1A, HMG20A/B, GSE1) show a dose-dependent reduction in affinity matrix binding. **d**, same as (c) but for lipoamide and including additional curves for MiDAC complex partners DNTTIP and MIDEAS. **e**, Competition assay for lipoic acid probing class IIa HDAC and MBLAC2 binding using established affinity matrix iC. Source data are provided as a Source Data file.

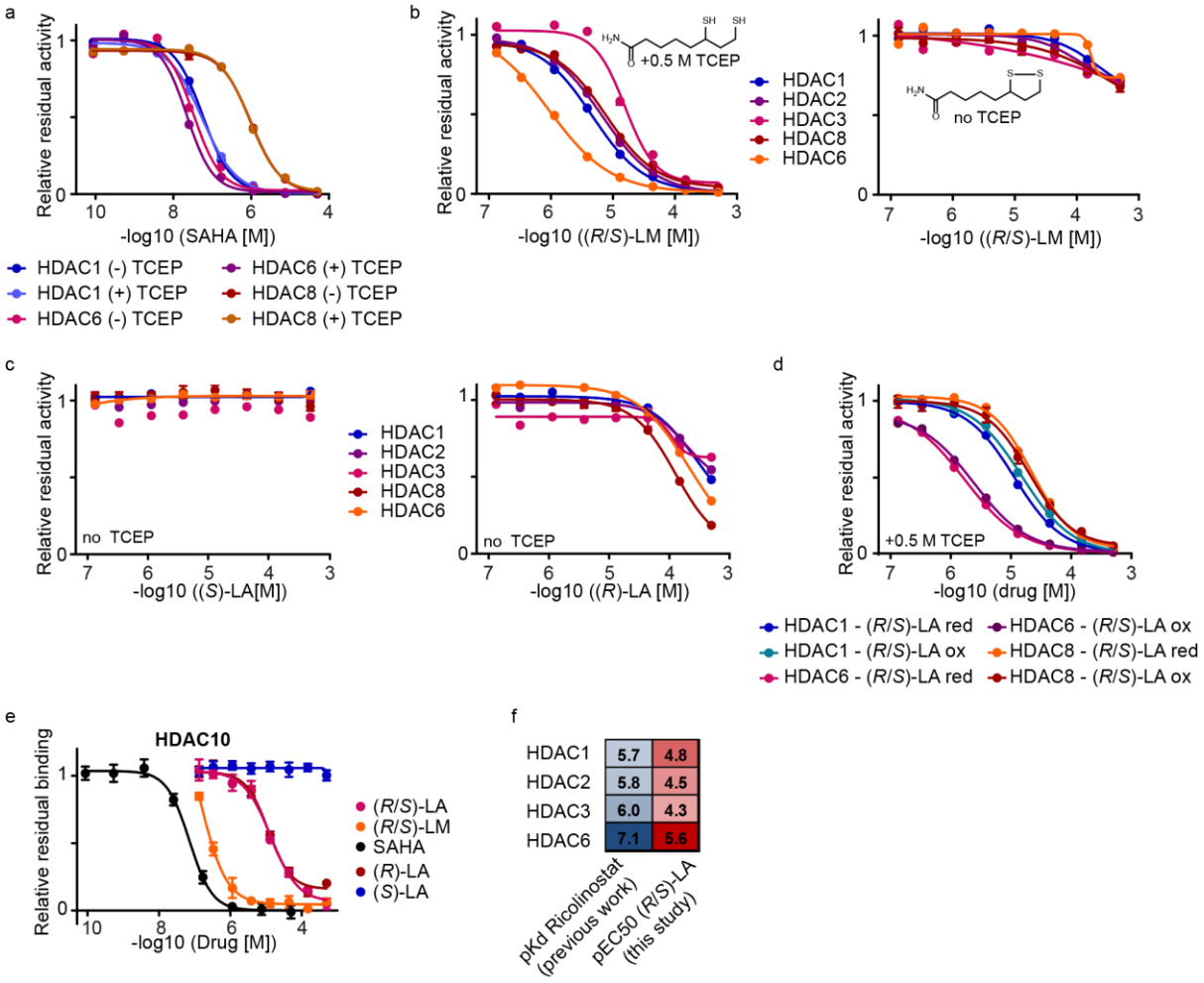

Supplementary Fig. 2|HDAC activity assays confirm the inhibitory effects of the reduced forms of (*R*)-lipoic acid, (*R/S*)-lipoic acid, and (*R/S*)-lipoamide. a, HDAC inhibition by SAHA (Vorinostat) in the Glo-assay setup is in the presence (+) or absence (-) of reducing agent TCEP (0.5 M) (n = 3 technical replicates for each drug dose, data are represented as mean value +/- SEM). **b,** influence of reducing agent TCEP (0.5 M) on Lipoamide mediated HDAC enzymatic inhibition via reduction and thiolane ring opening of the drugs (n = 3 technical replicates for each drug dose, data are represented as mean value +/- SEM). **c,** Dose-dependent effect of (*S*)- and (*R*)-lipoic acid on HDAC activity under non-reducing conditions (n = 3 technical replicates for each drug dose, data are represented as mean value +/- SEM). **d**, Comparison of effects of racemic reduced LA ((*R/S*)-LA red, i.e. dihydrolipoic acid) and oxidized (*R/S*)-LA on HDAC activity in the presence of reducing agent TCEP (0.5 M) (n = 3 technical replicates for each drug dose, data are represented as mean +/- SEM). **e**, FRET-based HDAC10 binding assay under reducing assay conditions (0.5 M TCEP) (n = 3 technical replicates for each drug dose, data are represented as mean value +/- SEM). **f**, lipoic acid pEC50 values from the Glo-HDAC activity assay are compared to the Ricolinostat pK_d^{app}s from ref.[1]. Source data are provided as a Source Data file.

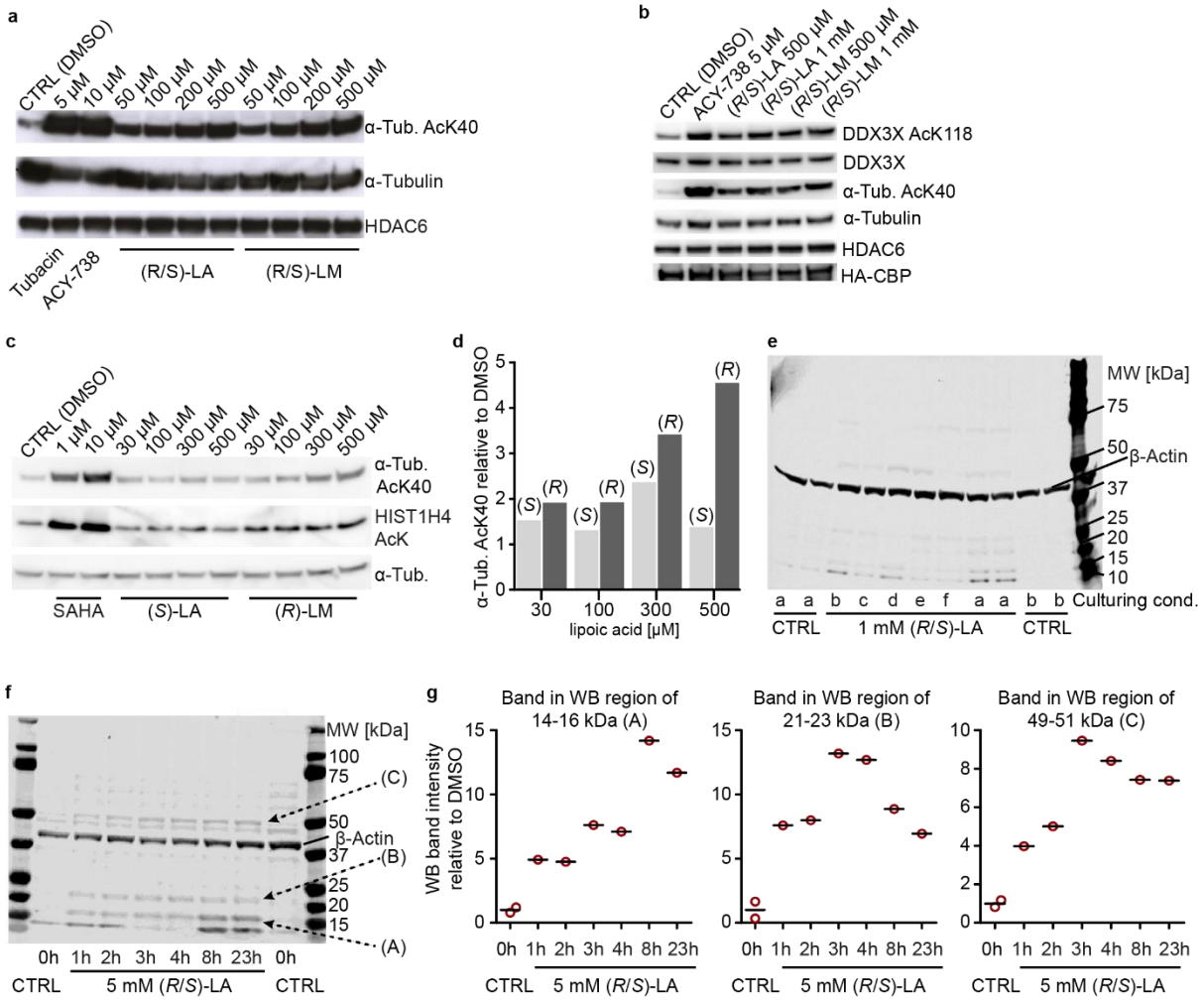

Supplementary Fig. 3|Lipoic acid and lipoamide treatment leads to hyperacetylation of HDAC substrate proteins. a, Western blot of CBP-HA (Acetyltransferase) transfected HEK293 cells that were incubated with HDAC6 inhibitor ACY-738, Tubacin, lipoic acid, or lipoamide for 7 h at indicated concentrations and probed for HDAC6 substrate protein acetylation site AcK40 of α-Tubulin as well as α-Tubulin and HDAC6 expression. **b**, Western blot of CBP-HA transfected HEK293 cells that were incubated with HDAC6 inhibitor ACY-738, lipoic acid, or lipoamide for 7 h at indicated concentrations and probed for HDAC6 substrate proteins and acetylation sites (Loading controls: HA-CBP and HDAC6). **c,** Western blot of HEK293T cells treated for 6 h with SAHA (Vorinostat), (*R*)-lipoic acid, or (*S*)-lipoic acid. **d,** comparison of dose-dependent effect of (*R*)-LA and (*S*)-LA treatment on α-tubulin AcK40 in HEK293 cells (quantification data from Supplementary Fig. 3c).**e**, Acetyl-lysine Western Blot of HeLa S3 cells cultured under various conditions and treated with 1 mM lipoic acid for 16 h. Culture conditions: a: DMEM (10% FBS), 95% confluency; b: DMEM (10% FBS), 70% confluency; c: IMDM (10% FBS), 70% confluency; d: supernatant of HeLa S3 cells after 3 d of culturing (old DMEM with 10% FBS), e: DMEM (10% FBS) plus 5 mM acetic acid, 70% confluency; f: DMEM (without FBS), 70% confluency. Biological replicates of condition 'a' treated with lipoic acid or vehicle control (DMSO) were used for quantification and plotting of Fig. 3c. **f** and **g**, Acetyl-lysine Western Blot of HeLa S3 cells treated with 5 mM (*R*/*S*)-lipoic acid for different periods (f) and intensity of bands (g) relative to control (DMSO, 0 h treatment) after normalization to β-actin loading control (n = 2 biologically independent samples for DMSO control CTRL, data of control is represented as mean value). Source data are provided as a Source Data file.

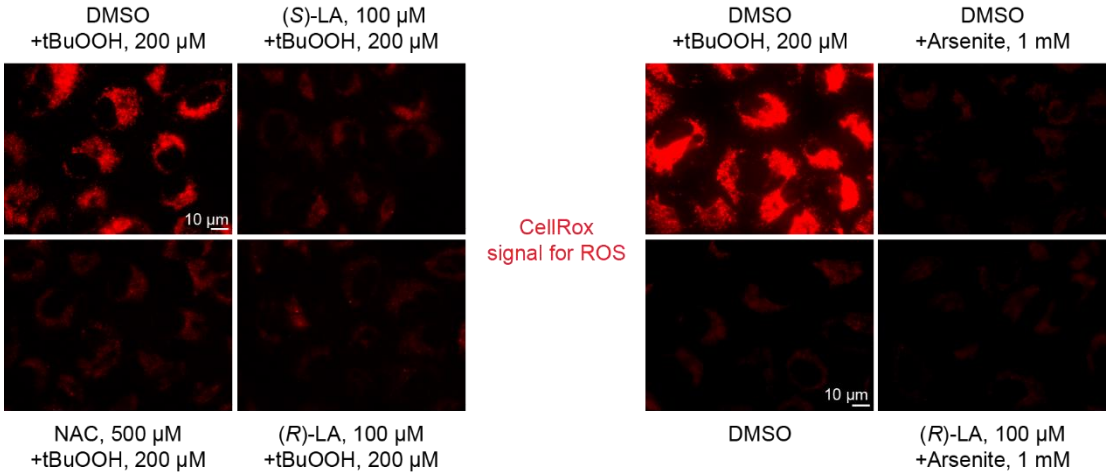

Supplementary Fig. 4|Small molecule ROS buffering effect under tertbutylhydroperoxide (tBuOOH) or arsenite stress. Cells were pretreated with drug molecules and then exposed to stress inducers tBuOOH or arsenite. ROS was quantified by microscopy via CellRox deep red signal intensity.

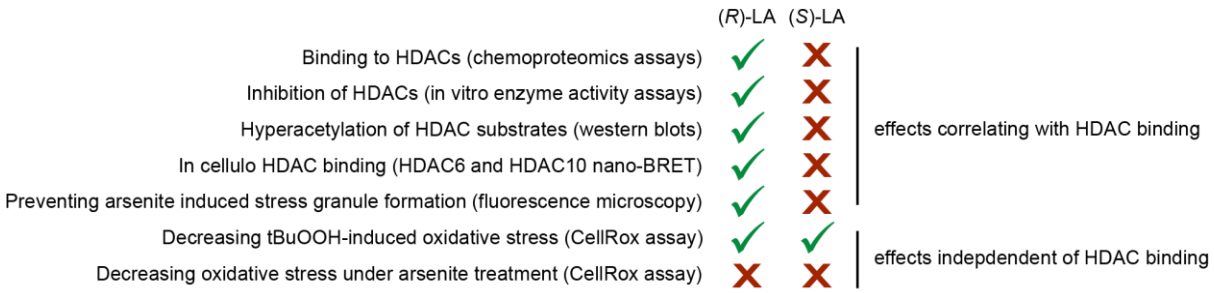

Supplementary Fig. 5|Overview of enantioselective effects of (*R*)-LA and of effects independent of the stereochemistry of LA. Assays used for the readout of the effects are provided in brackets.

Supplementary References

1. Lechner, S. *et al.* Target deconvolution of HDAC pharmacopoeia reveals MBLAC2 as common off-target. *Nat Chem Biol* **18**, 812-820 (2022).